Alfred-Wegener-Institut für Polar- und Meeresforschung
Universität Potsdam, Institut für Erd- und Umweltwissenschaften

Glaciomarine sedimentation at the continental margin of Prydz Bay, East Antarctica: implications on palaeoenvironmental changes during the Quaternary

Dissertation
zur Erlangung des akademischen Grades
Doktor der Naturwissenschaften
(Dr. rer. nat.)
in der Wissenschaftsdisziplin “Geowissenschaften”

eingereicht an der
Mathematisch-Naturwissenschaftlichen Fakultät
der Universität Potsdam

von

Andreas Borchers

Potsdam, 30. November 2010

Das Höchste, wozu der Mensch gelangen kann,
ist das Erstaunen.

J. W. von Goethe

Acknowledgements

This dissertation would not have been possible without the support and help of numerous people to whom I would like to express my gratitude.

First, I am highly indebted to PD Dr. Bernhard Diekmann for the possibility to conduct this work under his supervision and for his constant support, whenever discussion or advice was needed. I appreciated his vast expertise and knowledge of marine geology, sedimentology and Quaternary Science that he so enthusiastically shared with me, adding considerably to my experience. Besides being a full-hearted geologist, he is also a great guitarist, which I enjoyed during the past years, especially during the expeditions I had the chance to participate.

I would also like to thank Prof. Dr. Hans-Wolfgang Hubberten for his general support and understanding, giving me the opportunity to broaden my knowledge of marine geology in the field. Using the infrastructure of the institute in Potsdam, Bremerhaven and on the world's oceans has made a major contribution realizing this work.

I am deeply grateful to Prof. Dr. Ulrike Herzschuh and Dr. Gerhard Kuhn who provided a large part of assistance by discussions, constructive advices and moral support.

Dr. Oliver Esper, Dr. Thomas Frederichs and Dr. Rainer Gersonde are acknowledged for close collaboration, quick and straightforward help and a great time during our expedition to the North Pacific.

This PhD project was funded by the 'Deutsche Forschungsgesellschaft' (DFG) within the scope of priority program 1158 'Antarctic research with comparative studies in Arctic ice regions' through grant DI 655/3-1. During the last years I had the opportunity to be a member of the Potsdam Graduate School (POGS) and the Helmholtz Graduate School for Polar and Marine Research (POLMAR). I like to thank Dr. Claudia Sprengel, Dr. Claudia Hanfland and Dr. Heike Küchmeister for making it possible for me to attend several professional courses. I also thank the German Polar Society (DGP) and SCAR-ACE for travel grants to scientific conferences.

For the instruction and support in analytical work I like to express my gratitude to the laboratory staff at AWI Potsdam and AWI Bremerhaven, namely Ute Bastian, Antje Eulenburg, Rita Fröhlking, Norbert Lensch, Ute Bock and Susanne Wiebe. Bernd Hoffmann

and Anna Plotzki amongst other students doing internships at the AWI are acknowledged for their involvement in the sample preparation.

Many thanks also to the AWI Potsdam administration, in particular Christine Litz. Thanks to Heiko Gericke and Tobias Schmidt for solving plotter and network problems.

Stephan, Boris, Jens, Ulrike – even in an office half the size of ours it would have been a splendid time. I very much enjoyed our A.-coffee breaks, scientific discussions and our "group suffering" from everything that life offers.

The open and pleasant atmosphere amongst the young researchers on the Telegrafenberg contributed to a great time over the past years. For many humorous conversations and philosophical talks regarding scientific and non-scientific issues I especially thank Larsen, Jule, Micha, Torsten, Mathias, Thomas, Seb and Seb, Bernhard and Bernhard, Lise, Josi, Ines, Katja, Maria and others.

It is a valuable gift to have people close even though they are far away.
Uta, Anja and Gregor – I am deeply grateful for lots of talks and, unfortunately, less frequent activities helping me get my mind free. Maike – I am very much indebted to you for a great time and your unwavering support and patience.

Most of all, I would like to thank with all my heart my parents and my entire family for their support and encouragement and dedicate this work to them.

Contents

List of figures

List of tables

List of abbreviations

AABW	Antarctic Bottom Water
AAIW	Antarctic Intermediate Water
AAZ	Antarctic Zone
ACC	Antarctic Circumpolar Current
AD	Antarctic Divergence
AIS	Amery Ice Shelf
ANDRILL	Antarctic Geological Drilling
AR4	Assessment Report 4
ASC	Antarctic Slope Current
BB	Burton Basin
CCD	Calcite Compensation Depth
CDW	Circumpolar Deep Water
CoC	Coastal Current
DWBC	Deep Western Boundary Current
EAIS	East Antarctic Ice Sheet
FM	Fisher Massif
GTHC	Global Thermohaline Circulation
GSD	Grain-Size Distribution
HSSW	Hypersaline Shelf Water
IODP	Integrated Ocean Drilling Program
IPCC	Intergovernmental Panel on Climate Change
IRD	Ice-Rafted Debris; Ice-Rafted Detritus
ISW	Ice Shelf Water
LAIS	Lambert Glacier-Amery Ice Shelf
LD	Lambert Deep
ODP	Ocean Drilling Program
PCM	Prince Charles Mountains
PF	Polar Front
PFZ	Polar Front Zone
SACCF	Southern Antarctic Circumpolar Current
SAF	Subantarctic Front
SAZ	Subantarctic Zone
SB	Southern Boundary of the Antarctic Circumpolar Current
SLE	sea-level equivalent
WAIS	West Antarctic Ice Sheet

Abstract

The Antarctic plays an important role in the global climate system. On the one hand, the Antarctic Ice Sheet is the largest freshwater reservoir on Earth. On the other hand, a major proportion of the global bottom-water formation takes place in Antarctic shelf regions, forcing the global thermohaline circulation.

Previous research mainly focused on the long-term development of the West- and East Antarctic Ice Sheets and on the short-term variability of the West Antarctic Ice Sheet. Investigations regarding the variability of the East Antarctic Ice Sheet (EAIS) on Milankovitch timescales were mostly done in the Weddell Sea and South Atlantic sector of the Southern Ocean. In contrast, comparatively little palaeoenvironmental studies were conducted on sediment records from the Indian sector of the Southern Ocean.

The main goal of this dissertation is to provide new insights into the dynamics and stability of the EAIS during the Quaternary. Additionally, variations in the activity of bottom-water formation and their causes are investigated. The dissertation is a German contribution to the International Polar Year 2007/ 2008 and was funded by the 'Deutsche Forschungsgesellschaft' (DFG) within the scope of priority program 1158 'Antarctic research with comparative studies in Arctic ice regions'.

During RV Polarstern expedition ANT-XXIII/9, glaciomarine sediments were recovered from the Prydz Bay-Kerguelen region. Prydz Bay is a key region for the study of East EAIS dynamics, as 16% of the EAIS are drained through the Lambert Glacier into the bay. Thereby, the glacier transports sediment into Prydz Bay which is then further distributed by calving icebergs or by current transport. The scientific approach of this dissertation is the reconstruction of past glaciomarine environments to infer on the response of the Lambert Glacier-Amery Ice Shelf system to climate shifts during the Quaternary. To characterize the depositional setting, sedimentological methods are used and statistical analyses are applied. Mineralogical and (bio)geochemical methods provide a means to reconstruct sediment provenances and to provide evidence on changes in the primary production in the surface water column. Age-depth models were constructed based on palaeomagnetic and palaeointensity measurements, diatom stratigraphy and radiocarbon dating.

Sea-bed surface sediments in the investigation area show distinct variations in terms of their clay minerals and heavy-mineral assemblages. Considerable differences in the mineralogical composition of surface sediments are determined on the continental shelf. Clay minerals as well as heavy minerals provide useful parameters to differentiate between sediments which originated from erosion of crystalline rocks and sediments originating from Permo-Triassic deposits. Consequently, mineralogical parameters can be used to reconstruct the provenance of current-transported and ice-rafted material.

The investigated sediment cores cover the time intervals of the last 1.4 Ma (continental slope) and the last 12.8 cal. ka BP (MacRobertson shelf). The sediment deposits were mainly influenced by glacial and oceanographic processes and further by biological activity (continental shelf), meltwater input and possibly gravitational transport.

Sediments from the continental slope document two major deglacial events: the first deglaciation is associated with the mid-Pleistocene warming recognized around the Antarctic. In Prydz Bay, the Lambert Glacier-Amery Ice Shelf retreated far to the south and high biogenic productivity commenced or biogenic remains were better preserved due to increased sedimentation rates. Thereafter, stable glacial conditions continued until 400 - 500 ka BP. Calving of icebergs was restricted to the western part of the Lambert Glacier. The deeper bathymetry in this area allows for floating ice shelf even during times of decreased sea-level. Between 400 - 500 ka BP and the last interglacial (marine isotope stage 5) the glacier was more dynamic. During or shortly after the last interglacial the LAIS retreated again due to sea-level rise of 6 - 9 m. Both deglacial events correlate with a reduction in the thickness of ice masses in the Prince Charles Mountains. It indicates that a disintegration of the Amery Ice Shelf possibly led to increased drainage of ice masses from the Prydz Bay hinterland.

A new end-member modelling algorithm was successfully applied on sediments from the MacRobertson shelf used to unmix the sand grain size fractions sorted by current activity and ice transport, respectively. Ice retreat on MacRobertson Shelf commenced 12.8 cal. ka BP and ended around 5.5 cal. ka BP. During the Holocene, strong fluctuations of the bottom-water activity were observed, probably related to variations of sea-ice formation in the Cape Darnley polynya. Increased activity of bottom-water flow was reconstructed at transitions from warm to cool conditions, whereas bottom-water activity receded during the mid-Holocene climate optimum.

It can be concluded that the Lambert Glacier-Amery Ice Shelf system was relatively stable in terms of climate variations during the Quaternary. In contrast, bottom-water formation due to polynya activity was very sensitive to changes in atmospheric forcing and should gain more attention in future research.

Kurzfassung

Die Antarktis spielt im globalen Umweltsystem eine tragende Rolle. Mit ihrem mächtigen Eispanzer ist sie nicht nur der größte Süßwasserspeicher auf der Erde, in ihren Schelfregionen wird auch ein Großteil der globalen Bodenwassermassen gebildet, welche die globale thermohaline Zirkulation antreiben.

Vorangegangene Forschungshaben konzentrierten sich auf die langfristige Entwicklung von West- und Ostantarktischem Eisschild, bzw. auf die kurzfristige Dynamik der Westantarktis. Untersuchungen zur kurzfristigen Dynamik des Ostantarktischen Eisschildes konzentrierten sich auf den Atlantischen Sektor des Südozeans und das Weddellmeer. Im indischen Sektor des Südozeans dagegen war die Forschungsaktivität bisher vergleichsweise gering.

Hauptziel dieser Arbeit, welche einen deutschen Beitrag zum Internationalen Polarjahr 2007/ 2008 liefert und im Rahmen des DFG Schwerpunktprogramms 1158 "Antarktisforschung mit vergleichenden Untersuchungen in arktischen Eisgebieten" finanziert wurde, war es, neue Erkenntnisse hinsichtlich der Stabilität des Ostantarktischen Eisschildes während des Quartärs zu liefern. Weiterhin sollten Aussagen über Variationen in der Bildung von Antarktischem Bodenwasser und deren Ursachen getroffen werden.

Dazu wurde im Rahmen der ‚Polarstern' Expedition ANT-XXIII/9 eine Beprobung glaziomariner Sedimente zwischen Pryzd Bucht und Kerguelen Plateau durchgeführt. Diese Region eignet sich zur Untersuchung der Ostantarktischen Eisdynamik besonders gut, da hier der weltweit größte Gletscher, der Lambert Gletscher, etwa 16% des Ostantarktischen Eispanzers drainiert. Er transportiert dabei Sediment nach Norden, das schließlich die Prydz Bucht erreicht und durch direkten Transport über kalbende Eisberge oder durch Umlagerung und Verteilung mithilfe von Meeresströmungen weiter verfrachtet wird. Der wissenschaftliche Ansatz dieser Arbeit besteht darin, über die Verteilung dieser Sedimente in Raum und Zeit, d.h. über Variationen des glaziomarinen Paläoregimes, die Reaktion des Lambert Gletschers und des vorgelagerten Amery Schelfeises auf Klimaschwankungen während des Quartärs zu rekonstruieren. Dabei werden sowohl sedimentologische Methoden unter Einbeziehung neuer statistischer Möglichkeiten angewandt, um Sedimentationsprozesse zu charakterisieren, als auch mineralogische und (bio)geochemische Parameter verwendet, um Aussagen über die Herkunft der Sedimente und Änderungen in der Produktivität im Oberflächenwasser treffen zu können. Die Altersbestimmung der Sedimentkerne erfolgte mittels Paläomagnetik, Paläointensitäten, Biostratigraphie und Radiokarbondatierungen.

Die Oberflächensedimente im Untersuchungsgebiet zeigen deutliche Unterschiede sowohl hinsichtlich ihrer Tonmineral- als auch Schwermineralzusammensetzung. Beide mineralogischen Parameter zeigen die größten Differerenzen auf dem Schelf. Dort lassen

sich deutlich Sedimente der Prydz Bucht, die vorwiegend von Kristallingestein abstammen, von Sedimenten des MacRobertson Shelfes, die aus permotriassischen Ablagerungen hervor gehen, differenzieren. Sie stellen daher ein gutes Hilfsmittel dar, um sowohl die Herkunft von eis- als auch strömungstransportiertem Material zu rekonstruieren.

Die untersuchten Sedimentkerne decken den Zeitraum der letzten 1,4 Millionen Jahre (Kontinentalhang) bzw. der letzten 12,8 tausend kal. Jahre v. H. ab (MacRobertson Schelf). Die abgelagerten Sedimente wurden im Wesentlichen durch glaziale und ozeanographische Einflüsse geprägt, aber auch durch Bioproduktion (Schelf) bzw. durch Schmelzwassereinträge und möglicherweise gravitative Prozesse (Kontinentalhang).

In den Sedimenten des Kontinentalhangs sind zwei starke Enteisungsereignisse überliefert: Das erste Ereignis steht mit dem mittelpleistozänen Klimaoptimum in Verbindung, das auch in anderen antarktischen Regionen nachgewiesen wurde. Es führte in der Prydz Bucht zu einem weitreichenden Rückzug des Lambert Gletscher-Amery Schelfeises (LAIS) und gleichzeitig zu einer hohen Primärproduktion bzw. einer verbesserten Überlieferung der biogenen Komponenten. Danach herrschten bis etwa 400 - 500 tausend Jahre v. H. stabile glaziale Bedingungen. Kalbung von Eisbergen war wahrscheinlich auf den westlichen Teil des Lambert Gletschers begrenzt, wo eine tiefere Bathymetrie auch bei niedrigerem globalen Meeresspiegel noch Aufschwimmen des Gletschereises erlaubt. Zwischen 400 - 500 tausend Jahren v. H. und vermutlich dem letzten Interglazial wurde der Gletscher schließlich wieder dynamischer, um mit oder kurz nach dem letzten Interglazial (Meeresspiegel etwa 6 - 9 m höher) eine weitere Phase deutlichen Rückzuges zu durchlaufen. Beide Ereignisse lassen sich mit Phasen der Eisreduktion in den Prinz Charles Bergen korrelieren, d.h. der Rückzug des Lambert Gletschers hatte möglicherweise ein erhöhtes Nachfließen von Eismassen aus dem Hinterland zur Folge.

An den Sedimenten des Schelfkernes wurde ein neu entwickeltes Verfahren der Endmember-Modellierung erfolgreich getestet. Dabei konnte der strömungstransportierte Anteil des Sandes vom eistransportierten Anteil getrennt werden. Der Eisrückzug auf dem MacRobertson Schelf begann etwa 12,8 tausend kal. Jahre v. H. und war gegen 5,5 tausend kal. Jahre v. H. abgeschlossen. Während des Holozäns kam es zu starken Schwankungen in der Bodenwasseraktivität, die höchst wahrscheinlich mit der Neubildungsrate von Meereis in der Kap Darnley Polynia in Zusammenhang stehen. Besonders auffallend war eine erhöhte Bodenwasseraktivität am Übergang von Warm- zu Kaltphasen bzw. ihr extremer Rückgang während des Mittel-Holozänen Klimaoptimums.

Insgesamt zeigen die Ergebnisse der Arbeit, dass sich das LAIS während des Quartärs relativ stabil gegenüber Klimaveränderungen verhalten hat. Die Bodenwasserproduktion in Polynien dagegen reagierte sehr empfindlich auf relative geringe atmosphärische Veränderungen und bedarf in Zukunft verstärkter Aufmerksamkeit.

1. Introduction

During Earth`s geological history, long-term changes in global climate were controlled by several factors including e.g. orbital forcing, tectonic activity, configuration of continents and the response of the ecosystem to these external and internal influences. In this context, the Earth experienced strong glaciations during the Early Proterozoic, Late Proterozoic, Ordovician, and the Permo-Carboniferous with associated variations in global sea level.

During the late Cenozoic, most continents had reached their modern position and tectonic activity receded. The Antarctic continent became thermally isolated and continental ice sheets developed (Barker and Thomas, 2004). Eventually, the closure of the Isthmus of Panama around 3.0 - 2.5 Ma led to a strengthening of particularly the North Atlantic Thermohaline Circulation with intensified supply of moisture to northern high latitudes and in turn to built up of the Northern Hemisphere Glaciation (Bartoli et al., 2005).

Since then, the Global Thermohaline Circulation (GTHC) constitutes a key factor in controlling global climate by exchanging heat and salt between low and high latitudes (Schmitz, 1995; Rahmstorf, 2002). In a simplified way, near-surface waters flow towards the main areas of bottom-water formation – in the Weddell Sea, the Ross Sea and the Northern Atlantic – and recirculate at depth. The Antarctic shelf regions, holding vast floating ice shelves, play an essential role in terms of bottom-water formation as they contribute to it at a rate of 21 ± 6 Sv in contrast to the Northern Atlantic with about 15 ± 2 Sv (Rahmstorf, 2002). Unfortunately, only little is known about the vulnerability of the whole GTHC system and its variability during history.

In the recent past, the dynamics of Antarctic ice sheets, accompanied by the behaviour of the Greenland inland ice masses in response to global change, gained great popularity and thoughtfulness, especially during the fourth International Polar Year (IPY) in 2007/2008 and by publication of the fourth Intergovernmental Panel on Climate Change Assessment Report (IPCC AR4). This is not surprising, because the Antarctic ice sheet is the largest body of fresh water on our planet, amounting to 70% of the total. The complete disappearance of the East Antarctic Ice Sheet (EAIS) would result in 55 m of sea-level rise (Huybrechts et al., 2000). In contrast, the storage of the Greenland and West Antarctic ice sheets is calculated to a sea-level equivalent of ‘only’ about 7 m each. According to the IPCC AR4 (Bindoff et al., 2007), since 1961 global average sea level has risen at an average rate of 1.8 (1.3 to 2.3) mm/yr and since 1993 at 3.1 (2.4 to 3.8) mm/yr, with contributions from thermal expansion, melting glaciers and ice caps, and polar ice sheets.

As a consequence, it is inevitable to draw conclusions on the stability of global ice masses, ice shelves and ocean circulation in terms of global change to better predict future scenarios of sea-level rise and climate change. Following the principle of actualism, the main goal of this

thesis is to provide clues on the response of the EAIS and the East Antarctic margin to the significant fluctuations in global climate during the Quaternary, when time intervals with global mean temperatures close to those predicted for the 21st century occurred. For this purpose, sediment cores were retrieved from the Prydz Bay-Kerguelen area during RV 'Polarstern' expedition ANT-XXIII/9 in early 2007. In this region, the world's largest fast flowing glacier – the Lambert Glacier – drains a great proportion of the EAIS and is therefore an important glaciological feature to be studied.

The PhD project has been part of the German IPY activity and was funded by the Deutsche Forschungsgemeinschaft (DFG) priority program SPP 1158 "Antarctic research with comparative studies in Arctic ice regions" through grant DI 655/3-1.

1.1 Regional setting

1.1.1 Topography

The Prydz Bay-Kerguelen region (Fig. 1.1A) is situated between 50°S and 69°S latitude and 65°E and 85°E longitude. Prydz Bay represents the third largest shelf sea of the Antarctic margin and is the prolongation of the Lambert Graben (Fig. 1.1B) extending about 700 km inland. The shelf region is covered by seasonal sea ice and is bounded to the east by Princess Elizabeth Land and to the west by MacRobertson Land (Fig. 1.1A). In the hinterland, along the eastern side of the Lambert Graben, some bedrock exposures with a total length of about 400 km rise up to 3200 m a.s.l. and constitute the Prince Charles Mountains (Fig. 1.1B). Further mountain outcrops and nunataks are grouped in the Grove Mountains, Framnes Mountains and in the Fisher Massiv (Fig. 1.1B).

The Prydz Bay continental shelf is 70 km to 250 km wide. Water depths in general increase from 200 m near the shelf edge to 1600 m farther inland due to over-deepening through former advances of the Lambert Glacier (Federov et al., 1982; Harris et al., 1997). MacRobertson shelf is situated on the East Antarctic margin north of MacRobertson Land and represents the continuation of the Prydz Bay-Amery Shelf about 400 km to the west (Fig. 1.1). It shows a typical width of about 90 km and an average depth of 350 m at the shelf break. Glacial incisions and rift basins have water depths of up to 1000 m (locally), Burton Basin has a maximum water depth of about 550 m.

Along Princess Elizabeth Coast, major groups of peninsulas and small islands form the Larsemann Hills (69°23'S, 76°10'E), Rauer Islands (68°50'S, 77°55'E) and Vestfold Hills (68°35'S, 78°10'E**,** Fig. 1.1B), covered with small lakes and ponds. North of the continental slope the Kerguelen Plateau separates the Weddell-Enderby abyssal plain from the Australian Antarctic Basin, both having maximum water depths between 4500 m and 5200

m. The Kerguelen Plateau is a submarine barrier separated from the Antarctic continent by the Princess Elizabeth Trough and rises up to 4 km above the surrounding deep sea regions. It represents one of the earth`s large igneous provinces (Frey et al., 2000) with volcanoes exceeding sea level at Heard Island and Kerguelen Island.

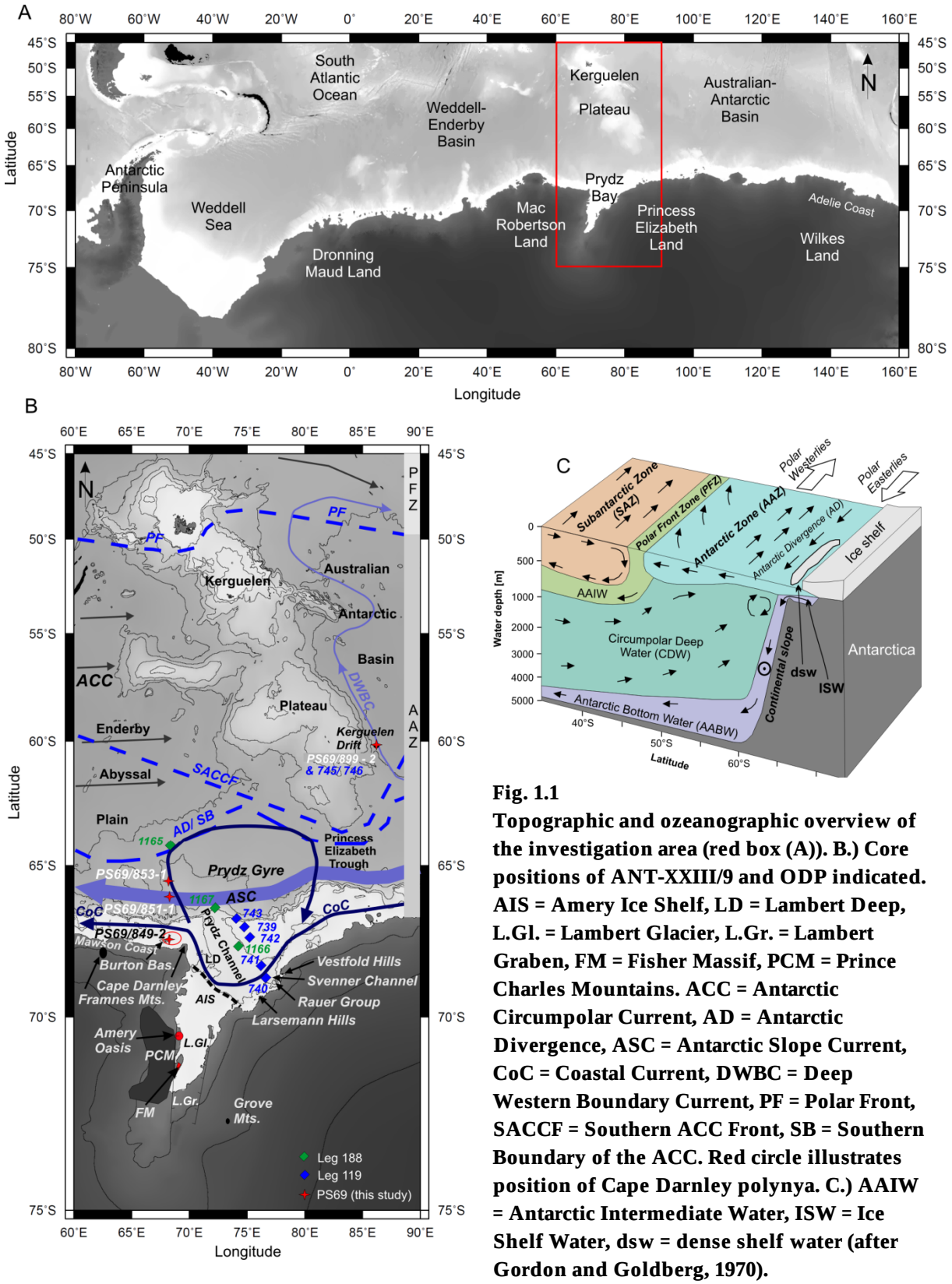

Fig. 1.1
Topographic and ozeanographic overview of the investigation area (red box (A)). B.) Core positions of ANT-XXIII/9 and ODP indicated. AIS = Amery Ice Shelf, LD = Lambert Deep, L.Gl. = Lambert Glacier, L.Gr. = Lambert Graben, FM = Fisher Massif, PCM = Prince Charles Mountains. ACC = Antarctic Circumpolar Current, AD = Antarctic Divergence, ASC = Antarctic Slope Current, CoC = Coastal Current, DWBC = Deep Western Boundary Current, PF = Polar Front, SACCF = Southern ACC Front, SB = Southern Boundary of the ACC. Red circle illustrates position of Cape Darnley polynya. C.) AAIW = Antarctic Intermediate Water, ISW = Ice Shelf Water, dsw = dense shelf water (after Gordon and Goldberg, 1970).

1.1.2 Geology

East Antarctica once formed a central part of the Gondwana supercontinent (Tingey, 1991). Most of the bedrock is composed of Archean, Proterozoic and Cambrian metamorphic rocks and intrusives (Tingey, 1991). Prydz Bay and Lambert Graben (Fig. 1.1B) are incised in the East Antarctic shield and represent the failed arm of a triple junction associated with breakup of India and Antarctica/Australia during early Cretaceous times, at approximately 130 Ma.

The largest outcrop of bedrock is located on the western flank of the Lambert Graben (Fig. 1.1B). There, the Prince Charles Mountains (PCM) form the best-exposed cross section through the East Antarctic shield comprising metamorphic rocks grading from granulite-facies gneisses with intrusions of charnockite plutons, pegmatite veins and alkaline dykes in the northern province of the bedrock outcrop to amphibolite-facies and greenschist-facies gneisses in the southern province (Tingey, 1991). Other bedrock exposures can be found along the Princess Elizabeth Coast showing predominantly mafic rocks in the Vestfold Hills and Rauer Group (Tingey, 1991; Thost et al., 1998).

During the Permian and Mesozoic, up to 5 km thick continental deposits comprising sandstones, shales, coal and conglomerates of alluvial origin accumulated in the Lambert Graben (Cooper et al., 1991b; Tingey, 1991). The deposits also constitute the Amery Group best studied in the Prince Charles Mountains around Beaver Lake (Tingey, 1991; Webb and Fielding, 1993). Since the Palaeocene these sediments have been re-deposited several times (Whitehead et al., 2006) and formed the sediment sequences of the Pagodroma Group (Hambrey and McKelvey, 2000a, 2000b) also exposed in the Prince Charles Mountains and in the Fisher Massiv.

1.1.3 Glaciology

The most prominent glaciological feature in the study area is the Lambert Glacier (Fig. 1.1B), the world`s largest outlet glacier being approximately 400 km in length, 100 km wide and 2500 m deep. It drains about 16% of the East Antarctic Ice Sheet (EAIS) (Fricker et al., 2000) and flows northward to the Amery Ice Shelf. Ice thickness at the seaward boundary of the Amery Ice Shelf is about 300 m. The Glacier system is fed by four major tributaries (Charybdis Glacier and Nemesis Glacier, Fisher Glacier, Mellor Glacier) and is predominantly responsible for the supply of terrigenous sediments to Prydz Bay and adjacent areas. The whole Lambert Glacier-Amery Ice Shelf (LAIS) grounded-ice region has an area of $1.34*10^6$ km^2 (Wen et al., 2008). Most of the Lambert Glacier has velocities between 400 - 800 m/yr. As the glacier extends across Amery Ice Shelf, velocities increase to 1000 -

1200 m/yr (http://earthobservatory.nasa.gov/IOTD/view.php?id=1199) because the ice sheet spreads out and thins.

In Prydz Bay, sea-ice formation starts during mid-February, and maximum ice thickness occurres in late November. During austral winter, annual sea ice extends north of 60°S, whereas multi-year sea ice is mainly restricted to coastal areas. Snow cover remains thin the whole time, and blowing snow causes frequent redistribution of the snow (Lei et al., 2010).

1.1.4 Oceanography

The surface waters in the Prydz Bay-Kerguelen region are highly variable throughout the year and linked to the local ice conditions. Surface circulation (Fig. 1.1B) is related to the prevailing wind systems. Along the Antarctic continent, the polar easterlies force the Antarctic Coastal Current (CoC, Fig. 1.1B). Within the bay, circulation is dominated by a cyclonic gyre (Fig. 1.1B) with cold-water inflow from the east, and outflow along the western side of the embayment (Smith et al., 1984). Prydz Bay gyre is a summer feature, with both the strength and direction of the gyre is controlled by the production of dense water from local coastal polynyas (Galton-Fenzi et al., 2010). There is evidence for Antarctic Bottom Water (AABW) formation due to polynya activity in Prydz Bay and on the MacRobertson Shelf (Cape Darnley polynya, Fig. 1.1B; Tamura et al., 2008; Yabuki et al., 2008; Meijers et al., 2010). Surface circulation in the study area also controls the velocity and direction of sea-ice motion and iceberg drift (Schmitt et al., 2004).

The deepwater movements on the continental slope and in the open ocean are attributed to three large-scale ocean systems: 1.) the Antarctic Slope (or Polar) Current (ASC, Bindoff et al., 2000), which is a boundary current enforced by prevailing winds and by input of dense waters from coastal areas; at 100°E, a branch of the ASC divertes to the north and flows along the eastern flank of the Kerguelen Plateau as Deep Western Boundary Current (DWBC); 2.) the Antarctic Divergence (AD) at approximately 64°N producing cyclonic gyres over the slope and inner rise; and the 3.) eastward-flowing strong band of the Antarctic Circumpolar Current (ACC) driven by strong westerly winds (Fig. 1.1B). It extends from the sea surface to depths of 2000 - 4000 m and can be as wide as 2000 km. Most of the deep and bottom-water masses of the ACC consist of Circumpolar Deep Water (CDW) representing a mixture of water masses from the Atlantic, the Antarctic, the Indian and Pacific Oceans. The ACC reveals a frontal system with different zones separated by oceanic fronts identified as narrow regions of sharp horizontal density gradients and by increasing nutrients levels. From the north to the south these are: the Subantarctic Zone (SAZ), separated from the Polar Frontal Zone (PFZ) by the Subantarctic Front (SAF); the Antarctic Zone (AAZ) is bounded to the

north by the Polar Front (PF, Fig. 1.1B; e.g. Orsi et al., 1995). The interaction of downslope density (e.g. turbidity) currents and along-slope (contour) currents, e.g. the ASC, control sedimentation on the continental slope (Kuvaas and Leitchenkov, 1992).

1.2 Scientific background

1.2.1 Long-term dynamics of the East and West Antarctic Ice Sheets since the onset of Antarctic glaciation

Intense marine geological investigations on the Antarctic continental margin and in the Southern Ocean have greatly increased our knowledge of the palaeoenvironmental history of Antarctica. Activities of the Ocean Drilling Program (ODP) aimed at the onset and evolution of Antarctic glaciation and on discrimination between the development of the West Antarctic and East Antarctic ice sheets during the Cenozoic (e.g. Barker and Thomas, 2004; Barker et al., 2007; Peters et al., 2010). Results from onshore investigations (Whitehead et al., 2006) and ocean drilling at the Antarctic continental margin in Prydz Bay (Barron et al., 1991; Cooper and O'Brien, 2004), the Ross Sea (Barrett, Sarti and Wise, 2000) and Wilkes Land margin (IODP Leg 318; Expedition 318 Scientists, 2010.) indicate two general states of the Antarctic ice sheets: 1.) an early phase with strong cyclic waxing and waning due to less stable ice cover lasting from about 34 Ma to 14 Ma (Pälike et al., 2006; Zachos et al., 2008) and 2.) a later phase with permanent and more stable features such as indicated by deep-sea isotope records (e.g. Flower and Kennett, 1994).

During the Pliocene and Pleistocene, however, the comparatively stable ice sheets may have experienced considerable fluctuations in size, possibly by as much as 25 m of sea-level equivalent (SLE; Naish et al., 2009; Pollard and DeConto 2009). These fluctuations were obviously obliquity-paced, as evidenced from the ANDRILL project (ANtarctic geological DRILLing; Naish et al., 2009) and from marine $\delta^{18}O$ records (e.g. Raymo et al., 2006). Taking into account a contribution of 7 m SLE from both the West Antarctic and the Greenland ice sheets it is implied that a substantial volume of the present EAIS must have melted (Raymo et al., 2006). This raises questions regarding the stability of the EAIS in terms of global warming, because in contrast to the less stable (because predominantly grounded below sea level) West Antarctic Ice Sheet (WAIS), the continental EAIS is considered stable and believed to respond only slowly to changes in climate.

1.2.2 Quaternary EAIS dynamics and bottom-water formation at the East Antarctic continental margin

Focussing on the Quaternary, ocean drilling in the Atlantic sector (Weddell Sea, South Atlantic) and Indian sector (Prydz Bay, Wilkes Land) of the Southern Ocean was conducted to answer outstanding questions whether or not the EAIS experienced periods of instability in response to the cyclic variations in global climate such as recorded in Antarctic and Greenland ice cores (e.g. Grootes et al., 1993; Petit et al., 1999; North Greenland Ice Core Project members, 2004; EPICA Community Members, 2006; Steig et al., 2006; Jouzel et al., 2007) and in marine $d^{18}O$ records (Lisiecki and Raymo, 2005). Additionally, the applicability of ice-rafted debris (IRD) as a means to trace periods of ice sheet instability in the open ocean was tested. Insights into the dynamics of ice rafting arose from ODP Site 177-1090 which was drilled north of the northern boundary of the present-day Polar-Front Zone (PFZ; the zone of major iceberg melting and boundary between different sedimentary provinces) being a very sensitive location to record both ice rafting and stable-isotopic-ratio changes. Results obtained from this record may be characteristic for the subantarctic South Atlantic showing IRD input during 1.) glacials and 2.) strong stadials within cool interglacials ends before the peak of each glaciation (Diekmann et al., 2000; Diekmann and Kuhn, 2002; Becquey and Gersonde, 2003a; Diekmann et al., 2003; Teitler et al., 2010). This pattern suggests that the IRD record at this site is strongly depending on sea-surface temperatures. If temperatures are warm, icebergs are melting farther south and only occasional icebergs survive to deliver their debris to the site. Only during cold times, when the PFZ had shifted about 7° north (Becquey and Gersonde, 2002, 2003b) more icebergs survived to reach this distal location. Similar results were found from interpretation of IRD and physical properties of the ODP 177-1094 core (Kanfoush et al., 2002). Apart from temperature effects on iceberg survival, the interpretation of IRD fluxes in terms of Antarctic ice-sheet dynamics in the open ocean is further complicated because of IRD sources from offshore Antarctica, the possible sea-ice transport of volcanic ashes and the impact of episodic volcanic eruptions that are not coupled with climate variability (Diekmann et al., 2003).

To reduce the effect of sea ice and get a clearer picture of ice advance and retreat, in combination with dynamics of bottom-water activity, the investigation of sediment cores from the continental margin is necessary, too. In the Weddell Sea, Grobe and Mackensen (1992) provided a first sedimentation model to synthesize a general relationship between sediment facies and palaeoclimatic, palaeoceanographic and palaeoglacial conditions during the last four glacial cycles. It is summarized as follows: during interglacials, rising sea level causes the Antarctic ice shelves to float. Accompanied by intrusion of warmer CDW waters and reduced sea-ice coverage, the ice shelves destabilize and are reduced in size by intense

calving processes. IRD is released proximal to the calving line. Additionally, the interglacial environment is characterized by bottom-water formation due to super-cooling of surface waters underneath the floating ice shelves in combination with release of dense brines due to sea-ice formation in coastal polynyas. High biological primary production enhances the deposition of siliceous and subordinate calcareous microfossils. High CO_2 uptake in the water column raises the CCD to shallower depths. During glacial conditions, grounding lines of Antarctic ice shelves prograde to the north and in certain circumstances reach the shelf edge, bulldozing sediment material over the shelf break and initiating turbitidy currents. Whereas the latter can be recognized predominantly on the upper continental slope, on the lower slope, contour current deposits remain undestroyed due to a lack of bioturbation. Biological primary production is low because of multi-year sea-ice coverage, CCD is deeper. Icebergs show higher survivability and IRD is released in the distal to the calving line.

Similar to this sedimentation model, Melles (1991) reconstructed the late Quaternary palaeoenvironment in the Weddell Sea and gave detailed insights into the regional palaeoceanography during that time. During the last century, further advances were made in the interpretation of sediment compositions in terms of palaeoenvironmental implications, concerning contourites (e.g. Lucchi and Rebesco, 2007), turbidites (e.g. Close et al., 2010) and sediments deposited by meltwater plumes (e.g. Pudsey, 2000). Recent studies in the South Atlantic sector e.g. aim on short-term variations in the stability of ice masses on the Antarctic Peninsula since the last glacial (e.g. Domack et al., 2006; Yoon et al., 2007; Bentley et al., 2009) and during the Holocene (e.g. Heroy et al., 2008; Michalchuk et al., 2010). According to the authors, ice shelves decoupled from their bed between 9 and 11 cal. ka BP, major release of ice-transported material receded around 6 cal. ka BP. They further report two distinct intervals of warming, the early-Holocene warming and mid-Holocene hypsithermal with increased biological productivity. The warm periods might be explained by relatively abrupt shifts in the position of the southern westerlies, superimposed on slower solar insolation changes. A late Holocene shift to neoglacial conditions is widely recognized since ~2.5 cal. ka BP.

Abrupt instabilities of the Antarctic Ice Sheet during the last glacial analogous to the Heinrich events on the Northern Hemisphere were proposed by Kanfoush et al. (2000) from IRD events detected in sediment cores from the South Atlantic. Reevaluation of the data, however, turned out that most of the IRD is of volcanic origin and most mineral grains previously interpreted as to be quartz are plagioclase (Nielsen and Hodell, 2007). The authors conclude that sea ice was the dominant ice rafting agent in the PFZ of the Southern Ocean during the last glacial period whereas IRD variability during the Holocene reflects Antarctic ice sheet dynamics.

The above mentioned findings from the Weddell Sea realm coincide with results of multi-proxy studies performed on sediment cores taken along Wilkes Land and Adelie Coast. Sediment cores from the Wilkes rise consist of three main components: gravity flow deposits (i.e., debris flows and turbidites), contourites, and hemipelagic deposits (e.g. Busetti et al., 2003). A detailed picture of the Pleistocene evolution of the EAIS which is grounded below sea level on Wilkes Land, however, is to be expected from recently conducted ocean drilling IODP Leg 318 (Expedition scientists 318, 2010). More information is available regarding the Holocene environmental history in the region, especially in terms of sea-ice variations and polynya activity. The Mertz polynya and coastal polynyas west of the Mertz Glacier tongue are the source of AABW (e.g. Williams and Bindoff, 2003). Wilkes Land is thus an ideal location to study fluctuations in AABW production.

Interconnections evident between glacier, sea ice and ocean climatic components point out the important impact of sea ice as a link between glacier and deep water dynamics, and its complex role because of its strong sensitivity to seasonality (Denis et al., 2009a). Studies on diatom communities were conducted to reconstruct palaeoproductivity and sea-ice distribution (Crosta et al., 2008; Denis et al., 2009a, 2009b). It is concluded that rapid climate changes at high southern latitudes may be explained by a combination of external (solar) and internal (thermohaline circulation) forcings (Crosta et al., 2007). Diatom records and model output support each other, thereby implying a strong local insolation and local feedbacks control on Holocene climate evolution in the high-latitude Southern Hemisphere (Crosta et al., 2008).

However, comparisons of results obtained from Adelie Coast with other peri-Antarctic records and model simulations from high southern latitudes may suggest that interpretations on glacier-sea ice-ocean interactions and their Holocene evolutions reflect a more global Antarctic Holocene pattern (Denis et al., 2010).

1.2.3 Glacial palaeoenvironments in the Prydz Bay region – State of the art

Conclusions on the Quaternary evolution of the LAIS system were mainly drawn from long sediment cores recovered from the continental shelf and slope during two ocean drilling campaigns (ODP Legs 119 and 188; Barron et al., 1991; Cooper and O'Brien, 2004). Leg 119 (Fig. 1.1B) has provided information concerning the development of a continental margin under the prolonged influence of a major ice sheet. There is no doubt, that full-scale glaciation was underway by early Oligocene time, but late Pliocene-Pleistocene events are poorly constrained temporally on the continental shelf (Hambrey et al., 1991). According to the authors, they were dominated by successive advances of ice across the shelf and

continued build-up of flat lying sequences, accompanied by resumed progradation of the shelf margin under the influence of the ice sheet. From the structure of the glacier system and sediments recovered in Prydz Bay, the hypothesis of possible surging of the Lambert Glacier could be negotiated (Hambrey et al., 1991). However, ice-sheet development remained obscure by investigation of sediment sequences on the continental shelf, because of the poor recovery, major hiatuses in the record, and the problem of dating. Results from ODP Leg 188 Sites 745 and 746 indicated that ice rafting was less intensive during the late Pliocene to Quaternary time period, when ice shelves remained relative stable, compared to the late Miocene and early Pliocene epochs (Ehrmann and Grobe, 1991). To some degree, Sites 745 and 746 document, by their record of ice rafting and clay mineralogy, the Quaternary glacial history showing that most of the glacial debris was trapped on the shelf area, providing evidence for a relatively stable ice shelf (Ehrmann et al., 1991) since 2.0 Ma - 1.5 Ma. Weak maxima in the content of IRD at 2.4 - 1.6 Ma and 1.4 - 1.0 Ma correlate with relatively short-lived and minor rises of sea level.

To better unravel the Pliocene and Pleistocene ice sheet development, research during ODP Leg 188 concentrated on fan and drift deposits on the continental slope (Cooper and O'Brien, 2004; O'Brien et al., 2004). Sedimentation here is mainly controlled by turbidity activity and ocean currents (Kuvaas and Leitchenkov, 1992). Because the bulk of the Prydz Mouth Fan was deposited prior to 780 ka, it was concluded that extreme advances of the LAIS system ceased during the mid-Pleistocene (O'Brien et al., 2004). Possible causes for this change are progressive over-deepening of the inner shelf, a reduction in maximum ice volumes in the interior of the EAIS caused by temperature change, and a change in the interaction of Milankovich cycles and the response time of the ice sheet (Cooper and O'Brien, 2004; O'Brien et al., 2004, 2007; Taylor et al., 2004). During the mid-Pleistocene a major warming event was recognized in the region (e.g. Theissen et al., 2003) in association with extensive calving due to decoupling of the marine terminus from its bed in response to Northern Hemisphere deglaciations and associated sea-level rises (Passchier et al., 2003; Passchier, 2007; Villa et al., 2008). Clay-mineral studies, however, suggested that the EAIS may have behaved as a dynamic glacier for at least the past 5 Ma (Junttila et al., 2005).

More detailed information regarding ice-sheet development is available for the time interval since the last glacial. In Prydz Bay, the Lambert Glacier had not succeeded to the shelf edge since about 30 ka BP (Domack et al., 1998; O'Brien et al., 1999). Whether or not the Larsemann Hills and Vestfold Hills were ice-free during the Last Glacial Maximum remains controversial (Zwartz et al., 1998; Hodgson et al., 2001; Verleyen et al., 2004a). On MacRobertson shelf, grounded ice sheets may have reached the shelf edge but most probably covered the inner and middle shelf (Rathburn et al., 1997; Harris and O'Brien, 1998; Leventer et al., 2006). Ice retreat (deglaciation) in Prydz Bay and adjacent regions started between 13

cal. ka BP and 10 cal. ka BP and was accompanied by deposition of layered or varved biogenic sediments at many coring sites (Rathburn et al., 1997; Domack et al., 1998; Harris and O'Brien, 1998; Sedwick et al., 2001; Verleyen et al., 2004b; Stickley et al., 2005; Verleyen et al., 2005; Leventer et al., 2006; Wagner et al., 2007). In the Framnes Mountains, MacRobertson Land, the elevation of the inland ice sheet decreased in most cases between 13 ka BP and 5.1 ka BP, according to cosmogenic exposure ages from mountain dipsticks (Mackintosh et al., 2007). The timing of deglaciation in the Prydz Bay region suggests it was too late to contribute to meltwater pulse 1A, but early enough to contribute to meltwater pulse 1B (Leventer et al., 2006). During the Holocene, fluctuations in the biogenic primary production interpreted from biogenic opal, diatom concentrations and floral composition indicate shifts in the extent of sea-ice coverage (Rathburn et al., 1997; Harris and O'Brien, 1998; Harris, 2000; Verleyen et al., 2004). Some suggestions regarding Holocene variations in bottom-water flow possibly associated with Cape Darnley polynya were made by Harris and O'Brien (1998) and Harris (2000). In most sediment records from Prydz Bay and MacRobertson shelf, a mid-Holocene climate optimum was recognized showing increased productivities. Hemer and Harris (2003) also suggested that the Amery Ice Shelf retreated during that time. Data on the provenance of icebergs or ocean currents, however, is not available for the time period since the last glacial.

1.3 Objectives of this thesis

The overall aim of this dissertation is to broaden the understanding of past changes in the configuration of glaciological and oceanographic features along the East Antarctic margin. This includes glacier systems and inland ice sheets as well as sea-ice variability in polynya regions.
In particular, this thesis addresses the following questions:

1.) Are clay minerals and heavy minerals suitable indicators in the Prydz Bay-Kerguelen region to trace the provenance of ocean currents and icebergs?

2.) How did the Lambert Glacier-Amery Ice Shelf system respond to the cyclic climate variations during the Quaternary? Some evidences were already given by ODP Leg 188 drilling, but according to experience the disadvantage of the drilling procedure is bad recovery in the upper core meters covering the Quaternary. By investigation of gravity cores it was intended to overcome this problem and draw a more continuous picture of the Quaternary palaeoenvironmental development.

3.) If the glacial system did not remain stable, which conditions favoured ice retreat and advance?

4.) How did sea-ice cover fluctuate during the past and is it possible to draw conclusions on the mechanisms triggering sea-ice variations?

5.) Which factors controlled the formation and current speeds of bottom water in the study area and when did periods of increased/ decreased bottom-water activity occur?

6.) Is the palaeoenvironmental history in the study area comparable to that in other regions at the East Antarctic continental margin? Is the timing of events similar in the different regions? And, consequentially, is it possible to discriminate the impact of local and regional climate signals on the palaeoenvironmental evolution?

1.4 Scientific approach and methods

Modern changes in the Antarctic realm regarding the configuration of glaciological features or oceanographic conditions can be observed for example by means of remote sensing or *in situ* measurements. In contrast, past changes have to be inferred by indirect approaches. These approaches are based on the principle of actualism invented by James Hutton and Charles Lyell in the 18th and 19th century.

To gain integrated insights into the Quaternary evolution of the LAIS system, past glaciomarine environments, each characteristic of a certain glaciologic and oceanographic configuration, were reconstructed from the sedimentological, mineralogical and (bio)geochemical composition of sediments (Fig. 1.2). Studies from earlier works (e.g. the sedimentation model of Grobe and Mackensen, 1992) exemplified in chapter 1.2.2 were taken as a basis. In this regard, the reconstruction of

1.) ocean-current types and activity and
2.) ice-rafting activity

by grain-size analysis and sediment texture constitute the two main pillars. Because especially on the continental shelf it is hard to differentiate between current-transported particles and ice-transported material, end-member modelling was applied on grain-size data obtained from ‘Coulter Laser Particle Sizer’ measurements. Clay-mineral analysis (by use of X-ray diffraction, XRD) was conducted to draw conclusions on the provenance of water masses which also helps to discriminate between contour and turbidity current

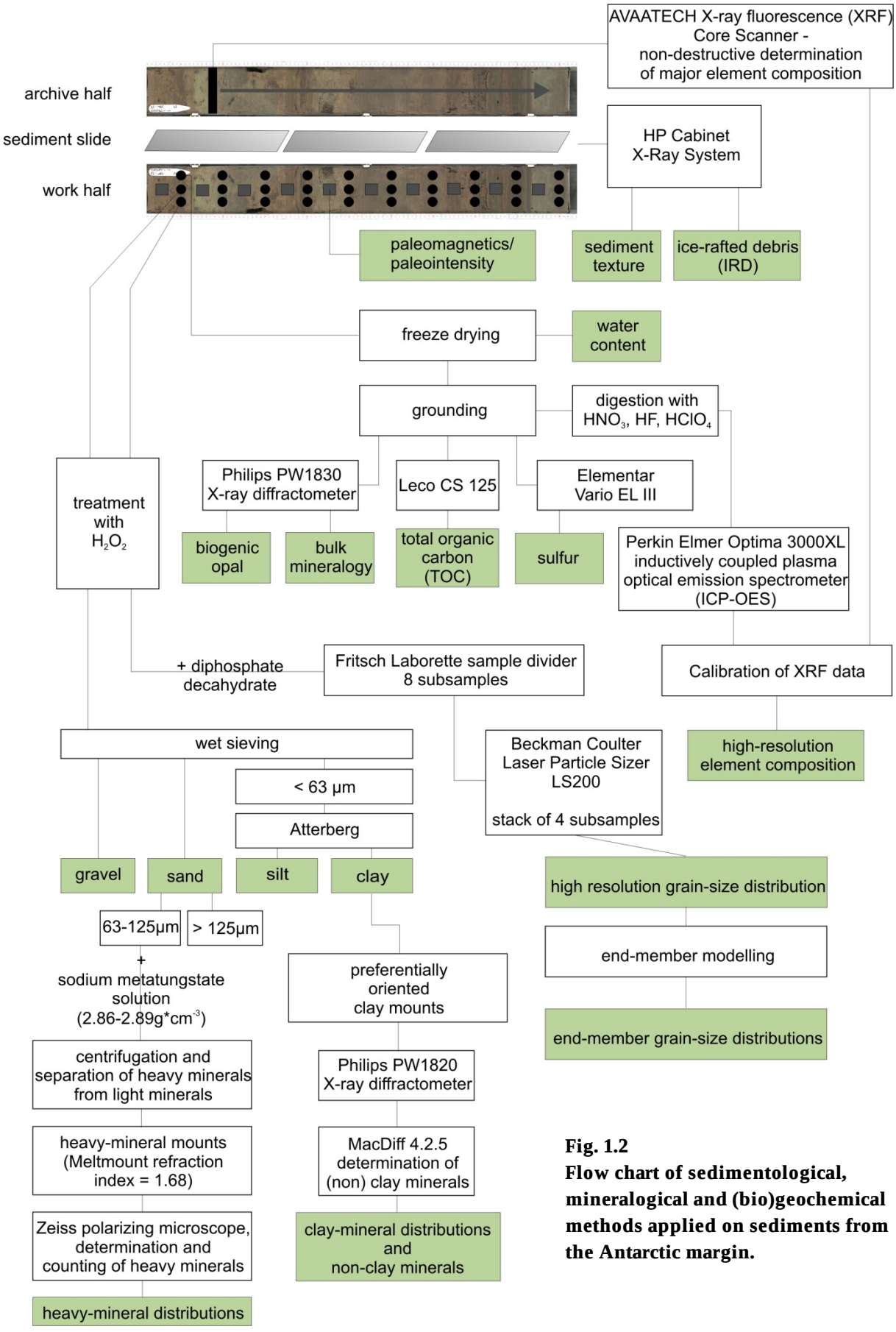

Fig. 1.2
Flow chart of sedimentological, mineralogical and (bio)geochemical methods applied on sediments from the Antarctic margin.

activity. The origin of material transported by icebergs was inferred from heavy-mineral distributions in the fine sand fraction associated with the geology of the Prydz Bay hinterland. The estimation of biological productivity and/or preservation versus terrigenous input by means of biogenic opal, total organic carbon, sulphur and water content, supplemented by element concentrations obtained from inductively coupled plasma optical emission spectrometry (ICP-OES) and X-ray fluorescence analysis (XRF) provided indirect clues on sea-ice coverage in the study area.

The combination of sediment cores recovered from the continental shelf and the continental slope maintained advantages compared to a solely interpretation:

1.) sediment cores from glacial incisions on the continental shelf provide temporal high-resolution records of the environmental evolution since at least the last glacial; the possible occurrence of grounded ice sheets can be better inferred than from continental slope records; the longer ice-sheet history is hard to reconstruct because of glacial erosion of previously deposited sediments due to glacial advances,
2.) sediment cores from the continental slope comprise lower temporal resolutions, but give insights into the longer history of glacial features; they record more regional signals rather than local signals recorded in shelf cores; often, interglacial sediments are winnowed,
3.) in the different environments, different processes leaving an impact on the sediment can be studied so the combined interpretation of cores from the shelf and from the slope helps to draw an integrated picture of the palaeoenvironmental development.

1.5 Overview of the manuscripts

In the main part of this thesis, three first-author manuscripts prepared for publication in international peer-reviewed journals are presented. Two further publications (co-author) are presented in the appendix, used to supplement the methodology of this paper and to supplement assumptions made on bottom-water activity during warm interglacial periods. An overview of all manuscripts is given in Table 1.

Tab. 1 Overview of manuscripts presented within this dissertation

Chapter	Publication/ main goals	Publication status
Chapter 2	Borchers, A., Voigt, I., Kuhn, G., Diekmann, B. Mineralogy of glaciomarine sediments from the Prydz Bay-Kerguelen region: relation to modern depositional environments.	*Antarctic Science* in press

	Main goals: To associate clay-mineral distributions and heavy-mineral distributions of surface sediments with modern oceanographic conditions and hinterland geology. The paper publishes own data and reviews mineralogical studies done so far.	
Chapter 3	Borchers, A., Dietze, E., Kuhn, G., Esper, O., Voigt, I., Hartmann, K., Diekmann, B. Holocene ice dynamics, bottom-water formation and polynya activity recorded in Burton Basin, East Antarctica. Main goals: To give insights into the deglaciation process after the last glacial and short-term fluctuations of bottom-water activity due to Cape Darnley polynya during the Holocene.	*Palaeogeography, Palaeoclimatology, Palaeoecology* in review
Chapter 4	Borchers, A., Frederichs, T., Esper, O., Kuhn, G., Grobe, H., Diekmann, B. Sedimentation on the continental slope off MacRobertson Land reveals major fluctuations of the East Antarctic Ice Sheet during the Pleistocene. Main goals: Inference of the stability of the Lambert Glacier-Amery Ice Shelf system during the Quaternary with a special focus on warmer-than modern times.	*Marine Geology* manuscript status
Appendix A1	Dietze, A., Hartmann, K., Diekmann , B., IJmker, J., Lehmkuhl, F., Opitz, S., Stauch, G., Wünnemann, B., Borchers, A. An end-member algorithm for deciphering modern detrital processes from lake sediments of Lake Donggi Cona, NE Tibetan Plateau, China. Main goal: To present an algorithm for end-member modelling of compositional data used to provide genetically meaningful, quantitative grain size end-members.	*Sedimentary Geology* in review
Appendix A2	Voigt, I., Borchers, A., Esper, O., Frederichs, T., Gersonde, R., Kuhn, G., Kretschmer, S., Mollenhauer, G., Diekmann, B. Antarctic bottom-water dynamics in the Indian sector of the Antarctic Ocean over the last 140 000 years. Main goal: Inference of bottom-water activity due to Mertz polynya dynamics during the last glacial cycle.	*Extended abstract Deep-water Circulation: Processes & Products International Congress, Baiona, Pontevedra, Spain, 16. - 18. 06. 2010*

1.6 The author's contribution to the individual manuscripts

Andreas Borchers entirely wrote all manuscripts presented in chapters 2-4, reviewed the relevant literature and prepared all figures and tables, except for figure 5 in manuscript I which was adopted and modified from the diploma thesis of Ines Voigt. Andreas Borchers built the general framework of all analytics, did the major part of laboratory work and interpreted the data with support from PD Dr. Diekmann.

Bernhard Diekmann and Gerhard Kuhn are the main supervisors of this thesis. They further did critical reviews and are therefore co-authors of all manuscripts.

Ines Voigt critically reviewed manuscript II and discussed the interpretation.

Gerhard Kuhn measured TOC, sulphur and water content of the sediment core presented in manuscript II. He further accomplished all XRD measurements of samples prepared by Andreas Borchers.

Elisabeth Dietze and Kai Hartmann were the main partners in establishing an end-member modelling algorithm which was applied to grain-size data presented in manuscript II. Elisabeth Dietze critically reviewed the second manuscript.

Thomas Frederichs conducted palaeomagnetic measurements at Bremen University, helped to establish an age model and critically reviewed manuscript III.

Oliver Esper supported the development of an age model for the sediment core presented in manuscript III by means of diatom stratigraphy. He further accounted for ideas regarding polynya dynamics discussed in manuscript II.

Hannes Grobe added comments regarding the interpretation of IRD and sediment textures.

Andreas Borchers was the main partner in establishing, writing and testing the algorithm of the Matlab script presented in manuscript IV (appendix A1) which he discussed and reviewed. He further supervised and discussed the studies of Ines Voigt presented in an extended abstract (appendix A2).

2. Mineralogy of glaciomarine sediments from the Prydz Bay-Kerguelen region: relation to modern depositional environments

Andreas Borchers*[1], Ines Voigt[2], Gerhard Kuhn[3] & Bernhard Diekmann[1]

[1]*Alfred Wegener Institute for Polar and Marine Research, Research Unit Potsdam*
Telegrafenberg A43, 14473 Potsdam, Germany
[2]*University of Bremen, Geosciences Postbox 330440, 28334 Bremen, Germany*
[3]*Alfred Wegener Institute for Polar and Marine Research, Research Unit Bremerhaven*
Columbusstrasse, 27568 Bremerhaven, Germany
* Corresponding author

Abstract

Surface mineralogical compositions and their association to modern processes are well known from the East Atlantic and Southwest Indian sectors of the Southern Ocean, but data from the interface of these areas – the Prydz Bay-Kerguelen region – is still missing. The objective of our study was to provide mineralogical data of reference samples from this region and to relate these mineralogical assemblages to hinterland geology, weathering, transport and depositional processes. Clay-mineral assemblages were analyzed by means of X-ray diffraction technique. Heavy-mineral assemblages were determined by counting of gravity-separated grains under a polarizing microscope.

Results show that by use of clay-mineral assemblages four mineralogical provinces can be subdivided: i. continental shelf, ii. continental slope, iii. deep sea, iv. Kerguelen Plateau. Heavy-mineral assemblages in the fine sand fraction are relatively uniform except for samples taken from the East Antarctic shelf.

Our findings show that mineralogical studies on sediment cores from the study area have the potential to provide insights into past shifts in ice-supported transport and activity and provenance of different water masses (e.g. Antarctic Slope Current and Deep Western Boundary Current) in the Prydz Bay-Kerguelen region.

Keywords: clay minerals, heavy minerals, ice rafting, bottom water, MacRobertson Land, East Antarctic Ice Sheet

2.1 Introduction

The Prydz Bay-Kerguelen area is one of the key regions in the Antarctic because it contains the world`s largest outlet glacier and three major areas of bottom-water production associated with sea ice formation. Total annual ice production in the most important area – the Cape Darnley polynya (180 km^{-3}) – equals about half of the production rate of ice of the Ross Ice Shelf Polynya (390 km^{-3}) and is comparable to that of Mertz Glacier Polynya (120 km^{-3}; Tamura et al., 2008).

In the recent past, research in the study area focused on oceanographic questions. Extensive oceanographic studies have been undertaken to infer the sources and flow routes of surface, deep and bottom waters (Smith et al., 1984; Nunes Vaz and Lennon, 1996; Bindoff et al., 2000; McCartney and Donohue, 2007; Roquet et al., 2009). Mineralogical surveys of modern sediments, however, are rare (Von der Borch and Oliver, 1967). Neither has the modern lateral distribution of mineralogical components on the sea floor been mapped nor the significance of different processes affecting these distributions been assessed. Consequently, the influence of modern transport and depositional processes on the composition of sediments in this region is poorly understood.

For palaeoenvironmental research, however, knowledge of present-day processes and their fingerprints in modern sediments is indispensable. In the Prydz Bay-Kerguelen region it is of major interest for the reconstruction of bottom-water activity and ice sheet dynamics, how sediments in different areas are affected by the flow of Circumpolar Deep Water (CDW), Antarctic Bottom Water (AABW), the Antarctic Slope Current (ASC) or input of ice-rafted material from the Lambert Glacier drainage basin and downslope transport.

Investigations of surface sediments, that place clay-mineral distributions in a modern oceanographical and sedimentological context, are available from the South Atlantic covering the area of 70°W - 40°E and 10°N - 80°S (Petschick et al., 1996; Diekmann et al., 2003). The authors concluded that most of the clay minerals are of terrigenous origin and relate marine clay-mineral assemblages to five main source regions. Input of the material is driven by a complex interaction of ocean currents, river, wind and ice activity, as well as turbidity and contour currents. Furthermore, Petschick et al. (1996) pointed out that clay-mineral assemblages of deep-sea sediments are not derived from a single source area nor along a single transport path, which complicates the connection of mineralogical compositions to certain provenances. Other investigations west of the study area have been accomplished by Moriarty (1977) who compiled clay-mineral maps of Southeast Indian Ocean sediments between 100°E - 170°E and 20°S - 70°S. Regarding the clay-mineral signature of ice-transported material he underlined the importance of sediments deposited prior to Antarctic glaciation, which are now partly hidden underneath the ice. Fluvial pre-

icecap sediments were also found in the Beaver Lake area, Prince Charles Mountains (Webb and Fielding, 1993; Whitehead et al., 2006) and are possibly more widespread than currently known. Kaolin-rich and smectite-rich sediments of the Pagodroma Group deposited in a fjordal marine environment (Hambrey and McKelvey, 2000b) provide excellent mineralogical tracers (Ehrmann et al., 2003).

Further mineralogical information on marine sediments within the Prydz Bay-Kerguelen region was provided by several palaeoenvironmental studies focussing on past variations of the Lambert Glacier drainage system (Ehrmann et al., 1991; Cooper and O`Brien, 2004; Junttila et al., 2005) and on palaeoceanography (Ehrmann et al., 1992; Cooper and O`Brien, 2004). In these studies, conclusions were drawn on provenance shifts using clay minerals and subordinate heavy minerals. An overview, however, on modern processes and related mineralogical signatures is still missing.

In this paper, we provide a set of reference data for clay mineral and heavy-mineral assemblages in the Prydz Bay-Kerguelen region. Ocean currents are used to aid the interpretation of clay-mineral trends. Heavy-mineral assemblages are tested for suitability to reflect differences in the geologic background between the relevant drainage areas. In this regard, samples taken from pre-Holocene deposits play a major role as they probably reflect the direct influence from the hinterland. Mineralogical proxies are examined as tracers of Late Quaternary shifts in the glaciomarine environment and provenances in response to climate changes.

2.2 Regional setting

The Prydz Bay-Kerguelen region (Fig. 2.1) is situated between 50°S and 69°S latitude and 65°E and 85°E Longitude and includes four main topographic features:

i. Lambert Glacier (Fig. 2.1), approximately 400 km in length, is the world`s largest outlet glacier. It drains about 16% of the East Antarctic Ice Sheet (EAIS) (Fricker et al., 2000) and is predominantly responsible for the supply of terrigenous sediments to Prydz Bay and adjacent areas.

ii. Prydz Bay represents the largest shelf sea on the East Antarctic margin, though smaller than the Weddell Sea or Ross Sea. The shelf region is covered by seasonal sea ice and is bounded to the east by Princess Elizabeth Land and to the west by MacRobertson Land (Fig. 2.1). Continental shelf width varies between 70 km and 250 km. Water depths in general increase from 200 m near the shelf edge to 1600 m farther inland due to overdeepening through advances of the Lambert Glacier (Federov et al., 1982; Harris et al., 1997). Glacial incisions and rift basins have water

depths of up to 1000 m (locally).

iii. The Kerguelen Plateau, which is a NW-SE tending 2500 km long submarine barrier reaching widths of up to 600 km (Fig. 2.1). It rises up to 4 km above that sea floor, but rises above sea level only in the area of Kerguelen Islands and Heard Island.

iv. Enderby abyssal plain (Fig. 2.1), which comprises water depths between 4000 m and 5000 m. Sedimentation to a large part takes place by turbidity currents and by pelagic rain of biosilicous remains (Goodell, 1973; Kuvaas and Leitchenkov, 1992).

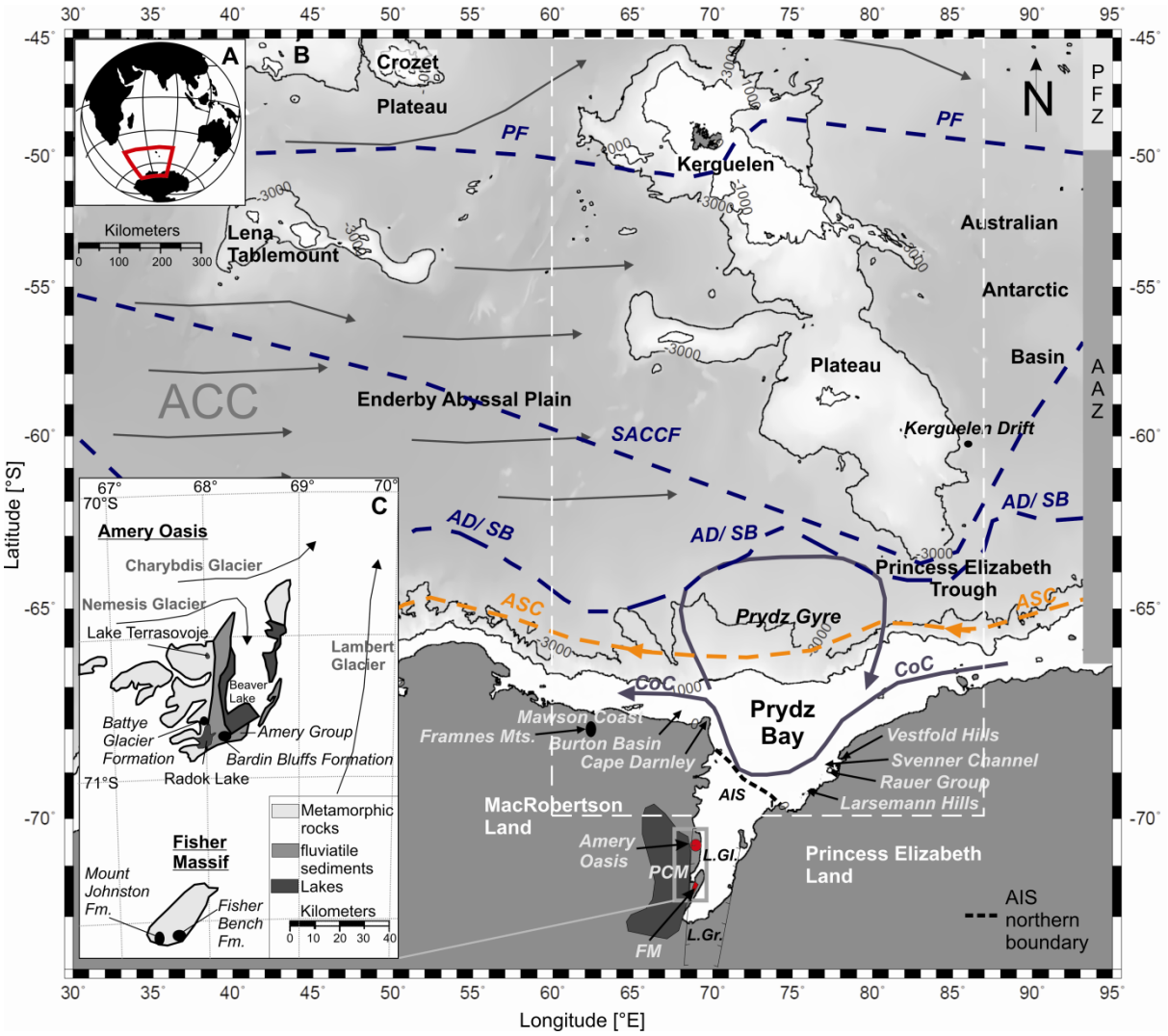

Fig. 2.1 Topographic and oceanographic features in the Prydz Bay-Kerguelen region (white box) and surrounding areas. A. Location of the investigation area B. AIS = Amery Ice Shelf, FM = Fisher Massif, L.Gl. = Lambert Glacier, L.Gr. = Lambert Graben, PCM = Prince Charles Mountains, ACC = Antarctic Circumpolar Current, CoC = Antarctic Coastal Current, ASC = Antarctic Slope Current (McCartney and Donahue, 2007), AAZ = Antarctic Zone, AD = Antarctic Divergence (Roquet et al., 2009), PF = Polar Front, PFZ = Polar Front Zone, SACCF = Southern ACC Front, SB = Southern Boundary of the ACC (Orsi et al., 1995), Prydz Gyre adopted from Smith et al. (1984). Map scale at 65°S. C. Enlarged picture of Amery Oasis and Fisher Massif with Pagodroma Group (black dots; Battye Glacier Fm., Bardin Bluffs Fm., Mount Johnston Fm. and Fisher Bench Fm.) and Amery Group indicated (modified after Ehrmann et al., 2003).

2.2.1 Oceanography, icebergs and sea ice

Surface circulation (Fig. 2.1) in the Prydz Bay-Kerguelen region is related to the prevailing wind systems. Near to the continent the Antarctic Coastal Current (CoC; Nunes Vaz and Lennon, 1996) and the Antarctic Continental Slope (or Polar) Current (ASC; Bindoff et al., 2000) are forced by the polar easterlies and move to the west (Fig. 2.1). At approximately 64°N the Antarctic Divergence (AD) delineates the boundary of the eastward-flowing strong band of the Antarctic Circumpolar Current (ACC) driven by strong westerly winds (Fig. 2.1). The opposing surface current directions generate a cyclonic gyre in Prydz Bay (Fig. 2.1) with cold-water inflow from the east, and outflow along the western side of the embayment (Smith et al., 1984). Circulation in the embayment is also enhanced by intense polynya activity that leads to bottom-water formation (Tamura et al., 2008) favouring downslope currents beyond the shelf edge. Sedimentation on the continental slope is controlled by the interaction of downslope density (e.g. turbidity) currents and along-slope (contour) currents (Kuvaas and Leitchenkov, 1992), e.g. the ASC.

The most prominent oceanographic feature in the study area is the Antarctic Circumpolar Current (Fig. 2.1). It extends from the sea surface to depths of 2000 m - 4000 m and can be as wide as 2000 km. Most of the deep and bottom-water masses of the ACC consist of Circumpolar Deep Water (CDW) that represents a mixture of water masses from the Atlantic, the Antarctic, the Indian and Pacific Oceans. Several oceanic fronts (e.g. Orsi et al., 1995) identified as narrow regions of sharp horizontal density gradients and by increasing nutrients levels subdivide the ACC from north to south into Subantarctic Zone (SAZ), Polar Frontal Zone (PFZ) and Antarctic Zone (AAZ; Fig. 2.1).

A comprehensive overview of sea-ice concentration and sea-ice motion is provided by Schmitt et al. (2004). The speed and direction of ice drift is dependent on the winds and surface currents. In Prydz Bay, ice follows the Antarctic Coastal Current to the west and is deflected to the north by southerly winds. North of the Antarctic Divergence, ice then diverges to the east. During austral winter, annual sea ice extends north of 60°S, whereas multi-year sea ice is mainly restricted to coastal areas.

2.2.2 Geology

Prydz Bay and Lambert Graben (Fig. 2.1) are incised in the East Antarctic shield, which is built up of Archean, Proterozoic and Cambrian metamorphic rocks and intrusives. East Antarctica once formed a central part of the Gondwana supercontinent (Tingey, 1991).

South of Prydz Bay the Lambert Graben extents 700 km inland. It represents the failed arm of a triple junction associated with breakup of India and Antarctica/Australia during early

Cretaceous times, at approximately 130 Ma. During the Permian and Mesozoic, sequences up to 5 km thick of continental deposits comprising sandstones, shales, coal and conglomerates of alluvial and glacial origin accumulated on the mostly Proterozoic basement (Cooper et al., 1991; Tingey, 1991). In the Prince Charles Mountains around Beaver Lake (Fig. 2.1) these deposits constitute the Amery Group (Fig. 2.1; Tingey, 1991; Webb and Fielding, 1993). Since the Palaeocene these sediments have been re-deposited several times (Whitehead et al., 2006) forming the sediment sequences of the Pagodroma Group (Fig. 2.1; Hambrey and McKelvey, 2000b).

The largest outcrop of bedrock is located on the western flank of the Lambert Graben (Fig. 2.1), where the Prince Charles Mountains (PCM) form the best-exposed cross section through the East Antarctic shield. The mountains consist of isolated nunataks and steep-sided, flat-topped massifs that stand up to 1000 m above the surrounding ice-sheet (Tingey, 1991). They are composed of Precambrian metamorphic rocks grading from granulite-facies gneisses with intrusions of charnockite plutons, pegmatite veins and alkaline dykes in the northern province of the bedrock outcrop to amphibolite-facies and greenschist-facies gneisses in the southern province (Tingey, 1991).

Along the eastern side of Prydz Bay, in the Larsemann Hills, Vestfold Hills and Rauer Islands (Fig. 2.1), several rock outcrops give insights into the petrography of the high-grade Archean and Proterozoic metamorphic rocks. The Larsemann Hills in largely consist of garnet-bearing gneiss with subordinate blue cordierite (Tingey, 1991; Thost et al., 1998). To the north, there is a scattering of smaller outcrops of Cambrian granites and Proterozoic gneisses. The Rauer Group, situated 100 km northeast of the Larsemann Hills (Fig. 2.1) comprises granulite-facies tonalitic orthogneisses with intrusions of mafic to ultramafic dykes (Tingey, 1991). Subsidiary paragneisses, marbles and skarn rocks can be found. Following to the northeast the Vestfold Hills offer the third large outcrop of bedrock off Princess Elizabeth Land (Fig. 2.1). The rock suite comprises Archean granulite facies gneisses intersected by several mafic dyke swarms with an interlayering of metavolcanics, pyroxenites, metagabbros, felsic orthogneisses and paragneisses (Tingey, 1991; Thost et al., 1998).

West of Prydz Bay, on MacRobertson Land (Fig. 2.1), bedrock is exposed along Mawson coast (Fig. 2.1). Rocks mainly consist of high-grade granulite-facies gneisses intruded by large charnockite plutons (Tingey, 1991). South of Mawson Station, bedrock of the Framnes Mountains (Fig. 2.1) crops out over an area of about 2000 km^2 comprising a variety of hypersthene-bearing felsic intrusives, granodiorites and tonalities (Tingey, 1991).

2.3 Material and methods

Twelve undisturbed sea-bottom surface samples were taken during Polarstern cruise ANT-XXIII/9 by use of giant-box corer and multicorer (Fig. 2.2). Additionally, three sediment samples from piston cores and gravity cores retrieved from the continental shelf were investigated for clay mineral and heavy-mineral distributions (Table 2.1). Samples obtained from sediment cores were taken from terrigenous sediment units directly underlying diatom oozes. They are thus tentatively assigned to the last glacial. The advantage of mineral distributions gathered from these glacial environments is that they directly display the composition of material derived from the hinterland (Ehrmann et al., 1992; Diekmann and Kuhn, 1999). In this paper, however, we use the term `pre-Holocene` to refer to these

Table 2.1 Overview of sample sites and devices used for retrieval of surface samples and pre-Holocene samples.

Site	Device	Latitude	Longitude	Water depth (m)
PS69/793-1	MultiCorer	-68.01	72.89	-703
PS69/793-2	Gravity corer (Kiel type)	-68.01	72.89	-673
PS69/794-2	MultiCorer	-68.72	76.68	-850
PS69/820-2	MultiCorer	-60.95	72.72	-4161
PS69/847-1	MultiCorer	-61.85	72.73	-4104
PS69/849-1	MultiCorer	-67.58	68.13	-553
PS69/849-2	Gravity corer (Kiel type)	-67.58	68.12	-559
PS69/851-2	MultiCorer	-66.37	69.01	-2036
PS69/853-2	MultiCorer	-66.00	69.22	-2365
PS69/855-1	Piston corer (BGR type)	-68.70	76.72	-848
PS69/878-4	Giant box corer	-65.34	82.66	-3093
PS69/885-1	Giant box corer	-63.84	82.87	-3702
PS69/891-5	Giant box corer	-62.66	82.84	-2290
PS69/895-1	MultiCorer	-61.70	82.83	-2352
PS69/899-1	MultiCorer	-59.62	85.67	-4126
PS69/903-1	MultiCorer	-57.23	79.38	-1713
PS69/907-3	MultiCorer	-55.00	73.33	-2251
PS69/912-5	MultiCorer	-50.31	71.57	-565

samples. In addition one should note that because of different accumulation rates in the different environments the term `modern` for surface samples is not to be taken *sensu stricto.* From each site, one 1 cm slice from the upper sediment was used for clay mineralogy. A second sample from each site with a thickness of 5 cm was used for heavy-mineral determination. Both samples were treated with 10% hydrogen peroxide for disaggregation and elimination of organic matter until chemical reaction ceased. Sample one, assigned to clay-mineral analysis, was wet-sieved through 63 µm and 2000 µm meshes to isolate the fines from the sand fraction and gravel fraction. Silt and clay were separated by Stokes´ Law using

Atterberg settling tubes (Müller, 1967).

Some sediment samples included high concentrations of biogenic opal with potential to bias the determination and quantification of clay minerals (Petschick et al., 1996). Therefore biogenic opal was dissolved by heating the material of the clay fraction at 85°C in a 1.5 M sodium hydroxide solution for two hours. After smear slides were inspected to verify that all biogenic opal had been removed, the suspension was washed to pH of 7 - 8 by centrifuging with demineralized water and dried at 50°C. Preferentially oriented clay-mounts were produced following the method and precisions explained in detail elsewhere (Ehrmann et al., 1992; Petschick et al., 1996). Clay mineralogy was determined semiquantitatively by X-ray diffraction measurements conducted on a Philips PW1820 diffractometer system (CoK-alpha radiation at 1600 W, 40 kV, 40 mA). Mineral proportions of the main clay-mineral groups smectite, illite, kaolinite and chlorite were determined with the help of MacDiff 4.2.5 program (freeware, http://www.geologie.uni-frankfurt.de/Staff/Homepages/Petschick/Classicsoftware.html, date accessed 11th August 2010) from weighted peak areas recorded in the X-ray diffractograms. For simplification, the terms smectite, kaolinite, illite and chlorite are here used as a general expression for the relevant mineral groups. The distribution of clay minerals was calculated using empirically estimated weighting factors (Biscaye, 1965). The 5/10 Å ratio gives evidence on the illite octahedral composition. According to Esquevin (1969) low 5/10 Å values (< 0.15) are characteristic of Fe, Mg-rich (biotitic) illites. Substitution of Mg and Fe by Al increases the ratio with values exceeding 0.4 corresponding to a muscovitic composition. For analysis of the `crystallinity´ of smectite and illite, the integral breadth of the glycolated 17 Å-smectite and 10 Å-illite peaks were measured (Petschick et al., 1996). Crystallinity usually provides a qualitative index for lattice order and crystallite size but it can also be used as a tracer for source regions and transport path of young sediments (Petschick et al., 1996).

Subsidiary to the clay-mineral assemblages, the occurrence of other minerals in the clay mineral fraction like quartz, plagioclase, K-feldspar, hornblende and pyroxene was determined. These minerals can provide adjuvant information on the provenance of the material and reveal information on weathering, transport and deposition mechanisms of sediment material.

Heavy-mineral analysis: In sediment sample two the 63 - 125 µm fine sand fraction was isolated from the rest of the sand fraction by wet sieving. Approximately 2.7 g of fine sand was dispersed in 10 ml of sodium-metatungstate solution (density 2.86 - 2.89 g/cm^3) in centrifuge tubes. The heavy-mineral fraction was separated from the light minerals by centrifuging (20 minutes at 3000 rpm), subsequent freezing in liquid nitrogen and staged melting. The heavy minerals were mounted on glass slides using Meltmount (refraction index = 1.68). A minimum of 300 translucent grains were counted along traverses under a

polarizing microscope. Gale and Hoare (1991) recommend counting a minimum of about 300 grains to determine the broad distribution of species in a sample. Improvement in the precision is very small with counts greater than 500 grains.

The results are presented as grain percentages in the heavy-mineral fraction, corrected for opaque and weathered grains. Additionally the ratio of opaque to translucent grains and the ratio of altered to translucent grains was calculated.

All specifications of sample locations and data can be extracted from the information system 'Pangaea' (http://www.pangaea.de/PHP/CruiseReports.php?b=Polarstern; PS69 (Prydz Bay); Borchers 2010).

2.4 Results

2.4.1 Clay-mineral assemblages

Clay-mineral assemblages in the twelve studied samples show distinct regional variations in the study area (Fig. 2.2; Table 2.2). South of 57°S, illite is the dominant clay mineral with values ranging between 10% on the northern Kerguelen Plateau and 77% on the Kerguelen Drift and in the Svenner Channel situated on Prydz Bay shelf (Fig. 2.2). It is followed by smectite, making up to 89% of the clay-mineral assemblage at site PS69/912 on the northernmost Kerguelen site. However, south of 58°S smectite does not exceed 30%. Kaolinite occurs with about 10% to 15%, except for the continental shelf, where it can reach concentrations of 24% in surface samples and up to 41% in sediment samples from pre-Holocene deposits. Concentrations of kaolinite and smectite in sediment samples from the continental shelf are higher in the pre-Holocene sections compared to the surface samples at the same site, except for samples from Svenner Channel.

Illite chemistry shows distinct variations between strong biotitc to strong muscovitic compositions as indicated by 5/10 Å values that range between 0.07 and 0.64. The highest values are found on the topmost positions of the Kerguelen Plateau (Fig. 2.2). Results show no significant difference in the geochemical composition of the illites there. To the south, 5/10 Å ratios decrease to values between 0.1 and 0.2 on the continental slope adjacent to Prydz Bay. In Prydz Bay and in Burton Basin (Fig. 2.2), medium 5/10 Å ratios of 0.21 to 0.38 hint to mixing of illites of biotitic and muscovitic composition, while the sediment sample from the pre-Holocene sample in the Svenner Channel exhibits a clear biotitic character.

In addition to clay minerals, non-clay minerals in the clay fraction also show spatial differences. Both extreme values of the quartz/feldspar ratio (minimum 0.1, maximum 2.8) are found in the Kerguelen region. The ratio of hornblende/quartz is relatively uniform in the investigation area with most values ranging between 0.02 and 0.09. The minimum was found

in the Burton Basin whereas an extraordinary high ratio of 0.23 was determined on the northern Kerguelen Plateau. A similar regional pattern of extreme values is obtained by analysis of the K-feldspar/plagioclase ratios.

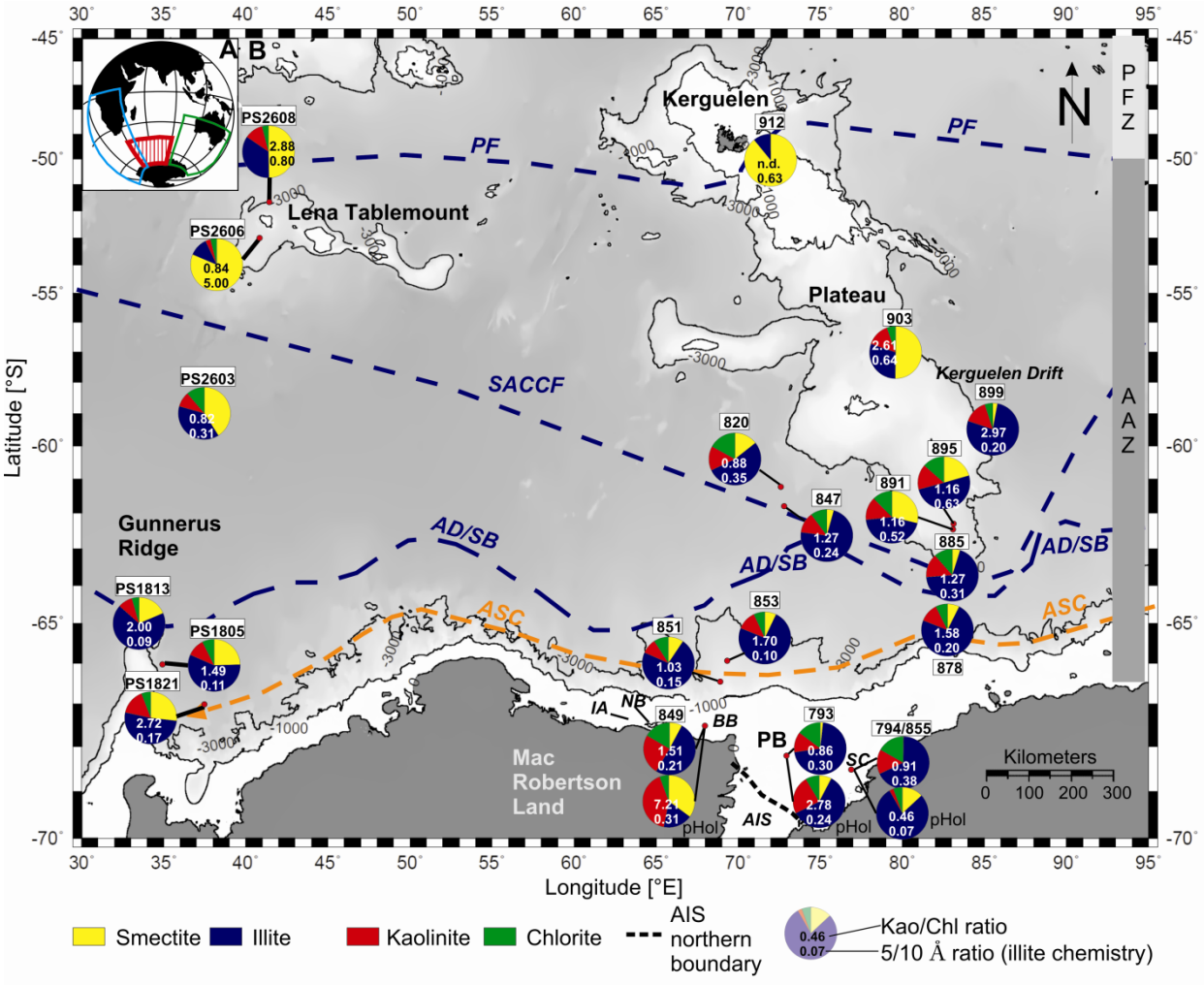

Fig. 2.2 Clay-mineral assemblages of sea-bed surface sediments in the Prydz Bay-Kerguelen region and of pre-Holocene deposits (pHol) on the East Antarctic shelf. A. Location of the investigation area (red, vertical lines) and areas of previous clay-mineral studies of sea surface sediments indicated (green polygon: Moriarty 1977, blue polygon: Petschick et al., 1996). B. Surface samples PS1805 to PS2608 published by Diekmann et al. (2003). AIS = Amery Ice Shelf, BB = Burton Basin, IA = Iceberg Alley, NB = Nielsen Basin, PB = Prydz Bay, SC = Svenner Channel. AAZ = Antarctic Zone, AD = Antarctic Divergence, ASC = Antarctic Slope Current, PF = Polar Front, PFZ = Polar Front Zone, SACCF = Southern ACC

Table 2.2 Mineralogical composition of the clay fraction determined from sea-bed surface sediments and pre-Holocene sediment samples (with core depth in cm in brackets) from the Prydz Bay-Kerguelen region.*

Pos.	Sm %	Ill %	Kao %	Chl %	K/C	5/10 Å	Ill 10 Å IB	Sm 17 Å IB	Q/Fsp	KFsp/ Plag	Px/ Q	Hb/ Q	Province
Surface samples													
793-1	1.7	71.0	12.6	14.7	0.9	0.3	0.5	-	1.7	0.2	0.1	0.07	Shelf
794-2	0.3	67.6	15.3	16.8	0.9	0.4	0.5	-	1.6	0.2	0.1	0.09	Shelf
820-2	14.4	53.6	15.0	17.0	0.9	0.3	0.4	1.0	1.9	0.3	0.1	0.05	Deep Sea
847-1	4.4	72.7	12.9	10.1	1.3	0.2	0.7	1.1	1.5	0.3	0.1	0.07	Deep Sea
849-1	7.8	50.7	24.9	16.5	1.5	0.2	0.4	0.9	2.2	0.5	0.1	0.02	Shelf
851-1	9.4	72.2	9.3	9.1	1.0	0.1	0.6	0.9	1.6	0.3	0.1	0.05	Slope
853-1	7.1	74.1	11.9	7.0	1.7	0.1	0.6	1.4	1.6	0.3	0.1	0.07	Slope
878-4	7.4	73.6	11.7	7.4	1.6	0.2	0.6	1.4	2.0	0.4	0.0	0.05	Slope
885-1	4.9	68.9	14.7	11.6	1.3	0.3	0.7	-	1.7	0.3	0.1	0.06	Deep Sea
891-5	28.7	44.7	14.3	12.3	1.2	0.5	0.4	1.1	2.8	0.3	0.1	0.03	Kerguelen
895-1	20.5	50.3	15.6	13.5	1.2	0.6	0.5	1.2	2.4	0.2	0.1	0.04	Kerguelen
899-2	2.9	77.2	14.9	5.0	3.0	0.2	0.8	0.8	1.6	0.3	0.1	0.09	Deep Sea
903-1	50.3	30.0	14.3	5.5	2.6	0.6	0.3	0.9	2.3	0.3	0.1	0.05	Kerguelen
912-5	89.1	10.7	0.2	0.0	n.d.	0.6	0.1	1.0	0.1	1.5	2.3	0.23	Kerguelen
pre-Holocene samples													
849-2 (370)	35.1	18.0	41.2	5.7	7.2	0.3	0.5	1.2	2.3	1.1	0.1	0.02	Shelf
793-2 (96)	7.7	60.0	23.8	8.5	2.8	0.2	0.4	1.0	1.9	0.3	-	0.06	Shelf
855-1 (1528)	13.1	78.7	2.6	5.6	0.5	0.1	0.5	0.8	1.2	0.2	0.1	0.14	Shelf

***Sm = smectite, Ill = illite, Kao = kaolinite, Chl = chlorite, K/C = kaolinite/chlorite ratio, IB = Integral breadth used as crystallinity index, 5/10 Å = illite chemistry, Q/Fsp = quartz/feldspar ratio, KFsp/Plag = K-feldspar/plagioclase ratio, Px/Q = pyroxene/quartz ratio, Hb/Q = hornblende/quartz ratio, n.d. = not determined. The assignment of each sample to a certain mineralogic province is shown. Schelf = 'continental shelf province', Slope = 'continental slope province', Deep Sea = 'deep sea province', Kerguelen = 'Kerguelen Plateau province'.**

2.4.2 Heavy-mineral assemblages

Heavy-mineral assemblages were obtained from seven sites (Fig. 2.3, Table 2.3). Samples from other sites exhibited either low contents of sand-sized material or a pronounced dilution of lithogenic matter with biogenic (primarily opaline) components. On the continental shelf, the mineralogical composition of sediments from three sites was analyzed (Fig. 2.3). In Prydz Bay it was only possible to isolate heavy-mineral grains from the sand fraction of the pre-Holocene deposits. Surface sediments were strongly diluted by biogenic material. In contrast to Prydz Bay, high amounts of sandy material in the Burton Basin (Fig. 2.3) favoured mineralogical analysis of both modern and glacial sediments. Samples from

Prydz Bay and Burton Basin show conspicuous differences in the content of garnet and hornblende with strong supply of garnet (79 - 83%) to Burton Basin and high amounts of hornblende (42 - 69%) in Prydz Bay, well expressed in differences of the garnet/ hornblende ratio. This ratio can be used to trace back sediments of the open ocean to the two possible source regions: garnet/ hornblende < 1 indicates provenance from

Prydz Bay, whereas garnet/ hornblende > 1 indicates sediment sources on MacRobertson Shelf (Fig. 2.3). Heavy-mineral assemblages on the continental shelf furthermore can be distinguished by high concentrations of orthopyroxene in the Svenner Channel and lower orthopyroxene contents in the Burton Basin (Fig. 2.3).

Three samples were counted from the continental slope west and east of Prydz Bay. Heavy-mineral distributions show similar pictures with slightly increasing garnet/hornblende ratios and slightly decreasing orthopyroxene/clinopyroxene ratios from the east to the west. North of Princess Elizabeth Trough (Fig. 2.1), at site PS69/885, values of biotite, hornblende and zircon reach their maximum (9%, 65% and 6%, respectively), whereas garnet is of minor abundance. The northernmost site on Kerguelen Plateau, PS69/899, is characterized by the highest amount of apatite in the study area. Examination of translucent/opaque grains ratio and translucent/altered grains ratio reveals decreasing trends from Svenner Channel to Burton Basin and from the shelf to the southern Kerguelen Plateau.

Table 2.3 Heavy-mineral composition of sea-bed surface sediments and pre-Holocene sediment samples (with core depth in cm in brackets) from the Prydz Bay-Kerguelen region.*

	Bio	Gn	Hb	Cpx	Opx	Ap	Ep+Cz+Z	Sill	Stau	Zir	Rut	Opx/Cpx	Gn/Hb	Tr/Op	Tr/Alt	counts
Surface samples																
849-1	0.8	82.9	1.9	1.2	3.5	2.7	0.0	5.8	0.0	0.8	0.0	3.0	42.6	17.1	64.3	257
851-1	2.0	39.8	44.9	4.0	5.4	1.1	0.0	0.7	0.0	2.0	0.0	1.3	0.9	15.3	40.5	445
853-1	3.5	21.0	57.2	3.2	6.4	2.4	1.3	2.7	0.0	1.9	0.5	2.0	0.4	20.9	22.1	376
878-4	4.9	15.6	55.6	3.9	9.2	3.1	2.1	2.1	0.0	1.8	1.2	2.4	0.3	8.9	28.6	487
885-1	8.9	4.7	65.4	2.8	5.6	3.7	1.9	0.0	0.0	5.6	1.4	2.0	0.1	5.6	12.6	214
899-1	2.7	14.5	43.5	4.3	9.0	12.9	3.9	2.0	0.0	4.7	2.4	2.1	0.3	3.3	8.2	255
pre-Holocene samples																
793 (125)	1.7	13.9	68.9	3.6	5.8	2.4	0.7	0.5	0.5	1.9	0.0	1.6	0.2	12.8	41.1	411
849 (330)	4.0	78.8	1.7	2.3	4.8	4.5	0.0	1.7	0.0	1.7	0.3	2.1	46.5	6.4	39.3	354
855 (1528)	0.2	29.6	42.9	4.0	21.8	0.9	0.2	0.0	0.0	0.2	0.0	5.4	0.7	14.1	60.3	422

*Bio = biotite, Gn = garnet, Hb = hornblende, Cpx = clinopyroxene, Opx = orthopyroxene, Ap = apatite, Ep+Cz+Z = sum of epidote, clinozoisite and zoisite, Sill = sillimanite, Stau = staurolilthe, Zir = zircon, Rut = rutile, Tr/op = ratio of translucent to opaque grains, Tr/Alt = ratio of translucent to altered grains.

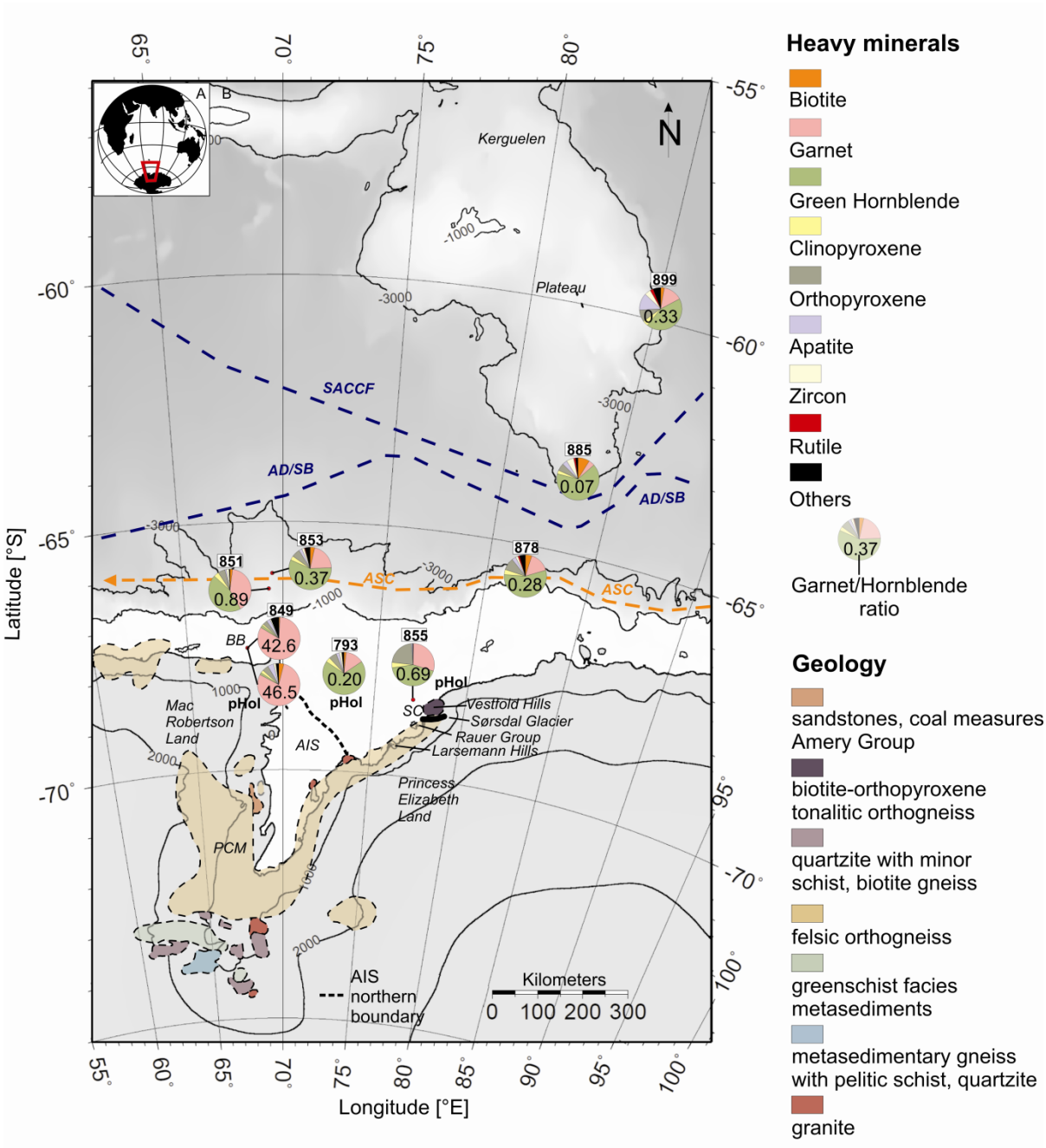

Fig. 2.3 Map of heavy-mineral assemblages determined from sea-bed surface sediments in the Prydz Bay-Kerguelen region and pre-Holocene deposits (pHol) on the East Antarctic shelf. A. Location of the investigation area. B. Geology of the Lambert Glacier drainage basin and Prydz Bay after Tingey (1991) and Thost et al. (1998). AIS = Amery Ice Shelf, BB = Burton Basin, SC = Svenner Channel, PCM = Prince Charles Mountains. AD = Antarctic Divergence, ASC = Antarctic Slope Current, SACCF = Southern ACC Front, SB = Southern Boundary of the ACC. Map scale at 65° S. Map courtesy of Australian Geological Survey Organisation © Commonwealth Australia 1998.

2.5 Discussion

The interpretation of both clay minerals and heavy-mineral assemblages requires understanding of the interaction of different factors that influence the mineralogical composition of the sediment samples with distance from source (e.g. Petschick et al., 1996; Diekmann and Kuhn, 1999). These factors include:

i. the geology of source rocks in the hinterland, which is responsible for the primary mineralogical composition of the material
ii. erosion and weathering conditions, controlled by local climate and hydrographic conditions. According to the mechanical and chemical stability of minerals, mechanical and/or chemical conversion can lead to first *in situ* modifications of the mineral suite.
iii. transport by water and ice can cause reduction in grain size and selective enrichment of different mineral groups
iv. authigenesis and sediment diagenesis

2.5.1 Clay Minerals

Four clay-mineral provinces (Fig. 2.4) can be distinguished in the study area by combination of similar clay-mineral assemblages: a 'continental shelf province', 'continental slope province', 'deep-sea province' and 'Kerguelen Plateau province'. All clay-mineral assemblages comprise high concentrations of illites characteristic of an East Antarctic provenance. They are considered as a detrital product of subglacial erosion and weathering products of crystalline rocks in high latitude marine sediments (Petschick et al., 1996). Illites in most samples from the continental shelf, the continental slope and from deep sea sediments show neither clear biotitic nor muscovitic signature reflecting the mixing of both illite types. Nonetheless, relatively low 5/10 Å values argue for a preponderance of biotites produced by physical weathering of biotite-rich rocks in the Prydz Bay hinterland, including gneisses, granulites, granites/granitoids and subordinate metamorphosed mafic dykes (Tingey, 1991).
In the following section the single clay-mineral provinces are described:

'Continental shelf province' – pre-Holocene sediments.
The 'continental shelf province' (Fig. 2.4) comprises distinct variations in the concentration of clay-mineral groups in surface and diamict samples. The general increase in smectite and kaolinite in a westward direction particularly hints at a provenance of fine grained material from different sources.

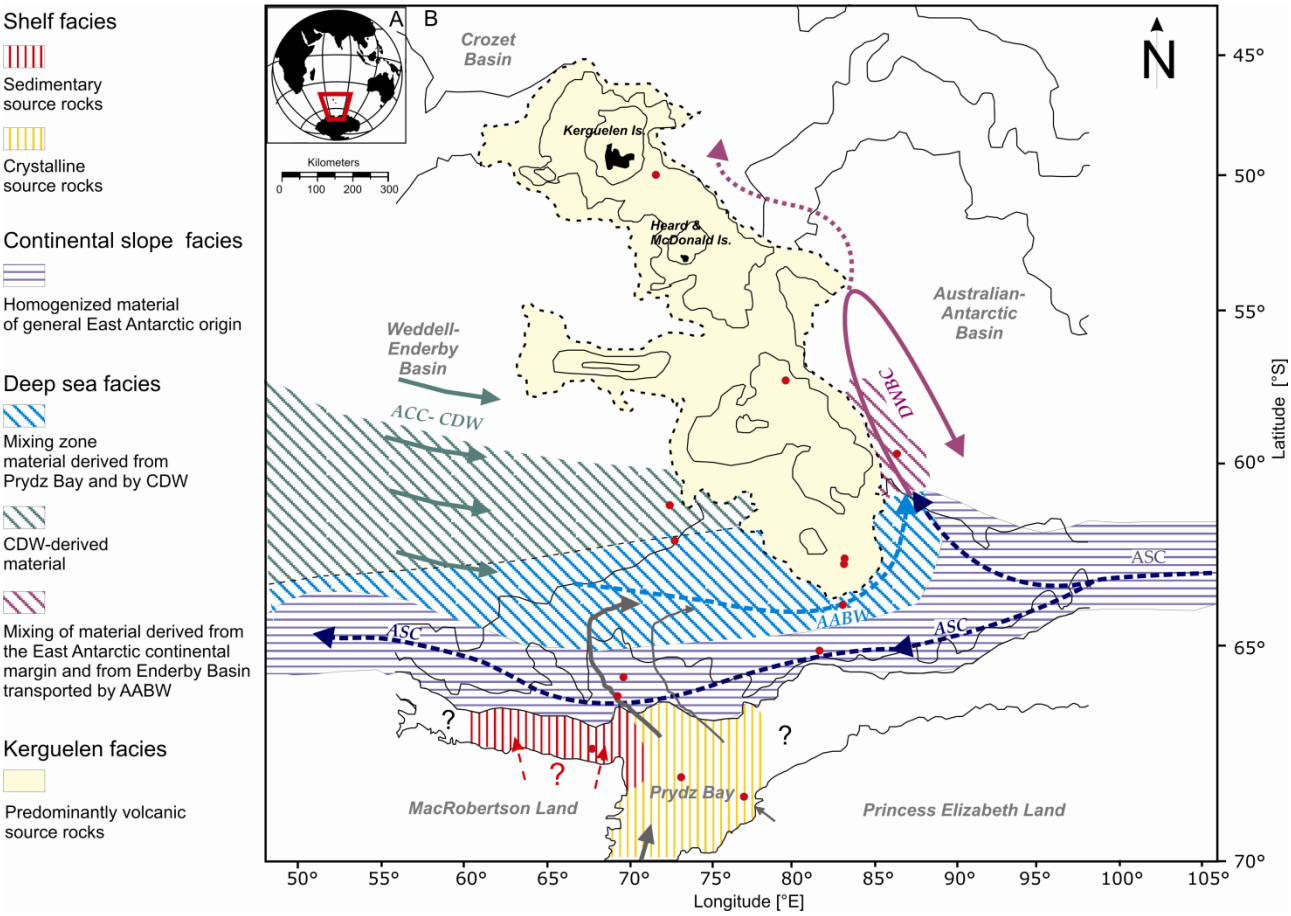

Fig. 2.4 Synopsis of mineralogical provinces in the Prydz Bay-Kerguelen region. A. Location of the investigation area. B. On the continental shelf, differences in the mineralogical assemblages are attributed to the primary composition of source rocks. 'Continental slope province' shows clay-mineral signatures of East Antarctic provenance homogenized by a strong contour current following the continental slope. In the southern 'deep sea province' terrigenous material is supplied from Prydz Bay (Goodell, 1973) and surrounding shelf areas, whereas sedimentation of fines in the northern 'deep sea province' is CDW-dominated. In the area of the Deep Western Boundary Current, fines supplied by AABW from the Weddell-Enderby Basin and from the East Antarctic continental margin are mixed. 'Kerguelen province' comprises generally high smectite contents associated with local transport of pyroclastic material. AABW = Antarctic Bottom Water, ACC = Antarctic Circumpolar Current, ASC = Antarctic Slope Current, CDW = Circumpolar Deep Water, DBWC = Deep Western Boundary Current. Map scale at 65°S.

Sediment samples from Svenner Channel (Fig. 2.2) show very high abundances of illite. 80% illite in the sample is tentatively assigned to the last glacial. The enrichment of Mg-Fe-rich illites in the pre-Holocene sample can be related to biotite-bearing highly metamorphic rocks found on the East Antarctic craton (Tingey, 1991). The mineralogy is consistent with the geology in the adjacent hinterland of Princess Elizabeth Coast (Fig. 2.3), which comprises granulite facies felsic and mafic layered orthogneiss, mafic gneisses and schists, minor calcsilicates and metapelitic gneisses (Tingey, 1991; Thost et al., 1998). A physical degradation

in glacial regimes, such as grain size reduction, preserves the chemical and structural properties of the low-ordered biotitic illites that are then supplied to the ocean (Petschick et al., 1996).

Sediment samples from Burton Basin (Fig. 2.2) show high contents of kaolinite and smectite, which is remarkable in the study area. Source rocks in the investigation area contain high amounts of feldspar and are therefore suitable to form kaolinite. However, kaolinite cannot be produced under modern weathering conditions. Thus ancient sediments have to be taken into consideration. The only local sedimentary remnants of formerly widespread deposits in the Prydz Bay hinterland are exposed in the area of the Prince Charles Mountains (Fig. 2.3), where two sedimentary units can be distinguished:

i. Permo-Triassic continental deposits of the Amery Group (red-beds, Fig. 2.1, Fig. 2.3) containing feldspathic sandstones with a kaolinitic matrix (Tingey, 1991; Webb and Fielding, 1993). This kaolinite is probably a product of early diagenesis (Ehrmann et al., 2003). The Permo-Triassic deposits are of fluviatile origin and crop out at Beaver Lake (Fig. 2.1). The material was probably derived from a rapidly uplifted block of Upper Proterozoic and Archean gneisses (Turner, 1991).
ii. glaciomarine sediments of the Pagodroma Group (Fig. 2.1), cropping out in the regions of Fisher Massiv and Amery Oasis (Hambrey and McKelvey, 2000b; Whitehead et al., 2006). In the latter area the Bardin Bluffs formation is characterized by high kaolinite concentrations of 46% - 64%. Bardin Bluffs formation constitutes re-worked material from underlying Amery Group strata (Ehrmann et al., 2003).

Mineralogical results obtained from the site within Burton Basin bear a strong resemblance to results from Bardin Bluffs formation, Battye Glacier formation (Ehrmann et al., 2003), Beaver and Radok Lakes (Fig. 2.1, Hultzsch et al., 2008) and Permo-Triassic samples (Turner, 1991) respectively: similarities comprise very high kaolinite contents together with enrichment in K-feldspar compared to plagioclase and only very small amounts of amphibole. Medium 5/10 Å values point to a mixture of illites of biotitic and muscovitic composition. Because other source rocks or sediment deposits with analogous mineralogical fingerprints are not known, both Permo-Triassic sedimentary rocks as well as their re-worked analogues are the most likely sources for the provenance of material deposited in Burton Basin.

The origin of high amounts of smectite in the diamict of the Burton Basin, however, is difficult to explain with an exclusive origin from the mentioned formations. Marine authigenic formation of smectite is generally possible, but hard to assess, because the degree of authigenic smectite formation is subjected to the age of the material. Rather, a detrital origin from possible occurrences of volcanic material identified on the continental slope off Cape Darnley (Fig. 2.1) as revealed by seismic investigations of Stagg (1985) seems possible.

The underlying seismic reflectors decrease landward in depth making it possible that volcanic material could be accumulated in shallow depths near Burton Basin.

On the continental shelf, the amount of smectite is generally higher in the pre-Holocene deposits compared to modern sediments. The fact that the shelf areas were glaciated to a wide extent during the last glacial stage (Domack et al., 1998; Harris and O'Brien, 1998) suggests that the smectite preferentially was derived or re-deposited from direct glacial input rather than by dispersal by ocean currents. Apparently there are no sediments known from the Prydz Bay hinterland that bear such high concentrations of smectite with exception of lacustrine sediments deposited in Lake Terrasovoje, Amery Oasis (Fig. 2.1). Smectite in these deposits holds values between 3 % and 69 % (Hultzsch et al., 2008). According to Hultzsch et al. (2008) and other authors (Ehrmann et al., 1992; Ehrmann et al., 2003) smectite could have formed by chemical weathering of mafic rocks (e.g. mafic dykes, volcanics or mafic gneisses). Because only a minor number of outcrops of basaltic rocks is known from the Lambert Glacier area, a wider distribution of hidden subglacial mafic rocks must be taken into consideration.

The question arises whether material was transported from the Amery Oasis to Burton Basin. By examination of Lambert-Glacier ice-flow rates and directions (http://earthobservatory.nasa.gov/IOTD/view.php?id=1199, date accessed 13th August 2010) and ice-drift paths in the Prydz Bay area (Schmitt et al., 2004) it becomes obvious that transport of material derived from Amery Oasis by Lambert Glacier to the Burton Basin is nearly impossible. Firstly, Beaver Lake is characterized by glacier inflow from Nemesis and Charybdis Glaciers (Fig. 2.1) avoiding a discharge of sediment-laden ice to the main axis of Lambert Glacier. Apart from that, icebergs calving from the Amery Ice Shelf leave Prydz Bay north of Cape Darnley, which forms a natural barrier for direct iceberg drift and IRD release to the Burton Basin.

The consolidated character of the pre-Holocene sample from Burton Basin points to direct subglacial release of sediment load from grounded ice probably arriving from MacRobertson Land. This glacial source would suggest undiscovered kaolinite sources on MacRobertson Land; however, it is also possible that consolidated material in the Burton Basin represents a natural outcrop of pre-glacial sediments of Cenocoic age exposed by glacial incision. Similar material, underlying glaciomarine sediments of Pliocene to Pleistocene ages, was recovered in eastern Prydz Bay during ODP Legs 119 and 188 (Turner, 1991; Cooper and O`Brien, 2004). It was also identified on the eastern continental slope off Prydz Bay (Kemp, 1972) and in western Prydz Bay according to seismic interpretation (Stagg, 1985; O`Brien, 1994) and sedimentological information (Domack et al., 1998). Additional evidence comes from Nielsen Basin and Iceberg Alley located on MacRobertson shelf west of Burton Basin (Fig. 2.1). Sediments there contain palynomorphs of Early and Middle Jurassic, Early Cretaceous and

middle Eocene age (Harris and O'Brien, 1998; Truswell et al., 1999). The basins also bear microfossils of definite Late Palaeocene to Oligocene ages (Quilty et al., 1999). However, the exact composition and provenance of the sediment underlying MacRobertson shelf is poorly known (Truswell et al., 1999) and needs further investigation.

In conclusion, pre-Holocene material recovered from Burton Basin has its source in ancient sediments equivalent to the Permo-Triassic sediments of the Amery Group or their re-worked Cenozoic correspondents, possibly hinting at pre-Pliocoene sedimentation patterns in the Prydz Bay-MacRobertson region. In contrast, glacial material recovered in Svenner Channel is probably related to mechanical weathering of rocks cropping out in the direct vicinity of the site.

'Continental shelf province' – modern sediments.

Clay-mineral assemblages of modern sediments show more uniform distributions. The samples from Prydz Bay are in particular good agreement, hinting at a mixing of material by the Antarctic Coastal Current and Prydz Gyre which certainly strengthened during the Holocene due to decreased ice cover and raised sea level. The Antarctic Coastal Current also influences the Burton Basin, as indicated by lower concentrations of kaolinite and increased illite content compared to the pre-Holocene sample. Nevertheless, the atypically high amounts of kaolinite and smectite provide evidence for either active reworking of pre-Holocene material or ongoing input of sediment from a local source.

The relatively low concentrations of smectite in modern shelf sediments not only indicate a reduced supply of glacial sedimentary input, but could also be explained by size-sorting effects. This would have led to wash-out of smectites and transport to more distal sites where current velocities are sufficient low to allow deposition of very fine material (Grobe and Mackensen, 1992). In contrast, sites proximal to the grounding line of the ice-sheet and reduced current velocities during the last glacial, preserved the smectites from this wash-out process.

'Continental slope province'.

Clay-mineral assemblages of the 'continental slope province' (Fig. 2.4) are quite uniform laterally and over a range of water depths. Comparison of mineral contents and illite composition from sites east and west of Prydz Bay suggests that input of sediment material from Prydz Bay is a minor influence on the sedimentation of the slope under modern conditions.

An explanation for this lack of sensitivity can be provided by the westward flowing Antarctic Slope Current (ASC). It represents a very powerful contour current with transport of 45 Sv at the Princess Elizabeth Trough (Fig. 2.1) at speeds of 30-40 cm s^{-1} (Bindoff et al., 2000;

McCartney and Donohue, 2007). That is much more water than is contributed by input from Prydz Bay.

The mineralogy of sediment samples taken from the ASC sphere of influence therefore represents a homogenized picture of East Antarctic provenance with mixing of material supported by several glaciers along the East Antarctic margin. High illite contents with high biotite composition, which are also documented in surface samples from the continental slopes off Adelie Land and Wilkes Land (Damiani et al., 2006), the Lambert Graben area (this paper) to Gunnerus Ridge, Enderby Land (Fig. 2.2; Diekmann et al., 2003), reflect a general source of clayey material associated with the East Antarctic shield. The latter comprises predominantly Proterozoic high grade metamorphic rocks and granitoids including charnockites (Tingey, 1991). Relatively low but constant kaolinite concentrations provide evidence for subordinate but widespread occurrences of ancient kaolinite-bearing sediments in the East Antarctic region. The material is glacially eroded, mechanically weathered and contributed to the ASC by subglacial deposition on the shelves followed by current reworking or by turbitity currents mostly initiated by ice-sheet dynamics (Kuvaas and Leitchenkov, 1992).

Clay-mineral assemblages similar to those of the 'continental shelf province' were also determined by Petschick et al. (1996) in surface sediments taken on or proximal to the continental shelf west of the investigation area. It is therefore feasible to connect the continental shelf province with the southern part of the East Antarctic province of Petschick et al. (1996).

'Kerguelen Plateau province'.

Clay-mineral assemblages from Kerguelen Plateau province (Fig. 2.4) show moderate to very high concentrations of well-crystallized smectite. Increasing trends of smectite content correlate with shallower water depths and the proximity to volcanic areas, respectively. Similar smectite patterns were observed from volcanic areas in the Atlantic region, e.g. west of the Antarctic Peninsula and its offshore islands, in the area around the South Sandwich Islands and at the Southwest Indian Ridge (Petschick et al., 1996). Smectite contents even rise to 90% in the vicinity of young volcanoes like Deception or Bouvet Island similar to that documented in the investigation area at site PS69/912, northern Kerguelen Plateau. The latter site is close to Kerguelen Island, which comprises a suite of primarily tholeiithic basalts with subordinate trachyte and Quaternary pyroclastic deposits (Parra et al., 1991). Local volcanogenic sedimentation of smectites from Kerguelen Plateau seems very likely. A local source of the clayey material is also suggested by the exceptionally high ratios of K-feldspar/ plagioclase, pyroxene/quartz and amphibole/quartz. Whereas amphibole, pyroxene and plagioclase are important constituents of basaltic rocks, K-feldspar is commonly found in

felsic extrusive or plutonic rocks, e.g. in trachytes or syenites that crop out on the Rallier du Baty peninsula in the southwestern part of Kerguelen Island (Parra et al., 1991). Illites are also very abundant and 5/10 Å values exceed 0.5 typical for Al-rich composition. Low integral widths reflect very good to good crystallinities favouring a detrital source of the illites with only minor structural and/or chemical degradation. According to the ten main clay-mineral provinces proposed by Petschick et al. (1996), material deposited on Kerguelen Plateau is most likely derived from the Circumantarctic province. The transport of this material is tentatively assigned to Circumpolar Deep Water, which represents the dominant water mass of the ACC in the relevant water depths above 2300 m (Orsi et al., 1995). According to Petschick et al. (1996) illites (together with chlorite) transported by CDW are derived from low-grade metamorphic rocks mainly found in the Andean chain on the Pacific side of the Antarctic Peninsula and southermost America (Patagonia).

According to the different provenances of smectites and illites in surface samples recovered from Kerguelen archipelago, their relationships are suggested to illustrate the dominance of either CDW influence or volcanogenetic influence. To the south a very sharp boundary, associated with changes in the dominant water mass, separates the 'Kerguelen Plateau province' from the 'deep-sea province'.

'Deep-sea province'.

Much work on clay-mineral distributions has been done on modern sediments from the deep sea of the East Atlantic and South Indian sector of the Southern ocean (Moriarty, 1977; Petschick et al., 1996). In contrast, little information is available for the Southern Ocean between 45°E and 100°E. Unfortunately, surface sediment samples obtained for this study could only be retrieved from the region between 65°E and 85°E. The 'deep-sea province' (Fig. 2.4) includes information from sites PS69/820, 847, 885 and 899.

Sites PS69/847, 885 in particular and subordinary site 899 bear strong similarities in terms of illite and smectite contents and illite crystallinity. These parameters can be clearly distinguished from those of close-by samples from the Kerguelen Plateau province. The fine-scale spatial separation between sites 847/885 and 899 is probably related to channelized flows of Antarctic Bottom Water (AABW) which derive from two main sources (McCartney and Donohue, 2007): i. AABW from the Weddell-Enderby basin passes Princess Elizabeth Trough at the southern tip of the Kerguelen Plateau (sites 847 and 885, Fig. 2.4) and turns northward at about 85° East (Donohue et al., 1999). It merges south of site PS69/899 with ii. water from the continental slope adjacent to the Australian-Antarctic Basin, which originate in the Ross Sea and along the Adèlie coast (Donohue et al., 1999; Bindoff et al., 2000) to form the Western Boundary Current (Fig. 2.4).

The mineralogical composition of samples from sites PS69/847 and 885, which shows low

smectite content, medium 5/10 Å ratios and moderate illite crystallinities (Fig. 2.2), most resembles to the composition of samples taken from Prydz Bay compared to that of samples taken on a transect from Gunnerus Ridge to Lena Tablemount (Fig. 2.2; Diekmann et al., 2003). This finding indicates, that material supported to the 'deep-sea province' at sites PS69/847 and 885 probably derived from the adjacent Antarctica continental margin. Increased input of material from the Antarctic continent is also suggested by generally high contents of terrigenous material (Goodell, 1973). Most likely, fine-grained material from Prydz Bay is transported to the sites by dense water, which originates on the shelf (Nunes Vaz and Lennon, 1996; Tamura et al., 2008) and is spilled over the shelf break (Smith et al., 1984; Yabuki et al., 2006). The dense water mass proceeds to the northwest triggered by the Antarctic Slope Current and when it enters the latitude of CDW dominance, it is looped to the east by the strong band of the ACC (Fig. 2.4) where it underlies and mixes with CDW and passes the Northern Prinzess Elizabeth Trough as a boundary current (McCartney and Donohue, 2007). The suggestion of Donohue et al. (1999) that water masses entering into the Deep Western Boundary Current could be sourced from the Weddell Gyre could neither be supported nor negated by this mineralogical study.

Differences in the illite chemistry and kaolinite/chlorite ratio of sample PS69/899 compared to the clay-mineral assemblages of sites PS69/847 and PS69/885 hint to mixing with material from another source. In particular, the low 5/10 Å ratio is hard to explain as solely derived from the boundary current south of the Kerguelen Plateau, because of the eastward increasing 5/10 Å trend. In addition, re-deposition of material from Kerguelen Plateau can be excluded, because material obtained from there is clearly of muscovitic composition.

It seems more consistent with the evidence, that biotite-like illites are directly derived from a branch of the Antarctic Slope Current that bifurcates in the southwestern Australian Antarctic Basin (Donohue et al., 1999) and contributes to the Western Boundary Current. Although no modern clay-mineral data are available from the continental slope off Wilhelm II Land and Queen Mary Land to test this assumption, the following data hint at similar illite compositions as obtained from the continental slope off Prydz Bay:

i. illite chemical compositions and crystallinities of surface samples recovered from the continental slopes off Adelie Land (Damiani et al., 2006), Prydz Bay (this paper) and Gunnerus Ridge (Diekmann et al., 2003) spanning about 110° of longitude are very similar and reflect the homogenization of material by the Antarctic Slope Current
ii. the geology of the hinterland along these areas (Tingey, 1991) is assumed relatively uniform with little input of material that might alter the clay mineral signature along the Antarctic Slope Current path (see section continental slope province)

As a consequence, the clay-mineral assemblage of site PS69/899 provides a sedimentological clue to the oceanographical circulation pattern in the southern Kerguelen region summarized

by McCartney and Donohue (2007).

Other important oceanographic features in the investigation area are the Southern ACC Front (SACCF) and the Southern Boundary of the ACC (SB). The latter roughly follows the Antarctic Divergence (Fig. 2.1). The influence of the SACCF and SB is possibly responsible for the differences in clay-mineral assemblages obtained from sites PS69/847 and PS69/820. The fine fraction of the latter site is enriched in smectite and chlorite. Illites comprise a more muscovitic composition. In conjunction with results obtained from the CDW-dominated site PS2603 (Diekmann et al., 2003), it therefore seems very likely, that clayey material deposited at site PS69/820 is of overall CDW provenance. The decreasing trend of smectite content to the east is attributed to subordinate contribution of illites with AABW from Prydz Bay or adjacent areas. Following these mineralogical indications and observations by Park et al. (2009), the sharp boundary between CDW-dominated flow at site PS69/820 and AABW dominated flow at site PS69/847 (see above) could be attributed to the deep prolongation of the Southern ACC Front or the Southern Boundary of the ACC. However, the position of both the Southern ACC Front and southern Boundary of the ACC is still under debate (e.g. Orsi et al., 1995; Park et al., 2009).

2.5.2 Heavy minerals

Heavy minerals are a valuable tool for determining the provenance of ice-rafted or fluvial-derived material, because they are more resistant to destruction by transport or chemical weathering than their lighter counterparts (e.g. Diekmann and Kuhn, 1999).

The heavy-mineral assemblages in the study area are very similar to each other, apart from the sample recovered from site PS69/849. Green hornblende comprises the dominant species, and shows highest abundance in the pre-Holocene sample from central Prydz Bay (Fig. 2.3, Table 1). Green hornblendes are ubiquitous components of many intrusive and metamorphic rocks. In conjunction with observation of high amounts (commonly 15-40%) of translucent to reddish garnets, this reflects the preponderance of high-grade metamorphic rocks in the Lambert-Glacier drainage area. In particular, erosion of amphibolite-facies and granulite-facies rocks exposed in the Northern Prince Charles Mountains (Fig. 2.3) leads to enrichments in hornblende in the heavy-mineral assemblages. The predominance and survival of chemically unstable hornblende is additionally attributed to its very good preservation because of the polar arid conditions during rock breakdown and thus restricted chemical weathering.

The overall East Antarctic signal, however, is modified in places by material supplied from local sources. In eastern Prydz Bay, for example, sedimentary material was probably derived

from the Vestfold Hills (Fig. 2.3). The latter mostly consist of Archean granulite facies gneisses intersected by mafic dyke swarms (Tingey, 1991). Intermediate metavolcanic rocks and metagabbros, in connection with Mossel gneiss and layered paragneisses of the Chelnok supracrustal assemblage, which mostly consist of garnet, biotite, orthopyroxene, quartz and feldspar (Tingey, 1991), obviously account for about 15% higher orthopyroxene and garnet contents in pre-Holocene sediments from Svenner Channel compared to central Prydz Bay (Fig. 2.3). According to Stone et al. (1993), cosmogenic exposure ages of the Vestfold Hills suggest that last glacial ice advances where peripheral to the oases. As a result, the inner part of Vestfold Hills has not been glaciated since before the Late Pleistocene. Any later glacial influence was due to expansion of the Sørsdal Glacier (Fig. 2.3), which will have made it likely, that rock types found in the Vestfold Hills extend into the Sørsdal drainage basin and may thus account for the mineralogical composition of Late Quaternary material deposited in the Svenner Channel. In connection with moderate smectite contents attributed to derivation from mafic source rocks (see section 2.5.1), a grain-size-independent transport mechanism suggesting movement by ice is most plausible.

In Burton Basin it seems likely that the composition of source rocks has overprinted the widely present East Antarctic heavy-mineral signature. The main constituent of the heavy-mineral assemblages here is garnet, which is characterized by high resistance in terms of chemical and mechanical weathering. Its extreme enrichment to about 80% clearly indicates repeated recycling of sediments, which originated from the breakdown of primary metamorphic rocks in the Lambert-Graben drainage area. Sediments of the Beacon Supergroup, for example, contain garnet as a major constituent of the heavy-mineral fraction (Diekmann and Kuhn, 1999) and may be the major and parent source of sediments in the Burton Basin. Following the interpretation of clay minerals in this paper (section 2.5.1) and results from palynomorphs provided by Truswell et al. (1999) and Quilty et al. (1999), the underlying sediments of MacRobertson shelf could be of Eocene age. According to Truswell et al. (1999) deposition of material close to the outcrop of the source sediments is most probable. By comparing the pre-Holocene with the modern heavy-mineral assemblage from Burton Basin, no major differences can be recognized. This situation could be ascribed to a stable source region, as well as similar transport mechanisms during pre-Holocene and modern times. In any case, input of material derived from Prydz Bay or other source regions is of negligible importance. This can be discounted, because sea-ice and icebergs calving in Prydz Bay are observed to make their way to the west, north of the continental shelf break (Schmitt et al., 2004), as indicated by generally increased hornblende contents in sediments from the continental slope off MacRobertson Land. This observation could – to a certain extent – also explain the northward trend of increased hornblende content at the expense of garnet with water depth.

Although heavy minerals are a valuable tool for determining the provenance of ice-rafted debris along the Antarctic margin (Diekmann and Kuhn, 1999), in the study area, other sedimentary processes may also influence the dispersal of sand-sized heavy minerals. It must be considered, that the dominant transport media for sand-sized material deposited on the continental slope are sediment gravity flows, especially turbidity currents (Kuvaas and Leitchenkov, 1992). Within these density flows sorting of material takes place according to the hydraulic characteristics of the grains. By comparing the density and shape of garnet and hornblende, conclusions can be drawn about the transport width of these minerals in liquified sediment flows. Garnet shows higher density (d = 3.5 - 4.3 g cm^{-3}) and rounded shape whereas hornblende is characterized by platy habit and has densities of 3.0 - 3.4 g cm^{-3}. According to these physical properties, hornblende is indicated to have a greater transport range than garnet, which is likely to lead to it accumulating in the lower part of the continental slope.

In the region of Kerguelen Plateau, most of the sandy material is suggested to have been derived from Prydz Bay by iceberg drift (Schmitt et al., 2004). Heavy-mineral assemblages resemble those of site PS69/793. Despite these similarities, local input of material should not be disregarded, because the amount of apatite at site PS69/899 exceeds values from all other sites by about 9% (Table 2.3). Apatite may have been derived from biotite-hornblende pyroxenites that represent constituents of Kerguelen volcanic rocks (Parra et al., 1991). Additional evidence for volcanic composition of the source material is given by slightly elevated zircon and rutile values, although apatite, zircon and rutile are also common constituents of calc-alkaline rocks such as granodiorite. Calc-alkaline rocks, however, are not found on Kerguelen Islands.

In summary, heavy-mineral assemblages in the Prydz Bay-Kerguelen region generally reflect an East Antarctic provenance of the material. Specific divergences from the overall East Antarctic signature were only detected in samples proximal to areas where source rocks with completely different primary composition crop out.

2.6 Conclusions and outlook

Clay minerals and heavy-mineral assemblages in modern sea-bottom surface sediments in the area between Prydz Bay and the Kerguelen Plateau trace the sedimentary sources and transport routes of glacigenic detritus delivered to the ocean.

Clay-mineral assemblages

Clay-mineral assemblages in the study area generally reflect an Antarctic source. In pre-Holocene deposits of the continental shelf, contrasting clay-mineral assemblages mirror

glacial input or alluvial input from local sources, respectively. During modern times, in contrast, clay minerals in the Prydz Bay region have been transported by ocean currents and were used to characterize four provinces, which reflect different transport and depositional regimes. Local clay-mineral signatures around the Antarctic, influenced by source rock composition, have been homogenized by the Antarctic Slope Current. Beyond the continental slope, the Antarctic clay-mineral signature reaches northward into the region of the Kerguelen Plateau, where it becomes modified by the Antarctic Circumpolar Current and local input of volcanic material.

Heavy-mineral assemblages

Heavy-mineral assemblages in the Prydz Bay-Kerguelen region are exclusively delivered from the East Antarctic shield. On the continental shelf it is possible to distinguish between different local sources of the ice-rafted material. Heavy-mineral grains of the fine sand fraction are mainly transported by glaciers as basal debris and then supplied to the ocean by drifting icebergs. In some regions such as the continental slope, however, heavy mineral transport and re-deposition by debris flows or turbidity currents cannot be excluded. In these cases, sorting of heavy minerals according to their hydrodynamic properties must be taken into account.

Application of clay minerals and heavy minerals for further palaeoenvironmental reconstructions

For the investigation of Late Quaternary East Antarctic Ice Sheet dynamics and connected ocean-atmosphere processes, clay minerals and heavy minerals are appropriate tools, although with some limitations.

The use of heavy-mineral assemblages for investigations of the provenance of ice-transported material is only suggested for sediments from the continental shelf. In this area, heavy-mineral distributions appear to match the primary mineralogy of source rocks. In areas distal to the source region, greater challanges in provenance analysis are anticipated. The material of various source rocks is mixed on its way to final deposition by sediment reworking processes leading to homogenization of heavy-mineral assemblages. It is thus difficult to clearly differentiate between primary signatures north of the continental shelf.

In the region influenced by the Antarctic Slope Current, the uniform clay mineral signature of sediments provides an opportunity to track back past changes in the local input of material to the continental slopes. Alternations between contour current activity and turbitity-current events can be documented, assuming turbitides with a distinct mineralogical composition. Therefore, future investigations of Late Quaternary East Antarctic Ice Sheet dynamics and bottom-water changes in particular should focus on the area west of Prydz Bay off MacRobertson Land, where clay-mineral and heavy-mineral

assemblages of the continental shelf show significant differences to those from the continental slope. The documentation of turbidity events there could provide information about the timing of advancing ice sheets that bulldoze material over the shelf edge or on turbidity events triggered by dense water pulses.

Acknowledgements

This investigation was funded by Deutsche Forschungsgemeinschaft priority program SPP 1158 through grant DI 655/3-1.

We kindly thank the master of research vessel ‘Polarstern’ captain Schwarze, the ship’s crew and the chief scientist of expedition ANT-XXIII/9, H.W. Hubberten, for their assistance and support. For sample preparation and technical support we are indepted to Ute Bastian, Rita Fröhlking, Norbert Lensch and interns onboard research vessel ‘Polarstern’. Map courtesy of Australian Geological Survey Organisation © Commonwealth Australia 1998.

Constructive reviews by Gavin Dunbar, Rob McKay and Alan P. M. Vaughan significantly improved the quality of the manuscript.

3. Holocene ice dynamics, bottom-water formation and polynya activity recorded in Burton Basin, East Antarctica

Andreas Borchers[1]*, Elisabeth Dietze[2], Gerhard Kuhn[3], Oliver Esper[3], Ines Voigt[4], Kai Hartmann[2], Bernhard Diekmann[1]

[1]*Alfred Wegener Institute for Polar and Marine Research, Telegrafenberg A43, 14473 Potsdam, Germany*

[2]*Freie Universität Berlin, Malteserstraße 74-100, 12249 Berlin, Germany*

[3]*Alfred Wegener Institute for Polar and Marine Research, Columbusstrasse, 27568 Bremerhaven, Germany*

[4]*University of Bremen, Klagenfurter Straße, 28359 Bremen, Germany*

*corresponding author

Abstract

A multi-proxy study including sedimentological, mineralogical and biogeochemical methods was conducted on sediment core PS69/849-2 retrieved from Burton Basin, MacRobertson shelf. The goal of this study was to depict the deglacial and Holocene environmental history of the MacRobertson-Prydz Bay region. A special focus was lain on the timing of ice-sheet retreat and the variability of bottom-water production due to sea-ice formation through the Holocene. The advantage of site PS69/849-2 is its location directly underneath Cape Darnley polynya, which is the second largest polynya in the Antarctic.

Methods included end-member modelling of laser-derived high-resolution grain-size data to reconstruct the depositional regimes, in particular bottom-water activity. The provenance of current-derived and ice-transported material was reconstructed using clay-mineral and heavy-mineral analysis. Conclusions on biogenic production were drawn by determination of biogenic opal and total organic carbon.

It was found that decoupling of the ice shelf from the ground around 32 ka BP (uncorr. ^{14}C age) coincides with results from other records in Prydz Bay and suggests global sea-level variation during Marine Isotope Stage 3 being the major trigger. Ice-rafted debris was then brought to the site until 5.5 cal. ka BP, when Holocene global sea-level rise stabilized and glacial rebound commenced. Throughout the Holocene, three episodes of enhanced bottom-water activity probably due to elevated brine rejection in Cape Darnley polynya were

recognized between 11.5 and 9 cal. ka BP, 5.6 and 4.5 cal. ka BP and since 1.5 cal. ka BP. These periods are related to cooler conditions commencing at the end of Holocene warm periods, in particular the early Holocene warm period, the hypsithermal and a late Holocene warm peak. Contrary, between 7.7 and 6.7 cal. ka BP, brine rejection ceased, maybe due to warm conditions and pronounced open-water intervals. Additionally, increased meltwater supply and subsequent stratification of the water column within the hypsithermal could be responsible for the mid-Holocene event.

Keywords: sea level, deglaciation, end-member modelling, Cape Darnley polynya, MacRobertson

3.1 Introduction

The knowledge of East Antarctic environmental history and its relationship to climate change has substantially been improved by investigation of ice cores (e.g. Masson et al., 2000), terrestrial records (e.g. White et al., 2009), lake sediments (e.g. Wagner et al., 2007) and marine sediment records (e.g. Cooper and O'Brien, 2004).

Focussing on the palaeoenvironmental history since the last glacial, especially sediment records retrieved from marine basins on the continental shelves provide excellent archives to reconstruct ice-sheet dynamics and shifts in the activity of oceanic currents (e.g. Domack et al., 1998; Harris, 2000; Leventer et al., 2006; Denis et al., 2009a). In this context, the activity of Antarctic Bottom Water (AABW) is noteworthy. Its contribution to the world ocean is essential as it comprises an important driver of the global thermohaline circulation which itself is a regulator of global climate. Dense brines produced by formation of sea ice in polynya areas, together with super-cooled water masses formed below ice shelves are important precursors of AABW (e.g. Tamura et al., 2008). Recent oceanographic studies turned out, that the eastern MacRobertson shelf hosts Antarctica`s second largest polynya and highlight the potential of polynya activity to bottom-water formation (Tamura et al., 2008). This bottom water partially fills Burton Basin to merge with the Antarctic Coastal Current at the northern shelf edge (K. Ohshima, pers. comm.). Steering mechanisms of polynya activity were modelled by Marsland et al. (2007). Palaeoenvironmental records of polynya activity, however, remain sparse (e.g. Harris, 2000; Smith et al., 2010).

The goal of this study is to reconstruct Holocene fluctuations in the activity of bottom currents in Burton Basin by means of sedimentological and biogeochemical methods. End-member modelling is applied to high-resolution grain-size data to unravel different sedimentation processes (Weltje, 1997; Weltje and Prins, 2003; Dietze et al., in review). Inferred oscillations in bottom-water activity are interpreted in relation to changes in the configuration of Cape Darnley polynya. These changes are discussed regarding their correlation to shifts in external forcing during the Holocene to provide clues on possible responses of polynya systems to future climate change. Additionally, we present data of the deglaciation history of eastern MacRobertson shelf. Results are compared with data from other marine and terrestrial sediment cores taken from MacRobertson shelf, Prydz Bay and other locations along the Antarctic margin to discuss the influence of global sea-level rise and glacial rebound.

3.2 Study area

MacRobertson shelf is situated on the East Antarctic margin north of MacRobertson Land and represents the continuation of the Prydz Bay-Amery Shelf about 400 km to the west (Fig. 3.1). It shows a typical width of about 90 km and an average depth of 350 m at the shelf break.

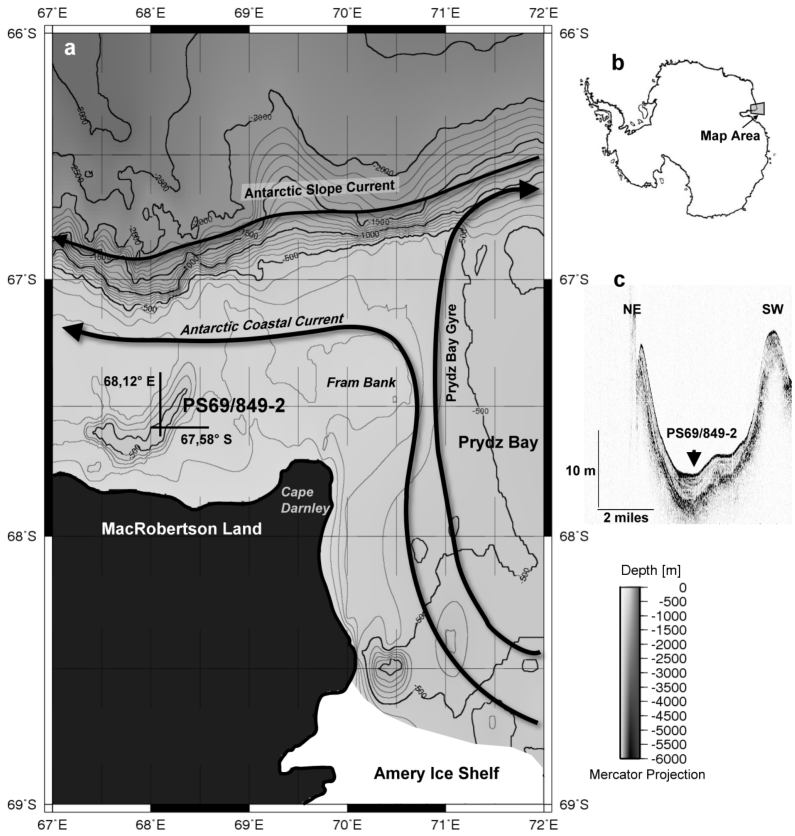

Fig. 3.1
Topographic overview (a) and location of the study area (b) with near-surface acoustic echosounder profile (c) of the coring site. Important oceanographic features are indicated.

3.2.1 Geomorphology

In general, MacRobertson shelf shows a more erosive surface than Prydz Bay (Harris and O`Brien, 1996). A conspicuous geomorphologic feature of MacRobertson shelf is the alternation of shallow banks and north-south tending basins. Burton Basin constitutes a U-shaped depositional valley that is connected to the continental slope and separated from Prydz Bay by Cape Darnley and Fram Bank (Fig. 3.1). The Basin is characterized by high-relief ridge-valley structures in the south and muds which locally drape the floor to the north. The flanks are steep-sided and consist of overconsolidated and/or coarse grained sandy and gravely sediments, indicated by Parasound survey (Fig. 3.1) conducted during expedition ANT-XXIII/9 and mentioned from other locations on MacRobertson shelf (Harris

and O'Brien, 1996; Harris et al., 1998). Burton Basin shows strong morphologic similarities to other basins on MacRobertson shelf, e.g. Nielsen Basin and Iceberg Alley.

3.2.2 Regional geology and sediments

The inner part of MacRobertson shelf probably consists of Precambrian metamorphic rocks and metasediments (Stagg, 1985), comprising charnockites and gneisses similar to those exposed in the Framnes Mountains on MacRobertson Land (Tingey, 1991).
Although there are no onshore outcrops of Cenozoic strata adjacent to MacRobertson shelf, information on a considerable sediment cover was obtained by seismic survey (Stagg, 1985) and from sediment cores taken during ANARE cruises in 1993, 1995 and 1997 (O'Brien, 1995; Harris et al., 1997; Quilty, 2001). A comprehensive overview of the provenance of pre-Holocene sediments on MacRobertson shelf is given by Borchers et al. (in press). The distribution of surficial sea-bottom sediments was investigated by Harris et al. (1998). They summarize, that sediments of the outer MacRobertson shelf include coarse-grained terrigenous and biogenic material. In contrast, sediments from the inner shelf comprise fine-grained muds and biosiliceous ooze.
In contrast to MacRobertson shelf, pre-Cenocoic and Cenozoic sediment packages in Prydz Bay are covered by massive glaciomarine sediments (e.g. Cooper and O'Brien, 2004) predominantly derived from the Lambert Glacier system, that drains about 16% of the East Antarctic Ice Sheet (Fricker et al., 2000). High-resolution Late Quaternary deposits were retrieved including diamictons, re-worked sediments from continental red-beds and diatom oozes (e.g. Domack et al., 1998).

3.2.3 Hydrography and ice-drift paths

At present, MacRobertson shelf and Prydz Bay are influenced by several surface and deep-water masses. The study area is situated south of the frontal system of the Antarctic Circumpolar Current (ACC) that flows to the east forced by westerly winds. It is subdivided by oceanic fronts separating zones with different physical properties and nutrient contents (Orsi et al., 1995). Most of the transport of water takes place within the prominent Circumpolar Deep Water (CDW) that represents a mixture of water masses from the Atlantic, the Antarctic, the Indian and Pacific Oceans. A minor deeper inflow of upwelled Circumpolar Deep Water (CDW) across the shelf break mixes with recirculated Prydz Bay waters.

South of the Antarctic Divergence easterly winds become more important and drive the westward flowing Antarctic Slope Current (ASC) as well as the Antarctic Coastal Current (CoC; Fig. 3.1). The ASC follows the East Antarctic continental slope over long distances (Bindoff et al., 2000; McCartney and Donohue, 2007) and extends from the surface to the seafloor. It is characterized as a contour current that homogenizes material supplied from the East Antarctic (Borchers et al., in press). The Antarctic Coastal Current is a strong surface current that reaches mean velocities of 0.14 m/s to 0.49 m/s with peak velocities of up to 1.96 m/s (Hodgkinson et al., 1991; Harris and O'Brien, 1998). It enters Prydz Bay after crossing the West Ice Shelf (Nunes Vaz and Lennon, 1996) and is deflected by the clockwise flowing Prydz Bay Gyre. After the Antarctic Coastal Current leaves the shelf area along the western embayment (Wong, 1994; Nunes Vaz and Lennon, 1996), it proceeds to the west on the northern MacRobertson shelf. The flow path of surface waters is associated with the drift path of sea ice and icebergs calving in the whole Prydz Bay region (Heil and Allison, 1999; Schmitt et al., 2004). Icebergs calving in Prydz Bay are looped to the west by the Prydz Bay Gyre and pass Cape Darnley north of Fram Bank which represents a natural barrier. North of the Antarctic Divergence, sea ice and icebergs are retroflected to the east and cross the Kerguelen Plateau.

A very important hydrographical feature on MacRobertson shelf and in Prydz Bay is the occurrence of coastal polynyas. Cape Darnley polynya constitutes the second largest ice free area in Antarctica with considerable sea-ice formation that equals half of the sea-ice formation in Ross Sea (Tamura et al., 2008). Associated with sea-ice production is the occurrence of dense High Salinity Shelf Water (HSSW) that is formed by brine rejection (Harris and O'Brien, 1998; Tamura et al., 2008). The dense water sinks and flows downslope off the shelf probably crossing and filling glacial troughs (Harris, 2000; K. Ohshima, pers. comm.) and possibly triggering turbidity currents there (Nunes Vaz and Lennon, 1996; Baines and Condie, 1998).

3.3 Material and methods

Gravity core PS69/849-2 was retrieved from Burton Basin (67°35`S, 68°7`31``E, 559 m water depth) on MacRobertson shelf during R/V Polarstern expedition ANTXXIII/9 in spring 2007. The site is situated at the southern end of a core transect taken along the continental slope off MacRobertson Land over the central Wild Drift. The sediment core provides a 3.8 m long sediment record extending back to the last glacial.

3.3.1 Sample preparation

After the sediment core was opened and described, sediment samples were collected at 10 cm intervals and divided into three subsamples. Subsample 1 was analyzed for bulk mineralogy. The other two subsamples were treated with 10% hydrogen peroxide and 10% acetic acid for disaggregation, elimination of organic material and calcium carbonate, respectively. Subsample 2 was analyzed for clay mineralogy and heavy minerals. In subsample 3, grain-size distribution was determined by Laser Particle Size technique.

3.3.2 IRD counting

After the sediment core had been split into an archive and a work unit, X-radiographs were taken from 1*10*25 cm sediment slices with the help of a HP Cabinet X-Ray System, Faxitron Series (radiation about 3 minutes, 40 kV, 4 mA). Rock fragments >2 mm, which represent an indicator for the amount of ice-rafted debris (IRD), were counted at 1 cm intervals (Grobe, 1987). Bedding characteristics were documented to get clues on the depositional environment and to identify units with possible sediment reworking.

3.3.3 Bulk mineralogy and determination of biogenic opal

Subsample 1 was freeze-dried, ground and measured for bulk mineralogy deduced from X-ray powder diffraction (XRD) with a Philips X`Pert system (PW3020 goniometer, CoK-alpha radiation, 1600 W, 40 kV, 40 mA). Biogenic opal was determined from X-ray diffractograms. For calibration, the height (intensity) of the hump generated by biogenic opal was measured in ten reference powder samples with given opal contents of 0% to 100% (in steps of 10%) and a linear regression (with $r^2 = 0.987$) was performed. After calibration, the hump in each sediment sample was determined and the opal content calculated by use of the linear regression.

3.3.4 Clay minerals

Subsample 2 was wet-sieved through 63 µm and 2000 µm meshes to isolate the fines from the sand fraction and gravel fraction. Silt and clay were separated by Stokes´ Law using Atterberg tubes. Prior to clay-mineral analysis, material of the clay fraction was treated for two hours at 85°C in a 1.5 M sodium hydroxide solution to dissolve biogenic opal.

Mineralogical analyses were carried out by X-ray diffraction measurements on glycolated preferentially oriented clay mounts. X-ray diffraction measurements were conducted on a Philips PW1820 diffractometer system (CoK-alpha radiation at 1600 W, 40 kV, 40 mA). Sample preparation and semiquantitative evaluation of X-ray diffractograms using MacDiff 4.2.5 program followed techniques explained in detail elsewhere (Ehrmann et al., 1992; Petschick et al., 1996). The distribution of clay minerals was calculated using empirically estimated weighting factors (Biscaye, 1965). According to Ehrmann et al. (1992) the relative analytical precession of this method is 6 - 9% for major clay components and 8 - 14% for minor clay components.

3.3.5 Heavy minerals

The fine sand fraction (63 – 125 µm) was isolated from the sand fraction of subsample 2 by wet sieving. Heavy-mineral separation and preparation was conducted as explained elsewhere (Borchers et al., in press). After heavy minerals were mounted on glass slides using Meltmount (refraction index = 1,68) a minimum of 300 grains comprising translucent, opaque and weathered minerals were counted along traverses under a polarizing microscope. The results are presented as grain percentages in the heavy-mineral fraction corrected for opaque and weathered grains.

3.3.6 Grain-size analysis with the Laser Particle Sizer

Biogenic opal was removed by treating the material in a 1.5 M sodium hydroxide solution at 85°C for 2 hours. Afterwards, the sodium hydroxide was removed by centrifugation with demineralized water to pH 7 - 8. After one spattle of tetra-sodium diphosphate decahydrate was added for disaggregation the material was split into eight subsamples by use of a rotary sample divider (Fritsch laborette 27). Measurement was conducted on a Beckman Coulter Laser Particle Sizer LS200 comprising 92 grain-size classes. Measurements of four subsamples were stacked.

3.3.7 Determination of TOC, sulphur, water content and mean density

A Leco CS125 device was used to determine bulk organic carbon on ground and decalcified sediment samples. The relative precession of the method is ± 3%. Water content of each sediment sample was calculated by the proportion of freeze-dried and wet sediment mass

times 100. Ground sediment samples were analyzed for sulphur content by use of Elementar Vario EL III. Mean density was obtained from Micromeritics Accupyc 1330 measurements.

3.3.8 End-member modelling

The statistical analysis of the polymodal grain-size distributions was performed using a Matlab end-member modelling algorithm generated by Dietze et al. (in review; [Appendix A1]) mainly following the general procedures of Weltje (1997). The advantage compared to other statistical methods like principal component or factor analysis is that end-member modelling provides a statistically rigorous and genetically meaningful solution by unmixing of compositional data (Weltje, 1997; Weltje and Prins, 2007). Important criteria to get geoscientifically feasible end-members are that they need to be nonnegative and to fulfil the constant-sum-constraints. End-members consist of loadings, which are typical process-related grain-size distributions and scores representing the quantitative downcore variation (i.e. composition in depth).

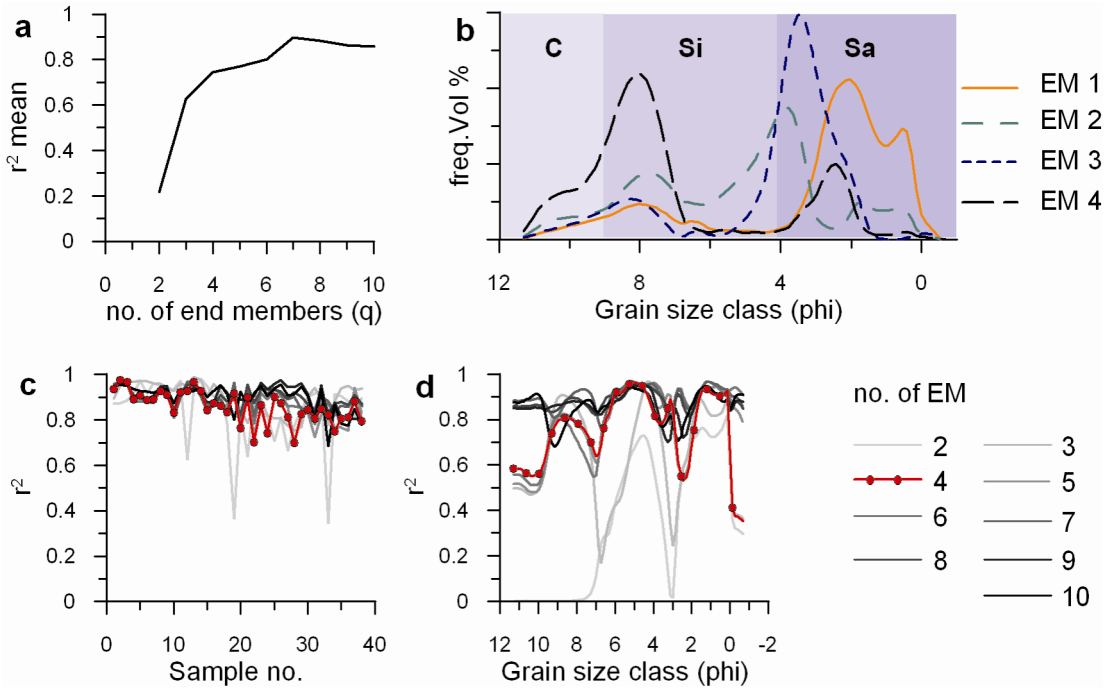

Fig. 3.2 End-member modelling results of grain-size data from sediment core PS69/849-2.
a) Mean coefficient of determination (r2) of all size classes for each end-member model.
b) Grain-size distributions of the four end-members.
c) Coefficients of determination (r^2) for each sample of models with 2-10 end-members.
d) Coefficients of determination (r^2) for each size class of models with 2-10 end-members.

The dataset was transformed by a W-transformation (Manson and Imbrie, 1964). The coefficients of determination (r^2) against grain size and samples are shown in Fig. 3.2 for models with 2-10 end-members. The coefficient of determination (r^2mean) represents the proportions of the variance of each grain-size class modelled by the approximated data (Weltje, 1997). It was calculated to estimate the minimum number of end-members for an appropriate representation of the original data by the modelled dataset.
Prins et al. (1999) showed, that the most likely number of end-members corresponds to the position of the inflection point of the q-r^2mean curve (Fig. 3.2a). For sediment core PS69/849-2, the coefficients of determination indicate that four end-members (Fig. 3.2b) are required to adequately describe the original grain-size data set by the modelled data (Fig. 3.2a, c, d). The four-end-member-model explains 74% of the total variance in the data set (r^2mean = 0.74).
The r^2 statistics of the single grain-size classes (Fig. 3.2c) reveals that highest uncertainties are found in the very fine (> 10 phi) and very coarse (< 0 phi) grain-size classes. They are attributed to the low absolute content of material within this grain-size classes and thus relative high modelling errors compared to grain-size classes with higher absolute values (Dietze et al., in review; [Appendix A1]).

All sample information and data lists are available via the PANGAEA data information system (www.pangaea.de).

3.4 Radiocarbon dating and age model

The radiocarbon age of eight sediment samples (Fig. 3.3, Tab. 3.1) was determined by accelerator mass spectrometry on decalcified bulk organic carbon at Poznan Radiocarbon Laboratory, Poland.
Due to upwelling of Circumpolar Deep Water, radiocarbon concentration in the Southern Ocean is depleted. This accounts for an older reservoir age than the global ocean mean. In order to ensure comparability to sediment records from other regions in the Antarctic, ^{14}C ages were corrected for the reservoir effect by 1300 ± 100 ^{14}C years as proposed by Ingolfsson et al. (1998) and Anderson et al. (2002) for Antarctic open waters. This reservoir age is in the range of dates determined from living mollusks of the circum-Antarctic (Berkman and Foreman, 1996) and similar to the surface age (1610 ± 30 ^{14}C years) determined in sediment core PS69/849-2 from the 1 cm depth sample. The time lag between the measured surface ^{14}C age and the proposed reservoir age suggests a lag equivalent to about 6 cm sediment with the given sedimentation rate in the upper section of the sediment core. Possibly, strong bottom currents with minor deposition, contamination with allochthonous recycled organic

matter due to bioturbation or addition of old carbon due to erosion and resedimentation affected the apparent surface age. Additionally, the marine radiocarbon reservoir of sediments dated in the vicinity to major ice-sheet masses of Prydz Bay and MacRobertson Land could be depleted by glacial meltwater or biological effects associated with the impact of sea-ice duration on CO_2 exchange (Andrews et al., 1999). Because the rate of glacial melting is very likely to have changed during the past as well as other parameters influencing the reservoir effect, one have to consider that the latter was not constant through time. However, in order to maintain consistency with previous works from the Antarctic shelf a constant reservoir effect was assumed in all ages of sediment core PS69/849-2.

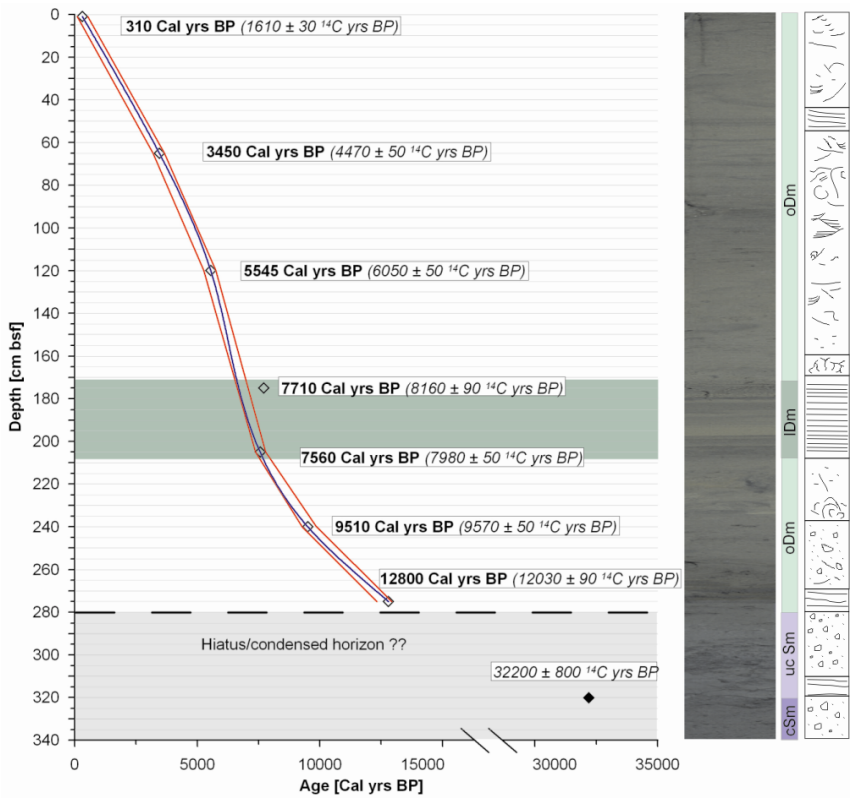

Fig. 3.3
Age-depth model with core picture, sedimentary units and sediment structures indicated. Black line: cubic spline model of most probable ages determined from the probability-density functions of each ¹⁴C age. Red line: 2s range of radiocarbon ages calculated with Calib6.0 software. cSm = consolidated sandy mud, ucSm = unconsolidated mud, oDm = oblique-bedded diatomaceous mud, lDm = laminated diatomaceous mud.

Conventional radiocarbon dates were calibrated to calendar ages BP. using Calib 6.0 software (Stuiver and Reimer, 1993). For calibration, model Marine09 (Reimer et al., 2009) was used, because calibration curve SHCal04 recommended for the Southern Hemisphere only extends back to 11 cal. ka BP. To construct an age-depth model (Fig. 3.3, Tab. 3.1) the most probable age within the 2s range was determined from the probability density distributions. Cubic spline interpolation done with Analyseries 2.0 (Paillard et al., 1996) was used to produce an overall smooth curve, and not change sedimentation rate abruptly at each data point. The resulting age-depth relationship was plotted against 2s ranges in order to guarantee that all ages are within the 95% confidence interval after the fitting procedure. The calibrated age of

sediment sample 175 cm was not included in the age-depth model because it was interpreted as an outlier due to too low TOC content.

Tab. 3.1 Radiocarbon ages, calibrated ages and 95% confidence intervals of samples determined by accelerator mass-spectrometry (AMS) from bulk organic carbon in Burton Basin sediments. A reservoir age of 1300 ± 100 yrs was used, with 400 yrs already incorporated into Calib6.0 software.

Laboratory no.	Sample (depth)	Material	Conventional C14 age (yrs BP)	Marine reservoir age (dR)	Most probable age (cal. yrs BP)	Max. probability error (cal. yrs BP)	Range (2sigma) (cal. yrs BP)	
Poz-25396	1 cm	TOC	1610 ± 30	900 ± 100	310	214	106	524
Poz-29970	65 cm	TOC	4470 ± 50	900 ± 100	3450	251	3199	3661
Poz-25459	120 cm	TOC	6050 ± 50	900 ± 100	5550	287	5258	5754
Poz-31615	175 cm	TOC	8160 ± 90	900 ± 100	7710	269	7482	7979
Poz-29967	205 cm	TOC	7980 ± 50	900 ± 100	7560	228	7371	7788
Poz-25397	240 cm	TOC	9750 ± 50	900 ± 100	9510	347	9268	9857
Poz-29968	275 cm	TOC	12030 ± 90	900 ± 100	12800	487	12313	12940
Poz-25530	325 cm	TOC	32200 ± 800	--	--	--	--	--

3.5 Results and Discussion

3.5.1 Lithology

According to sediment texture and macroscopic core description, four sediment units can be distinguished. Unit 1 (cSm) characterizes the base of the core from 370 cm to 320 cm. It consists of consolidated, poorly sorted terrigenous muddy sand with only few diatoms. Unit 1 comprises low contents in total organic carbon (TOC, ~0.3%) and biogenic silica (BSi, ~20%; Fig. 3.4), the latter mainly derived from diatoms and subordinate radiolarians. These low proportions are accompanied by very low water content (~ 20%), which is likely due to the compaction of the sediment by grounded ice. Mean density is close to quartz, underlining the minerogenic character of unit 1. A clay horizon situated between 320 cm and 310 cm separates unit 1 from unit 2. It shows indistinct stratification and sharp boundaries to the bottom and to the top.

Unit 2 (ucSm) spanning from 310 cm to 240 cm is made up of poorly sorted, unconsolidated muddy sand. Water content increases to about 30 - 35% (Fig. 3.4). In connection with slightly elevated BSi (25%) and TOC (0.4 - 0.45%) this suggests lifting of the previously grounded ice masses. The onset of biogenic sedimentation is possibly related to higher primary production near the ice shelf edge with biogenic material spilled under the floating ice and trapped in the basin.

From about 280 cm to the top of the sediment core, units 3 (oDm) and 4 (lDm) consist of diatomaceous sandy mud. Unit 3 accounts for the largest part of sediments in the record comprising bioturbation and oblique-bedding (Fig. 3.3). The base of unit 3 shows abrupt but short increases in TOC, BSi, sulphur and water content, accompanied by reduced mean density (Fig. 3.4). The transition to more constant increased proportions of TOC (0.6 - 0.8%), BSi (~ 50%) and water content (70 - 80%) takes place in a sediment depth of 240 cm. This coincides with the reduction of ice-rafted material and possibly denotes the end of the deglaciation.

Between 210 cm and 160 cm, unit 4 consisting of stratified and laminated diatomaceous mud with minor sand and thin layers of "cotton-like ooze" intercalates unit 3. Within the intersected laminated diatomaceous mud, sulphur and water content reach their maximum with values about 0.8% and 80 - 90%, respectively (Fig. 3.4). In connection with a minimum in the mean density (2.3 - 2.4 g cm^{-1}) this suggests higher porosity of the sediment. Because this change is not clearly represented in a change in BSi or TOC, it hints to a shift in the diatom composition. Taking into account the laminated character and the sedimentation of fine material, unit lDm is assumed to have been deposited under calmer current condition and/or restricted water convection in the basin.

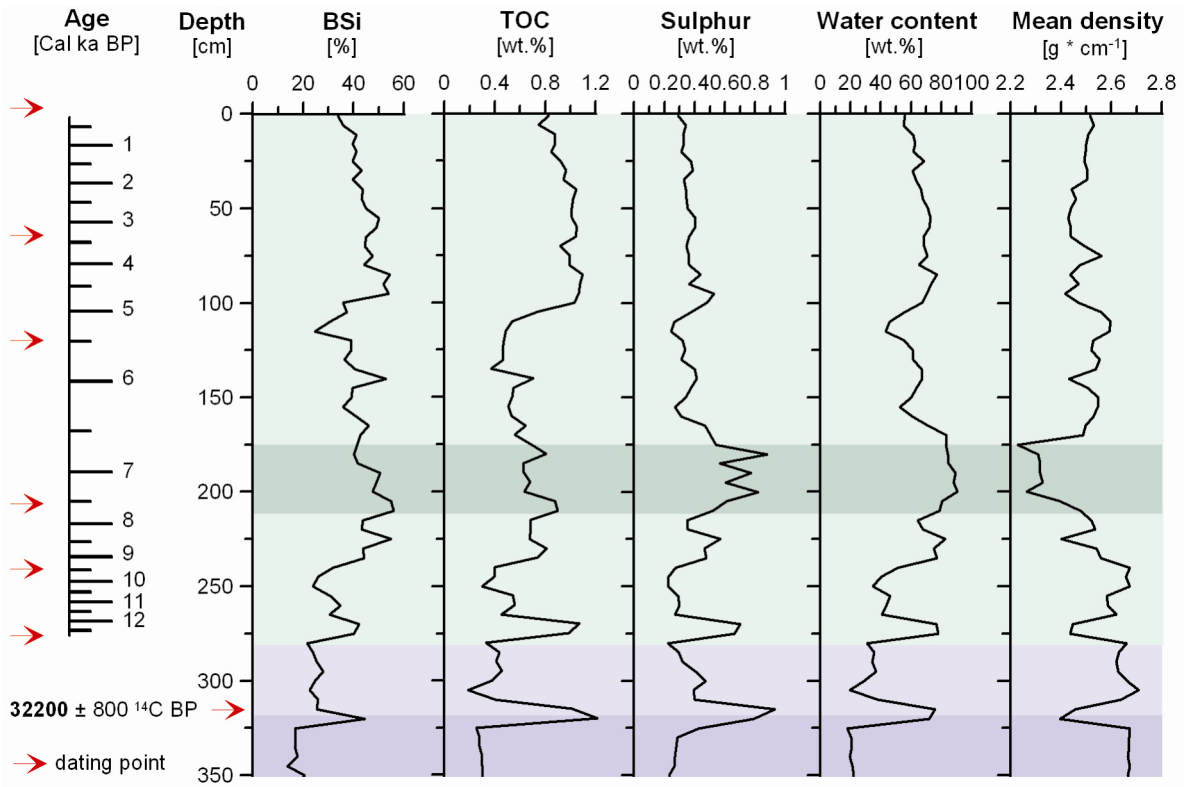

Fig. 3.4 Downcore variation in biogenic opal (BSi), total organic carbon (TOC), sulphur, water content and mean density. Background colours indicate sediment units according to Fig. 3.3.

Above the laminated section, mean density in unit 3 increases again to about 2.5 g cm^{-1} (Fig. 3.4). Sulphur and water content show reduced values. This correlates well with input of ice-rafted material. A major change occurs at 120 cm with a relatively sharp increase of TOC from 0.4 to 0.9 wt.%, which remains high to the top of the sediment core. This change is accompanied by a local minimum of BSi (30%) between 120 and 100 cm.
The consistency of TOC and BSi over the whole sediment core suggests them to represent primary production more likely than preservation, because both parameters have different stabilities regarding to biodegradation and diagenesis.

3.5.2 Grain-size distributions and sedimentation processes

End-member modelling of grain-size data from sediment core PS69/849-2 revealed four end-members. Its loadings differ from each other mainly in the sand fraction where the position of modi varies between 4 and 0.5 phi (Fig. 3.5). When interpreting the different end-members one has to keep in mind, that the core location is situated in an area of pronounced polynyas (Tamura et al., 2008). Thus, processes related to formation of polynyas exert an important influence on the grain-size distributions of the modelled end-members.
End-member one shows a maximum content of sand-sized particles offering a bimodal distribution and a shallow hump in the silt and clay size fraction (Fig. 3.5). The end-member is considered as parameter for transport of material by icebergs and release during melt-out. The good agreement in downcore variation with IRD and strong similarities of the end-member shape to original grain-size distributions of compacted sediments in the lower part of the sediment core underlines the interpretation. The bimodal composition probably evolves from glacial abrasion producing silt and clay-sized particles and plucking of bedrock that produces larger particles (Drewry, 1986). The resulting size spectra depend upon the mineralogy of the bedrock (Slatt and Eyles, 1981). Additionally, it can`t be excluded that some proportion of fine material might be blown in from limited exposed bedrock by strong catabatic winds. High content of sand-sized material in end-member one is attributed to the vicinity of the site to the Antarctic continent.
End-member two is characterized by a prominent and narrow peak in the fine sand fraction showing better sorting than any peak within the other end-members (Fig. 3.5). This leads to the conclusion of size sorting by relatively strong bottom current activity and winnowing of fines. According to the Hjulström diagram (http://www.terrestorm.com/press_research_Hjulstrom_Diagram.pdf) sediment particles of the fine sand fraction in a first approximation stay in suspension as long as fluid velocity exceeds 20 - 40 cm/s. In connection with only subordinate supply of fine material this end-

member represents strong bottom current activity and sediment reworking with winnowing and/ or resuspension of fines. Previous investigations of Harris and O`Brien (1998) also show, that the Antarctic Coastal Current at least at the outer continental shelf reaches velocities of 50 – 200 cm/s, capable to transport material of the fine sand fraction.

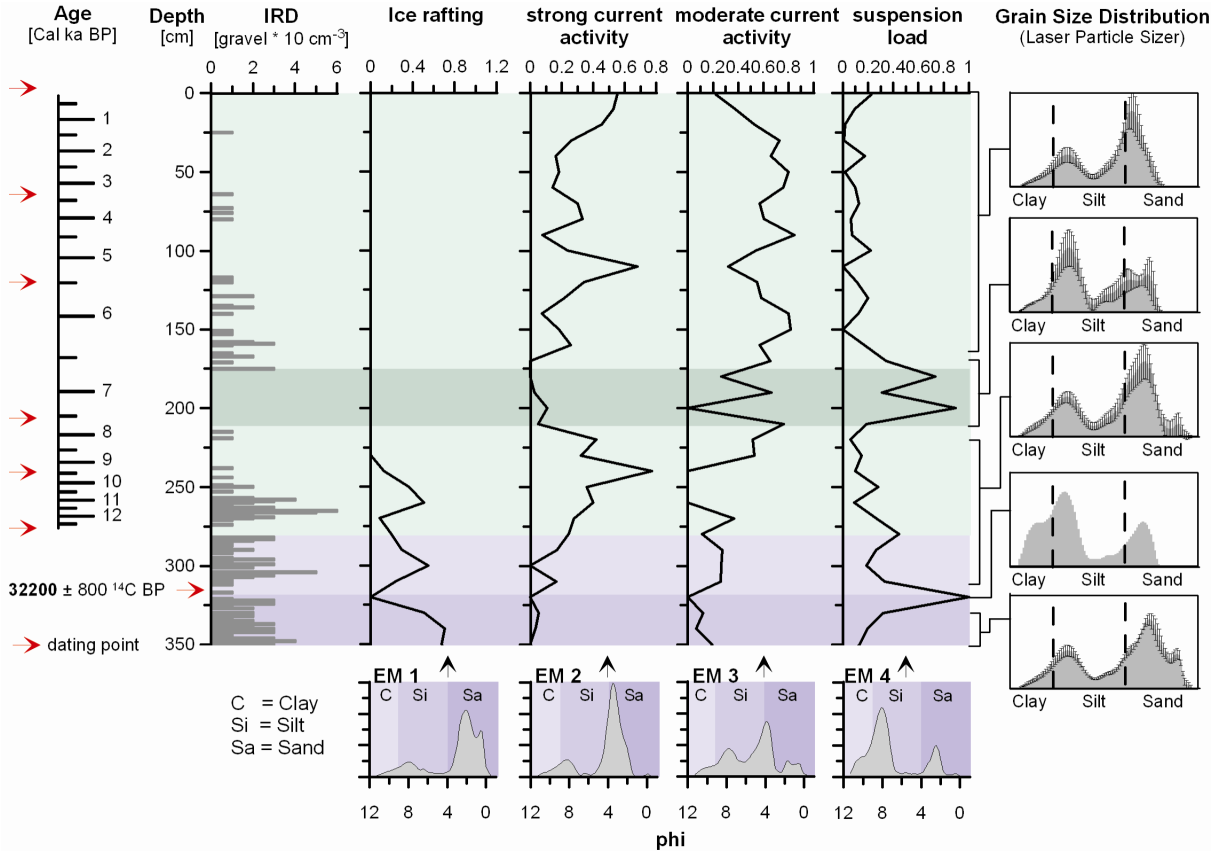

Fig. 3.5 Downcore variation of IRD and end-member scores. Laser-derived grain-size distributions (right) are stacked for sections with similar shape, and variability of each grain-size class within these sections indicated by error bars. Background colours indicate sediment units according to Fig. 3.3.

End-member three is characterized by a trimodal grain-size distribution with modi in the 8, 4 and 1 phi fraction (Fig. 3.5). It is associated with medium bottom-water activity and represents a mixture of processes. It has to be considered, that a one cm thick sample taken from the sediment core integrates seasonal fluctuations of several years. Since transport energy of the water and erosional stress varies with the seasons (Nunes Vaz and Lennon, 1996) the trimodal grain-size distribution could be interpreted as follows: silt-sized grains are transported during the whole year, as most currents are capable of transporting silt-sized material leading to the maximum peak of coarse silt. During late winter, when the site is covered by annual sea ice, bottom-water activity decreases because of reduced brine rejection and fines can be released from the lower sections of the water column within the narrow

basin. In contrast, increased brine rejection connected to formation of new sea ice and production of dense bottom water would favour winnowing of some fines at the bottom of the basin leading to a relative increase of the sand modus. Material of the sand fraction could also be derived from Fram Bank where relatively coarse sediments were discovered (Harris et al., 1998). This material could be eroded by the Antarctic Coastal Current or dense waters and transported into Burton Basin by downslope currents. However, it cannot be excluded, that some proportion of the coarse fraction is due to transport by ice-rafting and melt-out during summer. That would be consistent with findings from Gilbert et al. (2003) who deployed sediment traps near the Mueller Ice Shelf, Antarctic Peninsula, and recognized two to five times higher sand contents during the summer season than during winter, when minor but coarser sand was deposited. Additional indication for connection to ice-rafting can be inferred from the split shape of the sand peak which is very similar to sand in end-member one.

End-member four exhibits high amounts of fine silt and clay (Fig. 3.5). Given a modus at about 8 phi (~ 3 µm), water turbulence or current velocity in the Burton Basin must have fallen to very low values to abet the down-settling of fines, assuming single-grain sedimentation. In the marine environment, however, processes have to be taken into account leading to agglomeration of particles with sizes < 10 µm. Below 10 µm diameter, particles become cohesive because clay minerals, with their charge imbalances, enter the compositional spectrum and Van der Waals forces become significant in particle adhesion (McCave et al., 1995). Eventually, the agglomerated particles would then be deposited at elevated current velocities. Nevertheless, McCave et al. (1995) showed, that deposition of 10 µm particles takes place at velocities lower than 1 cm s^{-1} and that a well pronounced modus of 4 µm (7.9 phi) is indicative for very slow currents (much slower than 5 - 10 cm s^{-1}). In the Burton Basin, modern bottom currents are suggested to flow with velocities of 20-40 cm s^{-1} in times of polynya activity (Ohshima, pers. comm.).

3.5.3 Downcore changes of the depositional environment

The downcore variation of end-member scores is illustrated in Fig. 3.5 and shows major fluctuations which can be correlated with results from other parameters. From 370 cm to 240 cm, including unit cSm, ucSm and the lower part of oDm, sedimentation is dominated by IRD supply, taking place in three major episodes. Ice-supported sedimentation is interrupted at 320 cm, when suspension load settled down forming a clayey horizon. With the end of ice-rafting, strong current activity becomes dominant between 260 cm and 240 cm and is then superseded by moderate bottom-current activity below the laminated section (lDm).

Sedimentation within unit lDm is to a large extent characterized by downsettling of suspension load. In combination with the undisturbed fabric of the sediment this suggests only minor water convection in the Basin. A fourth episode of ice-rafting between 170 cm and 120 cm is solely represented by IRD. The missing signal of end-member one is related to mathematical difficulties of the end-member modelling algorithm to adequately represent grain-size classes with low content or barren of material (Dietze et al., in review). Between 120 cm and 170 cm, the content of sand-sized material is too low and loosely distributed to leave an impact on the end-member derivation. Major contributions to the end-member assemblages between 170 cm and 20 cm are given by end-member two, indicating moderate water convection. Shorter shifts to more turbulent conditions were identified between 120 cm and 100 cm and from 20 cm to the top of the sediment core.

3.5.4 Sources of fine-grained material

Clay-mineral distributions comprise two typical patterns over the sediment core (Fig. 3.6). In unit 1 (cSm) smectite and kaolinite constitute the main components of the clay-mineral assemblages (Fig. 3.6), each by about 40%. Illite accounts for 15%, chlorite is nearly absent (5%). This mineralogical signature indicates an input of fine grained material from local sediment sources (Borchers et al., in press) resembling the mineralogical composition of the Permo-Triassic Beacon Group or its re-worked analogues.

Within the clayey horizon and the overlying unit 2 (ucSm), illite becomes the dominant clay mineral to the cost of smectite. As illites are a typical weathering product of crystalline rocks in the East Antarctic they most likely document an increasing significance of material supported from Prydz Bay by the Antarctic Coastal Current (Borchers et al., in press). Illite abundance then remains high in the upper sections (oDm and lDm) of the sediment core with values ranging between 50% and 60%. It is accompanied by slightly reduced kaolinite abundance of about 25% to 30% compared to the consolidated sediment section. Chlorite concentration increases unobtrusively from 5% in the lower sediment core to 10% in the upper sediment core.

The differentiation between two typical clay-mineral distributions is also represented by illite chemistry, indicated by the 5/10 Å ratio (Fig. 3.6). Supply of illites of predominantly biotitic composition in the till (cSm and ucSm, mean 5/10 Å ratio = 0.25) shifts to illites of muscovitic composition (mean 5/10 Å = 0.38) in the post-glacial part (oDm and lDm) of the sediment core.

In addition to clay minerals, non-clay minerals in the clay fraction can be used to infer on sediment provenance and/or weathering processes. In the diamicton, K-feldspar is enriched

compared to plagioclase. According to Borchers et al. (in press) high contents of K-feldspar support findings from clay minerals, that fine-grained material in the diamicton is of sedimentary origin with a provenance from Beacon sandstone or its re-worked analogues.
A change in the weathering processes or sediment diagenesis can be inferred from the quartz/feldspar ratio that is detached from all other minerals in the clay fraction and also from other parameters investigated. Above 200 cm sediment depth, less feldspar survived compared to quartz than in the underlying section suggesting an intensification of chemical conversion of the deposited material.

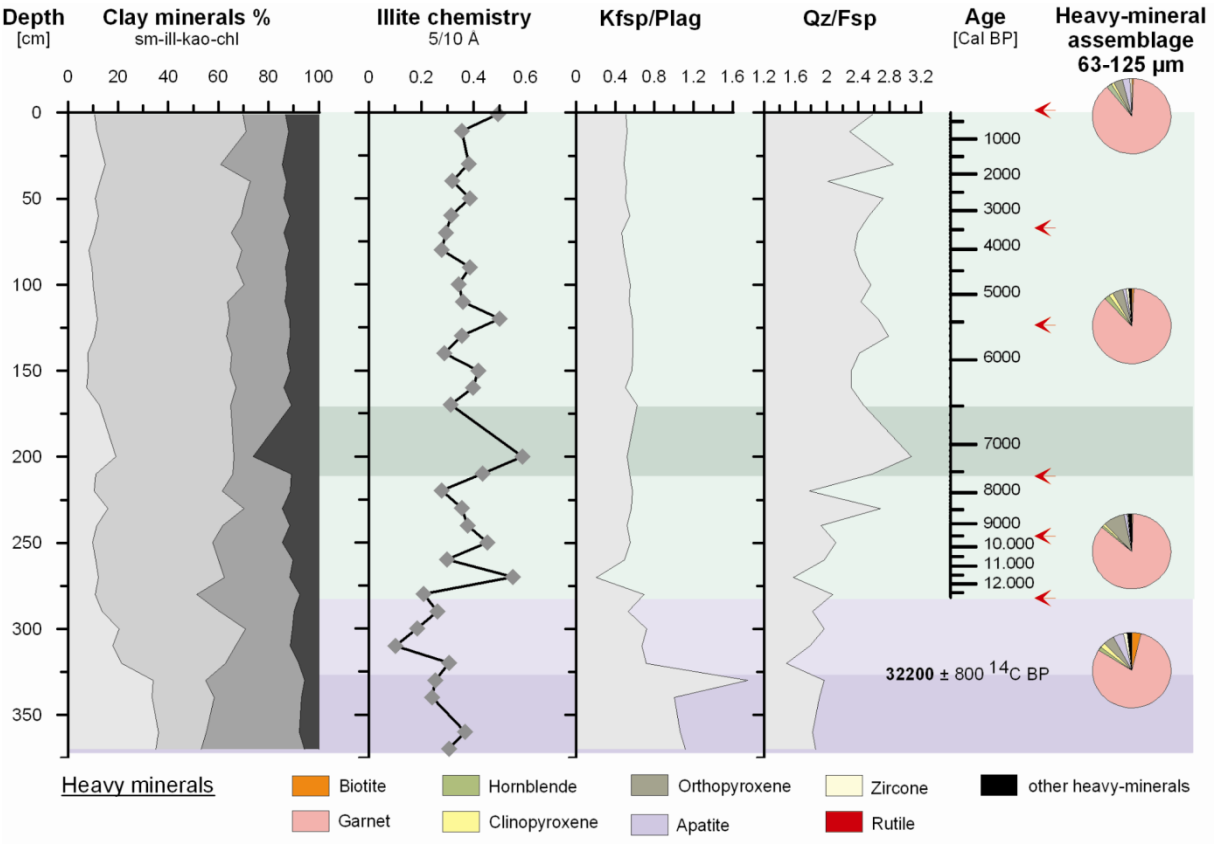

Fig. 3.6 Downcore variation of clay minerals and heavy-mineral assemblages of sediment core PS69/849-2. sm = smectite, ill = illite, kao = kaolinite, chl = chlorite. Background colours indicate sediment units according to Fig. 3.3.

3.5.5 Sources of coarse-grained material

Heavy-mineral assemblages (Fig. 3.6) of four sediment samples reveal a relatively constant distribution over the sediment core indicating a constant origin of ice-transported material. Garnet accounts for nearly the whole heavy-mineral assemblages and is probably derived from Permo-Triassic sediments or their re-worked analogues, where garnet enriched due to

weathering of crystalline rocks of the East Antarctic. Subordinate fluctuations can be observed in the content of orthopyroxene and apatite.

3.6 Late Quaternary environmental history in the Burton Basin

The sediment core from Burton Basin gives insights into environmental changes in the Prydz Bay-MacRobertson area since the last glacial. Our findings provide special insights into the deglacial history and bottom-water formation due to brine rejection associated with Cape Darnley polynya activity. Fig. 3.7 provides a general overview of the palaeoenvironmental development in the Burton Basin and its relation to sea-level rise and changes in the atmospheric pattern.

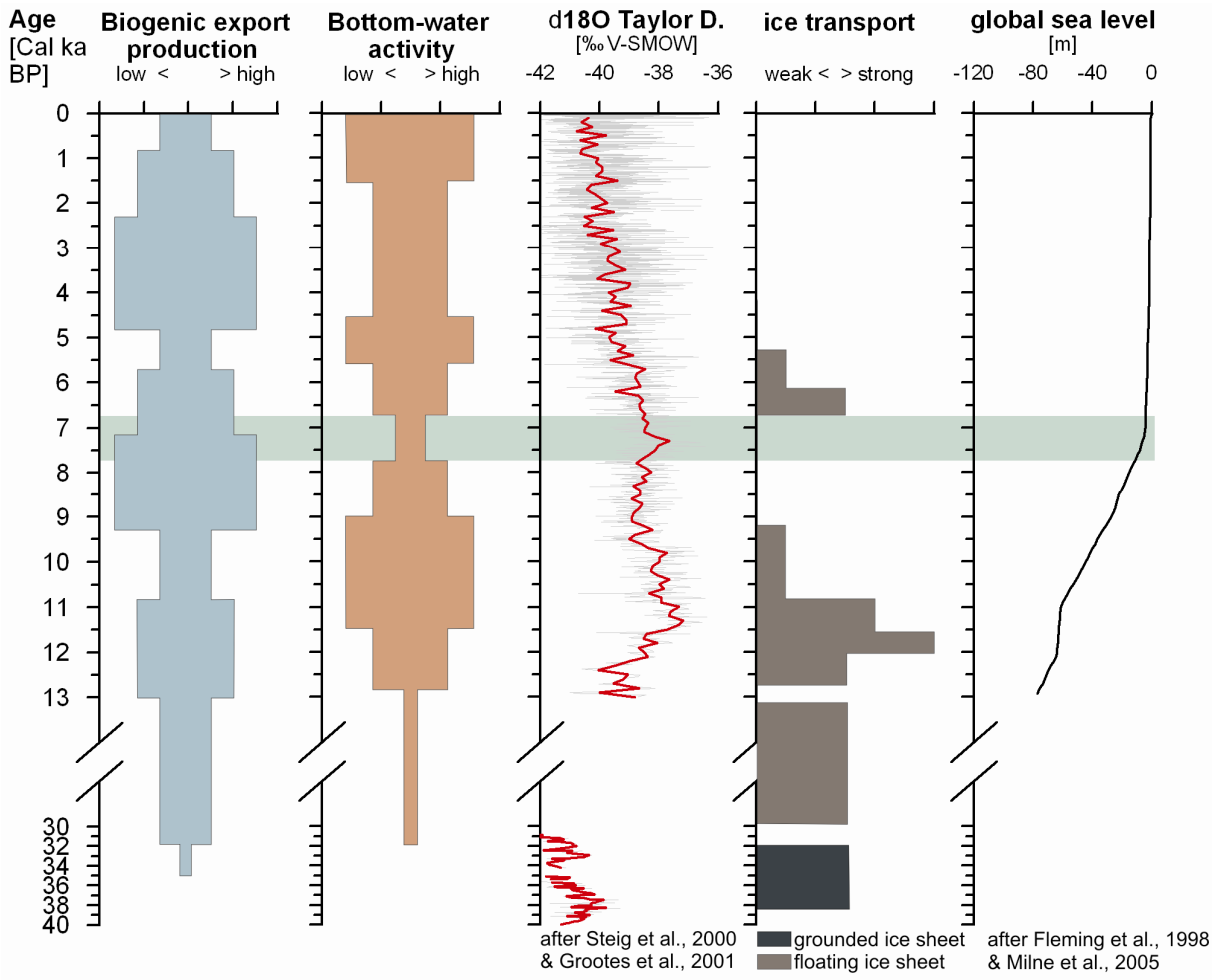

Fig. 3.7 Synthesis of the most important environmental changes in Burton Basin and correlation with ice core data (after Steig et al., 2000 and Grootes et al., 2001) and global sea-level rise (after Fleming et al., 1998 and Milne et al., 2005). Green horizon highlights the mid-Holocene warm event.

3.6.1 Pre-Holocene > 12.8 cal. ka BP

In sediment core PS69/849-2 a pre-Holocene age of the terrigenous sandy muds (cSm and ucSm) is indicated by radiocarbon ages older than 12.8 cal. ka BP. The definite timing of the deposition of the diamicts cannot be clearly determined. Dating of the clayey horizon at the transition from consolidated to unconsolidated sediment, suggests an age for the consolidated sandy mud older than 32.2 ka BP (uncorr. ^{14}C age). This radiocarbon age is, however, considered to be younger due to contamination of bulk carbon with older material. Nevertheless, it cannot be excluded, that the consolidated material was deposited prior to the last glaciation, possibly with a Pliocene/ Pleistocene age similar to the Bardin Bluffs formation of the Pagodroma Group (Borchers et al., in press). Evidence is provided by clay-mineral assemblages, which bear strong resemblance to results from Ehrmann et al. (2003), who investigated the mineralogical composition of the Cenozoic Pagodroma Group (Borchers et al., in press). It seems very likely, that a grounded ice sheet during the Pleistocene supported material from the interior of East Antarctica attended by syngenetic or postgenetic compaction of the deposited material. Lifting of the grounded ice-sheet at 32.2 ka BP (uncorr. ^{14}C age) initially led to deposition of fine-grained material trapped in the basin with subsequent support of diatoms from the open ocean spilled under the floating ice shelf in a low energy, fjord-like environment. Mixing of fine-grained material with different provenances is evident by clay and non-clay minerals. Material supported from local sources was diluted by material originating from Prydz Bay or farther east, with the Antarctic Coastal Current as a possible transport medium (Borchers et al., in press). Floating of the grounded ice and a resulting onset of the Antarctic Coastal Current at the proposed time coincides with a marine transgression into a near-coastal lake basin on the Larsemann Hills around 32 ka (Hodgson et al., 2009). Further implications for an early retreat of grounded ice from central Prydz Bay come from Domack et al. (1998) showing that diamicton similar in character to basal till was deposited prior to 32 ka BP (uncorr. ^{14}C age). Farther to the west, results from raised beaches along the margins of the Syowa Coast in Lützow-Holm Bay give evidence for ice-free conditions and a higher relative sea level in Marine Isotope Stage 3 (MIS 3) prior to the Last Glacial Maximum (Miura et al., 1998).

Despite these consistencies, glaciation history in Prydz Bay and adjacent regions is still under debate. This is, to a large extent, owed to the different local glacial advances and rebound effects, but certainly also a matter of dating problems.

3.6.2 Late Pleistocene to Early Holocene (12.8 – 9.5 cal. ka BP)

The transition from glacial to warmer conditions took place at 12.8 cal. ka BP, when deposition shifted from predominantly terrigenous material to biogenic material with strong IRD supply (Fig. 3.7). The slightly earlier onset of biogenic sedimentation compared to records presented by Leventer et al. (2006) could result from re-deposition of older material and thus some contamination of bulk carbon. This assumption is supported by deposition of diatomaceous muds commencing between 11.2 and 12.2 cal. ka BP at outer Nielsen Basin (Harris and O'Brien, 1998; Sedwick et al., 2001). In Prydz Bay, however, regional recession of the ice margin from the outer shelf commenced latest 13.4 cal. ka BP (Verleyen et al., 2005). Ice retreat from different lake sites in the Larsemann Hills and Vestfold Hills was accompanied with onset of biogenic sedimentation at 12.66 cal. ka BP (Verleyen et al., 2005). Ice retreat from Lake Terrasovoje and Beaver Lake, northern Amery Oasis, commenced 12.5 cal. ka BP (Wagner et al., 2007) and is contemporaneous with rapid retreat of the Lambert Glacier-Amery Ice Shelf system deduced from cosmogenic exposure ages (Fink et al., 2006). Eventually, the timing of the deglaciation corresponds to an Early Holocene climate optimum identified in all East Antarctic ice cores between 11.5 and 9 cal. ka BP (Masson et al., 2000)

In Burton Basin, retreat of the floating ice sheet led to strong supply of ice-rafted material, characterized by high abundances of garnet. This clearly shows that icebergs passing the core location derived from the floating ice sheet originating from MacRobertson Land. An influence of icebergs sourced in Prydz Bay can be excluded.

Whether the regional ice retreat in Prydz Bay and MacRobertson shelf with onset of biogenic sedimentation around 12.8 cal. ka BP and strong IRD supply between 11 cal. ka BP and 9.5 cal. ka BP in Burton Basin was triggered by global sea-level rise or the temperature optimum, is difficult to assess. Several records of sea-level change during the Late Quaternary (Fairbanks, 1989; Fleming et al., 1998) document two events of rapid sea-level rise. Meltwater pulse 1A (mwp-1A) has been dated to 14.2 cal. ka BP and the second event, termed meltwater pulse 1B (mwp-1B), began approximately 11 cal. ka BP (Fairbanks, 1989). The timing and regional correlation of the initial ice retreat with onset of biogenic sedimentation in Prydz Bay and from MacRobertson shelf suggests a response to global sea-level rise associated with mwp-1A. Whether the ice retreat in the East Antarctic was rapid enough to contribute to mwp-1A itself, is discussed elsewhere (Verleyen et al., 2005). Subsequent strong ice rafting was then possibly triggered by mwp-1B. Amendatory reconstructions of eustatic sea level from Huang Peninsula and Tahiti indicate, that sea-level rise between 12 cal. ka BP and 9 cal. ka BP may have been more rapid than assumed, if the single Barbados result at 11.1 cal. ka BP is ignored (Fleming et al., 1998). This may have lead to the major calving event in the study area during that period. The conclusion, that global sea-level rise is more likely the

driver for East Antarctic Ice Sheet retreat than changes in accumulation rate or atmospheric processes is supported by findings from Mackintosh et al. (2007), who compared exposure ages from MacRobertson hinterland with results from marine sediment records retrieved from the continental shelf.

A common feature of post-glacial sediment records from Prydz Bay, MacRobertson Land (Leventer et al., 2006) and the western Antarctic Peninsula (Leventer et al., 2002) is an early Holocene laminated section suggesting elevated biogenic productivity, also observed in sediment core PS69/849-2. Many early post-glacial laminated sediments are characterized by an annual alternation of biogenic and minerogenic compounds which can be explained by the calving bay reentrant model of Domack et al. (2006). According to the calving bay reentrant model, biogenic as well as terrigenous material should be derived from local sources, because outside the bay, the ice sheet is still grounded on the continental shelf. In the case of the sediment record from Burton Basin, however, the laminated section is not varved, because laminations are indistinct and irregular and the number of laminae is too small to represent annual sedimentation according to the age model. A rapid deposition during short time periods of high biogenic productivity is suggested rather than deposition on the basis of seasonal fluctuations of primary production in the surface water. Additionally, clay-mineral assemblages hint to another source of fine-grained material than MacRobertson Land. A possible explanation for the lack of varves could be the shallower geometry of the basin and narrower shape of the shelf preventing the formation of a calving bay reentrant and thus restricted oceanographic conditions (Leventer et al., 2006). Most likely, intense calving of icebergs prior to the deposition of the laminites lead to first temporary open-marine conditions with a proximal position of the calving line. Meltwater input and associated supply of nutrients favoured diatom blooms in the surface waters and rapid deposition of the material.

During or shortly after the deposition of the laminated section turbulent or pulsed water convection commenced in the basin, indicated by grain-size end-member composition and oblique-bedding of diatomaceous muds, with a maximum intensity during the early Holocene warm period around 9.5 cal. ka BP (Fig. 3.7). A widespread early Holocene optimum between 11 cal. ka BP and 9 cal. ka BP is documented in Antarctic ice cores (Masson et al., 2000) as well as in marine sediment records (Ingolfsson et al., 1998; Harris, 2000; Taylor and Leventer, 2003; Leventer et al., 2006).

The high-energy environment in Burton Basin during the early Holocene optimum is probably related to intense formation of Hypersaline Shelf Water (HSSW) triggered by formation of sea ice and associated brine rejection (Harris, 2000, Harris and O'Brien, 1998). Recent observations of Cape Darnley Polynya show strong production of dense water, merging with the Antarctic Slope Current, but also filling deeper parts of Burton Basin

(Tamura et al., 2008; K. Ohshima, pers. comm.). HSSW flow associated to polynya activity is also known to occur in Nielsen Shelf Valley (Harris, 2000).

Intensification of polynya activity and brine rejection between 12.0 cal. ka BP and 9.5 cal. ka BP was favored by the ongoing southward retreat of the calving zone. Brine rejection reached its maximum, when the calving front crossed the site at 9.5 cal. ka BP, indicated by the decrease in IRD. At the same time, a shift to higher primary production inferred from an increase in BSi and TOC also points to onset of open marine conditions (Fig. 3.7). It is assumed, that in the vicinity of the shelf ice edge, an interaction of super-cooling processes underneath the floating ice shelf and brine rejection resulting from sea-ice formation in front of the shelf ice lead to high overturning in the basin, as can be inferred from the extraordinary strength of bottom-water formation at 9.5 cal. ka BP. Strong Hypersaline Shelf Water (HSSW) production between 10.9 and 7.6 ka BP (corrected for reservoir age of 1.3 ka) was also inferred from cross-laminated sediments observed in a sediment core GC12 recovered from Nielsen Basin (Harris, 2000). The corresponding dense-water production in Nielsen Basin (Harris, 2000) and Burton Basin during the Early Holocene invokes strong sea-ice formation all over MacRobertson shelf. Possibly, dense-water production related to an immense Cape Darnley Polynya gained influence as far west as Nielsen Basin. Moreover, active deep-water formation at 10.6 and 9 cal. ka BP was also inferred from diatom associations investigated in core MD03-2601 retrieved off Adelie Coast (Denis et al., 2009b). These findings were supported by variations in Sortable Silt indicating generally high water activity between 11 and 7.4 cal. ka BP (Denis et al., 2009a).

3.6.3 The early to mid-Holocene (9.5 cal. ka BP – 4.9 cal. ka BP)

Ceasing of IRD supply correlating with a reduction of HSSW production from 9.5 cal. ka BP to 7.7 cal. ka BP after the Early Holocene Optimum might reflect longer annual to eventually perennial duration of sea ice that hampers the mobility of icebergs. Contrary, elevated productivity due to intermittent open marine conditions can be inferred from the deposition of sediments rich in BSi and TOC (Fig. 3.4, Fig. 3.7) and an elevated sedimentation rate. Thus, the strong decrease in input of ice-transported material (Fig. 3.7) suggests that the calving front receded to the south relative to the coring site.

On the outer shelf, productivity was variable nearly at the same time, between 9.1 and 10.3 cal. ka BP, maybe due to environmental fluctuations referred to the change from glacial to interglacial conditions (Rathburn et al., 1997). According to GC5 sediment core of Rathburn et al. (1997), on the Antarctic continental shelf, enhanced productivity typically results from changes in sea-ice conditions, stability of the water column, or physical oceanographic

factors, because nutrients are in general not limiting. Trusting radiocarbon dating of both GC5 and PS69/849-2 sediment cores, calving zone rapidly retreated from outer to mid MacRobertson shelf.

During a mid-Holocene event between 7.7 cal. ka BP and 6.6 cal. ka BP, exceptionally low water convection in Burton Basin is inferred from deposition of laminites and rainout of suspension load (end-member 4), suggesting undisturbed sedimentation. These findings imply cessation of brine rejection during this short time interval. To create conditions of low bottom-water activity in the basin, there are generally two possible explanations: 1. perennial thin sea-ice cover or at least long duration of annual sea ice due to a short glacial readvance reduced the formation of new sea ice due to a weak polynya. This coincides with the absence of IRD. Diatom production then would have taken place during short time periods of ice break-up or underneath thin ice with sufficient availability of light. Similar environments were described by Leventer et al. (2003), who suggest high productivity in regions with ice-free conditions for one to two months during the year. 2. In the case of continuing seasonal open marine conditions during warmer times, increased input of fresh water during spring from the floating ice shelf would supply nutrients to favour primary production in the surface water due to ice-edge blooms. Fresh water from rapidly melting sea ice contemporaneously lead to small to negligible vertical density gradients and stratification of the water column in the narrow basin, leading to undisturbed sedimentation. Possibly, production lasted longer than during earlier times. The comparatively short time period of ice built up might then leave a minor signal of dense water production in the sediments. The absence of IRD was referred to rainout of debris in more southerly latitudes or to dilution due to high biogenic input.

Diatom assemblages from sediment cores GC 33 and GC 5 hint to seasonally open water conditions on the outer MacRobertson shelf since 8 cal. ka BP (Rathburn et al., 1997). Results from sediment texture analysis conducted on core GC12 which is affected by downslope transport due to HSSW formation, indicate less downslope activity between 9.3 and 6.6 cal. ka BP. At a similar time, around 7.5 ka BP (uncorr. ^{14}C age), Taylor and McMinn (2001) report the deposition of sea-ice diatom assemblage in sediment core GC1 (Iceberg Alley) suggesting that perennial sea ice had persisted in the vicinity of the GC1 location since that time. Intersections of *Corethron*-rich layers in sediment core GC1 point to mid- to late Holocene high productivity events related to climate optima. In sediment core GC1, most of the *Corethron*-rich layers can be correlated with increases in Mo/Al and U/Al, suggesting anoxic to suboxic conditions during deposition (Sedwick et al., 2001). The most obvious *Corethron*-rich layer, however, post-dates the laminated horizon in sediment core PS69-849-2. It rather coincides with the time period of recurrent IRD supply and slightly decreasing BSi and TOC in Burton Basin. In Prydz Bay, Taylor and Leventer (2003) show that open marine conditions

prevailed during a climatically warm, stable mid-Holocene with high productivity. Contrary, the Amery Ice Shelf (AIS) was suggested to remain stable during that period. It started to retreat at 5.7 ka BP (uncorr. ^{14}C age), following results from sediment cores recovered from below the AIS (Hemer and Harris, 2003). However, radiocarbon dating of these cores is complicated, as surface ages of 6.5 ka BP (uncorr. ^{14}C age) and more display either exceptionally high reservoir ages due to sediment reworking or erosion of surface sediments. As the surface sediment, used to determine the reservoir age, was not verified to be of modern age, it cannot be excluded, that the recession of the AIS took place during the mid-Holocene.

Off Adelie Coast, diatom data of core MD03-2601 (Crosta et al., 2008) hints to warmer temperatures during the mid-Holocene and less extensive sea-ice cover, probably indicating earlier sea-ice breakup and later sea-ice freezing during autumn. This coincides with lower bottom-water formation, such as indicated by a low stand plateau of Sortable Silt between 7.4 and 5 cal. ka BP (Denis et al., 2009a). In the Palmer Deep region, Antarctic Peninsula, a bimodal mid-Holocene climate optimum is recognized by laminated sediments with a first section of elevated diatom abundance between 8.7 and 6.5 cal. ka BP reflecting high productivity (Sjunneskog and Taylor, 2002). Diatom assemblages (Taylor and Sjunneskog, 2002) are interpreted to reflect warm and stable oceanographic conditions during that time with present sea ice that broke up earlier during spring and formed later in autumn. These conditions were related to intrusion of warm, more subpolar surface waters into the area (Leventer et al., 2002)

In conclusion, most sediment records from the East Antarctic point to seasonally open marine conditions during the deposition of the laminated horizon due to warmer climate. Elevated rates of meltwater input from the MacRobertson ice shelf and melting sea ice and hence stratification of the water column therefore seems most likely to produce undisturbed sedimentation. A modelling study of Williams et al. (2002) conducted on the AIS reveals increased sub-ice melting during warming conditions and subsequent meltwater supply, with majority of basal IRD released under the floating ice shelf and not from calved icebergs.

Sediment cores used to compare studies of East Antarctic Holocene environmental change were all located in the vicinity or beneath prominent Antarctic polynyas. The simultaneous shifts in bottom-water production around Antarctica suggest a supraregional parameter possibly impacting polynya activity. The dependence of polynya activity on temperature, precipitation and wind stress was studied by Marsland et al. (2007). Results show that formation of dense water decreases significantly by temperature rise and, secondarily, by increasing precipitation. Whether the probable rise in ocean temperature in Burton Basin was triggered by warmer atmospheric temperatures or incursion of warmer subantarctic waters, cannot be assessed. The question remaining, however, is, why the mid-Holocene event

between 8 and 6 cal. ka BP is only distinctly recorded in Taylor Dome ice core (Masson et al., 2000; Steig et al., 2000; Grootes et al., 2001; Fig. 3.7). A possible explanation is that the near-coastal site of Taylor Dome was most sensitive to ocean-atmosphere interaction, especially to variations in the sea-ice extent.

Whether solar forcing or shifts of the Southern Westerlies are responsible for the environmental shifts during the Early and mid-Holocene, is discussed in detail for the Antarctic Peninsula region (Bentley et al, 2009). Concerning solar forcing, spring insolation which is modulated by precession, could trigger the reduction of sea-ice extent with a positive feedback on reducing albedo which in turn leads to further warming (Timmermann et al., 2009). Whether these mechanisms can be applied also in the Prydz Bay region, is still unclear.

From the end of mid-Holocene event to 5.4 cal. ka BP, last major occurrences of IRD suggest major calving from the floating ice shelf sourced on MacRobertson Land (Fig. 3.7). This corresponds well with still warm conditions (Ingolfsson et al., 1998) and global sea-level rise stabilized between 7 and 6 cal. ka BP (Fleming et al., 1998; Milne et al., 2005). The end of IRD supply might be due to glacial rebound of MacRobertson Land commencing around 6 ka BP (Mackintosh et al., 2007).

The end of the mid-Holocene period, between 5.5 and 4.7 cal. ka BP, is characterized by reduced proportions of BSi and TOC indicating lower productivity (Fig. 3.7). Around 5.2 cal. ka BP, medium productivity in combination with strong water convection in the basin suggest palaeoenvironmental conditions, which resemble those around 9.5 cal. ka BP. Both of these time periods marked the end of warmer-than-modern conditions obviously characterized by strong dense water production due to extensive sea-ice formation. In Nielsen Basin, Harris (2000) relates strong bottom-water activity between 6.5 and 3.6 cal. ka BP to the mid-Holocene climate optimum of Ingolfsson et al. (1998). Further evidences for warmer conditions in Prydz Bay come from Hemer and Harris (2003), who suggest a mid-Holocene retreat of the Amery Ice Shelf at 5.7 ka BP (uncorr. ^{14}C age). However, the interpretation of BSi, TOC and bottom-water activity in sediment core PS69/849-2 rather coincide with a cool phase in the Palmer Deep between 5.5 and 4.7 cal. ka BP, as suggested by Sjunneskog and Taylor (2002).

3.6.4 Mid to late Holocene, (4.9 – 1.5 cal. ka BP)

The period beginning at 4.9 cal. ka BP is characterized by deposition of sediments with elevated proportions of BSi and TOC under moderate bottom-current activity (Fig. 3.7).

This partly corresponds to results of Berg et al. (in review), although increased TOC around 5.7 cal. ka BP is not supported by BSi there, contrary to results from sediment record PS69/849-2. On Rauer islands, milder climate conditions with less sea ice and increased meltwater inflow are anticipated between 5.7 and 3.0 cal. ka BP. Between 2.7 and 3.1 ka BP (corrected for reservoir age of 1.3 ka), the outer Burton Basin experienced long intervals of open water and less extensive summer pack ice with higher production than today due to elevated meltwater input (Rathburn et al., 1997). Off Adelie Land, Denis et al. (2009b) found that the efficiency of the biological pump reached highest Holocene values between 5 and 1 cal. ka BP. They identified higher levels of both the macronutrient and the iron pool younger than 5 cal. ka BP, concomitant to decreasing nitrate relative utilization.

3.6.5 Late Holocene (Neoglacial, since 1.5 cal. ka BP)

During the Late Holocene, productivity proxies show slightly decreased proportions. Bottom-current activity strongly increased (Fig. 3.7). This development reflects increased annual sea-ice production and duration due to cooler climate and was also observed in outer Burton Basin starting 2.7 ka BP (corrected for reservoir age of 1.3 ka; Rathburn et al., 1997). Elevated bottom-water production due to sea-ice formation was possibly triggered by enhanced katabatic winds (Smith et al., 2010). On MacRobertson shelf, late Holocene cooling and longer sea-ice duration since 2.6 ka BP (corr. ^{14}C age) are inferred from diatom assemblages (Taylor and McMinn, 2001). Similar evidences were found in Prydz Channel (Taylor and Leventer, 2003). Additionally, ice advances have been observed in several records from coastal regions in East Antarctica (Cremer et al., 2003; Ingolfsson, 2004; Hall, 2009). On Rauer islands, late Holocene cooling since 1.7 cal. ka BP is accompanied by decreased productivity, though diatom assemblages argue against further increase in the duration of the sea-ice cover during summer (Berg et al., in review). A late Holocene cooling is widely recognized in both East and West Antarctic records and is termed Neoglacial (Taylor and Sjunneskog, 2002). Accordingly, palaeoenvironmental changes observed in Burton Basin may result from circum-Antarctic shifts in palaeoclimate and palaeoceanography.

3.7 Conclusions

The paper highlights major changes in the palaeoenvironmental conditions in the Burton Basin. These changes probably correspond to local shifts in the depositional setting and climate which were not always synchronous to adjacent regions. Important findings include:

1. The ice sheet originating from MacRobertson Land was not grounded since 32 ka BP (uncorr. ^{14}C age). Little current activity was probably due to either some perturbations induced by a weak Antarctic Coastal Current or by some CDW spilled over the shelf break.

2. Deglaciation commenced at coring site around 12.8 cal. ka BP, accompanied by increase in sedimentation rates and biogenic production. Continuing supply of IRD suggests the calving front was located in the vicinity and receded farther south from the coring site approximately 9.5 cal. ka BP, when the shift from deglacial to interglacial conditions occurred. At the same time, marking the end of the Early Holocene Optimum, strong bottom-water activity is referred to extensive sea-ice formation and associated brine rejection in connection with supercooling of waters underneath the proximal floating ice shelf.

3. During the mid-Holocene warm period (hypsithermal) a single event between 7.7 and 6.7 cal. ka BP with high biogenic production and ceasing bottom-water activity is superimposed on the general trend and provides evidences for reduced sea-ice formation. This is possibly related to high meltwater input, longer open-marine conditions and later ice built-up during the year. As a result, the signal of brine rejection was too weak to leave an impact on the terrigenous sediments. The timing of the mid-Holocene events correlates nicely with the mid-Holocene warm peak in near-coastal Taylor Dome ice core. Although the ice core is far from Burton Basin, it rather reflects the ocean-ice-atmosphere interaction and possible high sensitivity to sea-ice extent. The latter showed a similar pattern in Ross Sea and off Adelie Land.

4. At the end of this mid-Holocene warm period, around 5.2 cal. ka BP, there was a second optimum in bottom-water formation. The inferred palaeoenvironmental conditions obviously resembled to those around 9.5 cal. ka BP. IRD input finally ceased 5.5 to 6 cal. ka BP, probably due to a stabilized global sea level and commencing glacial rebound.

5. Around 4.9 cal. ka BP, mild climate conditions again favoured productivity and moderate bottom-water formation. Since 1.5 cal. ka a shift to widely recognized neoglacial conditions BP with enhanced sea-ice formation and associated brine rejection was recognized.

Downcore variations in biogenic production and bottom-water formation revealed three long-term cycles, characterized by 1. Warm climate with probably high spring insolation lead to high biogenic production with strong diatom blooms during spring. This was accompanied with moderate bottom-water activity. 2. At the end of warm periods or when cooler conditions commenced, respectively, enhanced bottom-water production was

observed, maybe due to earlier and more extensive sea-ice formation. Lower biogenic production suggests shorter periods of biogenic production.

In general, the above-mentioned findings are in good agreement with results from other records along the East Antarctic margin. Apart from dating uncertainties, discrepancies in the timing of climate events may reflect different local responses to atmospheric or oceanic circulation patterns or different configurations and responses of glacial features to climate variations.

Acknowledgements

This investigation was funded by Deutsche Forschungsgemeinschaft priority program SPP 1158 through grant DI 655/3-1. We thank the officers and crew of RV Polarstern and chief scientist H. W. Hubberten for their competent help in collecting the samples. R. Froehlking, N. Lentsch and U. Bastian are acknowledged for technical assistance. The manuscript benefited from comments and constructive suggestions of Sonja Berg and Bernd Wagner. Keiichiro Ohshima gave important insights into modern polynya activity and bottom-water flow paths on MacRobertson shelf.

4. Sedimentation on the continental slope off MacRobertson Land reveals major fluctuations of the East Antarctic Ice Sheet during the Pleistocene.

Andreas Borchers[1]*, Thomas Frederichs[2], Oliver Esper[3], Gerhard Kuhn[3], Hannes Grobe[3], Bernhard Diekmann[1]

[1]*Alfred Wegener Institute for Polar and Marine Research, Research Unit Potsdam, Telegrafenberg A43, 14473 Potsdam, Germany*

[2] *University of Bremen, Geosciences, Postbox 330440, 28334 Bremen, Germany*

[3] *Alfred Wegener Institute for Polar and Marine Research, Research Unit Bremerhaven, Columbusstrasse, 27568 Bremerhaven, Germany*

*Corresponding author

Abstract

Sediment core PS69/851-1, recovered from the continental slope off MacRobertson Land, provides insights into short-term changes in the Pleistocene glaciomarine palaeoenvironment in the Prydz Bay region. A multi-proxy study was applied to document changes in the depositional setting as well as in the provenance of current-transported and ice-rafted material in order to unravel the glacial history of the Lambert Glacier.

We found that deposition during the last 1.3 Ma was characterized by alternating sequences of hemipelagic sedimentation with dispersed input of ice-rafted material, fine-grained units accumulated from meltwater plumes and/or contourite currents and coarse layers reflecting intense calving from retreating ice streams. A prerequisite for the dynamic behaviour of the Lambert Glacier-Amery Ice Shelf system during the middle and late Pleistocene was the change from a terrestrial-based feature to a marine-based feature around 1.25 Ma. Thereafter, two episodes of deglaciation occurred around 1 Ma during the mid-Pleistocene, and during or shortly after the last interglacial. Differences in the sedimentological and mineralogical characteristics between both events display changes in the drainage pattern of the Lambert Glacier-Amery Ice Shelf system during the late Pleistocene.

Keywords: Prydz Bay, Lambert Glacier, clay minerals, heavy minerals, ice sheet dynamics, IRD

4.1 Introduction

The Antarctic continent plays a key role in the global climate system because ice sheets there constitute the largest fresh water reservoir on Earth. Today, about 16% of the East Antarctic Ice Sheet is drained through the Lambert Glacier-Amery Ice Shelf system, the world's largest fast flowing ice stream, to the north into Prydz Bay (Fricker et al., 2000).

During the Neogene and Quaternary, the Lambert Glacier experienced some extreme advances and material was transported by grounded glaciers to the continental shelf break (Cooper and O'Brien, 2004; O'Brien et al., 2004), where they built up the Prydz Mouth Fan. Most of the successions there had formed by debris flows, turbidity currents and subordinary hemipelagic sedimentation (Passchier et al., 2003; Cooper and O'Brien, 2004). Results from a drift deposit which is stronger influenced by contour currents reflect the palaeoenvironmental history of the Prydz Bay region during the last 5.2 Ma (Passchier, 2007). On the continental shelf and along the western flank of the ice stream, the dynamic behaviour of the Lambert Glacier lead to deposition of predominantly diamictites separated by erosional structures (Barron et al., 1991; Cooper et al., 1991a; Hambrey et al., 1991) and glaciomarine sediments (e.g. Hambrey and McKelvey, 2000a). Results from previous studies indicated that the last major retreat of the Lambert Glacier has occurred around 1 Ma (Passchier et al., 2003; Cooper and O'Brien, 2004; Passchier, 2007; Villa et al., 2008). After this period, topographically controlled (Taylor et al., 2004) shifts in the drainage pattern of the Lambert Glacier-Amery Ice Shelf system prevented the ice stream to reach the shelf edge (O'Brien et al., 2007).

In this study, we investigate a sediment core recovered from Wild Drift situated on the continental slope off MacRobertson Land in the vicinity of Prydz Bay. The goal was to complement results from previous ODP investigations by giving insights into the short-term palaeoenvironmental history of the Prydz Bay region during the last 1.3 Ma. Within this study, we reconstructed the glaciomarine depositional regime by sedimentological means to infer on the activity of ocean currents and iceberg calving to provide clues on the dynamics of the Lambert Glacier-Amery Ice Shelf system. The use of geochemical and mineralogical parameters supported this approach by highlighting periods of high productivity and by adding information about the provenance of current-derived and ice-transported material.

4.2 Regional setting

Prydz Bay (Fig. 4.1) is situated at the northern end of the Lambert Graben which extends about 500 km inland and cut into the East Antarctic craton. The Lambert Graben represents the failed arm of a triple junction associated with breakup of India and Antarctica/Australia

during at least early Cretaceous times. It cut into mostly high-grade Precambrian metamorphic and intrusive rocks that crop out e.g. in the Prince Charles Mountains (PCM) along the western flank of the rift (Tingey, 1991).

Further isolated outcrops of basement rocks in the region comprise Cambrian granites and mafic dykes (Tingey, 1991). Since the initiation of the rift, the Lambert Graben and the Prydz Bay sedimentary basin filled with 5 km to 12 km thick sedimentary sequences (Cooper et al., 1991b) comprising Permo-Triassic alluvial sediments, Cretaceous coals and Cenozoic glacial sediments (Cooper et al., 1991a; Turner, 1991; Hambrey and McKelvey, 2000a) which also crop out in Amery Oasis (Fielding and Webb, 1996; McLoughlin and Drinnan, 1997).

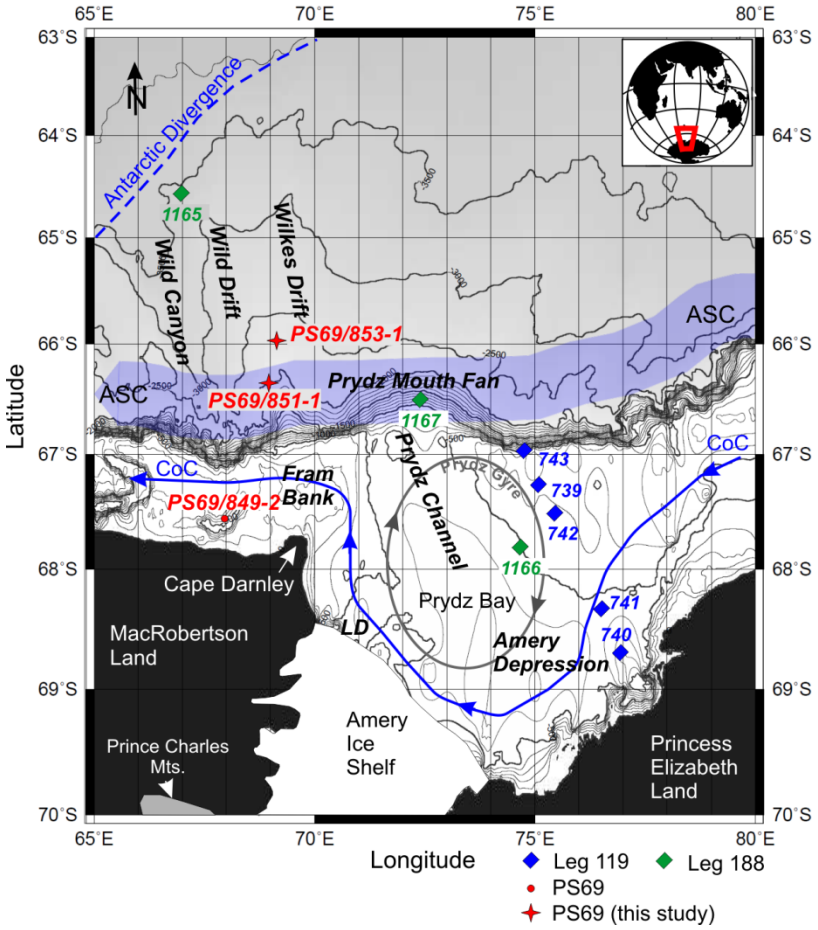

Fig. 4.1 Topographic and oceanographic overview of the study area with highlighted positions of previous investigations. LD = Lambert Deep. ASC = Antarctic Slope Current. CoC = Antarctic Coastal Current.

Today, the Lambert Graben is covered by the Lambert Glacier-Amery Ice Shelf (Fig. 4.1) system that drains about 16% of the East Antarctic Ice Sheet (EAIS; Fricker et al., 2000). The drainage system established during the Cenozoic with glaciations of the PCM at least since the Oligocene (Hambrey and McKelvey, 2000a). During the last five million years, the Lambert Glacier advanced several times to the continental shelf (Cooper and O'Brien, 2004). This lead to a morphology of the Prydz Bay continental margin characterized by a highly

eroded continental shelf, a trough-mouth fan on the slope and canyons and large drift deposits on the continental rise (Kuvaas and Leitchenkov, 1992).

Drift deposits on the continental rise therefore reflect the influence of ice activity and ocean currents on the depositional environment through the Cenozoic (Cooper and O'Brien, 2004). Sediment cores investigated in this study were taken from the Wild Drift (Fig. 4.1) located on the continental rise off MacRobertson Land. Sediments of Wild Drift were rapidly deposited during the Cenozoic on the flank of the long-established Wild Canyon system (Fig. 4.1) which originates from near the western side of Prydz Bay (Cooper and O'Brien, 2004).

Ocean-surface circulation in the study area is governed by the westward flowing Antarctic Coastal Current (Fig. 4.1) which is forced by the polar easterlies. In Prydz Bay, this current is deflected by the cyclonic Prydz Gyre with cold-water inflow from the east and outflow along the west side of the bay (Smith et al., 1984; Nunes Vaz and Lennon, 1996). The importance of Prydz Bay and adjacent shelf areas regarding dense-water production is still under debate. Whereas Smith et al. (1984) postulated that in Prydz Bay only little dense water is produced due to its geography and bathymetry, modern investigations of e.g. Tamura et al. (2008) point to considerable dense-water formation especially west of Cape Darnley (Fig. 4.1) associated with polynya activity. North of the shelf break, deep-water circulation is associated with three oceanographic features (Fig. 4.1): the Antarctic Slope Current, a cold and dense contour current following the continental slope to the west (Bindoff et al., 2000); the Antarctic Divergence, which is the boundary between eastward and westward moving currents, characterized by producing cyclonic gyres over the slope and inner rise and the Antarctic Circumpolar Current with most of its water transport associated with Circumpolar Deep Water (CDW; Orsi et al., 1995). Kuvaas and Leitchenkov (1992) showed that sediment deposition in the Prydz Bay region is controlled by the interaction of downslope (turbidity currents, debris flows) and along-slope currents (contour currents).

4.3 Material and Methods

Sediment cores PS69/851-1 and PS69/853-1 were recovered on a transect down Wild Drift located on the continental slope off MacRobertson Land. Diractly after splitting the core segments, core descriptions were made. Sediment cores comprised terrigenous muds to sandy muds nearly barren of microfossils with colours ranging from grey to reddish grey to greenish grey. In contrast to the sediment records from the slope positions, PS69/852-1 appeared more coarse-grained. Sediment core PS69/851-1 was sampled in 10cm intervals, core PS69/852-1 in 5 cm intervals and PS69/853-1 was only investigated by non-invasive means.

4.3.1 Magnetic volume susceptibility (k)

Susceptibility was measured on unopened 1-m core segments using a GEOTEK Multi-Sensor-Core-Logger (MSCL) with the following sensor and parameter settings: Bartington sensor MS-2C, loop sensor diameter 14 cm, alternating field frequency 565 Hz, counting time 10 s. Results are given in 10^{-5} SI.

4.3.2 X-radiographs

X-radiographs were taken from 25*10*1 cm sediment slices and photographed with a HP Cabinet X-Ray System, Faxitron Series (radiation about 3 minutes, 40 kV, 4 mA). The amount of ice-rafted debris (IRD) was obtained following the procedure described by Grobe (1987). Additionally, sediment texture (bedding characteristics, erosion horizons, lamination, bioturbation) was identified.

4.3.3 Grain-size analysis

Two sediment samples of each sample depth were treated with 10% hydrogen peroxide solution for disaggregation and removal of organic material. One sediment sample was wet-sieved through 2 mm and 63 µm meshes to separate gravel and sand from the fine fraction. Clay and silt fractions were split by Stokes' Law settling using Atterberg tubes. The weight percentages of the four major grain-size classes were calculated.
To the second sample, one spattle of tetra-sodium diphosphate decahydrate was added for disaggregation. The material was split into eight subsamples by use of a rotary sample divider (Fritsch laborette 27). Four subsamples were measured with a Beckman Coulter Laser Particle Sizer LS200 (comprising 92 grain-size classes) and stacked.

4.3.4 Bulk and clay-mineral composition

The bulk mineralogical composition of sediment samples was determined by Philips PW1830 step scan measurements (CoK-alpha radiation, 40 kV, 40 mA, 3-100° 2T at 0.02° 2T /1 sec) on random powder mounts.
Clay-mineral analysis of preferentially oriented clay mounts followed standard procedures described in Ehrmann et al. (1992) and Petschick et al. (1996) and was conducted on a Philips PW1820 diffractometer system (CoK-alpha radiation at 1600 W, 40 kV, 40 mA). Mineral proportions of the main clay-mineral groups smectite, illite, kaolinite and chlorite were

determined with the help of MacDiff 4.2.5 program (freeware, http://www.geologie.uni-frankfurt.de/Staff/Homepages/Petschick/Classicsoftware.html) from weighted peak areas (Biscaye, 1965) recorded in the X-ray diffractograms. The 5/10 Å ratio gives evidence of the illite octahedral composition. According to Esquevin (1969) low 5/10 Å values (< 0.15) are characteristic of Fe, Mg-rich (biotitic) illites, whereas values exceeding 0.4 corresponding to a muscovitic composition caused by substitution of Mg and Fe by Al. Hornblende (8.4 Å) and calcite (3.03 Å) were normalized against quartz (3.34 Å) and the ratio of kalifeldspar/plagioclase was calculated (3.24 Å/3.19 Å).

4.3.5 Heavy-mineral analysis

Heavy-mineral analysis followed the procedures explained in Borchers et al. (in press). The proportions of the main constituents (biotite, garnet, hornblende, clinopyroxene, orthopyroxene, apatite, zircon, rutile and others) were calculated as percentages of all counted transparent and unweathered grains.

4.3.6 Wet-geochemical analysis

Wet geochemical analysis was performed on 13 discrete bulk sediment samples of core PS69/851-1 to analyze the distribution of major elements (Al, Ca, K, Ti, Fe, Ba). Additionally, one standard sample (GSD-5) and one blank sample (ultra-pure water) were analyzed to prove the accuracy of the analysis and to exclude contamination of the samples during preparation. In a Teflon crucible, 100 mg of ground sediment was digested with 3 ml nitric acid, 4 ml fluoric acid and 3 ml perchloric acid. The crucibles were put under a pressure-resistant seal and the samples were boiled at 170°C for 22 hours to dissolve all particular matter. Subsequently, the acids were removed by vaporization due to heating the samples to 180°C for five hours. Afterwards, 1 ml nitric acid and 5 ml ultra-pure water were added to dissolve the residual and the solution was filled up to 50 ml (giving a dilution factor of 1:500).

Each dissolved sample was analyzed with an Inductively Coupled Plasma Optical Emission Spectrometer (ICP-OES, Perkin Elmer Optima 3000XL). Analysis of the standard sample revealed errors between 0% and 12.7% for each major element. The major elements Al, Ca, K, Ti, Fe are given in wt.%, whereas Ba is given in ppm.

4.3.7 XRF Core Scanning and calibration with ICP-OES results

To obtain continuous information about the distribution of major elements in sediment cores PS69/851-1 and PS69/853-1, the archive halves were measured at 1 cm intervals using an AVAATECH non-destructive X-ray Fluorescence Core Scanner (XRF-CS). Elemental XRF peak area intensities were measured in total counts per second (cps) using the following device settings depending on the investigated elements: 10 kV, 300 µA, counting time 30 s (Al, Ca, K, Ti, Fe); 50 kV, 1000 µA, 60 s (Ba).

For a detailed geochemical study of sediment core PS69/851-1, the XRF-CS data of the core was calibrated with the help of the geochemical composition of discrete samples obtained from ICP-OES measurements to eliminate the effects of water content, grain-size variations and surface roughness on XRF-CS measurements (Weltje and Tjallingii, 2008). The logarithm of the total counts of Al, Ca, K, Ti, Fe and Ba obtained from XRF-CS and the logarithm of the proportion of Al, Ca, K, Ti, Fe and Ba obtained from ICP-OES for each reference sample was calculated and a linear regression for each element was performed (Fig. 4.2). After that, the element-dependent regression formula was used to transform the total counts of each element into wt.%.

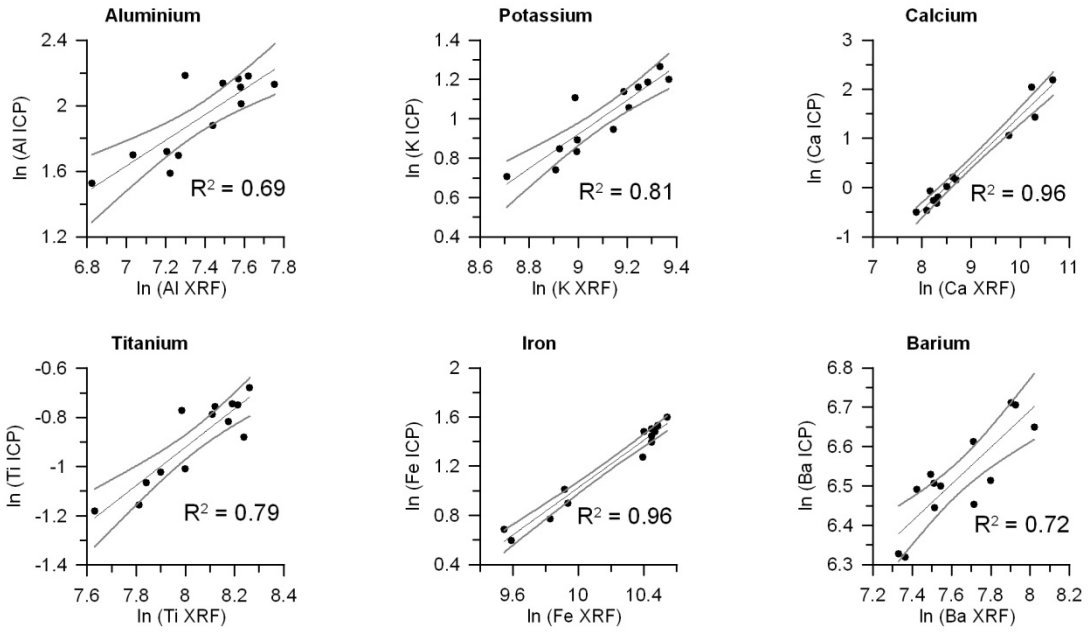

Fig. 4.2 Correlation of XRF data and ICP-OES reference data for each single element with 95% confidence interval indicated. Coefficients of determination range between R^2=0.69 and R^2=0.96. Highest reliability is suggested for calcium and iron.

4.3.8 Palaeomagnetics and stratigraphy

Age-depth relations for sediment cores taken from the continental slope were established by the combination of magnetic parameters with diatom data and correlation of these sediment cores with the help of magnetic susceptibility, XRD and XRF with ODP Leg 188 core 1165 (Fig. 4.3; Warnke et al., 2004).

Palaeomagnetic investigations (determination of intensity and direction of the Earth's magnetic field in the past) were conducted on discrete oriented samples taken at 5 cm intervals from cores PS69/851-1, PS69/853-1 with 2.2 cm*2.2 cm*1.8 cm cubic plastic boxes. The analysis was performed in the palaeomagnetic laboratory at the Departement of Geosciences, University of Bremen. Palaeomagnetic directions and magnetization intensities were measured with the help of a cryogenic magnetometer (model 2G enterprises 755 HR). Magnetization intensities included the determination of the natural remanent magnetization (NRM) and subsequent demagnetization treatment involving 16 steps with a peak alternating field of 100 mT and a biasing DC field of 40 µT to measure the anhysteretic remanent magnetization (ARM). A detailed vector analysis was applied to results to determine the characteristic remanent magnetization (ChRM).

In a first step, the inclination was used to correlate the Brunhes/ Matuyama boundary of sediment cores PS69/851-1, PS69/853-1 and ODP core 1165, which is situated above the drop of most prominent calcite deposition (Fig. 4.3, Florindo et al., 2003; Warnke et al., 2004). The Brunhes/ Matuyama boundary in all three cores lies in a similar depth suggesting comparable linear sedimentation rates of about 0.6 - 0.7 $cm*ka^{-1}$ at all core positions during the last 780 ka. In contrast to core 1165, the Jaramillo event in our sediment cores was not conflated with the Olduvai and could be clearly identified between 600 - 650 cm (PS69/853-1) and 480 - 550 cm (PS69/851-1). The Matuyama (C1r.2r) is well preserved in contrast to the ODP core. Relative palaeointensities of cores PS69/851-1 and PS69/853-1 were correlated with the standard curve SINT-2000 (Valet et al., 2005). Due to the fact that our sediment cores are barren of microfossils over nearly the whole core lengths, only two diatom dates from core PS69/851-1 could be obtained showing good agreement with the palaeomagnetic data. Nevertheless, erosion horizons such as determined in the X-radiographs suggest at least smaller hiatus maybe caused by non-deposition or erosion of sediment due to the Antarctic Slope Current. The temporal extent of such hiatus could not be determined due to the lack of further age data. Decoupled correlation of susceptibility, calcite contents (XRD) and calcium counts (XRF-CS), however, show good agreements between the age-depth models of both sediment records. It further suggests relatively continuous sedimentation at least during the Brunhes.

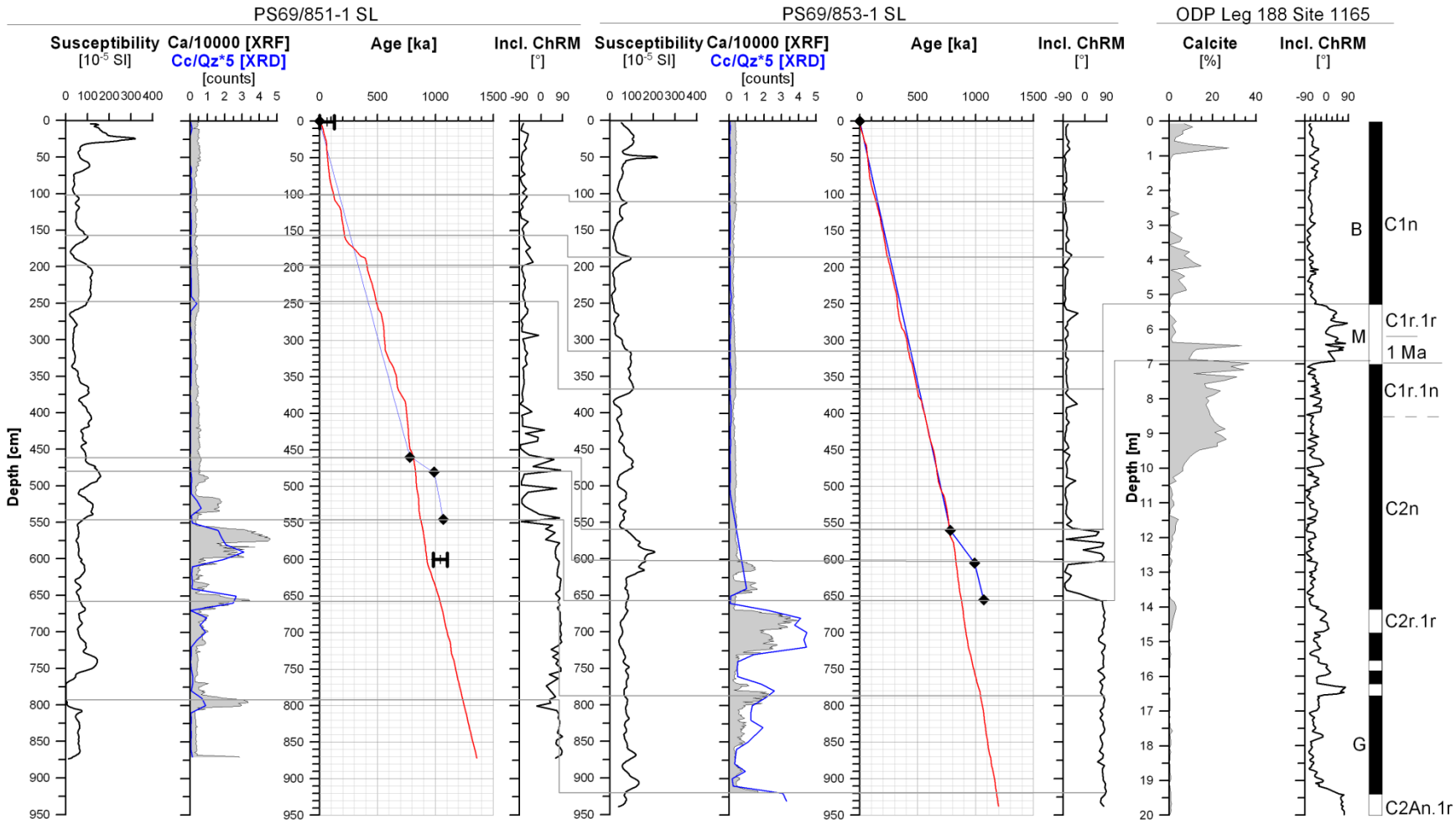

Fig. 4.3 Correlation of sediment cores PS69/851-1 (this study) and PS69/853-1 with ODP reference core 1165. Most prominent is the Brunhes (B)/Matuyama (M) boundary situated between 450 cm and 550 cm in all sediment cores, above the most prominent calcite deposition. In contrast to ODP core 1165, the geomagnetic Jaramillo polarity event could be clearly identified in both sediment cores from the continental slope. Further relative correlation between both PS69 cores was conducted using calcite content (blue line), calcium content and susceptibility (grey lines). Diatom age intervals in sediment core PS69/851-1 are indicated by black horizontal bars.

4.4 Results

4.4.1 Magnetic volume susceptibility (k)

Susceptibility in sediment cores PS69/851-1 und PS69/853-1 show mean values of $70*10^{-5}$ SI (Fig. 4.3) which is in the range typical of sediments, such as sand, clay and mud, taking into account the water content of marine sediments. Several optima can be observed with k exceeding $100*10^{-5}$ SI and maxima reaching up to $320*10^{-5}$ SI. A comparable down-core pattern of k of cores 851 and 853 allowed for a correlation of both sediment records.

4.4.2 IRD and sediment texture

Highest concentration of IRD with up to 5 grains*10 cm^{-3} was identified in the uppermost 50 cm of sediment core PS69/851-1 (Fig. 4.4). A more or less continuous input of 1-2

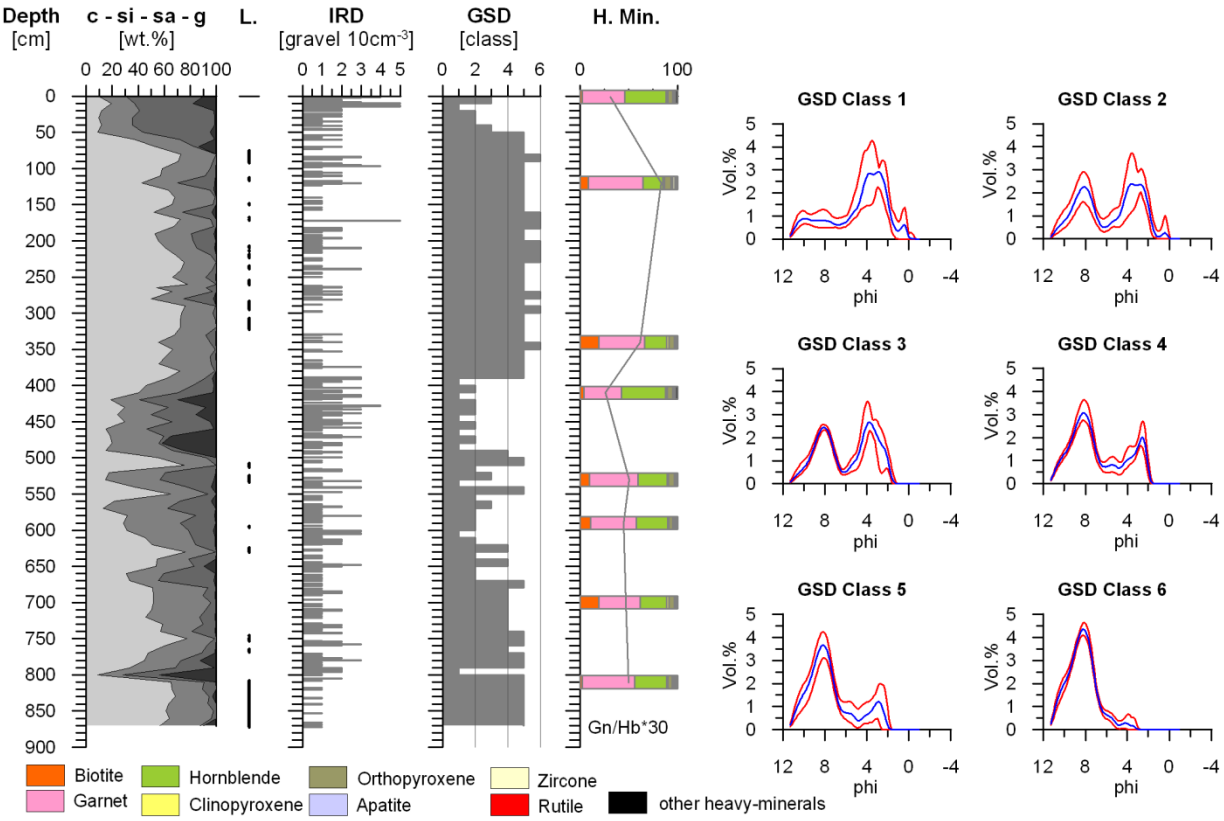

Fig. 4.4 Fluctuations in the depositional regime indicated by grain-size distribution from wet-sieving (c-clay, si-silt, sa-sand, g-gravel), sediment texture (L-lamination) and ice-rafted debris (IRD). High-resolution grain-size distributions (GSDs) obtained from Laser Coulter Counter measurements were grouped to six GSD classes. Their temporal distribution generally suits the results from wet-sieving with predominance of GSD classes one and two in core sections with high IRD and sand content. Heavy-mineral distributions (H. Min.) constitute garnet and hornblende the major minerals. Low garnet/hornblende ratios compared to the overall trend are observed in core sections with coarser sediments.

grains*10 cm^{-3} is regarded as the typical background sedimentation from icebergs crossing the core position. A distinct optimum in IRD deposition is observed between 400 cm and 500 cm. The mapping of sediment texture revealed several laminated horizons which typically occur in core sections barren of IRD and with increased contents of fine material (Fig. 4.4). Additionally, the position of possible hiatus could be identified by erosion marks at 70 cm, 175 cm, 260 cm, 390 cm, 485 cm, 515 cm, 555 cm, 620 cm, 635 cm, 645 cm, 755 cm, 805 cm and 870 cm.

4.4.3 Grain-size distributions

Grain-size data obtained from sieving displays major fluctuations in the content of clay, sand and gravel (Fig. 4.4). These observations are supported by high resolution grain-size distributions (GSDs) derived from Laser Particle Sizer measurements (Fig. 4.4). GSDs with similar shape were grouped, providing six GSD classes. GSDs assigned to class one and two show a trimodal distribution and differ from others by delivery of material < 2 phi. In class 1, additionally, the fraction > 6 phi is only weakly pronounced. GSD classes three to five show more or less bimodal GSDs. Class three comprises a similar content of material in the fractions < 6 phi and > 6 phi with a distinct coarse modus at four phi. It thus represents the transition from classes one and two to classes four and five, where the coarse modus is at 2.5 phi and the content of fine sand gradually decreases. This development continues for GSDs belonging to the nearly unimodal class six, where the 2.5 phi modus is only a residual.

Downcore, two intervals characterized by input of coarse material can be identified, which is in agreement with IRD disposal (Fig. 4.4): Between zero and 50 cm, grain-size distribution comprises sand contents up to 50% with subordinate deposition of gravel. In core section 420 cm - 670 cm, sand content ranges between 20% and 40% with high proportions of gravel in the top part (420 cm - 500 cm). In both intervals, GSDs one and two prevail.

In the rest of the sediment core, the fine fraction dominates. Between 50 cm - 390 cm and 800 cm - 870 cm, mean clay content is 60% and GSDs are dominated by those assigned to class five and six. These core sections also show discontinuous IRD supply. In the interval between 670 cm and 800 cm proportions of sand and especially silt are increased to the cost of clay (mean content 50%) and GSD class four is dominant, accompanied by continuous supply of IRD.

4.4.4 Mineralogical composition of the fine sand fraction

Heavy-mineral distributions (Fig. 4.4) to a great extent are composed by garnet (40% - 55%) and hornblende (20% - 45%). Garnet/ hornblende ratio ranges between 0.9 and 2.8 with low values being recognized in core sections with increased input of IRD and dominance of coarse material in the grain-size distributions. In some samples, considerable amounts of biotite were determined reaching maximum concentrations of 20%. The occurrence and variation of other heavy minerals is not noteworthy.

4.4.5 Mineralogical composition of the clay fraction

Illite and kaolinite constitute the main clay-mineral groups within the core, values range between 30% - 80% and 10% - 40%, respectively (Fig. 4.5). A monotonic 5/10 Å ratio of 0.2 over the whole core suggests the continuous dominance of illites of biotitic composition.

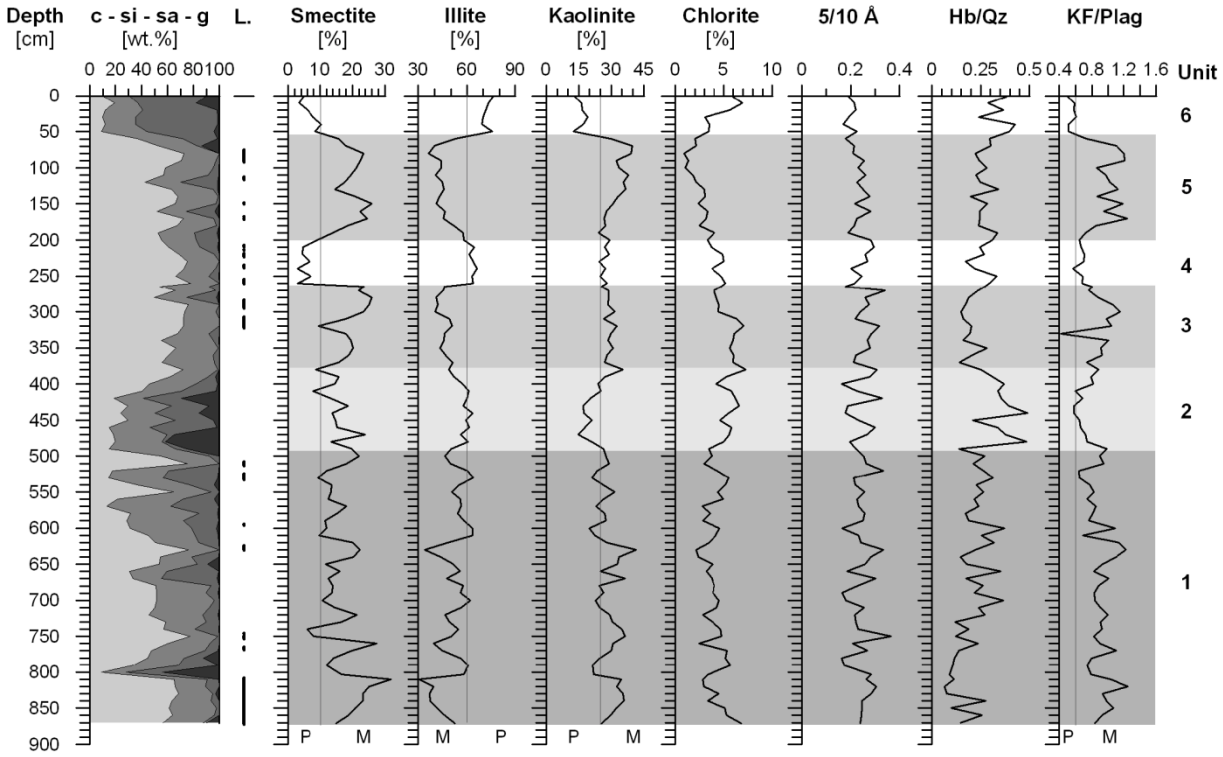

Fig. 4.5 Mineralogical composition of the clay fraction in comparison to grain-size distribution (c = clay, si = silt, sa = sand, g = gravel) and sediment texture (L = lamination). Sediment sections with similar contents and behaviour of clay minerals and non-clay minerals were grouped to units one to six. Light grey lines indicate concentrations of minerals in surface sediments to discriminate between provenance of material from sedimentary (M = MacRobertson Land) and crystalline sources (P = Prydz Bay and continental slope; Borchers et al., in press).

Smectite holds concentrations of 5% to 30% and is anti-correlated to illite over nearly the whole sediment core. Chlorite is of minor importance (max. 7%) and shows a long-term trend independent from other parameters.

According to the content of and relationship between smectite, illite, kaolinite and non-clay minerals, six mineralogical units can be distinguished (Fig. 4.5). The differentiation between the units is further accomplished by the use of reference data of surface mineral distributions representative of different sediment provenances (Borchers et al., in press). It can be concluded, that smectite, kaolinite and the kalifeldspar/ plagioclase ratio (KF/Plag) follow a similar trend especially in unit one, but also in unit six. In these units, the latter parameters are roughly anti-correlated to illite. Unit two exhibits a comparable development of KF/Plag and kaolinite which contrasts to that of smectite. No anti-correlation between smectite and illite is observed. The hornblende/quartz ratio reaches its maximum content. Units three and five comprise very high contents of smectite and kaolinite, along with high KF/Plag ratios. Noteworthy is the different behaviour of kaolinite with respect to the latter parameters and illite: in unit three, kaolinite varies independently of smectite, illite and KF/Plag, whereas in unit five, kaolinite is clearly anti-correlated to illite. The mineralogical composition of unit four is comparable to that of unit six except for the kaolinite concentration which shows only minor variations independent of those of smectite or illite. KF/Plag and smectite show an opposite trend to that of illite.

4.4.6 Geochemical composition of the bulk sediment

Analysis of the geochemical composition of the bulk sediment reveals that iron and calcium show the most reliable results (see Fig. 4.2) in the sediment core with concentrations varying between 1% - 5% and 1% - 9%, respectively (Fig. 4.6). Concentrations of aluminium range between 1% and 4%. Titanium comprises only low proportions ranging between 0.25% and 0.5%. Titanium, aluminium and iron exhibit a similar trend throughout the sediment core. The major fractions of these elements are generally associated with lithogenic material in pelagic and hemipelagic sediments (Sedwick et al., 2001).

Barium varies between 550 ppm and 850 ppm and shows a roughly opposite trend compared to the lithogenic elements. Biogenic barium (biogenic barium = barium – terrigenic barium) can be used to trace past productivity changes (Bonn, 1995; Klump et al., 2000). Biogenic barium even provides good estimates, when biogenic opal (which is commonly used to reconstruct biogenic productivity in surface waters) is dissoluted or advected and cannot be detected. For this purpose, the contents of biogenic and terrigenic barium have to be delineated by calculation of the Ba/Al ratio. According to Klump et al. (2000) the most

reliable method is to determine the terrigenic Ba/Al ratio from continental slope sediments barren of microfossils. In sediment core PS69/851-1, core section 50 cm – 350 cm was most reliable to do so and revealed a terrigenic Ba/Al ratio close to 0.0075 which corresponds to the global mean terrigenic Ba/Al (Klump et al., 2000) and is also in good agreement with results from the Weddell Sea region (Bonn, 1995). Values exceeding the Ba/Al ratio of 0.0075 can be interpreted to represent increased biogenic primary production in the surface water.

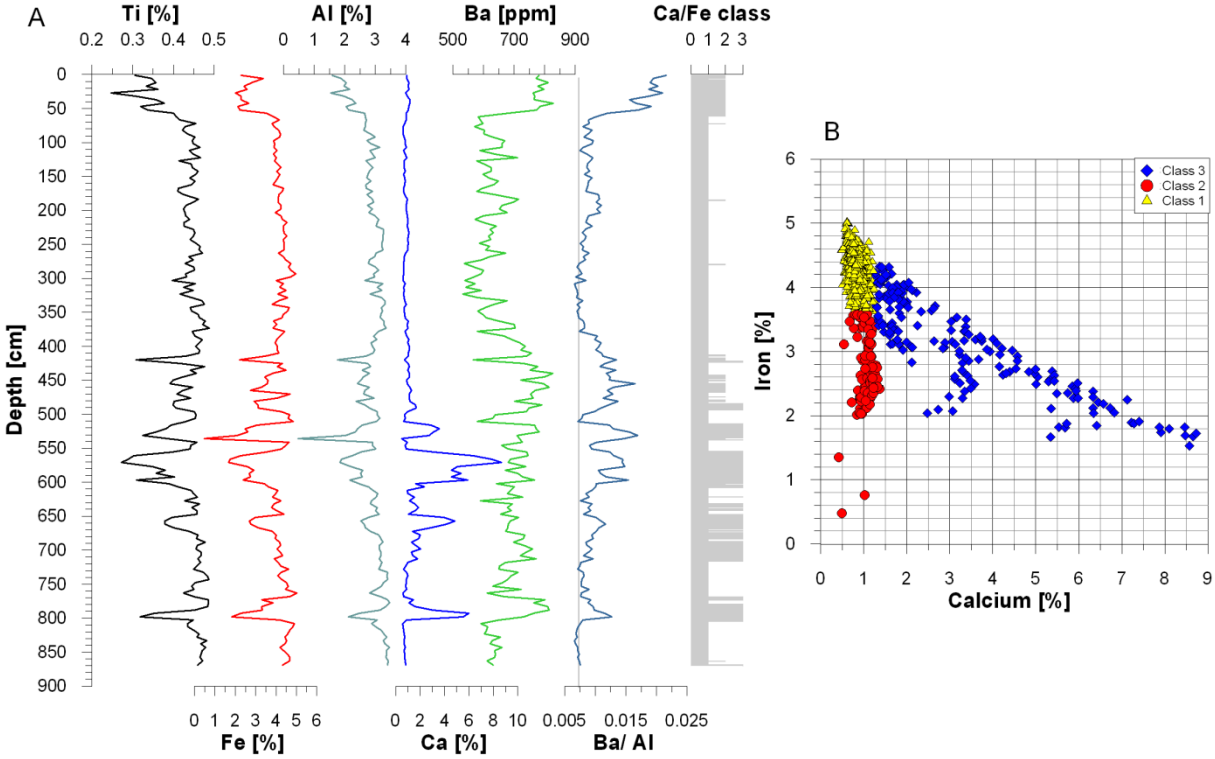

Fig. 4.6 Major element concentrations and downcore dependence of calcium and iron (Ca/Fe class) in sediment core PS69/851-1. A) Ti, Fe and Al exhibit good correlation throughout the sediment core with a generally opposite trend (B) compared to calcium and barium which are referred to biological processes.

With up to 9%, calcium exhibits the highest element concentrations in the sediment core. It shows similar temporal trends to Ba/Al in the lower 500 cm and top 50 cm of the core. The relationship of calcium and iron is illustrated in Fig. 4.6a and b. A clear anti-correlation of calcium and iron is observed in the sediment core below 500 cm (class 3), where samples comprise high proportions of calcium. Between 500 cm - 400 cm and within the top 50 cm of the core, the proportion of iron fluctuates independently of calcium content (class 2). Within the rest of the sediment core, iron concentration remains stable on a high level and calcium is nearly absent (class 1). Following these results and further observations from smear slides (not shown) most of the calcium content is referred to calcareous microfossils such as foraminifera.

4.5 Discussion

4.5.1 Stratigraphic distribution of different modes of glaciomarine sedimentation

Sedimentological, mineralogical and geochemical results from our sediment core display major shifts in the depositional environment on the continental slope during the last 1400 ka. Based on the sedimentological facies obtained from ODP Site 1167 (Passchier et al., 2003), most parts of sediment core PS69/851-1 can be classified as belonging to

- 'silty clay with dispersed clasts' (StC, predominance of GSD classes four to six),
- 'sandy mud with dispersed clasts' (SMm, predominance of GSD class two) and
- 'poorly sorted muddy sand with dispersed clasts' (MS-2, predominance of GSD classes one and two).

The interval between 870 cm and 670 cm, silty clay with dispersed clasts dominates and indicates glaciomarine deposition. Today, the position of the sediment core is influenced by the Antarctic Slope Current, a contour current characterized by a heterogenic clay-mineral distribution over wide areas. Although sediments between 870 cm and 800 cm, comprising clear lamination and low IRD imput, may be interpreted as glacial contourite deposits (e.g. Lucchi and Rebesco, 2007), the clay-mineral signature contradicts this assumption. It reflects a provenance of fine-grained material from Western Prydz Bay (Lambert Deep; Fig. 4.1) rather than down settling from the Antarctic Slope Current (Borchers et al., in press). In combination with distinct silt laminae, this probably indicates a contribution of a periodically more energetic downslope thermohaline flow associated with seasonal formation of sea ice (Passchier et al., 2003; Lucchi and Rebesco, 2007).

At 800 cm, a basal erosion mark and high contents of sand and gravel could be due to a strong flow regime with at least winnowing of fines. More likely, however, deposition of coarse debris due to a minor calving event associated with a retreat of the Lambert Glacier during warmer conditions seems plausible, as increased proportions of calcium and biogenic barium suggest an increased primary production. The transition to more hemipelagic sedimentation is interpreted from sediments between 780 cm and 670 cm, showing increased deposition of IRD. It indicates that icebergs continuously crossed the core position and released their load. Stronger fluctuation in grain-size distributions and clay-mineral distributions suggests a highly dynamic glaciomarine regime during the time of deposition. Strong variations in smectite and kaolinite content maybe indicate oscillations of coastal ice streams in addition to fluctuations of the Lambert Glacier.

Between 670 cm and 500 cm, sediments are characterized as 'sandy clay with dispersed clasts' (SMm, Passchier et al., 2003). In conjunction with continuous IRD supply, calcite

(foraminifera) deposition and increased contents of biogenic barium this unit reflects interglacial, open-marine conditions with hemipelagic deposition of muds. Variations in sea-ice concentration and shore-fast ice lead to fluctuations in the amount of coarse debris released by icebergs.

The interval 500 cm to about 400 cm comprises exceptionally high concentrations of coarse debris and is interpreted in terms of facies 'poorly sorted muddy sand with dispersed clasts' (MS-2; Passchier et al., 2003). It hints at an ice shelf advance far to the north. Although no dramatic changes in the provenance of fine material is observed, except for increased deposition of hornblende, supply of hornblende in the coarse fraction for the first time in the sediment record significantly increases to the cost of garnet. According to Borchers et al. (in press), sediments rich in hornblende are confined to the central and eastern coastal areas of Prydz Bay. It can be concluded, that Prydz Bay was glaciated to a large extent. As a result, not only sediments from the Lambert Deep were eroded and redeposited on the continental slope, but also sediments from eastern Prydz Bay gained influence.

Sediments deposited between 400 cm and 50 cm again belong to facies 'silty clay with dispersed clasts' (StC). IRD supply was discontinuous with coarse-grained material being delivered predominantly from Lambert Deep or MacRobertson Land. The clay-mineral distributions exhibit strong variations used to discriminate different sedimentation processes: associated with clay-mineral unit three (380 cm - 260 cm) and five (170 cm - 50 cm) is deposition of material originating in the Lambert Deep region and experiencing downslope transport by thermohaline flow due to seasonal formation of sea-ice. In contrast, downslope thermohaline flow probably was reduced and contour current activity dominated.

The topmost sediment unit (50 cm - 0 cm) most resembles to that between 500 cm and 400 cm and again suggests hemipelagic sedimentation of mud accompanied by deposition of ice rafted debris originating from Prydz Bay. Compared to the first major deglacial event observed, the ice-rafted material is finer. Results from glaciomarine sediments off Greenland exhibit release of IRD at the continental margin follows a power function with less coarse IRD deposited with distance (Andrews et al., 1997). Andrews (2000) suggests three possible scenarios for changes in coarse IRD supply: 1.) a change in the iceberg flux with sediment content and melt rate held constant; 2.) a change in sediment concentration, with the iceberg flux remaining steady and the rate of melt not varying, or finally; 3.) a change in the locus of the main zone of iceberg melting, due to changes in surface and subsurface temperature conditions. As the sediment load of Antarctic icebergs is relatively low compared to that of icebergs calving from the Greenland ice sheet, variations in the sediment concentration of icebergs are assumed to have only a minor impact on the sedimentation off Prydz Bay. More

likely, a southerly position of the calving line may have led to rainout of finer debris during the most recent deglacial event compared to the first one.

4.5.2 Pleistocene palaeoenvironmental history of the Prydz Bay region

Since its evolution during the Eocene, the East Antarctic Ice Sheet (EAIS) had experienced several cycles of waxing and waning (Barron et al., 1991; Cooper and O'Brien, 2004). These periods of ice advance and retreat are relatively well documented along the western flank of the Lambert Graben (Hambrey and McKelvey, 2000a) and in the marine realm (Barron et al., 1991; Cooper and OBrien, 2004). According to these results, the EAIS for the last time completely covered Prydz Bay shelf before 780 ka and since then remained relatively stable during the Pleistocene with only smaller phases of advance and retreat.

Results from sediment core PS69/851-1 generally support these previous finding, but add some detail and provide additional evidence for a Late Pleistocene decoupling of the marine ice shelf from its bed. Especially clay-mineral distributions at site PS69/851-1 show distinct fluctuations compared to findings from Junttila et al. (2005) and provide a better view on changes in the glacial regime in Prydz Bay.

Prior to 1.1 Ma - 1.25 Ma, sedimentation from glacial meltwater discharge of an ice shelf situated near the shelf break seems most plausible, explaining the very low content of IRD during that time and the clay-mineral signature. The possible advance of the Lambert Glacier to the shelf could be explained by a lower sea-level and lower sea surface temperatures (SSTs) due to the general cooling during the Late Pliocene/ Early Pleistocene (Villa et al., 2008). During the transitions to warmer conditions between 1.25 Ma and 1 Ma, the ice shelf became floating and the decoupling of the ice shelf from its bed led to deposition of coarse material in vicinity to the calving line. Hemipelagic sedimentation commenced accompanied by intense biogenic production in the surface water column. Ventilation of the deeper ocean advantaged benthic organisms and bioturbation destroyed primary sediment structures. Considering a transition from a grounded to a floating ice sheet between 1.25 Ma and 1 Ma, the change from a terrestrial based to a marine based EAIS margin could haven taken place during this time interval as proposed by Raymo et al. (2006). To explain this, fluctuations in sea level stronger than during earlier periods have to be invoked. These sea-level variations are referred to the waxing and waning of predominantly the northern hemispheric ice sheets and produced sea-level changes in the order of 80 m (Raymo et al., 2006). According to Passchier et al. (2003), changes in sea level induced the highly dynamic character of the Lambert Glacier during the middle Pleistocene with a fluctuating grounding line confined to Prydz Channel and Lambert Deep such as also suggested by strong variations in grain-sizes and garnet-rich sediments at site PS69/851-1.

A decoupling of the EAIS margin from its bed was then the prerequisite for the following deglaciation around 1 Ma. During this time, high productivity suggests strong interglacial conditions possibly associated with marine isotope stage 31 (MIS 31). During this time interval, the initial grounding line must have been located in the vicinity of the coring site, supplying very coarse ice-rafted debris. A change in the provenance of ice-rafted material to areas comprising crystalline bedrock indicates that glacial retreat was not only confined to that part of the Lambert Glacier following the Prydz Channel, but also affected eastern Prydz Bay, suggesting a major retreat of glacial features during this time interval. These findings support previous palaeoenvironmental reconstructions from other marine records (Passchier et al., 2003; Passchier, 2007; Villa et al., 2008) which also proposed significant warming, high productivity and major calving in the region. Especially the preservation of calcite below the CCD during interglacials could be explained by rapid burial during high primary production of siliceous and calcareous organisms (Pudsey, 2000). Due to the warm conditions, in the distal ocean only minor IRD was reported (Teitler et al., 2007; Scherer et al., 2008), owed to the low survivability of icebergs within warm surface waters. Whether these warm surface waters contributed to sub-ice melting leading to a more rapid decay of the ice shelf (e.g. Williams et al., 2002), can only be assumed. Modelling scenarios, however, suggest a mid-Pleistocene retreat of the Lambert Glacier far to the south (Pollard and DeConto, 2009). Although the retreat of the Lambert Glacier is small compared to the decay of the West Antarctic Ice Sheet during that time (Scherer et al., 2002; Pollard and DeConto, 2009), it has to be considered that ice masses calving in Prydz Bay possibly amplified sea-level rise to a certain extent and gave way to a faster flow of the Lambert Glacier from the hinterland. Rather, Scherer et al. (2008) suggest high Southern Hemisphere insolation led to strong interglacial conditions during MIS 31 with subsequent melting of the Antarctic margin which then triggered Northern Hemispheric ice sheet melt.

After the mid-Pleistocene retreat, from about 700 ka (or earlier, taking into consideration a non-linear but much higher sedimentation rate due to strong supply of terrigenous material), the Lambert Glacier-Amery Ice Shelf System stabilized. Most of the sediments deposited at site PS69/851-1 between 700 ka and 100 ka probably represent glacial material derived by meltwater plumes from Prydz Bay. Calving of icebergs was constricted to the (western) Lambert Glacier region, whereas coastal ice masses obviously remained stable. Predominantly stable glacial conditions with colder surface waters in Prydz Bay were also implied by Villa et al. (2008). According to the age model, distinct contour current activity took place between 400 ka and 300 ka. This time period is in the range of the warm interglacials MIS 11 and MIS 9 (Jouzel et al., 2007). In the Cape Basin and northwestern Weddell Sea, Diekmann et al. (2003) related increased contour current strength during interglacials to bottom-water formation permitted by floating ice shelves. Because in Prydz

Bay, only little or no bottom water is formed underneath the Amery Ice Shelf (Meijers et al., 2010) the ASC might have strengthened due to increased contribution of bottom water produced in regions east of Prydz Bay.

During the last 100 ka, increased terrigenous supply of predominantly sand-sized material again implies major ice-rafting activity when the ice shelf became buoyant probably in association with the warm interglacial MIS 5.5. Sediment records from coastal Prydz Bay underline ice-free conditions during that time (Hodgson et al., 2006). A deposition of the material after the Last Glacial Maximum, however, cannot be excluded. Similar to the mid-Pleistocene retreat of the Lambert Glacier, probably wide areas were affected by glacial recession. But more material such as eroded from the crystalline basement was deposited at site PS69/851-1, suggesting a deeper incision of Lambert Glacier into the Lambert Graben or erosion from more coastal areas, where crystalline basement constitutes the bedrock. The change in the ice drainage during the Pleistocene can be explained by progressive deepening of the inner shelf by glacial erosion (O'Brien et al., 2007) preventing ice streams to reach the shelf edge after the mid-Pleistocene. Changes in the topography of the Prydz Bay hinterland only leave an impact on the ice flow into the graben, with increasing velocity and ice flux due to raised boundary mountains (Taylor et al., 2004). Ice-sheet extent in terms of grounded ice on the continental shelf is unaffected, according to this modelling study. The dynamics of the ice stream further might have been influenced by oceanographic conditions changing during the mid-Pleistocene transition. During this time, spanning from about 900 ka to 450 ka, the Polar Front prograded to the north and major cooling of the oceans occured together with lower interglacial temperatures than those of the last 400 ka, evidencing less complete deglaciation (Kemp et al., 2010). In sediment core PS69/851-1, a less dynamic sedimentation of coarse material between 700 ka and 450 ka - 500 ka supports the assumption of an oceanographical influence on the development of the Lambert Glacier. Eventually, the deep excavation of the Lambert Graben and the inner shelf of Prydz Bay in combination with oceanographic conditions during the last one million years were responsible for the bad representation of glacial/ interglacial cycles in the sediment record.

In sediment core PS69/851-1, at least two periods of major glacial recession are documented. According to their inferred importance in the Prydz Bay region, they might have led an impact in the glacial regime of Prydz Bay hinterland. In situ ^{10}Be and ^{26}Al cosmogenic exposure ages of the Northern Prince Charles Mountains reflect the progressive emergence of McLeod Massif and Radok Lake basin from beneath the MacRobertson Land lobe of the EAIS (Fink et al., 2006). According to the authors, three major periods of ice thinning occured at 1.1 Ma, between 120 ka and 30 ka and through the Last Glacial Maximum resulting in a total reduction of ice thickness of about 1000m in the Battye Glacier-Radok Lake region. This data on the one hand supports findings from site PS69/851-1. But it furthermore implies, that

a retreat of the Lambert Glacier destabilizes terrestrial ice masses in the Prydz Bay hinterland which feed the main ice stream.

4.6 Conclusions

Results from this multi-proxy study in general supported previous findings from ODP Legs 119 and 188, but added important detail to the palaeoenvironmental history of the Lambert-Graben-Amery Ice Shelf system.

They suggest that the transition from a terrestrial-based to a marine-based ice system occurred around 1.25 Ma with sedimentation shifting from material derived from meltwater input to hemipelagic sedimentation with rainout of ice-rafted debris. After decoupling of the Lambert Glacier from its bed, glacial retreat culminated during the mid-Pleistocene around MIS 31. The inferred large retreat of the glacial system and coastal glaciers in Prydz Bay accompanied by a strong glacial recession around the Antarctic suggests melting significantly contributed to global sea-level rise and thus left an impact on Northern Hemispheric ice sheets. After the deglaciation, minor but persistent calving from the Lambert Glacier occurred. The relative stability of the ice stream is referred to the previous excavation of the inner shelf of Prydz Bay in combination with cold surface waters. Although of minor importance, the Lambert Glacier was slightly more dynamic after the mid-Pleistocene transition. A last major deglaciation commenced probably during or shortly after the last warm interglacial (MIS 5.5). The timing of deglaciations recognized from our sediment record is in agreement with that of major reductions of ice volume in the Prince Charles Mountains. This leads to the tentative conclusion that inland ice masses were affected by instabilities of the Lambert Glacier. Results further suggest possible future instabilities under MIS 5.5-like conditions.

Acknowledgments

This investigation was funded by Deutsche Forschungsgemeinschaft priority program SPP 1158 through grant DI 655/3-1.

We kindly thank the master of research vessel ‘Polarstern’ captain Schwarze, the ship’s crew and the chief scientist of expedition ANT-XXIII/9, H.W. Hubberten, for their assistance and support. Ute Bastian, Antje Eulenburg, Rita Fröhlking, Ute Bock, Norbert Lensch and interns onboard research vessel ‘Polarstern’ supported us in terms of sample preparation and technical questions. During her internship, Anna Plotzki did a great job in the sedimentology lab. Helpful comments of Carl Richter improved the quality of the magnetostratigraphy. For scientific ideas, we are indepted to Lora Teitler.

5. Synthesis

Within the central part of this dissertation, three first-author manuscripts were presented. In the first manuscript the relation of sea-bed surface mineralogical compositions to the modern current-flow patterns and ice transport was shown. This methodological aspect provided the basis for provenance studies made within the scope of palaeoenvironmental reconstructions presented in manuscripts II and III. The overall aim of reconstructing the glaciomarine environment during the Pleistocene (continental slope off Prydz Bay/ MacRobertson Land; manuscript III) and since the last glacial (Burton Basin, MacRobertson shelf; manuscript II) was to provide clues on the response of the LAIS, coastal glacial features (glaciers and polynyas) and bottom-water formation to climate variations during the Quaternary. The main outcomes of these investigations are presented in this chapter.

5.1 Applicability of mineralogical parameters to reconstructing palaeoenvironments in the Prydz Bay-Kerguelen region

The analysis of both clay minerals and heavy minerals was successfully applied on Quaternary sediments from around the Antarctic to decipher past shifts in the provenance of current-derived and ice-transported material (e.g. Diekmann and Kuhn, 1999; Damiani et al., 2006; Giorgetti et al., 2009). Building a basis for this thesis, it had to be assessed if there are substantial differences in the mineralogical composition of surface sediments which favour the use of clay minerals and heavy minerals to trace past provenances. Though the surficial sediment composition is related to modern processes, the term ‘modern’ for surface samples is not to be taken *sensu stricto* due to different accumulation rates in the different environments. Surface sediments therefore may represent different time spans of deposition.
According to the results presented in manuscript I, both mineralogical parameters comprise valuable tools, although with some limitations: the most significant differences in the mineralogical composition of sea-bed surface sediments were recognized on the continental shelf. With distance to the primary source of the material, mineral signatures become blurred and are – especially in case of heavy minerals – hard to differentiate.
On the continental shelf, two prominent mineral provinces occurred (Fig. 2.5): in eastern and central Prydz Bay, heavy minerals reveal very high abundances of hornblende (40%-70%) and illite is the main constituent of the clay fraction (60%-80%). Sediment input is therefore interpreted to have derived mainly from erosion and weathering of crystalline bedrock such as exposed in the Prince Charles Mountain, Groove Mountains, in the Vestfold Hills, Rauer Islands and Larsemann Hills (Tingey, 1991; Thost et al., 1998). Superimposed on the general

heavy-mineral composition smaller differences in the content of pyroxenes are addressed to input of material from local sources (Fig. 2.3).

On MacRobertson shelf, the high contents of garnet (~80%) and kaolinite (25%-41%) in both pre-Holocene and modern sediments indicate the presence of Permo-Triassic deposits of the Amery formation (Tingey, 1991; Webb and Fielding, 1993; Ehrmann et al., 2003) or their Neogene remnants of the Pagodroma Group (Hambrey and MacKelvey, 2000a,b; Ehrmann et al., 2003; Whitehead et al., 2006) as the primary source. A definite age of deposition for the pre-Holocene sediments recovered from MacRoberston shelf which extent to the east into the Lambert Deep cannot be given due to the problematic dating of glaciomarine sediments (see chapter 3.6.1). It cannot be excluded, that the recovered pre-Holocene material from MacRobertson shelf itself 1.) comprises an outcrop of Permo-Triassic material which also fills the deeper part of the Lambert Graben or 2.) uncovered Neogene sediments of the Pagodroma Group on MacRobertson shelf. The contrasting sediment compositions from Prydz Bay and MacRobertson shelf, however, allow for discrimination of material derived from these regions.

On the continental slope, clay-mineral and heavy-mineral assemblages from east and west of Prydz Bay yield similar results indicating only negligible impact of material derived from Prydz Bay on sedimentation on the continental slope. Rather, clay mineral assemblages from the continental slope resemble to those obtained from Adelie Coast/ Mertz Glacier region and Gunnerus Ridge, highlighting the importance of the Antarctic Slope Current on homogenizing material supplied to the continental margin predominantly by glaciers.

In the pelagic realm, minor variations of clay-mineral distributions are tentatively assigned to the modern flow patterns of CDW, AABW and the Deep Western boundary current (Fig. 2.5) and are supposed to serve as suitable tools to reconstruct Quaternary shifts in oceanic current patterns. Heavy-mineral assemblages show an overall East Antarctic crystalline origin. They support the general drift patterns of icebergs calving in Prydz Bay and being deflected across Kerguelen Plateau by the ACC as shown by Schmitt et al. (2004).

5.2 The stability of the Lambert Glacier-Amery Ice Shelf system and adjacent glacial features during the Quaternary

Conclusions on the long-term history of the Lambert Glacier-Amery Ice Shelf system (LAIS) were drawn by investigation of sediment cores recovered during ODP Legs 119 and 188 (Barron et al., 1991; Cooper and O'Brien, 2004). Regarding its behaviour during the Quaternary, only little is known. Results from the multi-proxy studies presented in manuscript II and III aimed on providing new insights into the dynamics of the LAIS during

this time period. According to the established age-depth models, sediment core PS69/851-1, from the continental slope off Prydz Bay/ MacRobertson Land covers the time interval since about 1.4 Ma, while sediment core PS69/849-2 from MacRobertson shelf documents the environmental history since the last glacial.

At least two phases of glacial retreat could be identified during the Pleistocene, associated with input of high amounts of coarse-grained material transported by sediment-laden icebergs to the continental slope (Fig. 4.4, 5.1). The precondition for these deglacial events to occur probably was the transition of the LAIS from a terrestrial-based to a marine-based ice sheet probably around 1.25 Ma BP. Ablation of the ice masses might have shifted from predominantly glacial melting at a terrestrial margin to calving of icebergs at the calving line as indicated by strong increase of IRD during this time and onset of hemipelagic deposition (Fig. 4.4). This would agree with modelling results of global $d^{18}O$ records by Raymo et al. (2006) suggesting that long-term cooling drove the EAIS margin into sea, so it was no longer warm enough for an extensive terrestrial melting margin. As a consequence, fluctuations of the LAIS after the transition were primarily controlled by sea-level variations driven by Northern Hemispheric ice-sheet fluctuations, whereas prior to the transition, Southern Hemisphere summer insolation was the primary control (Raymo et al., 2006). Eventually, the transition of the EAIS to a marine-based ice sheet explains the in-phase variation of ice sheets at both poles at both obliquity and precession frequencies such as determined in global $d^{18}O$ records.

In general, the LAIS remained relatively stable until about 1 Ma BP, when the grounding line of the LAIS retreated far to the south and very high proportions of IRD were deposited at the continental slope (Fig. 4.4, 5.1; Passchier et al., 2003; Passchier, 2007). Both clay minerals and heavy minerals (Fig. 4.4, 4.5) suggest that glacial recession was not only restricted to the Lambert Deep and western Prydz Bay but ice retreat also occurred in eastern Prydz Bay accompanied by receding glaciers along the continental margin of Princess Elizabeth Land. In the Prince Charles Mountains, ice thickness was reduced by about 400 m during this time (Fink et al., 2006), providing clues that the retreat of the glacier tongue also affected tributary glaciers of the LAIS. High contents of calcite and biogenic barium in sediments from the continental slope hint to strong interglacial conditions favouring high primary productivity in the surface water column possibly associated to the warm mid-Pleistocene with a peak of marine isotope stage 31 (MIS 31). During this time, surface waters in Prydz Bay were much warmer (Villa et al., 2005, 2008) and the Polar Front was displaced to the south (Flores and Sierro, 2007; Kemp et al., 2010) probably leading to enhanced preservation of calcareous material (Pudsey, 2000). A similar depositional regime occurred during or shortly after the last interglacial (MIS 5.5), when the LAIS retreated a second time (Fig. 5.1), probably due to raised global mean sea level by 6 m - 9 m (Hearty et al., 2007). The deglaciation of the LAIS

involved lowering of ice thickness by about 220 m in the Prince Charles Mountains between 120 ka and 28 ka (Fink et al., 2006). Sediment records from coastal Prydz Bay underline ice-free conditions during that time (Hodgson et al., 2006). In contrast to the glacial recession around 1 Ma, IRD delivered to the continental slope during the late Pleistocene was less coarse (Fig. 4.4) possibly implying a more southern position of the initial grounding line or higher sea-surface temperatures leading to stronger melting proximal to the calving line (Andrews et al., 1997; Andrews, 2000). It is, however, hard assess which factors influenced the different extent of advance of the LAIS to the north. It can be speculated that the duration of cold conditions prior to the deglaciation is of major importance for the growth of the glacial systems. So could also be the strength of glacial/ interglacial cyclicity. During long-lasting stable glacial conditions, such as observed prior to the mid-Pleistocene (Passchier, 2007), continuous cold temperatures in combination with only small fluctuations in global sea level might favour a steady growth of glacial systems.

Without a doubt, the relative stability of the LAIS to a certain extent can be explained by a reorganization of the drainage system during the Pleistocene. Very likely, progressive deepening of the inner shelf by glacial erosion (O'Brien et al., 2007) prevented the LAIS to reach the shelf edge after the mid-Pleistocene. Modelling results suggest that changes in the topography of the Prydz Bay hinterland only leave an impact on the ice flow into the graben, with increasing velocity and ice flux due to raised boundary mountains (Taylor et al., 2004). Ice-sheet extent in terms of grounded ice on the continental shelf is unaffected, according to this modeling study.

The reorganization in ice drainage provides a good explanation for the relatively stable LAIS during the Pleistocene with distinct glacial retreat obviously restricted to warmer-than modern interglacials. Still, there are some questions remaining, e.g.: why did the warm interglacials MIS 11 and MIS 9 (Fig. 5.1; Lisiecki and Raymo, 2005) leave no impact on the LAIS, although MIS 11 was the longest interglacial during the last 500 ka (Loutre and Berger, 2003)? To answer this question, the impact of the warm periods on global mean sea level (Fig. 5.1) has to be considered. According to Olsen and Hearty (2008) the MIS 11 highstand was in excess of 20 m. Estuarine environmental responses to sea-level change during MIS 11 revealed in Osaka Bay by diatom and sulphur analyses of high accumulation rate sediments suggest sea-level in the period from 426 ka to 366 ka was above -60 m and below 20 m (Kariya et al., 2010). In contrast, Bowen (2010) concluded from uplifted coastlines that the sea-level of MIS 11 at 406 ka was closer to present than previously suggested. Based on his results, a MIS 11 sea level at 20 m is not supported and consequently there is no need to invoke additional melting of the West Antarctic and Greenland ice sheets for the rise in sea-level from a MIS 12 low stand at - 140 m. For MIS 9, recent results from coral terraces on

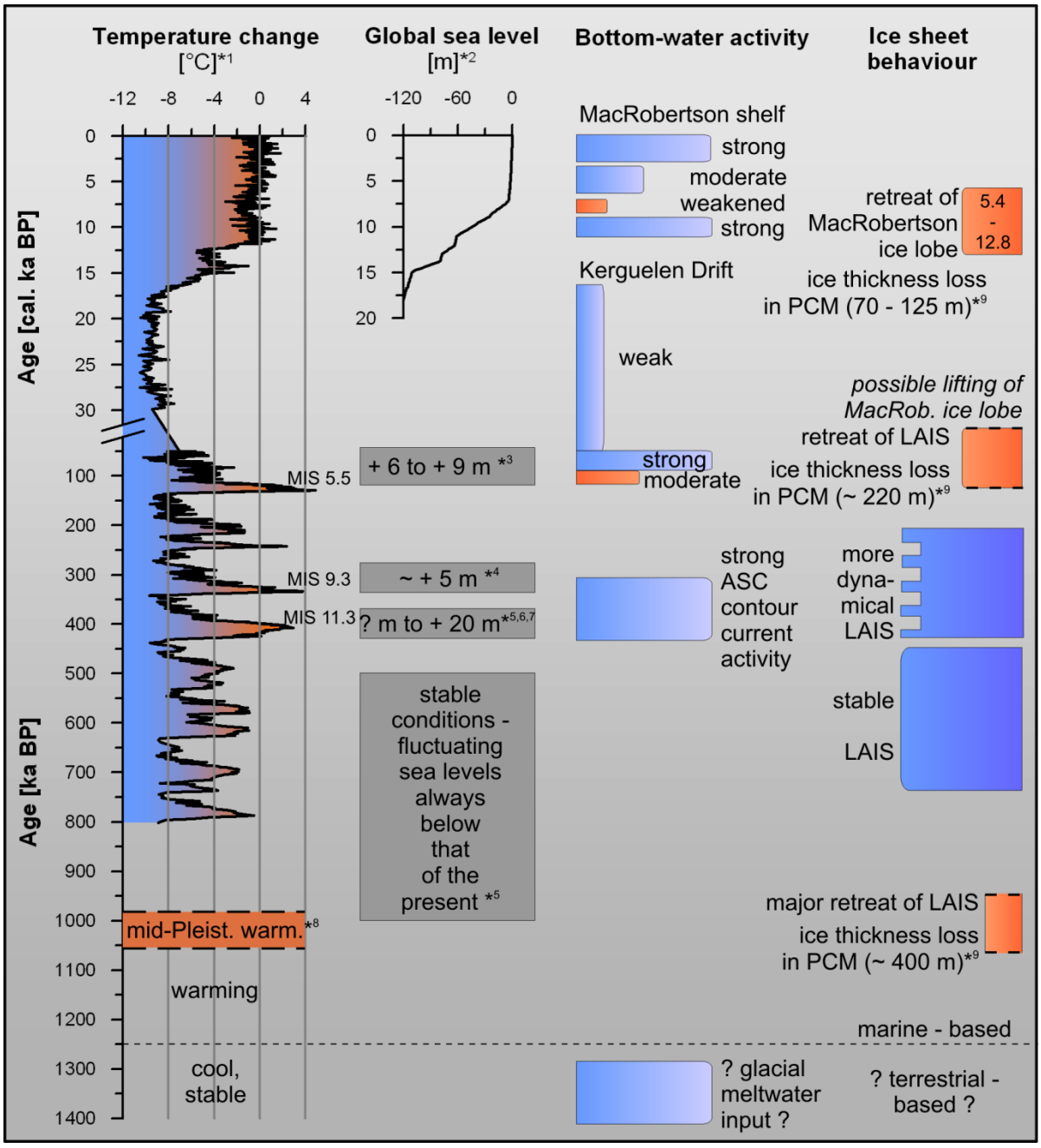

Fig. 5.1 Compilation of the environmental development in the Prydz Bay region during the Quaternary. Please note the changing time scale broken between 50 ka BP and 30 cal. ka BP. *[1]Antarctic temperature change data adopted from Jouzel et al., 2007. *[2]Sea-level history since the last glacial after Fleming et al. (1998) and Milne et al. (2005). Pleistocene sea-level data from *[3]Hearty et al. (2007), *[4]Stirling et al. (2001), *[5]Olsen and Hearty (2008), *[6]Bowen (2010), *[7]Kariya et al. (2010), *[8]Villa et al. (2008), *[9]Fink et al. (2006).

Henderson Island (Indo-Pacific region) indicate a sea level 5 m above modern values (Stirling et al., 2001). Eventually, the comparison of sea-level highstands during MIS 11, MIS 9 and MIS 5 leads to the tentative assumption that a disintegration of the LAIS might occur when sea level rises above 6 m. More specific conclusions regarding the sensitivity of the

LAIS to sea-level fluctuations, however, cannot be drawn until the sea-level history in combination with regional uplift history of the Prydz Bay region is fully understood and reliable relative sea-level data are available. Changes in the variability of sand input in the interval between the two major deglacial events might suggest that also minor variations of the sea-level during the Pleistocene left at least little impact on the LAIS extension. Between 700 ka and 450 ka, sand input was less dynamic than between 450 ka and about 100 ka (Fig. 4.4). According to Olsen and Hearty (2008) the time between 1.0 Ma and 0.5 Ma was a quiescent, stable period when fluctuating sea levels were always below that of the present. After 0.5 Ma until present, a turbulent period followed in which the amplitude of sea-level fluctuations was much greater, resulting more dynamical behaviour of the LAIS (Fig. 5.1).

The influence of sea-level rise on glaciers and inland ice masses in the Antarctic can probably be best assessed by investigation of young sediments with reliable core chronologies. Sediment core PS69/849-2 in this regard provides insights into the deglaciation history of MacRobertson shelf since the last glacial (manuscript III). The transition from a consolidated diamictite to unconsolidated material around 32.2 ka BP (taking into account ^{14}C dating uncertainties) suggests the decoupling of a grounded lobe from its bed (Fig. 5.1). According to clay mineral and heavy mineral data (Fig. 3.6), the lobe originated in the inland ice sheet on MacRobertson Land. This coincides with other records from Prydz Bay indicating a marine transgression into a near-coastal lake basin on the Larsemann Hills around 32 ka (Hodgson et al., 2009). Further implications for an early retreat of grounded ice from central Prydz Bay come from Domack et al. (1998) showing that diamicton similar in character to basal till was deposited prior to 32 ka BP (uncorr. ^{14}C age). After lifting of the marginal ice masses, deglaciation commenced on MacRobertson shelf around 12.8 cal. ka BP, accompanied by increased sedimentation rates and biogenic production (Fig. 3.3, 3.4, 3.7, 5.1). Continuing supply of IRD suggests the calving front was located in the vicinity and receded farther south from the coring site approximately around 9.5 cal ka BP, when the shift from deglacial to interglacial conditions took place (Fig. 3.4, 3.5, 3.7). In Prydz Bay, however, regional recession of the ice margin from the outer shelf commenced at latest at 13.4 cal. ka BP (Verleyen et al., 2005). Ice retreat from different lake sites in the Larsemann Hills and Vestfold Hills was accompanied with onset of biogenic sedimentation at 12.66 cal. ka BP (Verleyen et al., 2005). Ice retreat from Lake Terrasovoje and Beaver Lake, northern Amery Oasis, commenced 12.5 cal. ka BP (Wagner et al., 2007) and is contemporaneous with rapid retreat of the Lambert Glacier-Amery Ice Shelf system deduced from cosmogenic exposure ages (Fink et al., 2006). The timing of ice retreat in the Prydz Bay region suggests a connection to global sea-level rise. Several records of sea-level change during the Late Quaternary (Fairbanks, 1989; Fleming et al., 1998) document two events of rapid sea-level rise (Fig. 5.1): meltwater pulse 1A (mwp-1A) has been dated to 14.2 cal. ka BP and the second

event, termed meltwater pulse 1B (mwp-1B), began approximately 11 cal. ka BP (Fairbanks, 1989). In this regard, mwp-1A may have triggered the retreat of the ice margin rather than East Antarctic ice retreat contributed to global sea-level rise during mwp-1A. Possibly, the progressive waning of the ice sheets had an impact on mwp-1B. The conclusion, however, that global sea-level rise is more likely the driver for East Antarctic Ice Sheet retreat than changes in accumulation rate or atmospheric processes is supported by findings from Mackintosh et al. (2007). The authors showed that exposure ages from MacRobertson hinterland correlate well with the timing of the retreat of marine-based ice sheets as obtained from sediment records retrieved from the continental shelf. Last major occurrences of IRD around 5.4 cal. ka BP suggest major calving from the floating ice shelf sourced on MacRobertson Land (Fig. 3.5, 3.7, 5.1). This corresponds well with still warm conditions (Ingolfsson et al., 1998) and global sea-level rise stabilization between 7 and 6 cal. ka BP (Fleming et al., 1998; Milne et al., 2005). The end of IRD supply might be due to glacial rebound of MacRobertson Land commencing around 6 ka BP (Mackintosh et al., 2007). This pattern of deglaciation is also consistent with the modern observations of isostatic rebound. Tregonning et al. (1999) observe ~1 mm/y uplift at Mawson station, MacRobertson Land (67° 36'S, 62° 52'E). In contrast, no discernable trend is recognized at Davis Station in the Vestfold Hills (68° 35'S, 77° 58'E). While the magnitude of the change in former ice loads directly over each of these sites since the LGM is likely comparable, the timing of removal of this load is considerably different. Residual uplift occurring in the Mawson region is not surprising taking into account continued ice loss until 5-6 cal. ka BP, while it was more or less completed by 12 cal. ka at Davis.

To summarize, three times of glacial retreat were recognized in the Prydz Bay region. Major deglaciations occurred around 1 Ma and during or shortly after the last interglacial. A Holocene ice recession is associated to post-glacial sea-level rise. During most intervals since 1 Ma, the LAIS remained relatively stable, probably owed to the relatively low variations in global sea level (< 6 m) and over-deepening of the Lambert Graben after the mid-Pleistocene advance of the LAIS to the continental shelf break.

5.3 Bottom-water activity and sea-ice cover during the Quaternary

Antarctic coastal areas constitute important regions regarding the formation of dense water masses which to a large extent trigger the global thermohaline circulation and control global climate (Schmitz, 1995; Rahmstorf, 2002). The formation of dense waters is associated with two processes: super-cooling underneath large floating ice shelves and brine rejection due to

sea-ice formation (e.g. Rodehacke et al., 2007). To provide clues on past variations of bottom-water activity, it is therefore important to investigate both formation processes through time.
Within this study, an investigation of bottom-water activity covering the whole time interval since 1.4 Ma was impeded by the problematic depositional situation on the continental slope. Sedimentological data suggest that predominantly glacial sediments were recovered (manuscript III), because of winnowing of interglacial sediments by the Antarctic Slope Current (ASC), thus making it impossible to draw conclusions on the fluctuation of bottom-water activity on Milankovitch timescales. The clay mineralogy within the partly laminated horizons comprising high contents of kaolinite and high K-feldspar/plagioclase ratios (Fig. 4.5), however, point to western Prydz Bay or MacRobertson shelf as the possible source of mainly current-derived material. For this reason, a transport of the material by meltwater plumes or dense waters originating in Prydz Bay, filling Prydz Channel and eventually being spilled over the shelf break cannot be ruled out. During MIS 11 and MIS 9, well laminated sediments with clay-mineral assemblages suggest a deposition from the strong flowing band of the ASC (Fig. 5.1). It is forced by the polar easterlies, but also gains bottom-water input on its path along the East Antarctic margin. Maybe, increased bottom-water input intensified the ASC or at least strengthened its clay-mineral signature.
As a consequence of predominantly lacking interglacial deposits, the investigation of past variations of bottom-water activity focuses on the time interval of the last glacial cycle, comparing the situation during the last interglacial with that during the Holocene by investigation of sediment cores retrieved from MacRobertson shelf (Fig. 1.1, 3.1; manuscript III) and from Kerguelen Drift (Fig. 1.1; extended abstract, Appendix A2).
To better separate the ice-rafted from the current-transported fraction, end-member modelling was applied on grain size distributions determined in sediment core PS69/849-2 (manuscript II; manuscript IV, Appendix A1). This statistical analysis was necessary, because the sand fraction usually ascribed to transport by icebergs is affected by both current-sorting and ice transport on Antarctic continental shelf areas and especially at this site.
Results indicate that bottom-water strength was generally higher during interglacials compared to glacial times (Fig. 3.5, 3.7, A2.1). This is in agreement with earlier findings from the Antarctic margin (e.g. Melles, 1991; Grobe and Mackensen, 1992) providing evidences for decreased bottom-water formation during glacials because grounded ice shelves prohibited super-cooling of shelf waters at their base. Superimposed on this general pattern, it turned out that probably bottom-water strength diminished during warm interglacials such as MIS 5.5 (Fig. A2.1) and the mid-Holocene hypsithermal (Fig. 3.5, 3.7) compared to that during ‘moderate’ interglacials.
To prove this hypothesis, last interglacial sediments were investigated. Because deposits from the continental shelf and slope lack undisturbed sediments of the last glacial cycle,

pelagic sediment cores less affected by erosion and mass wasting processes provide a common means to infer on Late Quaternary palaeoceanography. For this reason, sediment core PS69/899-2 was recovered from a contourite drift along the eastern flank of the Kerguelen Plateau (Fig. 1.1). Sediments deposited here are current-sorted according to the strength of the Deep Western Boundary Current (DWBC; Fig. 1.1) which to a large extent is triggered by AABW that substantially originates along the Adelie Coast in the Mertz Glacier polynya (McCartney and Donohue, 2007; Williams et al., 2010; Fig. 1.1). Grain size-data indicate that enhanced bottom-water flow appeared during interglacial-glacial climate transitions and at recent times. During the last interglacial maximum (MIS 5.5) and during glacial phases (MIS 2, MIS 4, MIS 6), the DWBC weakened (Fig. A2.1, Fig. 5.1)). Clay minerals imply that during MIS 5.5 and during glacial phases, the DWBC probably was mainly controlled by AABW originating from Adelie Coast (Fig. A2.1). In contrast, during times of strong bottom-water activity, clay mineral signature is overprinted by material which probably derived from the adjacent Kerguelen Plateau (Fig. A2.1).

A similar pattern of bottom-water strength in terms of cold and warm phases can be drawn by investigation of sediment core PS69/849-2, which was recovered from Burton Basin in direct vicinity to Cape Darnley polynya. During the Holocene, bottom-water formation in Burton Basin commenced around 9.5 cal ka BP after the calving line of the floating ice shelf had retreated south of the coring site (Fig. 3.5, 3.7, 5.1). It is suggested that strong bottom-water activity is referred to extensive sea-ice formation and associated brine rejection in the Cape Darnley polynya in connection with super-cooling of waters underneath the proximal floating ice shelf. Later, enhanced bottom-water production was observed at the end of warm periods or when cooler conditions commenced (5.2 cal. ka BP, since 1.5 cal. ka BP), respectively, maybe due to earlier and more extensive sea-ice formation. Lower biogenic production suggests shorter periods of biogenic production (Fig. 3.4).

During the mid-Holocene hypsithermal (between 7.7 cal. ka BP and 6.7 cal. ka BP), high biogenic production and ceasing bottom-water activity were recognized providing evidences for reduced sea-ice formation in the polynya. This is possibly related to high meltwater input, longer open-marine conditions and later ice built-up during the year. As a result, the signal of brine rejection was too weak to leave an impact on the terrigenous sediments. Whether a retreated Amery Ice Shelf (Hemer and Harris, 2003) and, consequently, reduced super-cooling there, also contributed to the mid-Holocene reduction in bottom-water flow, remains questionable.

It is also possible that increased sub-ice melting of the Amery Ice Shelf during warm conditions, such as suggested by Williams et al. (2002), led to subsequent meltwater supply and consequently to dilution of former denser waters. The correlation of the mid-Holocene reduction in bottom-water activity, however, with a mid-Holocene warm peak in near-

coastal Taylor Dome ice core (Fig. 3.7; Steig et al., 2000; Grootes et al., 2001), though far away from each other, possibly reflects the ocean-ice-atmosphere interaction and a possible high sensitivity of signals in coastal ice cores to sea-ice extent.

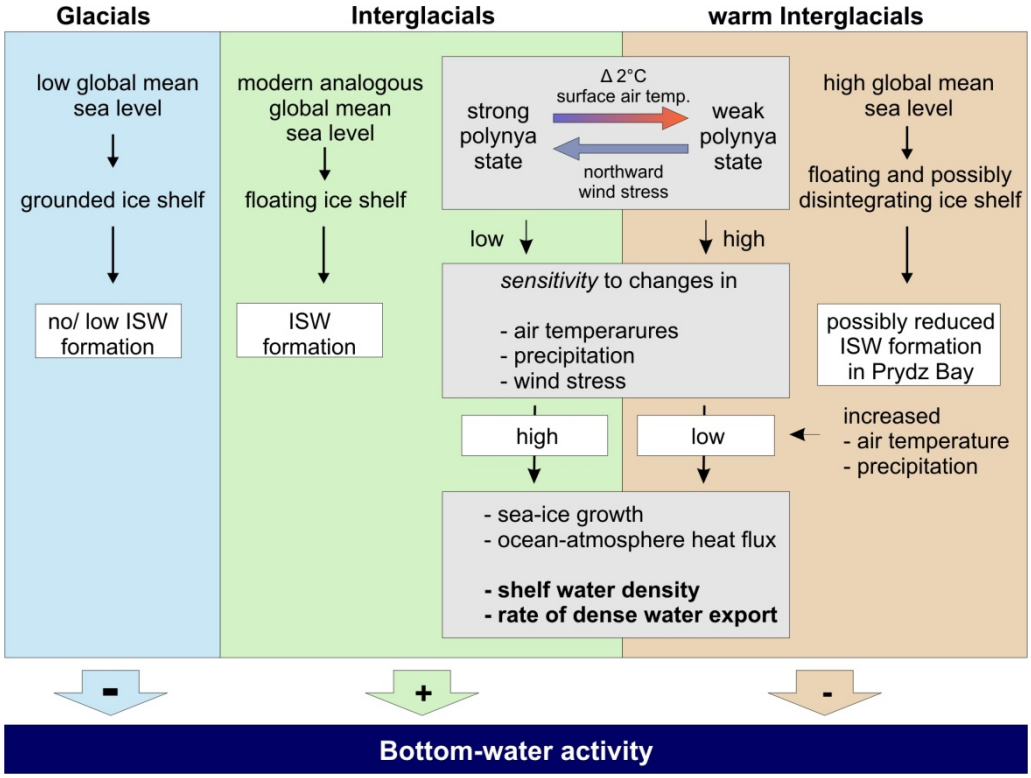

Fig. 5.1 Schematic of the main factors controlling bottom-water activity. Lowest bottom-water activity is recognized during glacial. During modern analogue interglacials, bottom-water activity is high due to formation of dense water in polynya regions in conjunction with super-cooling of shelf waters underneath floating ice shelves. For warmer-than-modern interglacial periods, palaeoenvironmental and modelling results (Marsland et al., 2007) provide evidence for reduced bottom-water activity due to diminished polynya activity.

The response of polynya systems to changes in atmospheric conditions is modelled by Marsland et al. (2007). The authors report two possible states of polynya activity: the strong phase is characterized by enhanced sea-ice formation resulting in much denser shelf waters. Consequently, the coastal polynya produces a much stronger outflow of shelf waters sufficiently dense to form bottom water. Due to either increase in air temperature and/ or decrease in precipitation, sea-ice production and sea-ice fraction are reduced. By an increase in air temperature of about 2°C, the polynya state changes to a weak polynya when shelf water export is much more sensitive to the atmospheric forcing (Fig. 5.2). As a result, it seems very likely that the slowdown in export of shelf water will increase over time if coastal polynya systems show a proclivity towards the weak polynya state as global warming progresses. The palaeoenvironmental implications from MacRobertson shelf and Kerguelen Drift feed the assumptions made by Marsland et al. (2007).

5.4 Palaeoenvironmental history of Prydz Bay compared to that from other sites around the East Antarctic margin

Today, scientific research along the East Antarctic margin is done focussing on three hotspot areas: the Weddell Sea/ Antarctic Peninsula (comprising the boundary of East and West Antarctica), Prydz Bay and off Wilkes Land. These areas comprise different morphologies and glacial configurations. In this regard, the comparison of the palaeoenvironmental evolution from the different regions helps to draw an integrated picture on the behaviour of the East Antarctic Ice Sheet and adjacent oceanographic and glaciologic features in terms of climate change. The Weddell Sea is a huge shelf margin hosting a wide ice shelf that is fed by several grounded inland glaciers. In contrast, large proportions of the inland ice on Wilkes Land are grounded below sea level and might respond very sensitively to changing environmental conditions. Prydz Bay is a comparable narrow shelf area hosting the Amery Ice Shelf which is fed by a giant outlet glacier.

Only little is known about the dynamics of ice masses in the Wilkes Land region during the Quaternary (Caburlotto et al., 2010), scientific research is still ongoing (e.g. Expedition 318 Scientists, 2010). Previous investigations of sediments from Wilkes Land continental slope revealed that the deposition of material resulted from alternation of gravity flows (slumps, debris flows, turbidity currents) and contourite flow (Busetti et al., 2003; Escutia et al., 2003) similar to results obtained from the Weddell Sea continental margin (e.g. Melles, 1991; Grobe and Mackensen, 1992; Bart et al., 1999). At the Prydz Bay continental margin, a similar alternation was not observed through the Quaternary, possibly owed to the particular shelf morphology and over-deepening of the drainage basin. Sedimentation on the continental slope rather took place by meltwater plumes and/ or dense water spilled over the shelf break and intense ice rafting during times of waning ice sheets. The LAIS drainage system therefore can be assumed as to be relatively stable with respect to the ice masses hosted in the Weddell Sea and on Wilkes Land. The mid-Pleistocene LAIS retreat, however, is part of a major palaeoenvironmental event observed in the Southern Ocean and also in the West Antarctic (e.g. Teitler et al., 2007; Scherer et al., 2008; Naish et al., 2009) and modelled by Pollard and DeConto (2009).

Ice retreat after the last glacial around 12.8 cal. ka BP inferred from sediment core PS69/849-2 is in the range of previous findings from Prydz Bay (e.g. Verleyen et al., 2005) and MacRobertson Land (e.g. Harris and O'Brien, 1998; Sedwick et al., 2001) and almost synchronous along the East Antarctic margin (Melles, 1991; Grobe and Mackensen, 1992; Anderson et al., 2002; Yoon et al., 2007; Heroy et al., 2008; Denis et al., 2009a). The synchronous timing of the decoupling of grounded ice sheets from their bed suggests an Antarctic-wide event the main trigger, probably mwp-1A (Fairbanks, 1989; Fleming et al.,

1998). Small variations in the onset of the deglaciation are possibly related to the different response time of the glacial features to sea-level rise or due to different shelf morphologies. Slow down of deglaciation in many areas is placed around 8 cal. ka BP to 9.5 cal. ka BP, correlating well with the end of the Antarctic early Holocene climate optimum observed in Antarctic ice core records (Masson et al., 2000). This correlation suggests an external forcing on ice dynamics additional to sea-level changes.

The mid-Holocene hypsithermal, as observed in the sediment core from Burton Basin between 7.7 cal. ka BP and 6.7 cal. ka BP, is widely recognized along the Antarctic margin. Its beginning as well as its duration, however, show strong variability between different regions. For example, the hypsithermal in the Antarctic Peninsula region occurred between 9.7 cal. ka BP and 3.4 cal. ka BP, depending on the type and location of the archives investigated (Bentley et al., 2009). Diatom data from Adelie Coast cores place the hypsithermal between 7.7 cal. ka BP and 3.9 cal. ka BP (Crosta et al., 2007, 2008; Denis et al., 2009a) and indicate warmer temperatures during the mid-Holocene and less extensive sea-ice cover, probably indicating earlier sea-ice breakup and later sea-ice freezing during autumn. This coincides with lower bottom-water formation, such as indicated by a low stand plateau of Sortable Silt between 7.4 and 5 cal. ka BP (Denis et al., 2009a). A mid-Holocene event is also recorded in Prydz Bay by a possible retreat of the LAIS around 5.6 ^{14}C ka BP (Hemer and Harris, 2003). Whether the differences in the timing of the hypsithermal are related to problems arising from radiocarbon dating (especially the estimate of possible reservoir ages) or different response times for the single proxies used to infer on palaeoenvironmental changes, remains questionable. Eventually, it cannot be excluded, that the factor triggering the palaeoenvironmental changes at the different sites – possibly the intrusion of warm subpolar waters onto the shelves (e.g. Bentley et al., 2009) – became important at different times. Regardless of the mechanisms responsible for the mid-Holocene hypsithermal it can be concluded that minor warming in the Antarctic led to reorganization of the ocean-ice-atmospheric system.

5.5 Further implications in conjunction with IPCC Assessment Report 4 (AR 4) predictions

In the recent past, the behaviour of ice masses at the Antarctic margin in response to global change gained great popularity and thoughtfulness, especially during the fourth International Polar Year (IPY) in 2007/2008. In the light of the ongoing climate change debate, the question arises, to which extent the Lambert Glacier-Amery Ice Shelf system could be affected by global warming. One could assume that increasing global temperatures and

rising sea level result in accelerated calving and/ or changes in the strength of bottom water formation. To draw some tentative conclusions on the sensitivity of glacial features in the Prydz Bay region to future warming, the recent environmental situation is compared to responses of the LAIS to past warming events.

According to the IPCC AR4 (Bindoff et al., 2007), since 1961 global average sea level has risen at an average rate of 1.8 (1.3 to 2.3) mm/yr and since 1993 at 3.1 (2.4 to 3.8) mm/yr, with contributions from thermal expansion, melting glaciers and ice caps, and polar ice sheets. During the 21st century, global sea level is projected to rise at a greater rate than during 1961 to 2003. Under the IPCC Special Report on Emission Scenarios (SRES) scenarios, the projected global sea-level rise during the 21st century will be 0.18 to 0.59 m above 1980 - 1990 levels (Meehl et al., 2007). According to the palaeoenvironmental reconstructions presented in this thesis (chapter 5.2), the LAIS remained stable unless sea-level rose at least ~ 6 m above present day levels. Thus, one can speculate that sea-level rise during the 21st century alone might probably be not sufficient enough to cause major disintegrations of the LAIS.

Assumptions on possible shifts in bottom-water formation in polynya regions strongly depend on future temperature trends. Multi-model global averages of surface warming for different scenarios suggest best estimates of temperature change during the 21st century between 1.8 and 4.0°C relative to the period between 1980 and 1999 (Meehl et al., 2007). In Antarctica, there are differences among the model projections concerning polar amplification of warming, especially over the continent (Parkinson, 2004). In several simulations, however, the warming is amplified over a narrow Southern Ocean band from which sea ice retreats (Anisimov et al., 2007). Palaeoenvironmental reconstructions indicated weakened polynya activity during MIS 5.5 and the mid-Holocene, when temperatures in Antarctica were 4°C or less above the modern level (chapter 5.3). Following these results and modelling scenarios of Marsland et al. (2007) suggesting a shift to a weak polynya state by 2°C temperature elevation, a decreased contribution of bottom water originating in polynya areas to the global thermohaline circulation cannot be excluded in terms of the predicted future temperature change.

5.6 Conclusions

By multi-proxy investigation of sediment cores recovered from the continental shelf, continental slope and deep ocean in the Prydz Bay-Kerguelen region, the following conclusions can be drawn:

- Heavy minerals provide a suitable tool to reconstruct the provenance of ice-rafted material at least on the continental shelf and adjacent slope. The garnet/ hornblende

(Gn/Hb) ratio has evolved the best parameter to distinguish between sediments originating from crystalline source rocks (Gn/Hb < 1) and ancient Permo-Triassic sediments (Gn/Hb > 1)

- Clay minerals nicely reflect the influence of oceanographic features on sedimentation and were used to establish sediment-hydrographic provinces. Consequently, they provide good tracers to reconstruct past shifts in oceanographic flow patterns.

- The LAIS experienced a transition from a terrestrial-based to a marine based ice sheet probably around 1.25 Ma

- Two major deglaciation events occurred. The first event took place around 1 Ma (possibly linked to the warm MIS 31) and is observed as a major event around the Antarctic. A second major retreat of the LAIS then occurred during or shortly after the last interglacial (MIS 5.5), when sea level was 6 m to 9 m higher than today.

- During the middle and late Pleistocene, the LAIS was relatively stable. This is mainly related to excavation and over-deepening of the Lambert Glacier drainage basin during the mid-Pleistocene. After that, sea-level fluctuations were probably insufficient to destabilize the LAIS.

- Post-LGM deglaciation on MacRobertson shelf commenced around 12.8 cal. ka BP and correlates well with findings from other regions along the East Antarctic margin suggesting melt-water pulse mpw-1A as the main trigger.

- Calving of icebergs ceased around 5.4 cal. ka BP, when global sea-level rise stabilized and MacRobertson Land experienced post-glacial rebound

- Bottom-water formation was more intense during interglacials compared to glacial times, as discovered in earlier studies. Superimposed on this general pattern, new findings indicate reduced bottom-water formation during warm interglacials exemplarily shown for the last interglacial (MIS 5.5) and the warm mid-Holocene.

- The reduction in bottom-water formation is related to shifts in the polynya activity, particularly to sea-ice formation. By global warming, a transition from a strong to weak polynya state is assumed with shelf water export being much more sensitive to atmospheric forcing. Increasing air temperatures and/ or precipitation would then result in reduced sea-ice production and sea-ice fraction, along with diminished dense water export.

Deduced from these findings, sea-level rise such as predicted by the IPCC AR4 for the 21st century, will probably have no major impact in terms of disintegration of the LAIS. Rather, major changes concerning polynya activity and thus in the strength of bottom-water formation could occur if IPCC AR4 predictions on temperature rise and modelling scenarios in terms of polynya dynamics turn into reality.

5.7 Outlook

Important future aspects of research along the East Antarctic margin could be to:

- narrow sea-bed surface sampling to guarantee a better sample coverage within the Prydz Bay-Kerguelen region. This would enable statistical analysis to group samples according to their mineral assemblages in a more objective way.

- establish a record of sea-surface temperatures for at least the Holocene in Prydz Bay (e.g. by applying transfer functions on diatom data). Ecological investigations on diatoms could help to draw more precise conclusions on sea-ice dynamics.

- extend the effort concerning palaeoenvironmental reconstruction of glacial-interglacial polynya dynamics to polynya regions along the East and West Antarctic margin and distal locations with sedimentation controlled by bottom-water formed due to polynya activity.

- continuously monitor the areal extent of the Cape Darnley polynya in response to atmospheric perturbations by means of remote sensing (passive microwave data, e.g. Special Sensor Microwave Imager (SSM/I)).

- continuously monitor the bottom-water export along the flow path by current-meter moorings synchronously to above mentioned remote sensing to gain clearer insights into the driving mechanisms of bottom-water formation in polynya areas.

- conduct further modelling approaches on polynya dynamics to assess the sensitivity of sea-ice variability and bottom-water formation to changing atmospheric forcing.

6. References

ANDERSON, J.B., SHIPP, S.S., LOWE, A.L., WELLNER, J.S., & MOSOLA, A.B. 2002. The Antarctic Ice Sheet during the Last Glacial Maximum and its subsequent retreat history: a review. *Quaternary Science Reviews,* **21**(1-3), 49-70.

ANDREWS, J.T., SMITH, L.M., PRESTON, R., COOPER, T., & JENNINGS, A.E. 1997. Spatial and temporal patterns of iceberg rafting debris (IRD) along the East Greenland margin, approximately 68°N, over the last 14 ka. *Journal Of Quaternary Science,* **12**, 1-13.

ANDREWS, J.T., DOMACK, E., CUNNINGHAM, W.L., LEVENTER, A., LICHT, K.J., JULL, A.J.T., DEMASTER, D.J., & JENNINGS, A.E. 1999. Problems and possible solutions concerning radiocarbon dating of surface marine sediments, Ross Sea, Antarctica. *Quaternary Research,* **52**, 206-216.

ANDREWS, J.T. 2000. Icebergs and iceberg rafted detritus (IRD) in the North Atlantic: facts and assumptions. *Oceanography*, **13**(3), 100-108.

ANISIMOV, O.A., VAUGHAN, D.G., CALLAGHAN, T.V., FURGAL, C., MARCHANT, H., PROWSE, T.D., VILHJÁLMSSON, H., & WALSH, J.E. 2007. Polar regions (Arctic and Antarctic). *In* PARRY, M.L., CANZIANI, O.F., PALUTIKOF, J.P., LINDEN, P.J.V.D., & HANSON, C.E. eds. *Climate Change 2007: Impacts, Adaptation and Vulnerability. Contribution of Working Group II to the Fourth Assessment Report of the Intergovernmental Panel on Climate Change.* Cambridge: Cambridge University Press, 653-685.

BAINES, P.G., & CONDIE, S. 1998. Observations and modeling of Antarctic downslope flows: A review. *In*: JACOBS, S.S., & WEISS, R.F., eds. *Ocean, Ice, and Atmosphere: Interactions at the Antarctic margin*. Washington, D.C.: Antarctic Research Series **75**, 29-49.

BARKER, P.F., & THOMAS, E. 2004. Origin, signature and palaeoclimatic influence of the Antarctic Circumpolar Current. *Earth-Science Reviews,* **66**(1-2), 143-162.

BARKER, P.F., DIEKMANN, B., & ESCUTIA, C. 2007. Onset of Cenozoic Antarctic glaciation. *Deep Sea Research Part II: Topical Studies in Oceanography,* **54**, 2293-2307.

BARRETT, P., SARTI, M., & WISE, S. 2000. Studies from the Cape Roberts Project Ross Sea, Antarctica: Initial Report on CRP-3. *Terra Antarctica,* **7**(1-2), 209 pp.

BARRON, J., LARSEN, B. & BALDAUF, J.G. 1991. Evidence for late Eocene to early Oligocene Antarctic glaciation and observations on late Neogene glacial history of Antarctica. *In*: BARRON, J., LARSEN, B., eds. *Proceeding of the Ocean Drilling Program, Scientific Results*, **119**. Texas A&M University, Ocean Drilling Program, College Station, TX, 869-891.

BART, P.J., DEBATIST, M., & JOKAT, W. 1999. Interglacial collapse of Crary Trough-mouth fan, Weddell Sea, Antarctica; implications for Antarctic glacial history. *Journal of Sedimentary Research,* **69**(6), 1276-1289.

BARTOLI, G., SARNTHEIN, M., WEINELT, M., ERLENKEUSER, H., GARBE-SCHONBERG, D., & LEA,

D.W. 2005. Final closure of Panama and the onset of northern hemisphere glaciation. *Earth and Planetary Science Letters*, **237**(1-2), 33-44.

BECQUEY, S., & GERSONDE, R. 2002. Past hydrographic and climatic changes in the Subantarctic Zone of the South Atlantic - The Pleistocene record from ODP Site 1090. *Palaeogeography Palaeoclimatology Palaeoecology*, **182**(3-4), 221-239.

BECQUEY, S., & GERSONDE, R. 2003a. Data report: early and mid-Pleistocene (MIS 65-11) summer sea-surface temperature, foraminiferal fragmentation, and ice-rafted debris records from the subantarctic (ODP Leg 177 Site 1090). *In:* GERSONDE, R., HODELL, D.A., & BLUM, P., eds. *Proceedings of the Ocean Drilling Program, Scientific Results*, **177**. Texas A&M University, Ocean Drilling Program, College Station, TX, 1-23.

BECQUEY, S., & GERSONDE, R. 2003. A 0.55-Ma paleotemperature record from the Subantarctic zone: Implications for Antarctic Circumpolar Current development. *Palaeoceanography*, **18**(1), 1014.

BENTLEY, M.J., HODGSON, D.A., SMITH, J.A., COFAIGH, C.O., DOMACK, E.W., LARTER, R.D., ROBERTS, S.J., BRACHFELD, S., LEVENTER, A., HJORT, C., HILLENBRAND, C.D., & EVANS, J. 2009. Mechanisms of Holocene palaeoenvironmental change in the Antarctic Peninsula region. *Holocene*, **19**(1), 51-69.

BERG, S., WAGNER, B., CREMER, H., LENG, M.J., & MELLES, M. in review. Late Quaternary environmental and climate history of the Rauer Group, East Antarctica. *Palaeogeography Palaeoclimatology Palaeoecology*.

BERKMAN, P.A., & FORMAN, S.L. 1996. Pre-bomb radiocarbon and the reservoir correction for calcareous marine species in the Southern Ocean. *Geophysical Research Letters*, **23**(4), 363-366.

BINDOFF, N.L., ROSENBERG, M.A. & WARNER, M.J. 2000. On the circulation and water masses over the Antarctic continental slope and rise between 80 and 150 °E. *Deep-Sea Research Part II-Topical Studies In Oceanography*, **47**(12-13), 2299-2326.

BINDOFF, N.L., WILLEBRAND, J., ARTALE, V., CAZENAVE, A., GREGORY, J., GULEV, S., HANAWA, K., LE QUÉRÉ, C., LEVITUS, S., NOJIRI, Y., SHUM, C.K., TALLEY, L.D., & UNNIKRISHNAN, A. 2007. Observations: Oceanic Climate Change and Sea Level. *In*: SOLOMON, S., QIN, D., MANNING, M., CHEN, Z., MARQUIS, M., AVERYT, K.B., TIGNOR, M., & MILLER, H.L., eds. *Climate Change 2007: The Physical Science Basis. Contribution of Working Group I to the Fourth Assessment Report of the Intergovernmental Panel on Climate Change.* Cambridge, United Kingdom and New York, NY, USA: Cambridge University Press.

BISCAYE, P.E. 1965. Mineralogy and sedimentation of recent deep-sea clay in the Atlantic Ocean and adjacent seas and oceans. *Geological Society American Bulletin*, **76**, 803-832.

BONN, W.J. 1995. Biogenic opal and barium: Indicators for late Quaternary changes in productivity at the Antarctic continental margin, Atlantic Sector, *Reports on Polar*

Research, 186 pp.

BORCHERS, A., VOIGT, I., KUHN, G., & DIEKMANN, B. 2010. Mineralogy of glaciomarine sediments from the Prydz Bay-Kerguelen region: relation to modern depositional environments. *Antarctic Science*, in press.

BOWEN, D.Q. 2010. Sea level ~400 000 years ago (MIS 11): analogue for present and future sea-level? *Climate Of The Past*, **6**, 19-29.

BUSETTI, M., CARBURLOTTO, L., DAMIANI, D., GIORGETTI, G., LUCCHI, R.G., QUILTY, P.G., & VILLA, G. 2003. Plio-Quaternary sedimentation on the Wilkes land continental rise: preliminary results. *Deep Sea Research Part II: Topical Studies in Oceanography*, **50**, 1529–1562.

CARBURLOTTO, L., LUCCHI, R.G., SANTIS, L.D., MACRI, P., & TOLOTTI, R. 2010. Sedimentary processes on the Wilkes Land continental rise reflect changes in glacial dynamic and bottom water flow. *International Journal Of Earth Sciences*, **99**, 909-926.

CLOSE, D.I. 2010, in press. Slope and fan deposition in deepwater turbidite systems, East Antarctica. *Marine Geology*, doi: 10.1016/j.margeo.2010.1003.1002.

COOPER, A.K., BARRETT, P.J., HINZ, K., TRAUBE, V., LEITCHENKOV, G., & STAGG, H.M.J. 1991a. Cenozoic prograding sequences of the Antarctic continental margin: a record of glacio-eustatic and tectonic events. *Marine Geology*, **102**, 175-213.

COOPER, A.K., STAGG, H.M.J., GEIST, E. 1991b. Seismic stratigraphy and structure of Prydz Bay, Antarctica: implications from Leg 119 drilling. *In*: BARRON, J., LARSEN, B., eds. *Proceeding of the Ocean Drilling Program, Scientific Results*, **119**. Texas A&M University, Ocean Drilling Program, College Station, TX, 5-26.

COOPER, A.K., O`BRIEN, P.E. 2004. Leg 188 synthesis: Transitions in the glacial history of the Prydz Bay region, East Antarctica, from ODP drilling. *In:* COOPER, A.K., O`BRIEN, P.E. & RICHTER, C., eds. *Proceedings of the Ocean Drilling Program, Scientific Results*, **188**. Texas A&M University, Ocean Drilling Program, College Station, TX, 1-42.

CREMER, H., GORE, D., MELLES, M., & ROBERTS, D. 2003. Palaeoclimatic significance of late Quaternary diatom assemblages from southern Windmill Islands, East Antarctica. *Palaeogeography Palaeoclimatology Palaeoecology*, **195**(3-4), 261-280.

CROSTA, X., DEBRET, M., DENIS, D., COURTY, M.A., & THER, O. 2007. Holocene long- and short term climate changes off Adelie Land, East Antarctica. *Geochemistry Geophysics Geosystems*, **8**(11), Q11009.

CROSTA, X., DENIS, D., & THER, O. 2008. Sea ice seasonality during the Holocene, Adelie Land, East Antarctica. *Marine Micropaleontology*, **66**(3-4), 222-232.

DAMIANI, D., GIORGETTI, G., & TURBANTI, I.M. 2006. Clay mineral fluctuations and surface textural analysis of quartz grains in Pliocene-Quaternary marine sediments from Wilkes Land continental rise (East-Antarctica): paleoenvironmental significance. *Marine Geology*,

226(3-4), 281-295.

DENIS, D., CROSTA, X., SCHMIDT, S., CARSON, D.S., GANESHRAM, R.S., RENSSEN, H., BOUT ROUMAZEILLES, V., ZARAGOSI, S., MARTIN, B., CREMER, M., & GIRAUDEAU, J. 2009a. Holocene glacier and deep water dynamics, Adelie Land region, East Antarctica. *Quaternary Science Reviews,* **28**(13-14), 1291-1303.

DENIS, D., CROSTA, X., SCHMIDT, S., CARSON, D.S., GANESHRAM, R.S., RENSSEN, H., CRESPIN, J., THER, O., BILLY, I., & GIRAUDEAU, J. 2009b. Holocene productivity changes off Adelie Land (East Antarctica). *Paleoceanography,* **24**, PA3207.

DENIS, D., CROSTA, X., BARBARA, L., MASSE, G., RENSSEN, H., THER, O., & GIRAUDEAU, J. 2010. Sea ice and wind variability during the Holocene in East Antarctica:insight on middle-high latitude coupling. *Quaternary Science Reviews*, in press, doi:10.1016/j.quascirev.2010.1008.1007.

DIEKMANN, B. & KUHN., G. 1999. Provenance and dispersal of glacial-marine surface sediments in the Weddell Sea and adjoining areas, Antarctica: ice-rafting versus current transport. *Marine Geology*, **158**(1-4), 209-231.

DIEKMANN, B., KUHN, G., RACHOLD, V., ABELMANN, A., BRATHAUER, U., FUTTERER, D.K., GERSONDE, R., & GROBE, H. 2000. Terrigenous sediment supply in the Scotia Sea (Southern Ocean): response to Late Quaternary ice dynamics in Patagonia and on the Antarctic Peninsula. *Palaeogeography Palaeoclimatology Palaeoecology*, **162**(3-4), 357-387.

DIEKMANN, B., & KUHN, G. 2002. Sedimentary record of the mid-Pleistocene climate transition in the southeastern South Atlantic (ODP Site 1090). *Palaeogeography, Palaeoclimatology, Palaeoecology*, **182**, 241-258.

DIEKMANN, B., FÜTTERER, D.K., GROBE, H., HILLENBRAND, C.D., KUHN, G., PETSCHICK, R. & PIRRUNG, M. 2003. Terrigenous sediment supply in the polar to temperate South Atlantic: land-ocean links of environmental changes during the Late Quaternary. *In:* WEFER, G., MULITZA, S. & RATMEYER, V., eds. *The South Atlantic in the Late Quaternary: Reconstruction of material budget and current systems*. Berlin: Springer, 375-399.

DIETZE, E., HARTMANN, K., DIEKMANN, B., IJMKER, J., LEHMKUHL, F., OPITZ, S., STAUCH, G., WÜNNEMANN, B., & BORCHERS, A. in review. An end-member algorithm for deciphering modern detrital processes from lake sediments of Lake Donggi Cona, NE Tibetan Plateau, China. *Sedimentary Geology*.

DOMACK, E., O'BRIEN, P., HARRIS, P., TAYLOR, F., QUILTY, P.G., DE SANTIS, L. & RAKER, B. 1998. Late Quaternary sediment facies in Prydz Bay, East Antarctica, and their relationship to glacial advance onto the continental shelf. *Antarctic Science*, **10**(3), 236-246.

DOMACK, E., AMBLAS, D., GILBERT, R., BRACHFELD, S., CAMERLENGHI, A., REBESCO, M., CANALS, M., & URGELES, R. 2006. Subglacial morphology and glacial evolution of the Palmer deep outlet system, Antarctic Peninsula. *Geomorphology,* **75**(1-2), 125-142.

DONOHUE, K.A., HUFFORD, G.E. & MCCARTNEY, M.S. 1999. Sources and transport of the deep western boundary current east of the Kerguelen Plateau. *Geophysical Research Letters*, **26**(7), 851-854.

DREWRY, D.J. 1986. *Glacial geological processes*. London: E. Arnold. 276 pp.

EHRMANN, W., & GROBE, H. 1991. Cyclic sedimentation at sites 745 and 746. *In* BARRON, J., LARSEN, B. eds. *Proceedings of the Ocean Drilling Program, Scientific Results*, **119.** Texas A&M University, Ocean Drilling Program, College Station, TX, 225-237.

EHRMANN, W., GROBE, H., & FÜTTERER, D.K. 1991. Late Miocene to Holocene glacial history of East Antarctica revealed by sediments from Sites 745 and 746. *In:* BARRON, J., LARSEN, B., eds. *Proceedings of the Ocean Drilling Program, Scientific Results*, **119**. Texas A&M University, Ocean Drilling Program, College Station, TX, 239-289.

EHRMANN, W., MELLES, M., KUHN, G. & GROBE, H. 1992. Significance of clay mineral assemblages in the Antarctic Ocean. *Marine Geology*, **107**, 249-273.

EHRMANN, W., BLOEMENDAL, J., HAMBREY, M.J., MCKELVEY, B., & WHITEHEAD, J. 2003. Variations in the composition of the clay fraction of the Cenozoic Pagodroma Group, East Antarctica: implications for determining provenance. *Sedimentary Geology*, **161**(1-2), 131-152.

EPICA COMMUNITY MEMBERS. 2006. One-to-one coupling of glacial climate variability in Greenland and Antarctica. *Nature*, **444**, 195 - 198.

ESCUTIA, C., WARNKE, D., ACTONC, G.D., BARCENA, A., BURCKLE, L., CANALS, M., & FRAZEE, C.S. 2003. Sediment distribution and sedimentary processes across the Antarctic Wilkes Land margin during the Quaternary. *Deep Sea Research Part II: Topical Studies in Oceanography*, **50**, 1481-1508.

ESQUEVIN, J. 1969. Influence de la composition chimique des illites sur le cristallinite. *Bulletin du Centre de Recherches de Pau, Société Nationale des Petroles d'Aquitaine*, **3**, 147-154.

EXPEDITION SCIENTISTS. 2010. Wilkes Land Glacial History: Cenozoic East Antarctic Ice Sheet evolution from Wilkes Land margin sediments. *IODP Preliminary Report*, **318**. Texas A&M University, Ocean Drilling Program, College Station, TX

FAIRBANKS, R.G. 1989. A 17,000-Year Glacio-Eustatic Sea-Level Record - Influence Of Glacial Melting Rates On The Younger Dryas Event And Deep-Ocean Circulation. *Nature*, **342**(6250), 637-642.

FEDEROV, L.V., GRIKUROV, G.E., KURININ, R.G., & MASOLOV, V.N. 1982. Crustal structure of the Lambert Glacier area from geophysical data. *In:* CRADDOCK, C. *ed. Antarctic geoscience.* Madison: University of Wisconsin Press, 931-936.

FIELDING, C.R., & WEBB, J.A. 1996. Facies and cyclicity of the Late Permian Bainmedart Coal Measures in the Northern Prince Charles Mountains, MacRobertson Land, Antarctica. *Sedimentology*, **43**, 295-322.

FINK, D., MCKELVEY, B., HAMBREY, M.J., FABEL, D., & BROWN, R. 2006. Pleistocene deglaciation chronology of the Amery Oasis and Radok Lake, northern Prince Charles Mountains, Antarctica. *Earth and Planetary Science Letters,* **243**(1-2), 229-243.

FLEMING, K., JOHNSTON, P., ZWARTZ, D., YOKOYAMA, Y., LAMBECK, K., & CHAPPELL, J. 1998. Refining the eustatic sea-level curve since the Last Glacial Maximum using far- and intermediate-field sites. *Earth and Planetary Science Letters,* **163**(1-4), 327-342.

FLORES, J.A., & SIERRO, F.J. 2007. Pronounced mid-Pleistocene southward shift of the Polar Front in the Atlantic sector of the Southern Ocean. *Deep Sea Research Part II: Topical Studies in Oceanography*, **54**(21-22), 2432-2442.

FLORINDO, F., BOHATY, S.M., ERWIN, P.S., RICHTER, C., ROBERTS, A.P., WHALEN, P.A., & WHITEHEAD, J. 2003. Magnetobiostratigraphic chronology and palaeoenvironmental history of Cenozoic sequences from ODP sites 1165 and 1166, Prydz Bay, Antarctica. *Palaeogeography Palaeoclimatology Palaeoecology,* **198**, 69-100.

FLOWER, B.P., & KENNET, J.P. 1994. The middle Miocene climatic transition: East Antarctic ice sheet development, deep ocean circulation and global carbon cycling. *Palaeogeography Palaeoclimatology Palaeoecology*, **108**(3-4), 537-555.

FREY, F.A., WEIS, D., YANG, H.J., NICOLAYSEN, K., LEYRIT, H., & GIRET, A. 2000. Temporal geochemical trends in Kerguelen Archipelago basalts: evidence for decreasing magma supply from the Kerguelen Plume. *Chemical Geology,* **164**(1-2), 61-80.

FRICKER, H.A., WARNER, R.C. & ALLISON, I. 2000. Mass balance of the Lambert GlacierAmery Ice Shelf system, East Antarctica: a comparison of computed balance fluxes and measured fluxes. *Journal of Glaciology,* **46**, 561-570.

GALE, S.J. & HOARE, P.G. 1991. *Quaternary sediments: petrographic methods for the study of unlithified rocks.* New York: Halsted Press, 323 pp.

GALTON-FENZI, B., MARSLAND, S., MEIJERS, A., & FRASER, A. 2010. The influence of coastal polynyas on the basal melting of ice shelves, EGU2010-14386. *EGU General Assembly.* Vienna. Geophysical Research Abstracts.

GILBERT, R., CHONG, A., DUNBAR, R.B., & DOMACK, E.W. 2003. Sediment trap records of glacimarine sedimentation at Muller Ice Shelf, Lallemand Fjord, Antarctic Peninsula. *Arctic Antarctic and Alpine Research,* **35**(1), 24-33.

GIORGETTI, G., TALARICO, F., SANDRONI, S., & ZEOLI, A. 2009. Provenance of Pleistocene sediments in the ANDRILL AND-1B drillcore: Clay and heavy mineral data. *Global and Planetary Change,* **69**(3), 94-102.

GOODELL, H.G. 1973. The sediments. *In:* GOODELL, H.G., HOUTZ, R., EWING, M., HAYES, D., NAINI, B., ECHOLS, R.J., KENNETT, J.P. & DONAHUE, J.G., eds. *Marine Sediments of the Southern Oceans.* New York: American Geographical Society: Antarctic Map Folio Series **17**, 1-9.

GORDON, A.L. & GOLDBERG, R.D. 1970. Circumpolar characteristics of Antarctic waters. American Geographie Society (New York), *Antarctic Map Folio Series*, **Folio 13**, 1-5.

GROBE, H. 1987. A simple method for the determination of ice-rafted debris in sediment cores. *Polarforschung,* **57**(3), 123-126.

GROBE, H. & MACKENSEN, A. 1992. Late Quaternary climatic cycles as recorded in sediments from the Antarctic continental margin. *In:* KENNET, J.P. & WARNKE, D.A., eds. *The Antarctic paleoenvironment: a perspective on global change.* Washington. D.C.: American Geophysical Union, 349-376.

GROOTES, P.M., STUIVER, M., WHITE, J.W.C., JOHNSEN, S.J., & JOUZEL, J. 1993. Comparison of oxygen isotope records from the GISP2 and GRIP Greenland ice cores. *Nature,* **366**, 552-554.

GROOTES, P.M., STEIG, E.J., STUIVER, M., WADDINGTON, E.D., MORSE, D.L., & NADEAU, M.-J. 2001. The Taylor Dome Antarctic 18O record and globally synchronous changes in climate. *Quaternary Research,* **56**(3), 289-298.

HALL, B.L. 2009. Holocene glacial history of Antarctica and the sub-Antarctic islands. *Quaternary Science Reviews,* **28**(21-22), 2213-2230.

HAMBREY, M.J., EHRMANN, W., & LARSEN, B. 1991. Cenozoic glacial record of the Prydz Bay continental shelf, East Antarctica. *In*: BARRON, J., LARSEN, B., eds. *Proceeding of the Ocean Drilling Program, Scientific Results*, **119**. Texas A&M University, Ocean Drilling Program, College Station, TX, 77-132.

HAMBREY, M.J., & MCKELVEY, B. 2000a. Major Neogene fluctuations of the East Antarctic ice sheet: Stratigraphic evidence from the Lambert Glacier region. *Geology*, **28**(10), 887-890.

HAMBREY, M.J. & MCKELVEY, B. 2000b. Neogene fjordal sedimentation on the western margin of the Lambert Graben, East Antarctica. *Sedimentology*, **47**, 577-607.

HARRIS, P.T., & O'BRIEN, P.E. 1996. Geomorphology and sedimentology of the continental shelf adjacent to Mac. Robertson Land, East Antarctica: a scalped shelf. *Geo-Marine Letters*, **16**, 287-296.

HARRIS, P., O`BRIEN, P.E., QUILTY, P.G., TAYLOR, F., DOMACK, E., DE SANTIS, L. & RAKER, B. 1997. Post Cruise Report, Antarctic CRC Marine Geoscience: Vincennes Bay, Prydz Bay and Mac. Robertson Shelf. *AGSO Rec., 1997/51,* 1-75.

HARRIS, P.T. & O'BRIEN, P.E. 1998. Bottom currents, sedimentation and ice-sheet retreat facies successions on the Mac Robertson shelf, East Antarctica. *Marine Geology*, **151**(1-4), 47-72.

HARRIS, P.T., TAYLOR, F., PUSHINA, Z., LEITCHENKOV, G., O`BRIEN, P.E., & SMIRNOV, V. 1998. Lithofacies distribution in relation to the geomorphic provinces of Prydz Bay, East Antarctica. *Antarctic Science,* **10**(3), 227-235.

HARRIS, P.T. 2000. Ripple cross-laminated sediments on the East Antarctic Shelf: evidence for episodic bottom water production during the Holocene? *Marine Geology,* **170**(3-4), 317-

330.

HEARTY, P.J., HOLLIN, J.T., NEUMANN, A.C., O'LEARY, M.J., & MCCULLOCH, M. 2007. Global sea-level fluctuations during the Last Interglaciation (MIS 5e). *Quaternary Science Reviews,* **26**(17-18), 2090-2112.

HEIL, P., & ALLISON, I. 1999. The pattern and variability of Antarctic sea-ice drift in the Indian Ocean and western Pacific sectors. *Journal Of Geophysical Research-Oceans,* **104**(C7), 15789-15802.

HEMER, M.A., & HARRIS, P.T. 2003. Sediment core from beneath the Amery Ice Shelf, East Antarctica, suggests mid-Holocene ice-shelf retreat. *Geology,* **31**(2), 127-130.

HEROY, D.C., SJUNNESKOG, C., & ANDERSON, J.B. 2008. Holocene climate change in the Bransfield Basin, Antarctic Peninsula: evidence from sediment and diatom analysis. *Antarctic Science,* **20**(1), 69-87.

HODGKINSON, R.P., COLMAN, R.S., ROBB, M., & WILLIAMS, R. 1991. *Current meter moorings in the region of Prydz Bay, Antarctica, 1987.* Australian Antarctic Division. 68 pp.

HODGSON, D.A., NOON, P.E., VYVERMAN, W., BRYANT, C.L., GORE, D.B., APPLEBY, P., GILMOUR, M., VERLEYEN, E., SABBE, K., JONES, V.J., ELLIS-EVANS, J.C., & WOOD, P.B. 2001. Were the Larsemann Hills ice-free through the Last Glacial Maximurn? *Antarctic Science,* **13**(4), 440-454.

HODGSON, D.A., VERLEYEN, E., SQUIER, A.H., SABBE, K., KEELY, B.J., SAUNDERS, K.M., & VYVERMAN, W. 2006. Interglacial environments of coastal east Antarctica: comparison of MIS 1 (Holocene) and MIS 5e (Last Interglacial) lake-sediment records. *Quaternary Science Reviews,* **25**, 179-197.

HODGSON, D.A., VERLEYEN, E., VYVERMAN, W., SABBE, K., LENG, M.J., PICKERING, M.D., & KEELY, B.J. 2009. A geological constraint on relative sea level in Marine Isotope Stage 3 in the Larsemann Hills, Lambert Glacier region, East Antarctica (31,366-33,228 cal. yr BP). *Quaternary Science Reviews,* **28**(25-26), 2689-2696.

HULTZSCH, N., WAGNER, B., DIEKMANN, B. & WHITE, D. 2008. Mineralogical implications for the Late Pleistocene glaciation in Amery Oasis, East Antarctica, from a lake sediment core. *Antarctic Science,* **20**(2), 169-172.

HUYBRECHTS, P., STEINHAGE, D., WILHELMS, F., & BAMBER, J.L. 2000. Balance velocities and measured properties of the Antarctic ice sheet from a new compilation of gridded data sets for modeling. *Annals of Glaciology,* **30**, 52-60.

INGOLFSSON, O., HJORT, C., BERKMAN, P.A., BJORCK, S., COLHOUN, E., GOODWIN, I.D., HALL, B., HIRAKAWA, K., MELLES, M., MOLLER, P., & PRENTICE, M.L. 1998. Antarctic glacial history since the Last Glacial Maximum: an overview of the record on land. *Antarctic Science,* **10**(3), 326-344.

INGOLFSSON, O. 2004. Quaternary glacial and climate history of Antarctica. *In:* EHLERS, J., &

GIBBARD, P.L. eds. *Quaternary Glaciations-extent and chronology*. Elsevier, 3-43.

JUNTTILA, J., RUIKKA, M. & STRAND, K. 2005. Clay-mineral assemblages in high-resolution Plio-Pleistocene interval at ODP Site 1165, Prydz Bay, Antarctica. *Global and Planetary Change*, **45**(1-3), 151-163.

JOUZEL, J., MASSON-DELMOTTE, V., CATTANI, O., DREYFUS, G., FALOURD, S., HOFFMANN, G., MINSTER, B., NOUET, J., BARNOLA, J.M., CHAPPELLAZ, J., FISCHER, H., GALLET, J.C., JOHNSEN, S., LEUENBERGER, M., LOULERGUE, L., LUETHI, D., OERTER, H., PARRENIN, F., RAISBECK, G., RAYNAUD, D., SCHILT, A., SCHWANDER, J., SELMO, E., SOUCHEZ, R., SPAHNI, R., STAUFFER, B., STEFFENSEN, J.P., STENNI, B., STOCKER, T.F., TISON, J.L., WERNER, M., & WOLFF, E.W. 2007. Orbital and Millennial Antarctic Climate Variability over the Past 800,000 Years. *Science*, **317**, 793-796.

KANFOUSH, S.L., HODELL, D.A., CHARLES, C.D., GUILDERSON, T.P., MORTYN, P.G., & NINNEMANN, U.S. 2000. Millennial-scale instability of the antarctic ice sheet during the last glaciation. *Science*, **288**(5472), 1815-1818.

KANFOUSH, S.L., HODELL, D.A., CHARLES, C.D., JANECEK, T.R., & RACK, F.R. 2002. Comparison of ice-rafted debris and physical properties in ODP Site 1094 (South Atlantic) with the Vostok ice core over the last four climatic cycles. *Palaeogeography Palaeoclimatology Palaeoecology*, **182**(3-4), 329-349.

KARIYA, C., HYODO, M., TANIGAWA, K., & SATO, H. 2010. Sea-level variation during MIS 11 constrained by stepwise Osaka Bay extensions and its relation with climatic evolution. *Quaternary Science Reviews*, **29**, 1863-1879.

KEMP, E.M. 1972. Reworked palynomorphs from West Ice Shelf area, East Antarctica, and their possible geological and paleoclimatological significance. *Marine Geology*, **13**(3), 145-157.

KEMP, E.M., GRIGOROV, I., PEARCE, R.B., & GARABATO, A.C.N. 2010. Migration of the Antarctic Polar Front through the mid-Pleistocene transition: evidence and climatic implications. *Quaternary Science Reviews*, **29**, 1993-2009.

KLUMP, J., HEBBELN, D., & WEFER, G. 2000. The impact of sediment provenance on barium-based productivity estimates. *Marine Geology*, **169**, 259-271.

KUVAAS, B. & LEITCHENKOV, G. 1992. Glaciomarine turbidite and current controlled deposits in Prydz Bay, Antarctica. *Marine Geology*, **108**(3-4), 365-381.

LEI, R.B., LI, Z.J., CHENG, B., ZHANG, Z.H., & HEIL, P. 2010. Annual cycle of landfast sea ice in Prydz Bay, East Antarctica. *Journal Of Geophysical Research-Oceans*, **115**.

LEVENTER, A., DOMACK, E., BARKOUKIS, A., MCANDREWS, B., & MURRAY, J. 2002. Laminations from the Palmer Deep: A diatom-based interpretation. *Paleoceanography*, **17**(2), 1027.

LEVENTER, A., DOMACK, E.W., DUNBAR, R.B., PIKE, J., STICKLEY, C.E., MADDISON, E., BRACHFELD, S., & MCCLENNEN, C. 2006. Marine sediment record from the East Antarctic

margin reveals dynamics of ice sheet recession. *GSA Today,* **16**, 4-10.

LISIECKI, L.E., & RAYMO, M.E. 2005. A Pliocene-Pleistocene stack of 57 globally distributed benthic d18O records. *Palaeoceanography,* **20**, PA1003.

LOUTRE, M.F., & BERGER, A. 2003. Marine isotope stage 11 as an analogue for the present interglacial. *Global and Planetary Change,* **36**, 209-217.

LUCCHI, R.G., & REBESCO, M. 2007. Glacial contourites on the Antarctic Peninsula margin: insight for palaeoenvironmental and palaeoclimatic conditions. *Geological Society, London, Special Publications,* **276**, 111-127.

MACKINTOSH, A., WHITE, D., FINK, D., GORE, D.B., PICKARD, J., & FANNING, P.C. 2007. Exposure ages from mountain dipsticks in Mac. Robertson Land, East Antarctica, indicate little change in ice-sheet thickness since the Last Glacial Maximum. *Geology,* **35**(6), 551-554.

MANSON, V., & IMBRIE, J. 1964. FORTRAN program for factor and vector analysis of geological data using an IBM 7090 or 7094/1401 computer system. *Kansas Geol. Survey Spec. Distrib. Publ.,* **13**, 46 pp.

MARSLAND, S.J., CHURCH, J.A., BINDOFF, N.L., & WILLIAMS, G.D. 2007. Antarctic coastal polynya response to climate change. *Journal Of Geophysical Research-Oceans,* **112**(C7), C07009.

MASSON, V., VIMEUX, F., JOUZEL, J., MORGAN, V., DELMOTTE, M., CIAIS, P., HAMMER, C., JOHNSEN, S., LIPENKOV, V.Y., MOSLEY-THOMPSON, E., PETIT, J.R., STEIG, E.J., STIEVENARD, M., & VAIKMAE, R. 2000. Holocene climate variability in Antarctica based on 11 ice-core isotopic records. *Quaternary Research,* **54**(3), 348-358.

MCCARTNEY, M.S. & DONOHUE, K.A. 2007. A deep cyclonic gyre in the Australian-Antarctic Basin. *Progress in Oceanography*, **75**(4), 675-750.

MCCAVE, I.N., MANIGHETTI, B., & ROBINSON, S.G. 1995. Sortable Silt and fine sediment size composition slicing - parameters for paleocurrent speed and paleoceanography. *Paleoceanography,* **10**(3), 593-610.

MCLOUGHLIN, S., & DRINNAN, A.N. 1997. Fluvial sedimentology and revised stratigraphy of the Triassic Flagstone Bench Formation, northern Prince Charles Mountains, East Antarctica. *Geological Magazine*, **134**(6), 781-806.

MEEHL, G.A., STOCKER, T.F., COLLINS, W.D., FRIEDLINGSTEIN, P., GAYE, A.T., GREGORY, J.M., KITOH, A., KNUTTI, R., MURPHY, J.M., NODA, A., RAPER, S.C.B., WATTERSON, I.G., WEAVER, A.J., & ZHAO, Z.-C. 2007. Global Climate Projections. *In* SOLOMON, S., QIN, D., MANNING, M., CHEN, Z., MARQUIS, M., AVERYT, K.B., TIGNOR, M., & MILLER, H.L. eds. *Climate Change 2007: The Physical Science Basis. Contribution of Working Group I to the Fourth Assessment Report of the Intergovernmental Panel on Climate Change.* Cambridge, United Kingdom and New York, NY: Cambridge University Press.

MEIJERS, A., KLOCKER, A., BINDOFF, N.L., WILLIAMS, G.D., & MARSLAND, S. 2010. The circulation and water masses of the Antarctic shelf and continental slope between 30° and 80°E. *Deep Sea Research Part II: Topical Studies in Oceanography*, **57**(9-10), 723-237.

MELLES, M. 1991. Late Quaternary paleoglaciology and paleoceanography at the continental margin of the Southern Weddell Sea, Antarctica. *Reports on Polar Research,* **81**, 190 pp.

MICHALCHUK, B.R., ANDERSON, J.B., WELLNER, J.S., MANLEY, P., MAJEWSKI, W., & BOHATY, S.M. 2010. Holocene climate and glacial history of the northeastern Antarctic Peninsula: the marine sedimentary record from a long SHALDRIL core. *Quaternary Science Reviews,* **28**, 3049–3065.

MILNE, G.A., LONG, A.J., & BASSETT, S.E. 2005. Modelling Holocene relative sea-level observations from the Caribbean and South America. *Quaternary Science Reviews,* **24**(10-11), 1183-1202.

MIURA, H., MORIWAKI, K., MAEMOKU, H., & HIRAKAWA, K. 1998. Fluctuations of the East Antarctic ice-sheet margin since the last glaciation from the stratigraphy of raised beach deposits along the Soya Coast. *In*: *Annals Of Glaciology,* **27**. Cambridge: International Glaciological Society, 297-301.

MORIARTY, K.C. 1977. Clay-Minerals in southeast Indian-Ocean sediments, transport mechanisms and depositional environments. *Marine Geology*, **25**(1-3), 149-174.

MÜLLER, G. 1967. *Methods in sedimentary petrography (Part I).* New York: Hafner Publishing Co., 283 pp.

NAISH, T., POWELL, R., LEVY, R., WILSON, G., SCHERER, R., TALARICO, F., KRISSEK, L., NIESSEN, F., POMPILIO, M., WILSON, T., CARTER, L., DECONTO, R., HUYBERS, P., MCKAY, R., POLLARD, D., ROSS, J., WINTER, D., BARRETT, P., BROWNE, G., CODY, R., COWAN, E., CRAMPTON, J., DUNBAR, G., DUNBAR, N., FLORINDO, F., GEBHARDT, C., GRAHAM, I., HANNAH, M., HANSARAJ, D., HARWOOD, D., HELLING, D., HENRYS, S., HINNOV, L., KUHN, G., KYLE, P., LAUFER, A., MAFFIOLI, P., MAGENS, D., MANDERNACK, K., MCINTOSH, W., MILLAN, C., MORIN, R., OHNEISER, C., PAULSEN, T., PERSICO, D., RAINE, I., REED, J., RIESSELMAN, C., SAGNOTTI, L., SCHMITT, D., SJUNNESKOG, C., STRONG, P., TAVIANI, M., VOGEL, S., WILCH, T., & WILLIAMS, T. 2009. Obliquity-paced Pliocene West Antarctic ice sheet oscillations. *Nature*, **458**, 322-327.

NIELSEN, S.H.H., HODELL, D.A., KAMENOV, G., GUILDERSON, T., & PERFIT, M.R. 2007. Origin and significance of ice-rafted detritus in the Atlantic sector of the Southern Ocean. *Geochemistry Geophysics Geosystems,* **8**, Q12005.

NORTH GREENLAND ICE CORE PROJECT MEMBERS. 2004. High-resolution record of Northern Hemisphere climate extending into the last interglacial period. *Nature,* **431**(7005), 147-151.

NUNES VAZ, R.A. & LENNON, G.W. 1996. Physical oceanography of the Prydz Bay region of

Antarctic waters. *Deep-Sea Research Part I: Oceanographic Research Papers*, **43**(5), 603-641

O`BRIEN, P.E. 1994. Morphology and late glacial history of Prydz Bay, Antarctica, based on echo sounder data. *Terra Antarctica*, **1**, 403-405.

O'BRIEN, P.E. 1995. Antarctic CRC marine geoscience, Prydz Bay, Mac.Robertson Shelf and Kerguelen Plateau, 1995: post-cruise report, AGSO cruise 149, ANARE voyage 6, 1994/95 (BANGSS). Australian Geological Survey Organisation, Canberra.

O'BRIEN, P.E., DE SANTIS, L., HARRIS, P.T., DOMACK, E., & QUILTY, P.G. 1999. Ice shelf grounding zone features of Western Prydz Bay, Antarctica: Sedimentary processes from seismic and sidescan images. *Antarctic Science*, **11**(1), 78-91.

O'BRIEN, P.E., COOPER, A.K., FLORINDO, F., HANDWERGER, D.A., LAVELLE, M., PASSCHIER, S., POSPICHAL, J.J., QUILTY, P.G., RICHTER, C., THEISSEN, K.M., WHITEHEAD, J.M. 2004. Prydz channel fan and the history of extreme ice advances in Prydz Bay. *In*: COOPER, A.K., O'BRIEN, P.E., RICHTER, C., eds. *Proceedings of the Ocean Drilling Program, Scientific Results*, **188**. Texas A&M University, Ocean Drilling Program, College Station, TX, 1-32.

O'BRIEN, P.E., GOODWIN, I., FORSBERG, C.F., COOPER, A.K., & WHITEHEAD, J. 2007. Late Neogene ice drainage changes in Prydz Bay, East Antarctica and the interaction of Antarctic ice sheet evolution and climate. *Palaeogeography, Palaeoclimatology, Palaeoecology*, **245**(3-4), 390.

OLSEN, S.L., & HEARTY, P.J. 2008. A sustained +21 m sea-level highstand during MIS 11 (400 ka): Direct fossil and sedimentary evidence from Bermuda. *Quaternary Science Reviews*, (doi:10.1016/j.quascirev.2008.11.001), 1-15.

ORSI, A.H., WHITWORTH III, T. & NOWLIN JR, W.D. 1995. On the meridional extent and fronts of the Antarctic Circumpolar Current. *Deep Sea Research Part I: Oceanographic Research Papers*, **42**, 641-673.

PAILLARD, D., LABEYRIE, L., & YIOU, P. 1996. Macintosh program performs time-series analysis. *EOS Trans. AGU*, **77**, 379.

PÄLIKE, H., NORRIS, R.D., HERRLE, J.O., WILSON, P.A., COXALL, H.K., LEAR, C.H., SHACKLETON, N.J., TRIPATI, A.K., & WADE, B.S. 2006. The Heartbeat of the Oligocene Climate System. *Science*, **314**(5807), 1894 - 1898.

PARK, Y.H., VIVIER, F., ROQUET, F. & KESTENARE, E. 2009. Direct observations of the ACC transport across the Kerguelen Plateau. *Geophysical Research Letters*, **36**, 5pp.

PARKINSON, C.L. 2004. Southern Ocean sea ice and its wider linkages: insights revealed from models and observations. *Antarctic Science*, **16**, 387-400.

PARRA, M., CHAPUY, B., PONS, J.C. & LATOUCHE, C. 1991. The nature and origin of smectites in the Kerguelen-Heard archipelagos of the Southern Indian Ocean. *Continental Shelf Research*, **11**(4), 347-364.

PASSCHIER, S., O'BRIEN, P.E., DAMUTH, J.E., JANUSZCZAK, N., HANDWERGER, D.A., &

WHITEHEAD, J.M. 2003. Pliocene-Pleistocene glaciomarine sedimentation in eastern Prydz Bay and development of the Prydz trough-mouth fan, ODP Sites 1166 and 1167, East Antarctica. *Marine Geology*, **199**(3-4), 279-305.

PASSCHIER, S. 2007. East Antarctic ice-sheet dynamics between 5.2 and 0 Ma from a high-resolution terrigenous particle size record, ODP Site 1165, Prydz Bay-Cooperation Sea. *In*: COOPER, A.K., RAYMOND, C.R., eds. *Antarctica: A Keystone in a Changing World – Online Proceedings of the 10th ISAES*. USGS Open-File Report 2007-1047, Short Research Paper 043, 4 pp.

PETERS, S., ANDERS, E.C., KELLY, D.C., & GINGERICH, P.D. 2010. Large-scale glaciation and deglaciation of Antarctica during the Late Eocene. *Geology*, **38**, 723-726.

PETIT, J.R., JOUZEL, J., RAYNAUD, D., BARKOV, N.I., BARNOLA, J.-M., BASILE, I., BENDER, M., CHAPPELLAZ, J., DAVIS, M., DELAYGUE, G., DELMOTTE, M., KOTLYAKOV, V.M., LEGRAND, M., LIPENKOV, V.Y., LORIUS, C., PEPIN, L., RITZ, C., SALTZMAN, E., & STIEVENARD, M. 1999. Climate and atmospheric history of the past 420,000 years from the Vostok ice core, Antarctica. *Nature*, **399**, 429-436.

PETSCHICK, R., KUHN, G. & GINGELE, F. 1996. Clay mineral distribution in surface sediments of the South Atlantic: sources, transport, and relation to oceanography. *Marine Geology*, **130**(3-4), 203-229.

POLLARD, D., & DECONTO, R.M. 2009. Modelling West Antarctic ice sheet growth and collapse through the past five million years. *Nature*, **458**, 329-332.

PRINS, M., STUUT, J.-B.W., LAMY, F., & WELTJE, G.J. 1999. End-member modelling of grain-size distributions of deep sea detrital sediments and its palaeoclimatic significance: examples from the NW Indian, E Atlantic and SE Pacific Oceans. *Geophys. Res. Abstr.*, **1**, 564.

PUDSEY, C.J. 2000. Sedimentation on the continental rise west of the Antarctic Peninsula over the last three glacial cycles. *Marine Geology*, **167**(3-4), 313-338.

QUILTY, P.G., TRUSWELL, E.M., O'BRIEN, P.E. & TAYLOR, F. 1999. Paleocene-Eocene biostratigraphy and palaeoenvironment of East Antarctica: new data from the Mac. Robertson Shelf and western parts of Prydz Bay. *AGSO Journal of Australian Geology and Geophysics*, **17**, 133-143

QUILTY, P.G. 2001. Reworked Paleocene and Eocene foraminifera, MacRobertson Shelf, East Antarctica: paleoenvironmental implications. *Journal of Foraminiferal Research*, **31**(4), 369-384.

RAHMSTORF, S. 2002. Ocean circulation and climate during the past 120,000 years. *Nature*, **419**, 207-214.

RATHBURN, A.E., PICHON, J.J., AYRESS, M.A., & DEDECKKER, P. 1997. Microfossil and stable-isotope evidence for changes in Late Holocene palaeoproductivity and palaeoceanographic conditions in the Prydz Bay region of Antarctica. *Palaeogeography*

Palaeoclimatology Palaeoecology, **131**(3-4), 485-510.

RAYMO, M.E., LISIECKI, L.E., & NISANCIOGLU, K.H. 2006. Plio-pleistocene ice volume, Antarctic climate, and the global delta O-18 record. *Science*, **313**(5786), 492-495.

REIMER, P.J., BAILLIE, M.G.L., BARD, E., BAYLISS, A., BECK, J.W., BLACKWELL, P.G., RAMSEY, C.B., BUCK, C.E., BURR, G.S., EDWARDS, R.L., FRIEDRICH, M., GROOTES, P.M., GUILDERSON, T.P., HAJDAS, I., HEATON, T.J., HOGG, A.G., HUGHEN, K.A., KAISER, K.F., KROMER, B., MCCORMAC, F.G., MANNING, S.W., REIMER, R.W., RICHARDS, D.A., SOUTHON, J.R., TALAMO, S., TURNEY, C.S.M., VAN DER PLICHT, J., & WEYHENMEYE, C.E. 2009. Intcal09 and Marine09 radiocarbon age calibration curves, 0-50,000 Years Cal Bp. *Radiocarbon*, **51**(4), 1111-1150.

RODEHACKE, C.B., HELLMER, H.H., HUHN, O., & BECKMANN, A. 2007. Ocean/ice shelf interaction in the southern Weddell Sea: results of a regional numerical helium/neon simulation. *Ocean Dynamics*, **57**(1), 1-11.

ROQUET, F., PARK, Y.H., GUINET, C., BAILLEUL, F. & CHARRASSIN, J.B. 2009. Observations of the Fawn Trough Current over the Kerguelen Plateau from instrumented elephant seals. *Journal of Marine Systems*, **78**(3), 377-393.

SCHERER, R.P., BOHATY, S.M., DUNBAR, R.B., ESPER, O., FLORES, J.A., GERSONDE, R., HARWOOD, D.M., ROBERTS, A.P., & TAVIANI, M. 2008. Antarctic records of precession-paced insolation-driven warming during early Pleistocene Marine Isotope Stage 31. *Geophysical Research Letters*, **35**(3), 5 pp.

SCHMITT, C., KOTTMEIER, C., WASSERMANN, S. & DRINKWATER, M. 2004. Atlas of Antarctic Sea Ice Drift, Karlsruhe. http://www.imk.uni-karlsruhe.de/seaiceatlas.

SCHMITZ, W.J. 1995. On the interbasin-scale thermohaline circulation. *Reviews of Geophysics*, **33**(2), 151-173.

SEDWICK, P.N., HARRIS, P.T., ROBERTSON, L.G., MCMURTRY, G.M., CREMER, M.D., & ROBINSON, P. 2001. Holocene sediment records from the continental shelf of Mac. Robertson Land, East Antarctica. *Paleoceanography*, **16**(2), 212-225.

SHIPBOARD SCIENTIFIC PARTY. 1999. Explanatory notes. *In:* GERSONDE, R., et al., eds. *Proceedings of the Ocean Drilling Program, Initial Reports Leg 177,* **177**. Texas A&M University, Ocean Drilling Program, College Station, TX, 1–57.

SJUNNESKOG, C., & TAYLOR, F. 2002. Postglacial marine diatom record of the Palmer Deep, Antarctic Peninsula (ODP Leg 178, Site 1098) 1. Total diatom abundance. *Paleoceanography*, **17**(3), 8003.

SLATT, R.M., & EYLES, N. 1981. Petrology of Glacial Sand - Implications for the Origin and Mechanical Durability of Lithic Fragments. *Sedimentology*, **28**(2), 171-183.

SMITH, N.R., DONG, Z.Q., KERRY, K.R. & WRIGHT, S. 1984. Water masses and circulation in the region of Prydz Bay, Antarctica. *Deep-Sea Research Part I: Oceanographic Research Papers*,

31(9), 1121-1147.

SMITH, J.A., HILLENBRAND, C.-D., PUDSEY, C.J., ALLEN, C.S., & GRAHAM, A.G.C. 2010. The presence of polynyas in the Weddell Sea during the Last Glacial Period with implications for the reconstruction of sea-ice limits and ice sheet history. *Earth and Planetary Science Letters*, **296**(3-4), 287-298.

STAGG, H.M.J. 1985. The structure and origin of Prydz Bay and MacRobertson Shelf, East Antarctica. *Tectonophysics*, **114**, 315-340.

STEIG, E.J., MORSE, D.L., WADDINGTON, E.D., STUIVER, M., GROOTES, P.M., MAYEWSKI, P.A., TWICKLER, M.S., & WHITLOW, S.I. 2000. Wisconsinan and Holocene climate history from an ice core at Taylor Dome, western Ross embayment, Antarctica. *Geografiska Annaler. Series A, Physical Geography*, **82**(2-3), 213-235.

STEIG, E.J. 2006. The south-north connection. *Nature*, **444**, 152-153.

STICKLEY, C.E., PIKE, J., LEVENTER, A., DUNBAR, R., DOMACK, E.W., BRACHFELD, S., MANLEY, P., & MCCLENNAN, C. 2005. Deglacial ocean and climate seasonality in laminated diatom sediments, Mac.Robertson Shelf, Antarctica. *Palaeogeography, Palaeoclimatology, Palaeoecology*, **227**, 290-310.

STIRLING, C.H., ESAT, T.M., LAMBECK, K., MCCULLOCH, M.T., BLAKE, S.G., LEE, D.-C., & HALLIDAY, A.N. 2001. Orbital Forcing of the Marine Isotope Stage 9 Interglacial. *Science*, **291**, 290-292.

STONE, J., BIRD, M.I., ZWARTZ, D., LAMBECK, K., FIFIELD, L.K. & ALLAN, G.L. 1993. Deglaciation and sea-level in the Vestfold Hills, East Antarctica. *EOS Transactions. American Geophysical Union*, **74**(43), 243.

STUIVER, M., & REIMER, P.J. 1993. Extended C-14 Data-Base and Revised Calib 3.0 C-14 Age Calibration Program. *Radiocarbon*, **35**(1), 215-230.

TAMURA, T., OHSHIMA, K.I. & NIHASHI, S. 2008. Mapping of sea ice production for Antarctic coastal polynyas. *Geophysical Research Letters*, **35**(7), 5 pp.

TAYLOR, F., & SJUNNESKOG, C. 2002. Postglacial marine diatom record of the Palmer Deep, Antarctic Peninsula (ODP Leg 178, Site 1098) 2. Diatom assemblages. *Paleoceanography*, **17**(3), 1026.

TAYLOR, F., & LEVENTER, A. 2003. Late quaternary palaeoenvironments in Prydz Bay, East Antarctica: interpretations from marine diatoms. *Antarctic Science*, **15**(4), 512-521.

TAYLOR, J., SIEGERT, M.J., PAYNE, A.J., HAMBREY, M.J., O'BRIEN, P.E., COOPER, A.K., & LEITCHENKOV, G. 2004. Topographic controls on post-Oligocene changes in ice-sheet dynamics, Prydz Bay region, East Antarctica. *Geology*, **32**(3), 197-200.

TEITLER, L., KUPP, G., WARNKE, D.A., & BURCKLE, L.H. 2007. Evidence for a long warm interglacial during Marine Isotope Stage 31: Comparison of two studies at proximal and distal marine sites in the Southern Ocean. *In:* COOPER, A.K., & RAYMOND, C.R., eds.

Antarctica: A Keystone in a Changing World – Online Proceedings of the 10th ISAES. USGS Open-File Report 2007-1047, Extended Abstract 013, 4 pp.

TEITLER, L., WARNKE, D.A., VENZ, K., HODELL, D.A., BECQUEY, S., GERSONDE, R., & TEITLER, W. 2010. Determination of Antarctic Ice Sheet stability over the last 500 ka through a study of iceberg-rafted debris. *Palaeoceanography,* **25**, PA1202.

THEISSEN, K.M., DUNBAR, R.B., COOPER, A.K., MUCCIARONE, D.A., & HOFFMANN, D. 2003. The Pleistocene evolution of the East Antarctic Ice Sheet in the Prydz bay region: Stable isotopic evidence from ODP Site 1167. *Global and Planetary Change,* **39**(3-4), 227-256.

THOST, D.E., LEITCHENKOV, G., O`BRIEN, P.E., TINGEY, R.J., WELLMAN, P. & GOLYNSKY, A.V. 1998. Geology of the Lambert Glacier - Prydz Bay region, East Antarctica. 1:1 000 000. Canberra: Australian Geological Survey Organisation.

TIMMERMANN, A., TIMM, O., STOTT, L., & MENVIEL, L. 2009. The Roles of CO_2 and Orbital Forcing in Driving Southern Hemispheric Temperature Variations during the Last 21,000 Yr. *Journal Of Climate,* **22**(7), 1626-1640.

TINGEY, R.J. 1991. *The geology of Antarctica*. Oxford: Clarendon Press, 680 pp.

TREGONING, P., TWILLEY, B., HENDY, M., & ZWARTZ, D. 1999. Monitoring isostatic rebound in Antarctica with the use of continuous remote GPS observations. *GPS Solutions,* **2**(3), 70-75.

TRUSWELL, E.M., DETTMANN, M.E. & O'BRIEN, P.E. 1999. Mesozoic palynofloras from the Mac. Robertson shelf, East Antarctica: geological and phytogeographic implications. *Antarctic Science*, **11**(2), 239-255.

TURNER, B.R. 1991. Depositional environment and petrography of preglacial continental sediments from Hole 740A, Prydz Bay, Antarctica. *In:* BARRON, J., LARSEN, B., eds. *Proceedings of the Ocean Drilling Program, Scientific Results*, **119**, 45-56.

VALET, J.P., MEYNADIER, L., & GUYODO, Y. 2005. Geomagnetic dipole strength and reversal rate over the past two million years. *Nature,* **435**, 802-805.

VERLEYEN, E., HODGSON, D.A., SABBE, K., & VYVERMAN, W. 2004a. Late Quaternary deglaciation and climate history of the Larsemann Hills (East Antarctica). *Journal Of Quaternary Science,* **19**(4), 361-375.

VERLEYEN, E., HODGSON, D.A., SABBE, K., VANHOUTTE, K., & VYVERMAN, W. 2004b. Coastal oceanographic conditions in the Prydz Bay region (East Antarctica) during the Holocene recorded in an isolation basin. *The Holocene,* **14**(2), 246-257.

VERLEYEN, E., HODGSON, D.A., MILNE, G.A., SABBE, K., & VYVERMAN, W. 2005. Relative sea-level history from the Lambert Glacier region, East Antarctica, and its relation to deglaciation and Holocene glacier readvance. *Quaternary Research,* **63**(1), 45-52.

VILLA, G., PALANDRI, S., & WISE, S. 2005. Quaternary calcareous nannofossils from Periantarctic basins: Paleoecological and paleoclimatic implications. *Marine*

Micropaleontology, **56**(3 4), 103-121.

VILLA, G., LUPI, C., COBIANCHI, M., FLORINDO, F., & PEKAR, S.F. 2008. A Pleistocene warming event at 1 Ma in Prydz Bay, East Antarctica: Evidence from ODP site 1165. *Palaeogeography Palaeoclimatology Palaeoecology*, **260**(1-2), 230-244.

VON DER BORCH, C.C. & OLIVER, R.L. 1967. Comparison of heavy minerals in marine sediments with mainland rock outcrops along the coast of Antarctica between longitudes 40°E and 150°E. *Sedimentary Geology*, **2**, 77-80.

WAGNER, B., HULTZSCH, N., MELLES, M., & GORE, D.B. 2007. Indications of Holocene sea-level rise in Beaver Lake, East Antarctica. *Antarctic Science*, **19**(1), 125-128.

WARNKE, D.A., RICHTER, C., FLORINDO, F., DAMUTH, J.E., BALSAM, W.L., STRAND, K., RUIKKA, M., JUNTTILA, J., THEISSEN, K., QUILTY, P.G. 2004. Data report: HiRISC (High-Resolution Integrated Stratigraphy Committee) Pliocene–Pleistocene interval, 0–50 mbsf, at ODP Leg 188 Site 1165, Prydz Bay, Antarctica. *In*: COOPER, A.K., O'BRIEN, P.E., RICHTER, C., eds. *Proceedings of the Ocean Drilling Program, Scientific Results*, **188**. Texas A&M University, Ocean Drilling Program, College Station, TX, 1-38.

WEBB, J.A. & FIELDING, C.R. 1993. Revised stratigraphical nomenclature for the Permo-Triassic Flagstone Bench Formation, northern Prince Charles Mountains, East Antarctica. *Antarctic Science*, **5**(4), 409-410.

WELTJE, G.J. 1997. End-member modeling of compositional data: Numerical-statistical algorithms for solving the explicit mixing problem. *Mathematical Geology*, **29**(4), 503-549.

WELTJE, G.J., & PRINS, M.A. 2007. Genetically meaningful decomposition of grain-size distributions. *Sedimentary Geology*, **202**(3), 409-424.

WELTJE, G.J., & TJALLINGII, R. 2008. Calibration of XRF core scanners for quantitative geochemical logging of sediment cores: Theory and application. *Earth and Planetary Science Letters*, **274**(3-4), 423-438.

WEN, J., WANG, Y., LIU, J., JEZEK, K.C., HUYBRECHTS, P., CSATHO, B.M., FARNESS, K.L., & SUN, B. 2008. Mass budget of the grounded ice in the Lambert Glacier-Amery Ice Shelf system. *Annals of Glaciology*, **48**, 193-197.

WHITE, D.A., BENNIKE, O., BERG, S., HARLEY, S.L., FINK, D., KIERNAN, K., MCCONNELL, A., & WAGNER, B. 2009. Geomorphology and glacial history of Rauer Group, East Antarctica. *Quaternary Research*, **72**(1), 80-90.

WHITEHEAD, J.M., QUILTY, P.G., MCKELVEY, B.C. & O'BRIEN, P.E. 2006. A review of the Cenozoic stratigraphy and glacial history of the Lambert Graben-Prydz Bay region, East Antarctica. *Antarctic Science*, **18**(1), 83-99.

WILLIAMS, G.D., & BINDOFF, N.L. 2003. Wintertime oceanography of the Ad!elie Depression. *Deep Sea Research Part II: Topical Studies in Oceanography*, **50**, 1373–1392.

WILLIAMS, M.J.M., WARNER, R.C., & BUDD, W.F. 2002. Sensitivity of the Amery Ice Shelf,

Antarctica, to changes in the climate of the Southern Ocean. *Journal Of Climate,* **15**(19), 2740-2757.

WILLIAMS, G.D., AOKI, S., JACOBS, S., RINTOUL, S.R., TAMURA, T., & BINDOFF, N.L. 2010. Antarctic Bottom Water from the Adélie and George V Land coast, East Antarctica (140–149°E). *Journal of Geophysical Research,* **115**, C04027, 29 pp.

WONG, A.P.S. 1994. *Structure and dynamics of Prydz Bay, Antarctica, as inferred from a summer hydrographic data set*. M.S. thesis, Univ. Tasmania, 104 pp.

YABUKI, T., SUGA, T., HANAWA, K., MATSUOKA, K., KIWADA, H. & WATANABE, T. 2006. Possible source of the Antarctic bottom water in the Prydz Bay region. *Journal of Oceanography*, **62**(5), 649-655.

YOON, H.I., KHIM, B.K., YOO, K.C., BAK, Y.S., & LEE, J.I. 2007. Late glacial to Holocene climatic and oceanographic record of sediment facies from the South Scotia Sea off the northern Antarctic Peninsula. *Deep-Sea Research Part Ii-Topical Studies In Oceanography,* **54**(21-22), 2367-2387.

ZACHOS, J.C., DICKENS, G.R., & ZEEBE, R.E. 2008. An early Cenozoic perspective on greenhouse warming and carbon-cycle dynamics. *Nature,* **451**, 279-283.

ZWARTZ, D., BIRD, M., STONE, J., & LAMBECK, K. 1998. Holocene sea-level change and ice-sheet history in the Vestfold Hills, East Antarctica. *Earth and Planetary Science Letters,* **155**(1-2), 131-145.

Appendix A

-

Further publications

A1 An end-member algorithm for deciphering modern detrital processes from lake sediments of Lake Donggi Cona, NE Tibetan Plateau, China

Elisabeth Dietze*[a], Kai Hartmann[a], Bernhard Diekmann[b], Janneke IJmker[c], Frank Lehmkuhl[c], Stephan Opitz[b], Georg Stauch[c], Bernd Wünnemann[a,d], & Andreas Borchers[b]

[a]*Institute of Geographical Sciences, Interdisciplinary Center of Ecosystem Dynamics of Central Asia (EDCA), Freie Universität Berlin*

[b]*Alfred Wegener Institute for Polar and Marine Research, Research Unit Potsdam, Telegrafenberg A43, 14473 Potsdam, Germany*

[c]*Department of Geography, RWTH Aachen University, Templergraben 55, 52056 Aachen, Germany*

[d]*now at: School of Geography and Oceanography, Nanjing University, 22 Hankou Road, Nanjing 210093, China*

* corresponding author

Abstract

Deciphering significant sedimentological processes from a set of sediment samples is an important step in reconstructing environmental changes. One approach going beyond classical methods is unmixing of grain size distributions. A new flexible end-member modelling algorithm is introduced, which bases on eigenspace analysis and considers inherent uncertainties. It has been applied to the detrital grain size components of lacustrine surface sediment samples of Lake Donggi Cona, Qinghai province, China. It allowed characterising and quantifying up to five grain size end-members in an optimal model. Three end-members in the fine sand to medium silt domains made up 60 % of lacustrine sedimentation. They may represent local to remote aeolian processes, which peak in winter time. An end-member with major mode in the clay domain accounted for 34 % of variance within the grain size data set. It may represent sedimentation of suspension load from linear and laminar runoff during heavy precipitation events in summer. A multimodal end-member explaining the remaining 6 % of variance may represent further fluvial and shore dynamics. Different model scenarios provided a suitable way to determine uncertainties inherent to the model. A comparison of 12 different scenarios and their respective uncertainties yielded a second model of invariant end-members. Thereby, the medium silt and clay end-members are robust features of detrital sedimentation within Lake Donggi

Cona. They alone explain 54.4 % of total variance in the data. However, no spatial pattern or relation to water depth is found for any of the grain size end-members. Thus, when reconstructing past detrital sedimentation at Lake Donggi Cona, a special focus should be on the invariant features attributed to aeolian and suspension-related sedimentation processes as well as on effective sediment mixing processes impeding a distinct correlation of grain size to spatial attributes. Further application of the end-member modelling algorithm are needed to reconstruct any type of modern or past depositional processes and to determine the most robust components in sediments.

Keywords: end-member modelling; grain size distribution; modern lake sediments; Tibetan Plateau

1. Introduction

Sediment archives are well-suited to study past climatic change, tectonic processes and human impact, though mostly sediment properties cannot be related to one of these external signal providers alone. A complete consideration of signal transmission from signal provider to the final archive is essential for understanding terrestrial archives, and thus, environmental processes.

An endorheic lake catchment may be regarded as a superordinate archive system in which e.g. climate change has left specific signatures. It consists of several geomorphological and sedimentological process units with appropriate (sub-) archives such as dust accumulation areas, fluvial terraces and a lake as a final storage system. These sediment archives are often topologically linked along sediment cascades displaying spatial connection of adjacent archive properties. Most times such catchments cannot be studied in a complete manner. The self-similarity of storage units in different spatial and temporal scales is then used to reconstruct effects of e.g. climate change on the entire process system.

The observable archive properties are thereby a result of complex process interactions. Depending on the geomorphological inventory, climatic signals (i.e. changes in temperature and precipitation) in sediments are buffered during and after deposition. Thus, physical and biological processes create a multidimensional fingerprint in sediments, which results in correlations between observed sediment parameters. For example, downstream sediment transport is influenced by grain size ranges in the source area, sediment supply, and runoff at least, though coarser grain sizes within a lake may also be related to a drop in lake level. Consequently, single archive properties alone are not sufficient to decipher process-related information, whereas correlated properties need to be “unmixed”.

For describing sediment properties and underlying geomorphological, sedimentological or hydrological processes a nearly infinite number of variables is possible. However, often only a limited number of properties, mostly physical (e.g. grain size distribution), geochemical (e.g. minerals composition) and biological (e.g. pollen content) variables, can be measured. Such variables principally belong to the group of compositional data, i.e. they are nonnegative and sum to a constant (e.g. 100%; Aitchison, 1986; Kucera and Malmgren, 1998; Buccianti et al., 2006). They are mostly expressed as proportions and for incomplete representations a residual variable should be considered. Aitchison (1986) provided first comprehensive approaches to deal with such data.

As an important precondition to extract signals from sediments and for further reconstruction of signal-related process parameters back in time, it is essential to study the modern spatial variation of sediment parameters within a known setting of external signal providers (climate, tectonics, man) and to test methodological concepts in evaluating these patterns (Folk and Ward, 1957; Diekmann and Kuhn, 1999; Orpin and Woolfe, 1999; McLaren et al., 2007). Thereby, consideration of concept-, method- and scale-depending uncertainties is crucial as they result in random noise (Hartmann, 2007). From a mathematical point of view, many methods provide fruitful ways to identify different signal-related processes and pathways from compositional data (Arhonditsis et. al., 2006; Dechert and O'Donnell, 2006; Christensen and Arora, 2007; Blanchet et al. 2008). In this study, we use one of the manifold opportunities of eigenspace analysis, which aim to reduce redundancy in a large set of measured variables and help to quantify the signal's contrast against random.
A Tibetan lake as a representative archive at the end of sediment cascades is studied. An algorithm for end-member modelling analysis (EMMA) is presented, which is applied to grain size distributions of lacustrine surface samples. An optimal end-member model and the most robust signals within these grain size distributions are derived from an array of different end-member models. They allow a quantitative estimation of dominant detrital processes within the lake at modern times.

2. Background of end-member modelling analysis

2.1 Mathematical concept of eigenspace analysis

For the extraction of palaeoclimatic and palaeohydrologic proxies representative for geomorphological, sedimentological and other processes it is possible to reduce multi-dimensional variables by connecting highly correlative ones, i.e. dimension reduction. Simple analyses of the covariance structure of compositional data are the calculation of

correlation coefficients r (or coefficients of determination r^2) and multiple regressions. They are often applied to geoscientific questions (e.g. Papatheodorou et al., 2006). Further procedures of dimension reduction in geosciences are principal component analysis (PCA), factor analysis (FA), and EMMA. They all base on eigenspace analysis, which aims at separating the data space into signal and noise.

A major pre-condition for eigenspace analyses is a metric scale of the variables. Large scale contrasts may result in weak or hidden correlation, which can be avoided by transformation of variables, e.g. standardisation by subtracting the mean and dividing by standard deviation. In a palaeoenvironmental sense, an eigenspace (German: eigen = innate, own) is an attribute space of interrelated processes or sources recorded in a geo-archive. The axes (i.e. eigenvectors, v_i) of this space are the underlying processes or sources as linear combination of measured sediment properties. These interrelated processes or sources are called principal components, factors or end-members and are defined as:

$$X_{mn} = M_{mn} * V_{nn}^T \qquad (1)$$

Matrix X_{mn} consists of original data of m observations (rows) concerning n measured variables (columns), e.g. sediment parameters. Observations can be samples from a record (in depth or time) or sites (in space). The right side of equation (1) indicates a linear combination of the matrix V_{nn} of n eigenvectors v_i (for i = 1, …, n variables) and the proportional matrix M_{mn} of m observations concerning the n eigenvectors. Thereby, the dimension of the eigenspace equals the dimension of measured variables.

For calculating matrices V and M from X different ways exist: a) extraction of the eigenspace from a similarity matrix A_{nn}, e.g. a correlation, covariance or the minor product or major product (X^T*X or $X*X^T$) matrix (Miesch, 1980; Weltje, 1997), b) by singular value decomposition (Renner et al., 1997 for geochemical data), or c) in a multiple way if different blocks of variables exist (Stanimirova et al., 2005).

Using A_{nn} we get V, the matrix of eigenvectors, from the relation

$$A_{nn} * V_{nn} = ?_n * V_{nn} \qquad (2).$$

Matrix V_{nn} contains the factor loadings, which represent the correlation between an abstract, independent factor and a variable. The smaller the angle (cosine) between factor and variable, the stronger is the correlation. The contribution of each factor to the variance of the total variable space is called eigenvalue ?.

Matrix M_{mn} contains the factor scores, i.e. the proportions of the compositions of a factor in sample space, and is determined from the relation

$$M_{mn} = X_{mn} * V_{nn} \qquad (3).$$

Equation (3) is invertible and can be used to quantify the uncertainty (i.e. error matrix E_{mn})

$$X_{mn}' = M_{mn} * V_{nn}^T + E_{mn} \qquad (4)$$

with X'_{mn} being the predicted data from the eigenspace. So far, the relative error as determined from the correlation matrix of X and X' has received more attention than the absolute error matrix E (Weltje, 1997; Weltje and Prins, 2007). A further compilation of the mathematical background of eigenspace analyses can be found in Reyment and Jöreskog (1993).

2.2 Application of eigenspace analysis

When sediments of different sources and transport processes are deposited in a sediment sink, they become mixed. Evaluation of this mixture gives a first hint of the main driving forces and directions in sedimentation. To "unmix" underlying and interrelated processes or sources from the properties of sediment archives, several ways of eigenspace analyses exist. We would like to introduce them in order of increasing complexity.

The simplest way is a principal component analysis (PCA). Thereby, any variance is explained by the eigenvectors (i.e. principal components, PCs). As many PCs as variables are produced containing both signal and noise, i.e. no dimension reduction. Furthermore, in PCA the first PC will move towards the greatest covariance and iteratively the next highest eigenvalues will load on the residual variance until no variance remains. The PCs are all orthogonal to each other and their eigenvalues are proportional to the variance of all vectors represented by the axes (Reyment and Jöreskog, 1993).

A step further goes factor analysis (FA). Not all variance within the original data set is aimed to be explained within the eigenspace. In the best case, factors are just representing the signal portion of variance. The variable dimensions are reduced and no order exists between the factors concerning their percentage of explained variance. Several criteria exist to decide how many factors are appropriate, e.g. the criteria of Guttman (1954) taking all factors with eigenvalues $?_i > 1$ or to use as many factors as needed to explain more than 95% of the cumulative variance (Reyment and Jöreskog, 1993). The variance of each PC or factor is at least as great as the internal variance of the prime variable (Hartmann and Wünnemann, 2009). To facilitate interpretation, a transformation by rotation of the axes is desirable, as there may remain some unexplained variance.

In mineralogy, petrology, geochemistry and provenance studies, principals of factor analysis have been applied to a variety of fields throughout the 20th century (Klovan, 1966; Solohub and Klovan, 1970; Zimmerman and Owen, 1990; Reyment and Jöreskog, 1993; Reimann et al., 2002; Juliá and Luque, 2006). However, PCs and factors are often abstract, what makes their interpretation towards underlying processes or sources difficult.

End-member analysis addresses this problem. After Weltje (1997), end-members "represent a series of fixed compositions, which can be regarded as distinct subpopulations within the dataset being analyzed". Mathematically, an end-member may be defined as either a concrete or an idealised population of one or more metric variables showing a characteristic frequency distribution.

In sedimentary basins, end-members represent involved sources and underlying processes more directly than PCs or factors. Comprising e.g. the geochemical components of pure rock, this rock can be regarded as an end-member described by its geochemical fingerprint. Unmixing the geochemical compositions of sediment samples allows deriving the original rock sources, a major topic of classical provenance and fingerprinting studies (Walling, 2005; Garzanti et al., 2009; Collins et al., 2010). Similarly, the grain size distribution of recently transported sediment collected from sites, which are obviously dominated by a single sedimentation process, is representative for the site and its typical process regime (Folk and Ward, 1957; McManus, 1988), a major assumption in all types of grain size analyses (e.g. in sediment trend analysis: McLaren et al., 2007).

However, the idea of end-members contrasts with the idea of descriptive moments of single samples used to characterize depositional environments in the sense of Krumbein (1936), Folk and Ward (1957) and McManus (1988). These get in trouble when being confronted with multi-modal distributions (see review in Hartmann, 2007). Thus, typical process-related sediments should rather be described by a grain size distribution with a limited range of possible distribution shapes. An idealised one is an end-member. It can be determined by fitting single grain size distributions with theoretical functions e.g. normal or log-normal distributions (Sun et al., 2002; Bartholdy et al., 2007). However, most times theoretical functions were selected in a quite subjective way with priory knowledge of natural end-members (Orpin and Woolfe, 1999; Flemming, 2007).

End-member modelling analysis (EMMA) combines eigenspace analysis with principals of compositional data analysis. It uses all available sediment samples from a mixture in space or within an archive to identify the respective, priory unknown end-members and their contributions to the final archive. This idea is supposed to be one of the most promising ways in analysis of multi-modal depositional processes from grain size distributions (Flemming, 2007). The important advantage over PCA and FA is the derivation of geoscientifically meaningful and quantitative end-member loadings and scores. EMMA keeps the compositional data constraints (i.e. constant sum and nonnegativity) by transformations, evaluates the modelling of the original data using rotated factors with goodness-of-fit tests, and improves this fit iteratively.

Ideas and functions used in EMMA go back to Imbrie (1963) and Klovan and Imbrie (1971) and are common in several fields of geosciences. For example in remote sensing, EMMA is

called spectral mixing analysis (SMA) and has been applied in the field of passive optical remote sensing associated to mapping of all kinds of land cover changes (Song, 2005; Robichaud et al., 2007; Sonnentag et al., 2007). In hydrology, an EM-algorithm by Christophersen et al. (1990) helped to distinguish hydrological flow paths from soil water chemistry (Burns et al., 2001; Bernal et al., 2006).
In sedimentology, integrative FORTRAN algorithms for the interpretation of geochemical and grain size data were designed by Renner et al. (1989 cit. in Renner et al., 1997) and Weltje (1997), respectively. Evaluations of their algorithms have been provided by modelling of artificial and extreme compositions (Renner, 1995, 1996; Weltje and Prins, 2007). They unmixed source end-members from the geochemical composition of marine sediments (Renner et al., 1997; Renner et al., 1998; Szefer et al., 2009) or quantified mainly aeolian and fluvial components mixed in the oceans from grain size distributions of marine sediments (Holz et al., 2007; Prins et al., 2007; Wan et al., 2007; Hamann et al., 2008).

Leaned towards the algorithm of Weltje (1997), we introduce a new MATLAB algorithm for the analysis of grain size distributions based on the general principles of eigenspace analysis mentioned above. Thereby, we go another step forward by introducing an additional opportunity to evaluate different variations of our EM-model. Thus, method-specific uncertainties can be considered in an objective way. The most relevant and robust end-members from the available data set are presented within the modern setting of a Tibetan lake system.

3. Data and methods

3.1 Geographical setting

Lake Donggi Cona, also referred to as Dongxi Co or Tuosu Hu, is situated at the northeastern margin of the Tibetan Plateau in Qinghai-Province, China (35°18'N, 98°32'E, 4090 m a.s.l., Fig. 1), northwest of the A'nyêmaqên and east of the Kunlun mountain ranges.
Summer climate is wet and warm, controlled by intense local convection, comparable to other high mountain areas (Schmidt, 1999). It is dominated by the monsoon system as the lake basin is located close to the western limit of the East Asian Summer Monsoon trajectories (Domrös and Peng, 1988; An et al., 2001). During the cold and dry winters extra-tropical westerlies prevail. Mean summer (May to October) and winter (November to April) precipitation is 278 mm and 26 mm, respectively. Mean January (July) air temperature is -16.8 (7.5) °C. Mean annual relative humidity, sunshine hours, total pan evaporation and

wind velocity are 59%, 61 %, 1375 mm and 3.4 m/s, respectively (data from Madoi climate station 1958-2007, Chinese Central Meteorological Office, 1984).

Lake Donggi Cona belongs to a series of pull-apart basins along the Kunlun Fault with a surface size of 229 km² and an asymmetric basin structure incised in heterogeneous Permian-Triassic and Neogene rocks (Dietze et al., 2010). Major perennial inflow along a large alluvial plain east of the lake drains the western A'nyêmaqên Shan with varying intra-annual discharge. Outflow of the lake towards the endorheic Qaidam Basin is currently directed through an artificial channel at the western lake margin (Fig. 1), which is controlled by a gauge station set up during the 1970s. However, morphological features like palaeo-shorelines and ancient on-shore terraces in the vicinity of the lake suggest former higher than present lake stands. Sedimentological and morphological indications for up to 57 m lower lake levels have been described by Dietze et al. (2010) for the Late Quaternary.

Currently the lake is an oligotrophic freshwater lake with oxygen supply down to the lake bottom and a maximum Secchi depth of 12 m (Mischke et al., 2010). The lake is frozen from late November to early April. It shows no distinct stratification pattern during the unfrozen period due to full circulation. Biological activity, i.e. ostracoda and aquatic macrophytes, shows a clear distribution with water depth (Mischke et al., 2010).

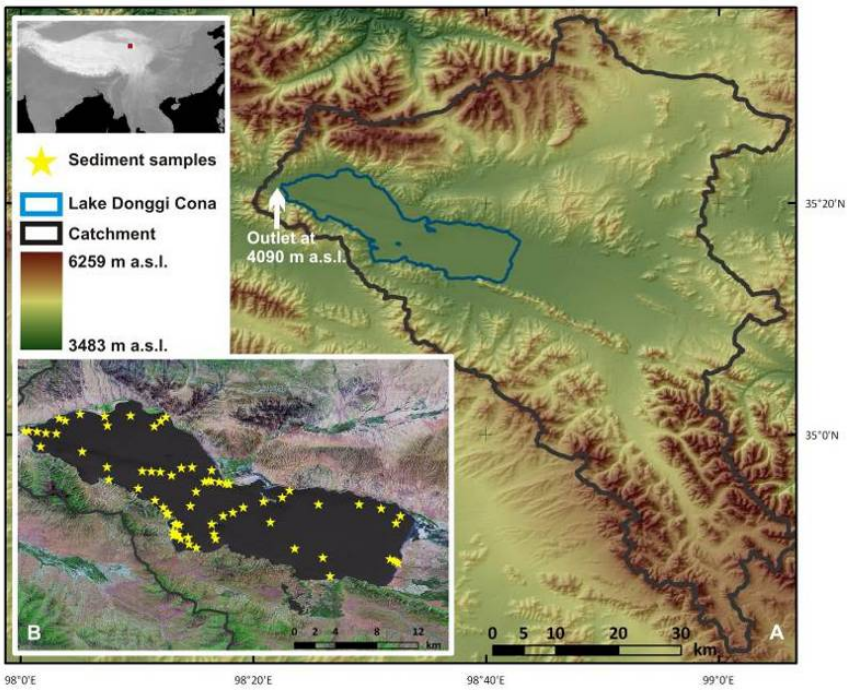

Fig. A1.1
Map of Lake Donggi Cona and its catchment (A), and sampling sites of lacustrine surface sediment samples (B). Background: SRTM3 heights and Landsat7 ETM+ MrSid image

At this high elevation site, climate influences the dominant modern geomorphological and depositional processes within the catchment. During summer, intense precipitation leads to fluvial erosion and alluvial, i.e. sheet flood, accumulation along the gentle slopes, which brings the main suspension load towards the lake. The few perennial, some seasonal inflows

and numerous short episodic inflows lead to alluvial cones of different size, which encircle the basin (Dietze et al., 2010; Fig. 1). During winter time, aeolian dislocation of sediment along the slopes and alluvial plain is forced by the dry winter monsoon and leads to loess-like sediments covering most of the slopes and several dune fields. Strong aeolian processes are supported by a sparse vegetation cover of alpine meadows and steppes (Kürschner et al., 2005), which are intensively grazed by yaks and sheep. In the past, glaciations in the northern catchment and at the outflow area provided huge amounts of glacio-fluvial sediments to the lake during times of substantially lower lake levels (Dietze et al., 2010).

3.2 Field and laboratory analyses

In August 2006, 77 surface sediment samples were collected from the upper 2 cm with a Hydro-Bios-Ekman grab from a boat (Mischke et al., 2010). Parallel to sampling, water depth at each site was measured and the position determined with a handheld GPS. With a second boat, a bathymetric survey of 3977 points using a Dual-Beam Garmin fishfinder and acoustic sub-bottom profiling has been conducted resulting in a bathymetric model of the lake basin (Dietze et al., 2010). All surface sediment samples covering a water depth range from 0.6 to 80 m have been used to analyse the detrital components of their grain size distribution. Therefore, they have been pre-treated with 35 % H_2O_2 to remove the organic matter and with 10 % acetic acid to remove the carbonate fractions before they went on an overhead shaker for minimum eight hours together with 10 mg of a dispersion agent ($Na_4O_7P_2$*10 H_20). Then, grain sizes less than 1 mm were finally measured with a laser diffraction particle size analyser (Coulter LS 200, Beckmann Coulter GmbH). Thereby, volume percentages of 85 grain size classes ranging from 0 to 11.31 phi have been measured and compiled in a data matrix.

3.3 Multivariate statistical analysis (EMMA)

Prior to end-member analysis, raw grain size distributions have been transformed to sum to 100 %. As first inspection, linear Pearson's correlation coefficients were used to detect the correlation structure in variable and sample space.

The EM-algorithm used in this study bases on Imbrie (1963), Manson and Imbrie (1964), Klovan and Imbrie (1971), Miesch (1976, 1980) and Weltje (1997; cf. Chap. 2). It allows two approaches: one being the iterative loop to find out the best fit of the EM model in relation to the original data, to determine the ideal number of end-members and best EMMA-internal

transformations. The other one defines the number of end-members manually, i.e. optimal EM model, and allows detailed estimation of uncertainty.

The principal steps for both approaches are:

Step 1. To minimize effects of scale a transformation becomes necessary (Hartmann and Wünnemann, 2009). Though often log-ratio transformations are quite popular with compositional data and suitable for geochemical data (Aitchison, 1986; Kucera and Malmgren, 1998), too many zero values exist within the grain size distribution space resulting in mathematical problems such as artificial extremes and divisions by zero. Thus, we apply a *weight transformation* as suggested by Manson and Imbrie (1964) and Klovan and Imbrie (1971):

$$W_{mn} = (X_{mn} - h_n)/ (g_n - h_n) \qquad (5)$$

with $h_n = Q_{0\%}$ (i.e. minimum value of x_n) and $g_n = Q_{100\%}$ (i.e. maximum value of x_n) after Miesch (1976), deriving the weighted matrix W from the original matrix X. Later on, variations of this weight transformation are tested using further quantile intervals as weights.

Step 2. The matrices of *eigenvectors* V and *eigenvalues* λ are extracted with a standard MATLAB routine LAPACK (Anderson et al., 1999; cf. equation (2), Chap. 2.1) from the minor product matrix Γ calculated by $\Gamma = W^T * W$ (cf. Chap. 2.1) as recommended by Weltje (1997). It is most suitable for the grain size data set. Normalisation of the eigenvalues give the degree of variance explained by the eigenvectors.

Step 3. A standard *varimax rotation* according to Kaiser (1958) represents our data optimal in comparison to e.g. an oblique Promax rotation after Henrickson and White (1964, cf. Chap. 2.2). Different numbers of end-members q to be rotated are used within the loop routine to evaluate overall goodness of fit. The optimal model then applies the manually defined end-member number in rotation.

Step 4. We then normalise the *preliminary factor loadings* (V_q) and estimate the *factor scores* (M_q) by a linear nonnegative least square algorithm after Lawson and Hanson (1974; standard MATLAB routine; cf. equation (3), Chap. 2.1).

Step 5. The initial *weight transformation* is then *reversed* using a scaling factor after Miesch (1976) with the respective initial values for h_n and g_n. This changes V_q and M_q to the original units of the initial data set. We now call them end-member loadings after a final normalisation to fulfil the initial 100%-sum constraint (V_q') and end-member scores (M_q'),

respectively. The variance explained by each end-member is the proportion of total scores variance.

Step 6. Now we calculate the modelled data set $X' = M_q' * V_q'^T + E$ according to equation (4) (Chap. 2.1) and compare it to the initial data set X. Goodness of fit is evaluated by calculating mean row- and column-wise linear coefficients of determinations (r^2), i.e. the declared proportion of variance of each sample and each variable, respectively.

As the true number of final end-members q in the system is generally unknown, Renner (1991) proposed to test if the logratios of error matrix E are normally distributed, which is probably valid for geochemical data. For derivation of the optimal q using grain size data, however, we follow Prins and Weltje (1999), who preferred to take q at the inflection point within the q-r^2_{mean} plot of the final goodness-of-fit test (step 6) in the loop routine of the model.
Furthermore, we test a range of end-member numbers to estimate the overall uncertainty of the model setup itself. Thereby, we assume that a minimum number of potential end-members is defined by taking at least as much eigenvectors into the varimax rotation (step 3) as needed to explain more than 95 % of total variance in the original data. As we encountered serious numerical instabilities during the model setup (cf. Chap. 4.1) we define the maximum number of end-members at the maximum value of r^2 within the q-r^2_{mean} plot. Minimum and maximum end-member numbers span the uncertainty range, wherein the optimal model is found at the inflection point.

4. Results

4.1 General characterisation of lake sediments and EMMA

Grain sizes of surface sediment samples of Lake Donggi Cona showed multimodal distributions with major modes at 4.2, 5.4 and 7.5 phi (Fig. 2A). However, they were highly variable in space and did not show a distinct relation to water depth (Fig. 2B). In the grain size classes < 1.4 phi, 62 % of the samples contained zero values. Linear Pearson's correlation coefficients revealed a highly correlative structure of adjacent grain size classes (not shown).
These intense correlations together with an unbalanced variable-to-sample ratio of 85 to 77 lead to a high degree of numerical instabilities during the EM model setup. Thereby, mathematically not defined negative eigenvalues occurred and factor rotation broke down during the loop. Thus, we summed up every two and the coarsest three grain size classes,

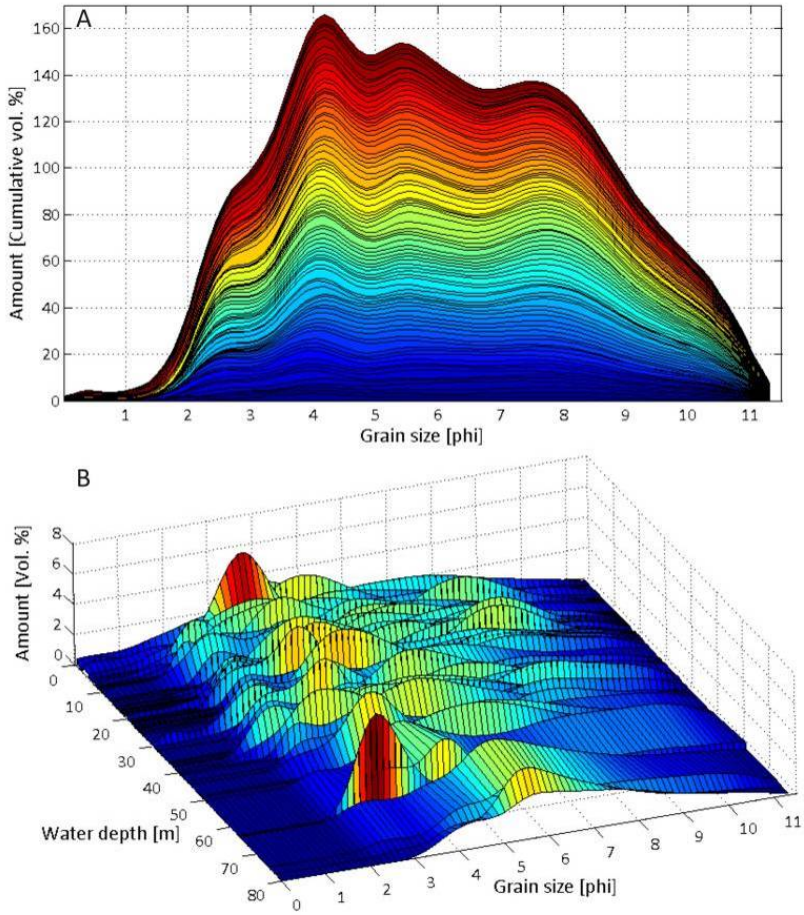

Fig. A1.2
Grain size distributions of lacustrine surface sediment samples from Lake Donggi Cona as cumulative volume percentages (A) and as individual representations against water depth at the sampling site (B).

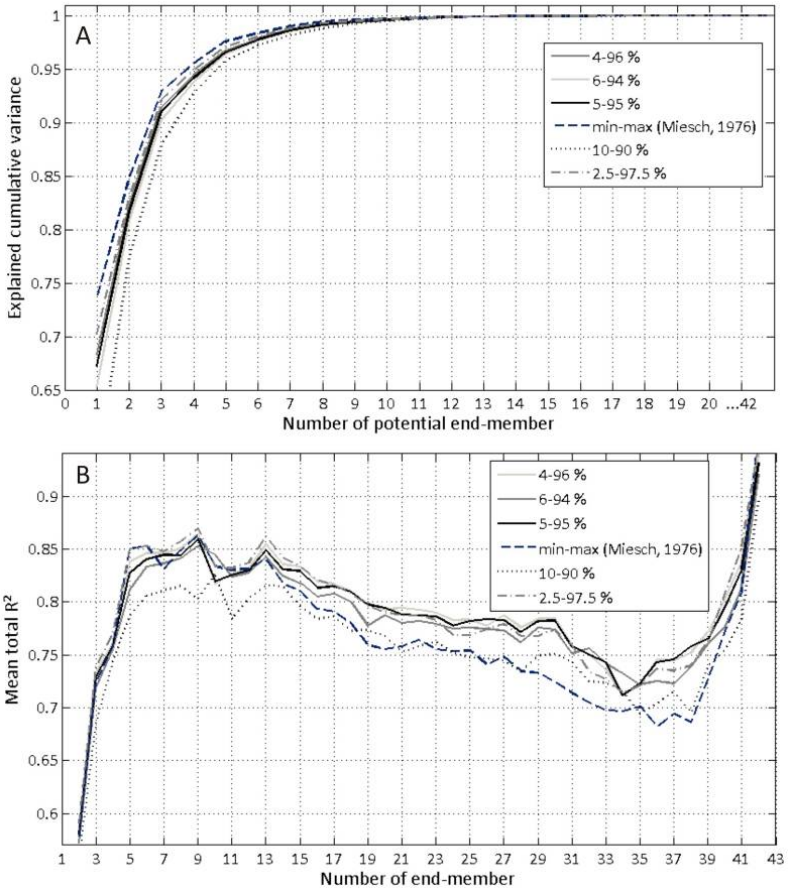

Fig. A1.3
Different weight transformations used within the end-member model. (A) The explained cumulative variance (ECV) of initial eigenvalues is a function of numbers of normalized eigenvectors (i.e. potential end-members q). The minimum number of end-member q is reached at ECV > 0.95. (B) The mean coefficient of determination r^2 as function of number of end-members q show the stability of the model and defines the maximum number of end-members at r^2_{max}.

which improved the variable-to-sample ratio to 42 to 77. This avoided negative eigenvalues and lead to a stable varimax rotation during the loop. However, some numerical instability persists, because two third of the samples still had zero values in the coarsest grain size classes. This instability became obvious when considering the final goodness-of-fit q-r^2_{mean} plot, where explained variance reduced unexpectedly when using more than 6 factors. Therefore, we tested further weight transformations using percentile intervals (Fig. 3).

4.2 The optimal end-member model

The optimal, i.e. most stable EM model had the following properties: a) it used the transformation interval of $h_n = Q_{4\%}$ and $g_n = Q_{96\%}$, b) was stable up to 8 end-members and c) yielded the highest coefficients of determination in the comparison of original with modelled data ($r^2_{max} = 0.86$). The inflection point after Prins and Weltje (1999) for this optimum model was reached when using five end-members. Its mean r^2 was 0.85, i.e. the signal to noise ratio in this optimal 5-EM model was 85 to 15.

Fig. 4A shows the end-member loadings, which are sedimentologically meaningful summing to 100 %. A clear unmixing of the former multi-modal grain size distributions has been achieved into end-members 1 to 5 with dominant modes at 3 phi (i.e. fine sand), 1.7 phi (coarse to medium sand), 6 phi (medium silt),4.4 phi (coarse silt), and 8.4 phi (clay domain). Each of them has some additional minor modes of subordinate importance, whereas EM 2 showed two prominent minor modes in the coarse silt (4.7 phi) and clay domain (8.4 phi). EM 1 to 5 represent 19.71 %, 6.22 %, 23.99 %, 16.44 %, and 33.64 % of the total variance explained by this end-member model, respectively.

End-member scores represent the degree to which an end-member contributes to each sample and are, therefore, the quantification of end-members in sample space. As in the original data, there was no significant relation to water depth at the sampling site (Fig. 4B). However, a dominance of the clay EM 5 appears visually in depth ranges around 24 m, which may correspond to a morphological level detected in bathymetry (Dietze et al., 2010).

The goodness-of-fit test showed an overall representation of grain size classes with $r^2 = 0.83 \pm 0.08$ and of samples with $r^2 = 0.85 \pm 0.08$. Fig. 4C indicates an almost complete representation of some coarse grain size classes (up to $r^2 = 0.96$ in the class of 0.9 phi), a slightly worse representation of phi-classes around 2 phi and a very good representation of phi-classes in the silt domain of $r^2 = 0.8$ to 0.9. Modelling of the smallest grain size classes then degrades slightly to $r^2_{min} = 0.6$ at 11.1 phi, a class instrumentally difficult to measure tending towards the Heisenberg uncertainty. Sample composition was explained by the 5-EM optimal model to always more than 67 % (Fig. 4D).

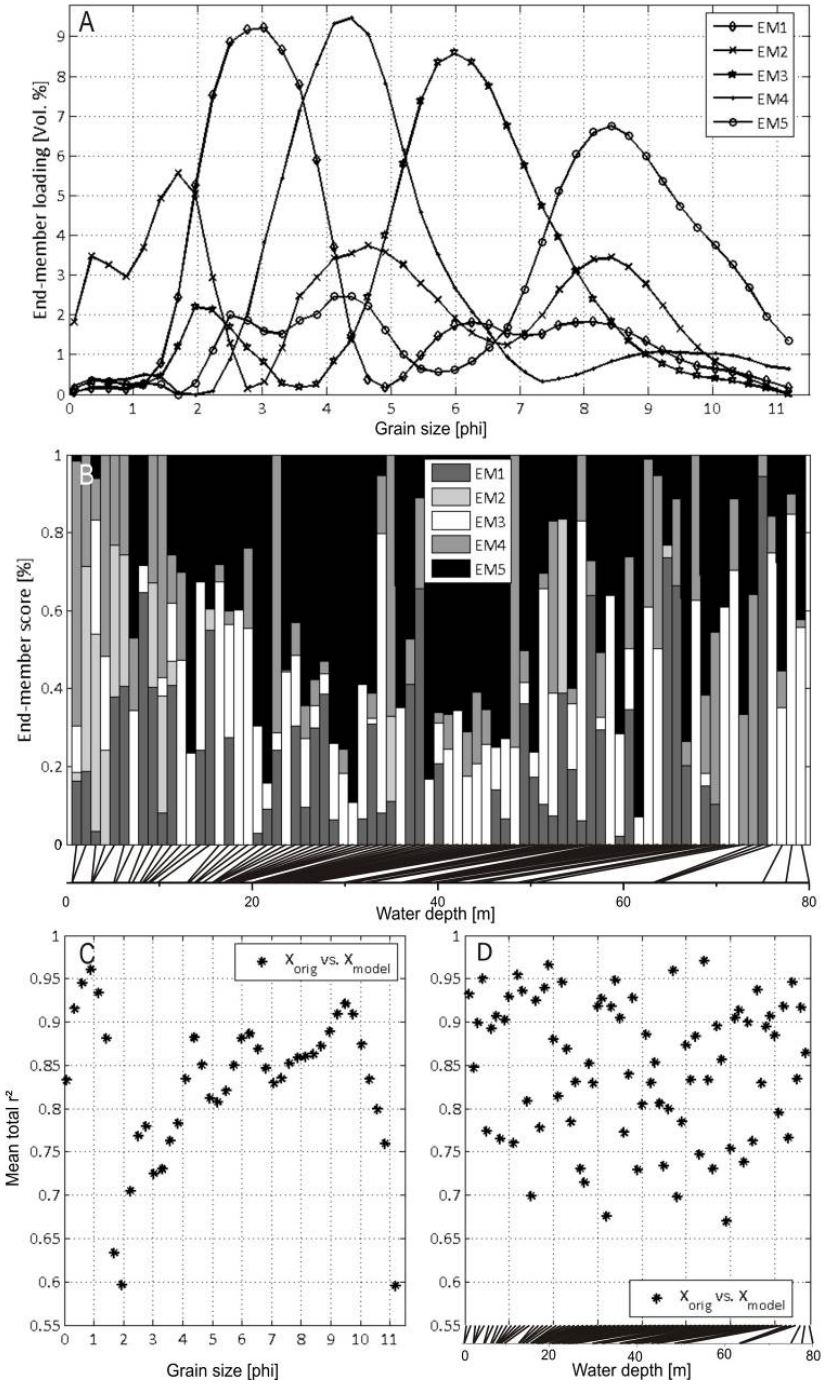

Fig. A1.4
Results of the optimal end-member model. A: End-member loadings representing geologically interpretable unmixed grain size distributions, B: End-member scores give the proportion of variance explained by the end-members for each surface sediment sample (sorted after water depth), C and D: mean variablewise and samplewise coefficient of determination (r^2) as quantitative error estimate.

4.3 The invariant end-member model

One single model is just a scenario with a given likelihood. However, the likelihood of a model itself can only be estimated in a reliable way by comparison of large sets of other similarly likely model scenarios. Thus, we calculated 12 different end-member models, which are supposed to be of similar probability. Thereby, we applied only the most stable weight transformations (quantile ranges 4-96 %, 5-95 % and 6-94 %) with a constant

minimum end-member number of 5, i.e. from more than 95 % of initially explained variance, and maximum numbers of 7 to 9, i.e. from the initiation of instability in the q-r^2_{mean} plot (Fig. 3).

Fig. 5A (grey graphs) shows a plot of all end-members between the minimum and maximum number of end-members possible within these scenarios. The representation of grain size classes < 5.2 phi appear highly depending on the model version showing no consistent end-member. However, the medium silt and clay end-members (i.e. EM 3 and 5 of Chap. 4.2 with major modes at 6 and 8.4 phi) were part of all of these end-member models. They represented highly invariant end-members and allowed a further determination of their range of uncertainty.

Therefore, we extracted the preliminary factor loadings V_q of these two invariant end-members from all 12 models and calculated their mean and standard deviation. Then, we put these mean V_q again to our end-member algorithm (to step 3) adding a residual member following the equation

$$V_{q\,res} = (1 - V_{q\,EM3invar}^2 - V_{q\,EM5invar}^2)/n$$

with n being the 42 grain size classes used in our case. For the reversal of the weight transformation (step 5) we applied the scaling factor with the 4-96% quantile weights.

The final end-member loadings $V_q'_{invar}$ are plotted in Fig. 5A (coloured) together with their range of uncertainty as calculated by adding and subtracting one standard deviation of V_q' to the mean V_q' of all 12 end-member models. The invariant end-member loadings $V_q'_{invar}$ were clearly within this uncertainty range, implying also a representative modelling of the residual member covering the coarser grain size classes (< 5.2 phi). Thereby, the medium silt EM and the clay EM explained 24.8 % and 29.6 % of the variance, respectively, i.e. both invariant end-members together represent 54.4 % of total variance within the original data set. In contrast, the residual member, i.e. the unexplained part of our model, accounted for 45.6 % of the data's variance.

End-member scores again did not show a significant relation to water depth as seen also in the quite complex pattern when plotted in space (Figs. 5B, 6). The residual member partly dominated samples of low water depths, especially close to the outlet of the lake and at the northern rim of the eastern sub-basin (Fig. 6C). The medium silt end-member never made up all of a sample ($M_q'_{max} = 0.94$; Fig. 6B).

Considering the goodness of variable and sample fit, we found a reasonably good modelling of variables with $r^2 = 0.54 \pm 0.20$ and of samples with $r^2 = 0.7 \pm 0.15$ in the invariant end-member model (Fig. 5C, D). As expected, grain size classes < 5.2 phi were poorly represented (i.e. only by the residual member) except for the classes where the two invariant end-members had their secondary modes. The finer grain size classes reached an $r^2_{max} = 0.8$. The majority of variance in sample space could be explained to always more than 36 % (Fig. 5D).

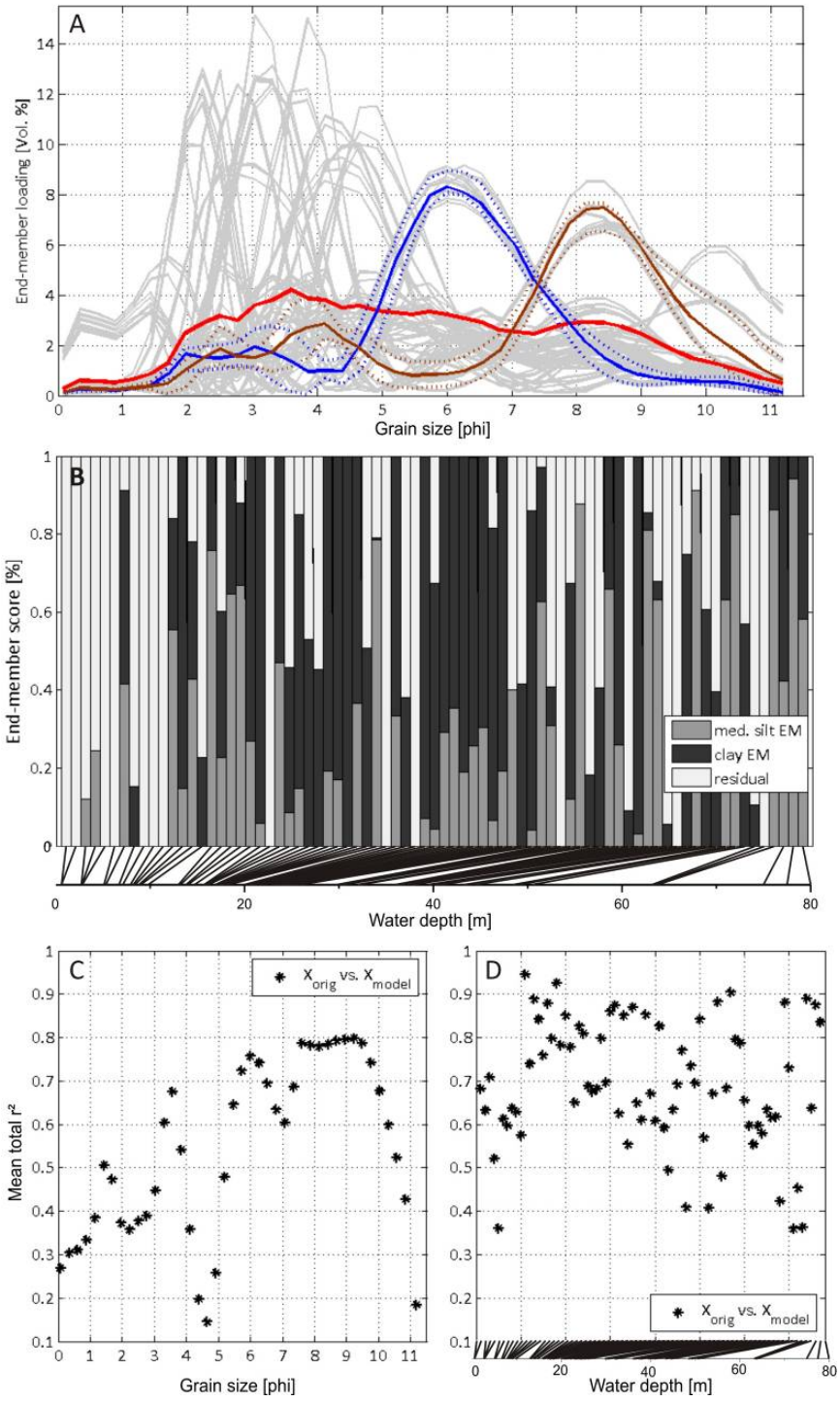

Fig. A1.5 Results of the end-member model using only the most invariant end-members. A: End-member loadings representing geologically interpretable unmixed grain size distributions (gray: all end-members from the 12 most stable EM model versions using their respective minimum to maximum number of end-members and different weight transformations; blue (dotted) graphs: mean μ (± standard deviation, s) of the invariant medium silt EM, brown (dotted) graphs: μ ± s of the invariant clay EM, red: residual; see Chap. 4.3 for details), B: End-member scores give the proportion of variance explained by the invariant end-members and the residual member for each surface sediment sample (sorted after water depth), C and D: mean variablewise and samplewise coefficient of determination (r^2) as quantitative error estimate.

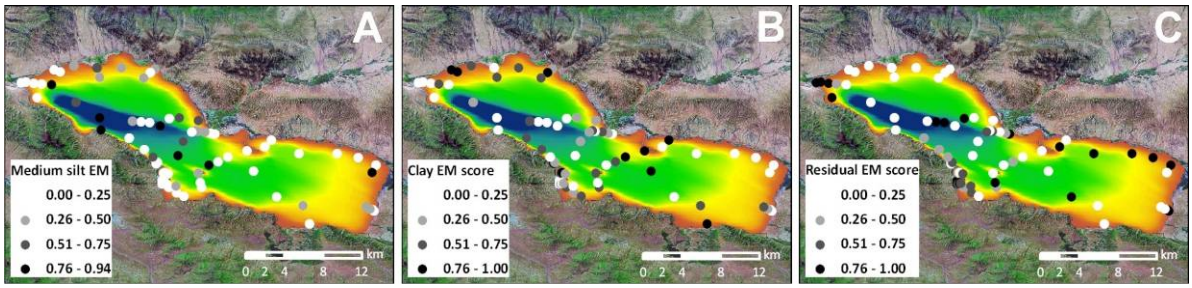

Fig. A1.6 High (black) to low (white) end-member scores of the invariant medium silt end-member (A), clay end-member (B) and the residual member (C) as the proportion of variance explained for each sample in space. Red to blue coloured bathymetry indicates a water depth range from 0 to -92 m (after Dietze et al., 2010).

5. Interpretation and Discussion

5.1 Evaluation of the end-member modelling algorithm

The overall gain of end-member modelling, i.e. the unmixing of geologically feasible, quantitative signals from a set of grain size distributions, has already been comprehensively discussed by Weltje (1997), Weltje and Prins (2007) and users of their algorithm (cf. Chap. 2.2). It overcomes most of the problems in grain size analyses associated with the methods of moments or subjectively fitting of theoretical functions (Flemming, 2007; Hartmann, 2007).
Our EM-modelling algorithm provides an additional flexible tool to study all kind of mixing problems associated with grain size distributions in all types of sediment archives. It is not restricted to study modern sediment compositions, it unmixes and derives meaningful end-members in a feasible way in the common programming environment of MATLAB and therefore contributes to a better operationalism in grain size analyses as demanded by Hartmann (2007).
Furthermore, the algorithm and its set-screws provide the opportunity to quantify the model's inherent setup uncertainty. Thereby, model scenarios can be run considering different numbers of end-members and flexible weight transformations. They are assumed of having a similar likelihood and avoid a fixed single outcome. The overall gain of considering these uncertainties is the possibility to detect invariant process components in any kind of sediment system. That brings end-member modelling to a higher level.

However, some limitations have to be mentioned, too. We had to deal with numerical instabilities, which could not be solved completely by the aggregation of grain size classes. However, we found that it is a data inherent problem, as we applied the same EM-algorithm to a data set of marine sediment core grain size distributions resulting in significantly

reduced numerical instabilities yielding likewise geologically meaningful end-members (Borchers et al., Holocene ice dynamics, bottom-water formation and polynya activity recorded in Burton Basin, East Antarctica, subm. to Paleo3). This suggests an overall suitability of our EMMA algorithm to unmix grain size distributions in further applications.
Our data inherent instabilities may result from problems related to the lacustrine sediment samples used in this study. They do not represent a purely random sampling strategy, as they have been chosen according to ecological considerations (Mischke et al., 2010). Thus, the deepest parts of the lake are poorly represented and a clustering of samples in around 24 m water depth occurs. Additionally, sedimentation rates cannot be assumed to be equal at all sites (Opitz et al., unpublished).

5.2 Detrital processes within Lake Donggi Cona

Within the mentioned limitations, detrital processes in Lake Donggi Cona can be interpreted from the end-members of the optimal 5-EM model. Typical distribution shapes may be linked with certain depositional processes following the classical understanding of grain size sorting and distribution processes during sedimentation (in tradition of e.g. Krumbein, 1936; Folk and Ward, 1957; McManus, 1988). Observations of sedimentological processes within the Donggi Cona catchment during field campaigns in summers 2006, 2009 and winters 2007, 2008 as well as reference surface samples from near-shore and catchment-wide characteristic depositional environments (IJmker et al., unpublished) allow further interpretation of the shapes of end-member grain size distributions. Thereby, we suggest that minor modes within the single end-members are more natural than an end-member from a fit with theoretical unimodal functions (Flemming, 2007).
Thus, we can specify EM 1 as sandy well-sorted, probably dune sediment and the well-sorted, silty EM 3 and 4 as remote and local dust, respectively. That implies that around 60 % of variance in modern lacustrine sediment composition may be attributed to aeolian sedimentation, which is the most characteristic transport process during winter time.
In contrast, the clay EM 5 may represent suspended sediment from fluvial and alluvial processes. During field campaigns in summer time a high load of suspension in linear and laminar runoff has always been observed during heavy precipitation events. Collected reference samples suggest multi-modal grain size distributions within the runoff, though with an obvious mode at the clay grain sizes, which has not been observed as such in reference samples of other depositional environments.
Sand EM 2 is rather poorly sorted and has actually three prominent modes representing sedimentation environments of more heterogeneity as typical for fluvial and on-shore

depositional dynamics. Nevertheless, as it explains only 6 % of total variance in the data, it may be also considered as a mathematical residual.

From the invariant EM model scenarios we learned that only the medium silt and clay end-members are robust features of surface sediment samples in Lake Donggi Cona. They are the most important detrital components of the lake sediments. Similar as in the optimal EM model they are interpreted as representing sediment contributions from remote dust and suspension load. Within a range of uncertainty they are signals which explain 25 % and 30 % of the variance in the sediment's grain size distributions, respectively. The residual variance represents different unspecific processes of higher energy during sedimentation, which may be linked with more random distribution of grain sizes at Lake Donggi Cona.

In contrast to biological activity (Mischke et al., 2010), a clear relation of grain size distributions to water depth and spatial pattern was missing (Fig. 6). Apart from the mentioned sampling limitations (Chap. 5.1), two reasons for the rather random grain size distribution of these sediments may be discussed. One is the biannual frozenness of the lake at a time, when aeolian processes peak. At that time, most of the sediment reaches the lake by wind, where it collects at ice cracks and on the partly snowed ice surface. It melts down during spring at random sites and contributes randomly to the surface sediment composition. Also a contribution of poorly sorted ice rafting debris may superimpose a continuous sedimentation.
Further influence of lake-internal transport by currents has to be considered. During spring and summer the lake is saturated by oxygen down to its bottom (Mischke et al., 2010) suggesting an intense water circulation, which can bring coarser material to deeper sites. Thereby, suspension load may be mainly distributed along the prominent -24 m morphological level, while the remaining high residual variation as representative for unspecific coarse grain sedimentation could partly be associated to the near-shore areas and more turbulent water flow close to the outlet. However, the relation of the clay end- member and the residual to water depth was not significant at all and may also be an artefact from sampling strategy.

The effective mixing processes play a major role at Lake Donggi Cona and might not be as strong in other sediment systems. They pose a special difficulty to the determination of process-related sediment properties, which we manage to deal with using the described EMMA algorithm. Within the given uncertainties we explained 55 % of variance by only two robust end-members attributed to aeolian and suspension-related sedimentation. This is a fairly good result, when we consider that deciphering all involved sedimentological

processes contributing to grain size variation within a lake would be an unrealistic high expectation.

6. Conclusion and Outlook

We presented a flexible end-member algorithm based on eigenspace analysis, which can be used to provide genetically meaningful, quantitative grain size end-members. These are representative for sedimentological and geomorphological processes within a sediment sink of highly correlative variable structure. Our algorithm helped to decipher robust, invariant sediment components of the modern detrital system within a Tibetan lake by integrating several similarly likely model scenarios. Thereby, end-member loadings allow characterising the respective end-members, while end-member scores give the proportion of variance of each end-member within a sample.

Concerning the specific local environmental conditions at Lake Donggi Cona we learned two things: first, the missing association of the grain size end-members to spatial sample distribution shows effective sediment mixing processes within the lake, which have to be considered when interpreting detrital sediment components from the past. Second, only two components are robust features of our lake system, i.e. the medium silt and clay end-members attributed to aeolian and suspension-related sedimentation processes. Consequently, we should focus on them when decomposing grain size data from sediments going back in time, as these are the main processes quantifiable in our lake system.

Our algorithm is not restricted to lacustrine depositional environments alone. It may be used in any grain size analysis studying any kind of modern or past sediment system. When studying a variety of sediment archives along a topologically linked sediment cascade, alteration of end-member scores can be used to assign significant environmental changes to certain signal providers such as climate change, tectonics or human impact.

Insight into past variations of the robust sedimentological processes at Donggi Cona area will be provided by end-member modelling using grain size components from lake sediment cores (Opitz et al., in prep.) and catchment-wide sediment archives (IJmker et al., in prep.) as proxies for limnological and environmental changes. Their contribution to sediment composition can then be compared to modern times allowing also a comparison of background sedimentation triggers.

Further alterations of the EMMA algorithm may be considered: the error estimation should include also Bayesian approaches such as Palmer and Douglas (2008) did with geochemical data. Background information can be derived from different model scenarios and the

modern climatic, tectonic and human setting. Additionally, initial tests using other compositional data such as raw element contents applying different transformations following the example of Renner (1996) showed promising results, implying that a use of our end-member algorithm beyond grain size analyses is possible.

7. Acknowledgements

We would like to acknowledge the financial support within the frame of DFG priority programme 1372 “Tibetan Plateau: Formation - Climate - Ecosystems“, which enabled a PhD-workshop on EMMA. Michael Dietze is warmly thanked for very constructive comments on manuscript.

References

Aitchison, J., 1986. The statistical analysis of compositional data. Monographs on statistics and applied probability, Chapman and Hall, London.

An, Z., Kutzbach, J.E., Prell, W.L., Porter, S.C., 2001. Evolution of Asian monsoons and phased uplift of the Himalaya-Tibetan plateau since Late Miocene times. Nature 411, 62-66.

Anderson, E., Bai, Z., Bischof, C., Blackford, S., Demmel, J., Dongarra, J., Du Croz, J., Greenbaum, A., Hammarling, S., McKenney, A., Sorensen, D., 1999. LAPACK User's Guide, third edition, SIAM, Philadelphia.

Arhonditsis, G.B., Stow, C.A., Steinberg, L.J., Kenney, M.A., Lathrop, R.C., McBride, S.J., Reckhow, K.H., 2006. Exploring ecological patterns with structural equation modeling and Bayesian analysis. Ecological Modelling 192, 385-409.

Bartholdy, J., Christiansen, C., Pedersen, J.B.T., 2007. Comparing spatial grain-size trends inferred from textural parameters using percentile statistical parameters and those based on the log-hyperbolic method. Sedimentary Geology 202, 436-452.

Bernal, S., Butturini, A., Sabater, F., 2006. Inferring nitrate sources through end member mixing analysis in an intermittent Mediterranean stream. Biogeochemistry 81, 269-289.

Blanchet, F.G., Legendre, P., Borcard, D., 2008. Modelling directional spatial processes in ecological data. Ecological Modelling 215, 325-336.

Buccianti, A., Mateu-Figueiras, G., Pawlowsky-Glahn (eds.), 2006. Compositional Data Analysis in the Geosciences. Special Publication 264, Geological Society, London.

Burns, D.A., McDonnell, J.J., Hooper, R.P., Peters, N.E., Freer, J.E., Kendall, C., Beven, K., 2001. Quantifying contributions to storm runoff through end-member mixing analysis and hydrologic measurements at the Panola Mountain Research Watershed (Georgia, USA). Hydrological Processes 15, 1903-1924.

Chinese Central Meteorological Office, 1984. Average climatology for 841 meteorological stations throughout China, 1951-1980 (Meteorological Data of China). Meteorology Press, Beijing.

Christensen, E.R., Arora, S., 2007. Source apportionment of PAHs in sediments using factor analysis by time records: Application to Lake Michigan, USA. Water Research 41, 168-176.

Christophersen, N., Neal, C., Hooper, R.P., Vogt, R.D., Andersen, S., 1990. Modelling streamwater chemistry as a mixture of soilwater end-members – A step towards second-generation acidification models. Journal of Hydrology 116, 307-320.

Collins, A.L., Walling, D.E., Webb, L., King, P., 2010. Apportioning catchment scale sediment sources using a modified composite fingerprinting technique incorporating property weightings and prior information. Geoderma 155, 249-261.

Dechert, W.D., O'Donnell, S.I., 2006. The stochastic lake game: A numerical solution. ournal of Economic Dynamics and Control 30, 1569-1587.

Diekmann, B., Kuhn, G., 1999. Provenance and dispersal of glacial-marine surface sediments in the Weddell Sea and adjoining areas, Antarctica: ice-rafting versus current transport. Marine Geology 158, 209-231.

Dietze, E., Wünnemann, B., Diekmann, B., Aichner, B., Hartmann, K., Herzschuh, U., IJmker, J., Jin, H., Kopsch, C., Lehmkuhl, F., Li, S., Mischke, S., Niessen, F., Opitz, S., Stauch, S., Yang, S., 2010. Basin morphology and seismic stratigraphy of Lake Donggi Cona, north-eastern Tibetan Plateau, China. Quaternary International 218, 131-142.

Domrös, M., Peng, G., 1988. The climate of China. Springer, Berlin, Heidelberg, New York.

Flemming, B.W., 2007. The influence of grain-size analysis methods and sediment mixing on curve shapes and textural parameters: Implications for sediment trend analysis. Sedimentary Geology 202, 425-435.

Folk, R.L., Ward, W.C., 1957. Brazos river bar: a study in the significance of grain size parameters. Journal of Sedimentary Petrology 27, 3-26.

Garzanti, E., Andò, S., Vezzosi, G., 2009. Grain-size dependence of sediment composition and environmental bias in provenance studies. Earth and Planetary Science Letters 277, 422-432.

Guttman, L., 1954. Some necessary conditions for common-factor analysis. Psychometrika 19, 149-161.

Hamann, Y., Ehrmann, W., Schmiedl, G., Krüger, S., Stuut, J.-B., Kuhnt, T., 2008. Sedimentation processes in the Eastern Mediterranean Sea during the Late Glacial and Holocene revealed by end-member modelling of the terrigenous fraction in marine sediments. Marine Geology 248, 97-114.

Hartmann, D., 2007. From reality to model: Operationalism and the value chain of particle-size analysis of natural sediments. Sedimentary Geology 202, 383-401.

Hartmann, K. Wünnemann, B., 2009. Hydrological changes and Holocene climate variations in NW China, inferred from lake sediments of Juyanze palaeolake by factor analyses. Quaternary International 194, 28-44.

Hendrickson, A.E., White, P.O., 1964. Promax: a quick method for rotation to oblique simple structure. British Journal of Statistical Psychology 17, 65-70.

Holz, C., Stuut, J.-B., Henrich, R., Meggers, H., 2007. Variability in terrigenous sedimentation processes off northwest Africa and its relation to climate changes: Inferences from grain-size distributions of a Holocene marine sediment record. Sedimentary Geology 202, 499-508.

Imbrie, J., 1963. Factor and vector analysis programs for analyzing geologic data. Technical Report 6, ONR Task No. 389-135, Office of Naval Research, Geography Branch.

Julià, R., Luque, J.A., 2006. Climatic changes vs. catastrophic events in lacustrine systems: A geochemical approach. Quaternary International 158, 162-171.

Kaiser, H.F., 1958. The varimax criterion for analytic rotation in factor analysis. Psychometrika 23, 187-200.

Klovan, J.E., 1966. The use of factor analysis in determining depositional environments from grain-size distributions. Journal of Sedimentary Petrology 36, 115-126.

Klovan, J.E., Imbrie, J., 1971. An Algorithm and FORTRAN-IV Program for Large-Scale Q-Mode Factor Analysis and Calculation of Factor Scores. Mathematical Geology 3, 61-77.

Krumbein, W.C., 1936. Application of logarithmic moments to size frequency distribution of sediments. Journal of Sedimentary Petrology 6, 35-47.

Kucera, M., Malmgren, B.A., 1998. Logratio transformation of compositional data- a resolution of the constant sum constraint. Marine Micropalaeontology 34, 117-120.

Kürschner, H., Herzschuh, U., Wagner, D., 2005. Phytosociological studies in the north-eastern Qinghai-Xizang Plateau (NW China) – A first contribution to the subalpine scrub and alpine meadow vegetation. Botanische Jahrbücher der Systematik 126, 273-315.

Lawson, C.L., Hanson, R.J., 1974. Solving Least Squares Problems. Prentice Hall, New Jersey.

Manson, V., Imbrie, J. 1964. FORTRAN program for factor and vector analysis of geologival data using an IBM 7090 or 7094/1401 computer system. Kansas Geological Survey Special Distribution Publications 13.

McManus, J., 1988. Grain size determination and interpretation, in: Tucker, M. (ed.), Techniques in sedimentology. Blackwell, Oxford, pp. 63-85.

McLaren, P., Hill, S.H., Bowles, D., 2007. Deriving transport pathways in a sediment trend analysis (STA). Sedimentary Geology 202, 489-498.

Miesch, A.T., 1976. Q-Mode factor analysis of geochemical and petrologic data matrices with constant row sums. U.S. Geological Survey Professsional Papers 574.

Miesch, A.T., 1980. Scaling variables and interpretation of eigenvalues in principal component analysis of geologic data. Mathematical Geology 12, 523-538.

Mischke, S., Bößneck, U., Diekmann, B., Herzschuh, U., Jin, H., Kramer, A., Wünnemann, B., Zhang, C., 2010. Quantitative relationship between water-depth and sub-fossil ostracod assemblages in Lake Donggi Cona, Qinghai Province, China. Journal of Paleolimnology 43, 589-609.

Orpin, A.R., Woolfe, K.J., 1999. Unmixing relationships as a method of deriving a semi-quantitative terrigenous sediment budget, central Great Barrier Reef lagoon, Australia. Sedimentary Geology 129, 25-35.

Palmer, M.J., Douglas, G.B., 2008. A Bayesian statistical model for end member analysis of sediment geochemistry, incorporating spatial dependences. Journal of the Royal Statistical Society Series C-Applied Statistics 57, 313-327.

Papatheodorou, G., Demopoulou, G., Lambrakis, N., 2006. A long-term study of temporal hydrochemical data in a shallow lake using multivariate statistical techniques. Ecological Modelling 193, 759-776.

Prins, M.A., Weltje, G.J., 1999. End-member modelling of grain-size distributions of sediment mixtures. In: Prins, M.A., Pelagic, hemipelagic and turbidite deposition in the Arabian Sea during the late Quaternary: Unravelling the signals of aeolian and fluvial sediment supply as functions of tectonics, sea-level and climate change by means of end-member modelling of siliciclastic grain-size distributions. Ph.D. Thesis, Geologica Ultraiectina, 168, Utrecht University, pp. 47-68.

Prins, M.A., Vriend, M., Nugteren, G., Vandenberghe, J., Lu, H., Zheng, H., Weltje, G.J., 2007. Late Quaternary aeolian dust input variability on the Chinese Loess Plateau: inferences from unmixing of loess grain-size records. Quaternary Science Reviews 26, 230-242.

Reimann, C., Filzmoser, P., Garrett, R.G., 2002. Factor analysis applied to regional geochemical data: problems and possibilities. Applied Geochemistry 17, 185-206.

Renner, R.M., 1991. An examination of the use of the logratio transformation for the testing of endmember hypotheses. Mathematical Geology 23, 549-563.

Renner, R.M., 1995. The construction of extreme compositions. Mathematical Geology 27, 485-497.

Renner, R.M., 1996. An algorithm for constructing extreme composition. Camp. Geosciences 21, 15-25.

Renner, R.M., Glasby, G.P., Walter, P., 1997. Endmember analysis of metalliferous sediments from the Galapagos Rift and East Pacific Rise between 2°N and 42°S. Applied Geochemistry 12, 383-395.

Renner, R.M., Glasby, G.P., Szefer, P., 1998. Endmember analysis of heavy-metal pollution in surficial sediments from the Gulf of Gdansk and the southern Baltic Sea off Poland. Applied Geochemistry 13, 313-318.

Reyment, R.A., 1963. Multivariate analytical treatment of quantitative species associations: An example from palaeoecology. Journal of Animal Ecology 32, 535-47.

Reyment, R.A., Jöreskog, K.G., 1993. Applied factor analysis in the natural sciences. Cambridge University Press, Cambridge.

Robichaud, P.R., Lewis, S.A., Laes, D.Y.M., Hudak, A.T., Kokaly, R.F., Zamudio, J.A., 2007. Postfire soil burn severity mapping with hyperspectral image unmixing. Remote Sensing of Environment 108, 467-480.

Schmidt, D., 1999. Das Extremklima der nordchilenischen Hochatacama unter besonderer Berücksichtigung der Höhengradienten. Dresdener Geographische Beiträge 4, in German.

Solohub, J.T., Klovan, J.E., 1970. Evaluation of grain-size parameters in lacustrine environments. Journal of Sedimentary Petrology 40, 81-101.

Song, C., 2005. Spectral mixture analysis for subpixel vegetation fractions in the urban environment: How to incorporate endmember variability? Remote Sensing of Environment 95, 248-263.

Sonnentag, O., Chen, J.M., Roberts, D.A., Talbot, J., Halligan, K.Q., Govind, A., 2007. Mapping tree and shrub leaf area indices in an ombrotrophic peatland through multiple endmember spectral unmixing. Remote Sensing of Environment 109, 342-360.

Stanimirova, I., Walczak, B., Massart, D.L., 2005. Multiple factor analysis in environmental chemistry. Analytica Chimica Acta 545, 1-12.

Sun, D., Bloemendal, J., Rea, D.K., Vandenberghe, J., Jiang, F., An, Z., Su, R., 2002. Grain-size distribution function of polymodal sediments in hydraulic and aeolian environments, and numerical partitioning of the sedimentary components. Sedimentary Geology 152, 263-277.

Szefer, P., Glasby, G.P., Geldon, J., Renner, R.M., Bjorn, E., Snell, J., Frech, W., Warzocha, J., 2009. Heavy-metal pollution of sediments from the Polish exclusive zone, southern Baltic Sea. Environmental Geology 57, 847-862.

Walling, D.E., 2005. Tracing suspended sediment sources in catchments and river systems. Science of the Total Environment 344, 159-184.

Wan, S., Li, A., Clift, P.D., Stuut, J.-B., 2007. Development of the East Asian monsoon: Mineralogical and sedimentologic records in the northern South China Sea since 20 Ma. Palaeogeography, Palaeoclimatology, Palaeoecology 254, 561-582.

Wang, Y., Yang, H., 2004. Middle Permian palaeobiogeography study in East Kunlun, A'nyêmaqên and Bayan Har. Science in China 47, 1120-1126.

Wang, Y., Xu, G., Lin, Q., Gong, S., 2001. Depositional model of Early Permian reef-island ocean in Eastern Kunlun. Science in China 44, 808-815.

Weltje, J., 1997. End-Member Modeling of Compositional Data: Numerical-Statistical Algorithms for Solving the Explict Mixing Problem. Mathematical Geology 29, 503-549.

Weltje, J., Prins, M.A., 2007. Genetically meaningful decomposition of grain size distributions. Sedimentary Geology 202, 409-424.

Zimmerman, A.R.B., Owen, R.M., 1990. A Quantitative Model of the Dispersal of Detrital Inputs and Minor Compositional Components in Lake Michigan Sediments. Journal of Great Lakes Research 16, 444-456.

A2 Antarctic bottom-water dynamics in the Indian sector of the Antarctic Ocean over the last 140 000 years

Ines Voigt[1], Andreas Borchers[2], Oliver Esper[3], Thomas Frederichs[4], Rainer Gersonde[5], Gerhard Kuhn[6], Sven Kretschmer[7], Gesine Mollenhauer[8] and Bernhard Diekmann[9]

1 University Bremen, Geoscience Department, P.O. Box 330440, 28334 Bremen, Germany ines.voigt@uni-bremen.de
2 Wegener Institute for Polar and Marine Research, Telegrafenberg A43, 14473 Potsdam, Germany Andreas.Borchers@awi.de
3 Alfred Wegener Institute for Polar and Marine Research, P.O. Box 12 01 61, 27515 Bremerhaven, Germany Oliver.Esper@awi.de
4 University Bremen, Geoscience Department, P.O. Box 330440, 28334 Bremen, Germany frederichs@uni-bremen.de
5 Alfred Wegener Institute for Polar and Marine Research, P.O. Box 12 01 61, 27515 Bremerhaven, Germany Rainer.Gersonde@awi.de
6 Alfred Wegener Institute for Polar and Marine Research, P.O. Box 12 01 61, 27515 Bremerhaven, Germany Gerhard.Kuhn@awi.de
7 Alfred Wegener Institute for Polar and Marine Research, P.O. Box 12 01 61, 27515 Bremerhaven, Germany Sven.Kretschmar@awi.de
8 Alfred Wegener Institute for Polar and Marine Research, P.O. Box 12 01 61, 27515 Bremerhaven, Germany Gesine.Mollenhauer@awi.de
9 Wegener Institute for Polar and Marine Research, Telegrafenberg A43, 14473 Potsdam, Germany Bernhard.Diekmann@awi.de

Abstract: *Today, the Deep Western Boundary Current (DWBC) off the Kerguelen-Plateau is one of the most important route for deep-water entering the Indian Ocean. Only few attempts have been undertaken to reconstruct late Quaternary bottom-water dynamics of the DWBC. Here we present a high-resolution record of bottom water variability from a sediment core recovered from a contourite drift along the eastern flank of the Kerguelen-Plateau. Large-scale changes in deep water circulation in the Indian sector of the Antarctic Ocean during the last 140 ka are associated with the formation of Antarctic Bottom Water (AABW) in the Mertz Glacier Polynya (MGP) on the Adélie Coast and show not a clear glacial/interglacial pattern.*

Key words: *Antarctic Bottom Water, Deep Western Boundary Current (DWBC), Kerguelen-Plateau, Adélie Coast, Mertz Glacier Polynya (MPG).*

INTRODUCTION

The exact sources of AABW found in the Australian-Antarctic Basin within the Southern Ocean have been controversial due to the distance from the major continental ice shelves in the Weddell- and Ross Sea which are traditionally associated with bottom water formation. However, more recent oceanographic surveys along the Adélie Coast suggest that this region is a significant source of AABW. The identification of the Mertz polynya, the second largest persistent polynya around East Antarctica, as a relevant source of bottom water has led to a reinterpretation of the volumetric census of AABW formed at the Adélie Coast (Rintoul, 1998). Thus, this region represents the second largest source after the Weddell Sea, and is responsible for 25% of the volume of AABW found in the world's ocean.

It can be expected that the relatively strong currents associated with AABW circulation effect sedimentary processes in the Australian-Antarctic Basin. Evidence for strong bottom-water current activity is found in drift deposits of the East Kerguelen Ridge (EKR), along the eastern margin of the Kerguelen-Plateau (Kolla et al., 1978). Here we present a record of late Quaternary bottom-water dynamics, inferred from a sediment core from the Kerguelen Drift.

STUDY AREA

The EKR lies at the western boundary of the Australian-Antarctic Basin. In the basin, the movement of Antarctic Bottom Water, which substantially originates along the Adélie Coast, is clockwise as a result of the northward extension of AABW east of the Kerguelen-Plateau (McCartney & Donohue, 2007). Along the eastern flank of the Kerguelen-Plateau, the influence of the Deep Western Boundary Current (DWBC) has been inferred from both current measurements and hydrographic observations and has been attributed to vigorous bottom-water flow (Kolla et al., 1978). Donohue et al. (1999) estimated a northward DWBC transport of 15–26 Sv.

METHODS

The terrigenous grain-size parameters, such as the sortable-silt fraction (10-63 µm) as a percentage of the fine-fraction (McCave, 1995a, 1995b), and the mean of the sortable-silt fraction (McCave, 1995a) are especially current sensitive and have been considered to be proxies for palaeo-current strenghts. In addition, we use clay minerals as tracers of current-transported sediment, to infer provenance and transport paths (Kuhn and Diekmann, 2002). Our age model is mainly based on paleomagnetic dating combined with biostratigraphy and relies for the last 30 ka on AMS ^{14}C dating.

DISCUSSION AND CONCLUSION

The variability of the DWBC, as indicated by the grain-size data, shows not a clear glacial/interglacial pattern. Enhanced near-bottom flow strength appears during the interglacial-glacial climate transitions between MIS 5 and MIS 4 and at recent times. During both the last interglacial maximum (MIS 5.5) and during glacial phases (MIS 2, MIS 4 and MIS 6) the DWBC strength weakened (see Fig.1).

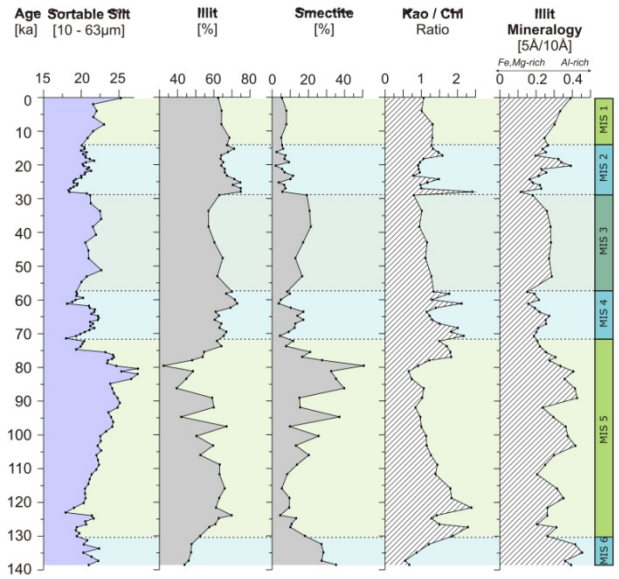

FIGURE 1. Sortable-silt and variability of clay mineralogy over time from the sediment core PS69/899-2 on the Kerguelen-Drift.

Changes in clay mineral composition of the drift deposits can be related to the hydrographic changes and are mainly controlled by the variability of the DWBC. Associated with the variations of near-bottom flow strength, two different source areas can be distinguished: a more local source and an easternmost source area. The influx of clay minerals from East Antarctica, indicated by Mg(Fe)-rich illite and kaolinite, is dectectable during phases with reduced near-bottom flow strength. That implies, that during the last interglacial maximum (MIS 5.5) and during glacial phases the DWBC probably was mainly controlled by the AABW from the Adélie Coast. During times of enhanced near-bottom flow, the clay mineral signature of East Antarctica is overprinted by an influx of (Al)-rich illite and smectite. The Kerguelen-Plateau and the adjacent Australian-Antarctic Basin represents a local source for (Al)-rich illite and smectite. Related to undercutting the basement by current erosion and reworking of basin sediments that occurs with enhanced bottom velocity, the clay minerals could be derived from more local sources. Thus, during the last 140 ka the variability of the DWBC is mostly affected by AABW which originates along the Adélie Coast.

The reduced near-bottom flow strength of the Deep Western Boundary Current during the maximum of the last interglacial (MIS 5.5) implies, that the formation of AABW at the Mertz polynya on the Adélie Coast is severely restricted during this stage. Modeling studies show a clear response in sea ice formation and dense shelf water production in the MPG related to the climate change perturbations (Marsland et al., 2007). Their model shows, that the dense shelf water export is reduced with increasing air temperatures and increasing surface fresh water influx (by precipitation, runoff or glacial melt water) – climate conditions that also marks the maximum of the last interglacial period (MIS 5.5). Thus, development of the Mertz polynya is prevented due to the extensive reduction of sea ice cover on the Adélie Coast which also implies a corresponding reduction in Antarctic Bottom Water formation in the area. By contrast, a very extensive sea-ice cover and/or the break-up of the Mertz glacier during glacial phases could also restricts the development of the Mertz polynya which generally reduces the intensity of bottom water formation. Only during the transition phases between the peaks of the climate cycles, the formation of AABW on the Adélie Coast is enhanced due to more or less instable sea ice cover, which guarantees the development and/or stability of the Mertz polynya system.

In conclusion, we see that the vigour of abyssal circulation off East Antarctica does not follow a simple glacial-interglacial pattern, as usually observed in the Atlantic sector of the Southern Ocean. In the Indian sector, times with most variable sea-ice formation determine AABW production and are related to modest interglacial stages.

ACKNOWLEDGEMENTS

We appreciate the kind assistance of several AWI colleagues and the crew and master of research vessel ‘Polarstern’ during the cruise ANTXXIII/9 to the Antarctic sea.

REFERENCES

Donohue, K., Hufford G. E. and McCartney, M.S., (1999): Sources and transport of the deep western boundary current east of the Kerguelen Plateau. *Geophysical Research Letters*, 26: 851-854.

Kolla, V., Henderson, L., Sullivan, L. & Biscaye, P.E., (1978): Recent sedimentation in the southeast Indian ocean with special reference to the e!ects of Antarctic bottom water circulation. *Marine Geology*: 27, 1-17.

Kuhn, G. & Diekmann, B. (2002). Late Quaternary variability of ocean circulation in the southeastern South Atlantic inferred from the terrigenous sediment record of a drift deposit in the southern Cape Basin (ODP Site 1089). *Palaeogeography Palaeoclimatology Palaeoecology*, 182, 287-303.

Marsland, S. J., Bindoff, N.L., Williams, G.D., Budd, W.F. (2004): Modeling water mass formation in the Mertz Glacier Polynya and Adelie Depression, East Antarctica. *Journal of Geophysical Research*, 109: C11003.

McCartney, M. S. and Donohue, K.A. (2007): A deep cyclonic gyre in the Australian-Antarctic Basin. *Progress in Oceanography*, 75 (4): 675-750.

McCave, LN., Manighetti, B. and Robinson, S.O., (1995): Sortable silt and fine sediment size/composition slicing: Parameters for paleocurrent speed and paleoceanography. *Paleoceanography*, 10, (3): 593-610.

Rintoul, S.R., (1998). On the origin and influence of Adélie Land Bottom Water. Ocean, Ice, and Atmosphere: Interactions at the Antarctic Continental Margin. *Antarctica Research Series*, 75, 151-171.

Appendix B

-

Data

All data presented in this thesis can be accessed at http://www.pangaea.de, including core descriptions, X-radiographs, physical properties (e.g. volume susceptibility), IRD data, XRF data *et cetera*.

B1: Heavy-mineral counts of sea-bed surface samples and sediment cores PS69/849-2 (manuscript II) and PS69/851-1 (manuscript III)

Depth	counts	biotite	garnet	horn-blende	clino-pyroxene	ortho-pyroxene	apatite	Ep./clinoz./ zoisite	silli-manite	stauro-lithe	zirkon	rutile	weathered	opaque
manuscript I														
PS69/849-1 SF	257	2	214	5	3	9	7	0	15	0	2	0	4	15
PS69/851-1 SF	445	9	177	200	18	24	5	0	3	0	9	0	11	29
PS69/853-1 SF	376	13	79	215	12	24	9	5	10	0	7	2	17	18
PS69/878-4 SF	487	24	76	273	19	45	15	10	10	0	9	6	17	55
PS69/885-1 SF	214	19	10	140	6	12	8	4	0	0	12	3	17	38
PS69/899-1 SF	255	7	37	111	11	23	33	10	5	0	12	6	31	77
PS69/793-2-125 cm	411	7	57	283	15	24	10	3	2	2	8	0	10	32
PS69/849-2-330 cm	354	14	280	6	8	17	16	0	6	0	6	1	9	55
PS69/855-1-1528 cm	422	1	125	181	17	92	4	1	0	0	1	0	7	30
manuscript II														
1 cm	257	2	214	5	3	9	7	0	15	0	2	0	4	15
20 cm	515	9	419	17	10	43	8	3	3	1	2	0	7	48
40 cm	319	8	265	7	5	24	5	1	3	1	0	0	2	17
115 cm	393	4	342	8	8	17	5	1	4	0	4	0	12	40
250 cm	368	2	315	3	4	32	5	1	4	0	2	0	7	15
280 cm	457	8	404	10	3	22	2	2	2	0	4	0	4	45
330 cm	374	14	300	6	8	17	16	0	6	0	6	1	9	55
manuscript III														
10 cm	492	11	216	207	8	26	5	6	4	0	6	3	5	51
120 cm	442	38	249	90	7	28	9	3	3	1	10	4	12	190
340 cm	554	106	261	127	11	31	7	2	4	0	5	0	9	113
410 cm	674	26	262	304	10	38	9	5	5	3	9	3	9	100
530 cm	409	41	204	121	4	25	2	1	3	1	5	2	8	66
590 cm	536	57	256	171	6	22	8	1	3	1	10	1	3	76
700 cm	560	108	239	152	11	32	4	2	1	2	8	1	3	72
810 cm	440	10	238	143	5	20	8	2	0	3	8	3	5	121

B2: Water content, bulk density, total organic carbon (TOC), sulphur (S) and biogenic silica content (= biogenic opal, BSi) of sediment core PS69/849-2

Depth [cm]	water content [wt.%]	mean density g cm^{-3}	TOC [wt.%]	S [wt.%]	BSi [%]
1	55.77	2.51	0.83	0.29	33.76
6	55.02	2.53	0.75	0.34	35.73
11	61.28	2.51	0.88	0.32	41.12
16	62.48	2.50	0.88	0.33	39.65
20	61.43	2.50	0.85	0.31	41.12
25	68.59	2.49	0.92	0.38	39.65
30	61.15	2.51	0.96	0.39	43.09
35	63.16	2.50	0.94	0.33	39.65
40	66.74	2.44	1.05	0.34	43.58
45	67.73	2.46	1.02	0.35	43.09
50	71.05	2.44	1.01	0.35	45.05
55	72.90	2.43	1.01	0.41	49.95
60	71.91	2.44	1.05	0.40	48.97
65	68.07	2.44	1.04	0.36	45.05
70	68.45	2.49	0.92	0.35	44.56
75	70.72	2.56	0.99	0.36	47.50
80	65.35	2.48	0.99	0.36	44.07
85	76.98	2.44	1.10	0.44	54.37
90	73.25	2.47	1.08	0.36	51.92
95	70.19	2.41	1.07	0.53	53.88
100	67.49	2.47	1.03	0.48	35.73
105	55.34	2.56	0.74	0.37	37.20
110	45.84	2.60	0.54	0.27	30.33
115	43.18	2.59	0.49	0.24	24.44
120	55.42	2.53	0.47	0.32	39.16
125	60.81	2.52	0.46	0.34	39.16
130	61.55	2.55	0.47	0.31	36.22
135	66.79	2.54	0.37	0.40	40.63
140	67.43	2.43	0.71	0.41	52.90
145	63.67	2.50	0.55	0.38	39.65
150	60.06	2.55	0.54	0.34	39.16
155	52.72	2.55	0.50	0.27	35.73
160	61.07	2.53	0.53	0.31	41.12
165	71.02	2.50	0.64	0.47	46.03
170	83.59	2.49	0.56		42.60
175	82.95	2.23	0.69	0.54	
180	84.53	2.31	0.81	0.88	40.14
185	84.72	2.32	0.62	0.57	41.61
190	89.14	2.32	0.63	0.77	50.45
195	88.25	2.33	0.68	0.61	48.97
200	90.61	2.26	0.64	0.82	47.50
205	80.46	2.39	0.88	0.61	54.86
210	78.87	2.48	0.90	0.52	55.84
215	64.45	2.52	0.69	0.35	43.58

Depth [cm]	water content [wt.%]	mean density g cm^{-3}	TOC [wt.%]	S [wt.%]	BSi [%]
220	67.92	2.54	0.68	0.36	43.09
225	82.52	2.40	0.67	0.57	54.86
230	74.89	2.54	0.81	0.46	43.58
235	76.95	2.56	0.73	0.48	44.07
240	51.35	2.67	0.40	0.28	31.80
245	40.16	2.66	0.39	0.23	25.91
250	35.00	2.67	0.30	0.22	23.95
255	46.26	2.58	0.55	0.29	30.82
260	43.63	2.59	0.56	0.30	34.75
265	40.70	2.62	0.45	0.27	30.33
270	76.56	2.45	1.07	0.70	42.10
275	77.96	2.44	0.99	0.66	40.14
280	31.10	2.66	0.33	0.22	21.50
285	35.51	2.63	0.43	0.30	23.95
290	34.40	2.62	0.41	0.32	25.42
295	36.94	2.63	0.45	0.41	27.88
300	28.82	2.66	0.38	0.47	24.44
305	19.54	2.71	0.19	0.39	22.48
310	38.18	2.64	0.41	0.40	25.91
315	75.70	2.46	1.01	0.93	25.42
320	71.89	2.40	1.21	0.79	44.56
325	17.74	2.67	0.25	0.43	16.59
330	20.27	2.67	0.28	0.29	17.08
335	20.95	2.67	0.28	0.28	16.59
340	19.71	2.67	0.30	0.27	17.57
345	21.11	2.67	0.30	0.27	13.65
350	21.98	2.66	0.30	0.23	20.52
355	19.95	2.67	0.30	0.25	17.57
360	20.76	2.66	0.30	0.23	15.61
365	17.41	2.66	0.31	0.22	17.08
370	17.03	2.67	0.31	0.25	17.08
375	19.50	2.67	0.30	0.28	20.52

B3: Results of the end-member modelling of grain-size data of sediment core PS69/849-2

B3.1 Goodness of fit (GOF) comparing the modelled dataset with the original data for 2 - 10 end member

No. of end-members	1	2	3	4	5	6	7	8	9	10
GOF r^2mean	0.00	0.22	0.63	0.74	0.77	0.80	0.90	0.88	0.86	0.86

B3.2 Coefficients of determination (r^2) against each sample for 2 – 10 end members

Depth [cm]	No. of end-members								
	2	3	4	5	6	7	8	9	10
1	0.87	0.89	0.94	0.95	0.96	0.95	0.95	0.95	0.95
11	0.87	0.95	0.98	0.96	0.97	0.97	0.97	0.97	0.95
20	0.88	0.98	0.97	0.97	0.95	0.96	0.96	0.95	0.95
30	0.92	0.97	0.89	0.89	0.88	0.90	0.90	0.91	0.94
40	0.97	0.97	0.91	0.91	0.88	0.90	0.90	0.90	0.93
50	0.92	0.97	0.89	0.89	0.88	0.89	0.89	0.89	0.92
60	0.96	0.96	0.89	0.90	0.87	0.89	0.89	0.91	0.92
70	0.95	0.96	0.93	0.92	0.93	0.95	0.94	0.94	0.93
80	0.91	0.94	0.91	0.90	0.93	0.95	0.94	0.95	0.94
90	0.94	0.93	0.83	0.84	0.81	0.82	0.82	0.84	0.87
100	0.97	0.96	0.92	0.92	0.90	0.91	0.91	0.93	0.94
110	0.63	0.95	0.93	0.96	0.97	0.96	0.96	0.92	0.92
120	0.94	0.99	0.97	0.97	0.97	0.97	0.95	0.94	0.93
130	0.98	0.98	0.93	0.93	0.90	0.91	0.91	0.92	0.94
140	0.95	0.91	0.84	0.86	0.83	0.86	0.84	0.88	0.90
150	0.90	0.96	0.87	0.88	0.87	0.88	0.86	0.88	0.93
160	0.93	0.93	0.86	0.86	0.87	0.89	0.91	0.95	0.95
170	0.78	0.87	0.83	0.86	0.84	0.84	0.88	0.92	0.91
180	0.37	0.90	0.92	0.92	0.92	0.97	0.90	0.89	0.80
190	0.84	0.85	0.76	0.79	0.79	0.79	0.82	0.89	0.93
200	0.64	0.79	0.90	0.90	0.94	0.95	0.96	0.89	0.87
210	0.90	0.86	0.70	0.74	0.78	0.82	0.87	0.90	0.92
220	0.83	0.89	0.86	0.84	0.92	0.94	0.93	0.96	0.95
230	0.81	0.82	0.74	0.75	0.89	0.92	0.93	0.93	0.91
240	0.71	0.81	0.90	0.89	0.94	0.94	0.93	0.96	0.94
250	0.81	0.81	0.87	0.90	0.91	0.91	0.92	0.98	0.96
260	0.66	0.78	0.81	0.85	0.86	0.89	0.89	0.95	0.91
270	0.77	0.75	0.70	0.70	0.86	0.90	0.92	0.94	0.91
280	0.84	0.77	0.83	0.82	0.85	0.85	0.90	0.96	0.95
290	0.90	0.90	0.85	0.83	0.84	0.85	0.87	0.91	0.90
300	0.92	0.94	0.80	0.72	0.78	0.82	0.85	0.82	0.80
310	0.93	0.89	0.85	0.82	0.87	0.90	0.93	0.95	0.94
320	0.35	0.78	0.82	0.83	0.87	0.88	0.83	0.80	0.69
330	0.91	0.88	0.75	0.77	0.82	0.83	0.87	0.88	0.87
340	0.91	0.94	0.81	0.77	0.81	0.86	0.88	0.81	0.78
350	0.88	0.95	0.81	0.75	0.81	0.86	0.87	0.80	0.77
360	0.80	0.93	0.88	0.94	0.88	0.91	0.91	0.81	0.85
370	0.89	0.94	0.80	0.83	0.81	0.86	0.87	0.80	0.78

B3.3 Coefficients of determination (r^2) against each grain-size class for 2 – 10 end members

phi	no. of end-members								
	2	3	4	5	6	7	8	9	10
11.31	0.00	0.50	0.58	0.52	0.56	0.88	0.86	0.85	0.87
11.18	0.00	0.50	0.58	0.52	0.56	0.88	0.86	0.85	0.88
11.04	0.00	0.50	0.59	0.52	0.56	0.88	0.86	0.85	0.87
10.91	0.00	0.50	0.58	0.51	0.55	0.88	0.86	0.85	0.88
10.77	0.00	0.49	0.57	0.51	0.54	0.88	0.86	0.85	0.88
10.64	0.00	0.48	0.57	0.50	0.53	0.88	0.86	0.85	0.89
10.50	0.00	0.47	0.56	0.49	0.52	0.88	0.86	0.85	0.89
10.37	0.00	0.47	0.55	0.48	0.51	0.89	0.86	0.85	0.90
10.24	0.00	0.47	0.55	0.48	0.51	0.89	0.86	0.85	0.91
10.10	0.00	0.48	0.55	0.48	0.51	0.89	0.86	0.85	0.91
9.97	0.00	0.50	0.56	0.49	0.52	0.89	0.86	0.85	0.91
9.83	0.00	0.53	0.58	0.52	0.55	0.89	0.86	0.85	0.89
9.70	0.00	0.59	0.61	0.56	0.59	0.88	0.85	0.84	0.85
9.56	0.00	0.67	0.66	0.62	0.66	0.86	0.84	0.85	0.79
9.43	0.00	0.75	0.71	0.69	0.72	0.84	0.84	0.85	0.73
9.29	0.00	0.81	0.74	0.74	0.77	0.82	0.83	0.86	0.70
9.16	0.00	0.86	0.77	0.78	0.80	0.81	0.83	0.86	0.68
9.03	0.00	0.89	0.79	0.80	0.82	0.81	0.84	0.86	0.69
8.89	0.00	0.90	0.80	0.82	0.82	0.83	0.85	0.86	0.71
8.76	0.00	0.91	0.80	0.82	0.81	0.85	0.86	0.87	0.74
8.62	0.00	0.91	0.81	0.83	0.80	0.87	0.88	0.87	0.77
8.49	0.00	0.90	0.81	0.82	0.78	0.89	0.89	0.88	0.79
8.35	0.00	0.89	0.80	0.82	0.77	0.90	0.89	0.88	0.81
8.22	0.00	0.88	0.80	0.81	0.74	0.91	0.90	0.88	0.83
8.08	0.00	0.86	0.79	0.79	0.72	0.92	0.90	0.88	0.84
7.95	0.00	0.84	0.78	0.78	0.70	0.93	0.89	0.88	0.85
7.81	0.01	0.82	0.77	0.77	0.68	0.93	0.89	0.88	0.86
7.68	0.01	0.79	0.76	0.75	0.66	0.93	0.88	0.87	0.87
7.54	0.01	0.76	0.75	0.73	0.63	0.93	0.87	0.87	0.88
7.41	0.02	0.71	0.73	0.71	0.60	0.93	0.85	0.86	0.89
7.28	0.04	0.65	0.70	0.67	0.57	0.91	0.84	0.86	0.88
7.14	0.06	0.54	0.67	0.64	0.55	0.89	0.83	0.84	0.86
7.01	0.11	0.40	0.64	0.61	0.55	0.84	0.82	0.83	0.84
6.87	0.19	0.24	0.65	0.63	0.63	0.79	0.83	0.82	0.83
6.74	0.25	0.17	0.69	0.69	0.73	0.76	0.86	0.82	0.85
6.60	0.29	0.22	0.76	0.76	0.79	0.79	0.88	0.84	0.86
6.47	0.29	0.30	0.80	0.79	0.81	0.83	0.90	0.85	0.86
6.33	0.30	0.35	0.82	0.81	0.81	0.87	0.90	0.85	0.87
6.20	0.34	0.39	0.86	0.85	0.85	0.91	0.90	0.86	0.89
6.06	0.41	0.41	0.90	0.90	0.90	0.93	0.90	0.87	0.90
5.93	0.46	0.43	0.92	0.93	0.92	0.94	0.89	0.88	0.91
5.80	0.49	0.44	0.91	0.93	0.92	0.93	0.89	0.89	0.91
5.66	0.52	0.47	0.92	0.93	0.93	0.94	0.89	0.90	0.92
5.53	0.56	0.52	0.93	0.95	0.94	0.94	0.90	0.91	0.93
5.39	0.59	0.57	0.95	0.96	0.95	0.95	0.92	0.93	0.94
5.26	0.62	0.64	0.96	0.97	0.96	0.96	0.93	0.94	0.94

phi	no. of end-members								
	2	3	4	5	6	7	8	9	10
5.12	0.65	0.70	0.96	0.97	0.96	0.96	0.94	0.95	0.94
4.99	0.67	0.76	0.96	0.97	0.95	0.95	0.95	0.95	0.94
4.85	0.70	0.81	0.96	0.96	0.95	0.95	0.95	0.95	0.93
4.72	0.72	0.86	0.96	0.95	0.95	0.95	0.95	0.95	0.93
4.58	0.73	0.90	0.95	0.94	0.95	0.94	0.95	0.95	0.93
4.45	0.73	0.94	0.93	0.93	0.95	0.95	0.95	0.95	0.92
4.32	0.71	0.97	0.91	0.91	0.95	0.95	0.95	0.95	0.92
4.18	0.67	0.96	0.88	0.89	0.96	0.96	0.95	0.94	0.90
4.05	0.61	0.93	0.84	0.87	0.96	0.96	0.94	0.92	0.87
3.91	0.55	0.89	0.81	0.86	0.96	0.95	0.93	0.88	0.83
3.78	0.49	0.83	0.79	0.85	0.95	0.93	0.92	0.84	0.79
3.64	0.42	0.76	0.78	0.85	0.94	0.91	0.90	0.80	0.77
3.51	0.34	0.68	0.78	0.86	0.91	0.88	0.89	0.76	0.77
3.37	0.25	0.59	0.81	0.89	0.87	0.85	0.87	0.72	0.78
3.24	0.14	0.48	0.85	0.91	0.82	0.81	0.85	0.70	0.80
3.10	0.03	0.34	0.89	0.91	0.78	0.80	0.82	0.71	0.82
2.97	0.02	0.25	0.85	0.82	0.79	0.83	0.83	0.79	0.80
2.84	0.19	0.30	0.73	0.69	0.88	0.90	0.89	0.85	0.74
2.70	0.41	0.44	0.61	0.60	0.94	0.94	0.91	0.82	0.70
2.57	0.53	0.54	0.55	0.56	0.93	0.92	0.89	0.75	0.72
2.43	0.59	0.59	0.53	0.55	0.90	0.89	0.86	0.72	0.77
2.30	0.63	0.62	0.54	0.56	0.87	0.85	0.83	0.73	0.81
2.16	0.66	0.67	0.59	0.60	0.85	0.84	0.81	0.78	0.83
2.03	0.70	0.74	0.66	0.67	0.85	0.85	0.82	0.82	0.85
1.89	0.72	0.82	0.75	0.75	0.86	0.86	0.85	0.85	0.88
1.76	0.73	0.87	0.83	0.83	0.87	0.89	0.89	0.89	0.91
1.62	0.75	0.89	0.89	0.89	0.90	0.91	0.92	0.92	0.93
1.49	0.76	0.89	0.92	0.92	0.93	0.94	0.93	0.93	0.94
1.36	0.76	0.87	0.94	0.94	0.95	0.96	0.94	0.94	0.94
1.22	0.75	0.84	0.93	0.95	0.96	0.97	0.94	0.94	0.95
1.09	0.73	0.83	0.92	0.94	0.96	0.97	0.93	0.93	0.94
0.95	0.72	0.82	0.92	0.94	0.96	0.96	0.92	0.92	0.93
0.82	0.72	0.82	0.91	0.94	0.95	0.96	0.91	0.92	0.92
0.68	0.73	0.82	0.91	0.95	0.94	0.95	0.91	0.91	0.91
0.55	0.75	0.83	0.90	0.95	0.93	0.95	0.91	0.91	0.89
0.41	0.76	0.83	0.90	0.94	0.92	0.94	0.91	0.91	0.88
0.28	0.79	0.86	0.91	0.93	0.92	0.93	0.91	0.91	0.88
0.14	0.82	0.90	0.93	0.92	0.92	0.93	0.92	0.90	0.89
0.01	0.60	0.68	0.67	0.90	0.93	0.92	0.87	0.84	0.84
-0.13	0.36	0.42	0.41	0.86	0.94	0.90	0.87	0.85	0.87
-0.26	0.32	0.38	0.38	0.85	0.94	0.90	0.88	0.87	0.90
-0.39	0.32	0.38	0.37	0.84	0.94	0.89	0.88	0.88	0.91
-0.53	0.31	0.37	0.36	0.82	0.93	0.88	0.87	0.88	0.91
-0.66	0.30	0.37	0.35	0.79	0.91	0.86	0.85	0.88	0.91

B3.4 Factor loadings and factor scores for each end-member for the 4-end-member model

phi	Strong Current loadings	Suspen-sion loadings	IRD loadings	Moderate Current loadings	Depth [cm]	Strong Current scores	Suspen-sion scores	IRD scores	Mod. Current scores
11,3	0,05	0,22	0,04	0,09	1	0,55	0,22	0,00	0,22
11,1	0,09	0,39	0,08	0,16	11	0,53	0,09	0,00	0,38
11,0	0,13	0,56	0,11	0,23	20	0,45	0,02	0,00	0,53
10,9	0,18	0,78	0,16	0,32	30	0,26	0,01	0,00	0,73
10,7	0,22	0,93	0,19	0,39	40	0,16	0,18	0,00	0,66
10,6	0,24	1,05	0,23	0,45	50	0,18	0,02	0,00	0,80
10,5	0,27	1,12	0,25	0,49	60	0,14	0,10	0,00	0,76
10,3	0,31	1,19	0,28	0,53	70	0,30	0,13	0,00	0,57
10,2	0,34	1,25	0,31	0,56	80	0,33	0,06	0,00	0,61
10,1	0,37	1,27	0,34	0,58	90	0,08	0,08	0,00	0,85
9,97	0,41	1,29	0,37	0,59	100	0,24	0,22	0,00	0,54
9,83	0,45	1,33	0,40	0,61	110	0,68	0,00	0,00	0,32
9,70	0,49	1,40	0,43	0,62	120	0,34	0,11	0,00	0,55
9,56	0,55	1,51	0,46	0,64	130	0,22	0,20	0,00	0,58
9,43	0,61	1,68	0,50	0,67	140	0,07	0,13	0,00	0,80
9,29	0,67	1,87	0,53	0,70	150	0,18	0,00	0,00	0,82
9,16	0,73	2,12	0,57	0,74	160	0,26	0,17	0,00	0,57
9,03	0,79	2,44	0,60	0,80	170	0,00	0,35	0,00	0,65
8,89	0,84	2,77	0,63	0,86	180	0,00	0,73	0,00	0,27
8,76	0,91	3,15	0,68	0,98	190	0,03	0,31	0,00	0,67
8,62	0,99	3,51	0,75	1,13	200	0,11	0,89	0,00	0,00
8,49	1,04	3,85	0,81	1,29	210	0,05	0,19	0,00	0,76
8,35	1,07	4,12	0,87	1,43	220	0,42	0,06	0,00	0,52
8,22	1,08	4,31	0,91	1,56	230	0,32	0,15	0,00	0,53
8,08	1,06	4,40	0,93	1,66	240	0,77	0,10	0,13	0,00
7,95	1,01	4,37	0,94	1,73	250	0,36	0,28	0,36	0,00
7,81	0,93	4,20	0,93	1,77	260	0,40	0,09	0,51	0,00
7,68	0,82	3,91	0,89	1,76	270	0,28	0,27	0,09	0,37
7,54	0,70	3,52	0,84	1,72	280	0,24	0,45	0,20	0,11
7,41	0,57	3,01	0,77	1,64	290	0,17	0,26	0,29	0,27
7,28	0,43	2,46	0,69	1,53	300	0,00	0,19	0,55	0,26
7,14	0,28	1,87	0,60	1,39	310	0,16	0,33	0,24	0,26
7,01	0,15	1,30	0,51	1,24	320	0,00	1,00	0,00	0,00
6,87	0,08	0,84	0,45	1,11	330	0,05	0,32	0,51	0,12
6,74	0,08	0,51	0,43	1,01	340	0,03	0,20	0,71	0,07
6,60	0,18	0,38	0,47	0,98	350	0,00	0,13	0,67	0,19
6,47	0,23	0,30	0,48	0,95	360	0,10	0,02	0,73	0,15
6,33	0,23	0,26	0,46	0,93	370	0,00	0,13	0,70	0,17
6,20	0,21	0,23	0,40	0,92					
6,06	0,14	0,20	0,32	0,93					
5,93	0,11	0,21	0,27	0,98					
5,80	0,11	0,24	0,25	1,08					
5,66	0,12	0,26	0,24	1,19					
5,53	0,18	0,27	0,24	1,31					
5,39	0,23	0,25	0,24	1,42					

phi	Strong Current loadings	Suspen-sion loadings	IRD loadings	Moderate Current loadings
5,26	0,32	0,22	0,23	1,53
5,12	0,43	0,19	0,22	1,63
4,99	0,56	0,18	0,22	1,77
4,85	0,74	0,19	0,23	1,94
4,72	0,95	0,19	0,23	2,13
4,58	1,23	0,18	0,21	2,33
4,45	1,60	0,16	0,18	2,53
4,32	2,14	0,18	0,21	2,82
4,18	2,83	0,20	0,25	3,12
4,05	3,61	0,23	0,28	3,35
3,91	4,40	0,27	0,32	3,49
3,78	5,09	0,33	0,37	3,48
3,64	5,66	0,47	0,51	3,31
3,51	5,93	0,62	0,70	2,93
3,37	5,90	0,77	0,95	2,38
3,24	5,55	0,91	1,27	1,73
3,10	4,96	1,03	1,64	1,05
2,97	4,32	1,20	2,12	0,56
2,84	3,80	1,51	2,75	0,42
2,70	3,30	1,77	3,29	0,34
2,57	2,88	1,95	3,69	0,29
2,43	2,56	2,01	3,96	0,28
2,30	2,29	1,88	4,10	0,29
2,16	2,07	1,62	4,21	0,45
2,03	1,81	1,24	4,24	0,68
1,89	1,44	0,80	4,13	0,89
1,76	1,01	0,46	3,90	1,00
1,62	0,62	0,28	3,58	0,99
1,49	0,31	0,19	3,22	0,91
1,36	0,11	0,13	2,87	0,80
1,22	0,04	0,12	2,63	0,76
1,09	0,02	0,12	2,50	0,76
0,95	0,01	0,12	2,48	0,77
0,82	0,00	0,14	2,60	0,80
0,68	0,00	0,16	2,78	0,82
0,55	0,03	0,20	2,94	0,83
0,41	0,05	0,21	2,87	0,77
0,28	0,08	0,18	2,25	0,55
0,14	0,10	0,10	1,35	0,29
0,01	0,16	0,08	0,66	0,17
-0,13	0,18	0,07	0,46	0,14
-0,26	0,13	0,04	0,33	0,11
-0,39	0,06	0,02	0,17	0,05
-0,53	0,02	0,00	0,04	0,01
-0,66	0,00	0,00	0,00	0,00

B4 Clay-mineral percentages and non-clay mineral ratios of minerals in the clay fraction (KFsp = K-feldspar, 3.24 Å; Plag = plagioclase, 3.19 Å; Qz = quartz, 3.34 Å; Fsp = Kfsp+Plag) of sediment core PS69/849-2

Depth [cm]	Sm [%]	Ill [%]	Kao [%]	Chl [%]	Qz/Fsp	KFsp/Plag	5/10 Å
1	10,72	58,95	17,04	13,29	2,58	0,51	0,49
11	11,51	59,53	16,97	11,98	2,29	0,52	0,36
30	14,87	46,13	24,45	14,56	2,85	0,49	0,38
40	12,69	60,10	14,40	12,80	2,02	0,52	0,32
50	11,00	59,59	15,40	14,00	2,72	0,51	0,38
60	12,14	57,09	19,20	11,57	2,53	0,55	0,31
70	10,75	54,38	20,99	13,88	2,39	0,47	0,29
80	8,45	60,94	18,78	11,83	2,35	0,49	0,28
90	9,66	57,51	19,54	13,30	2,42	0,52	0,39
100	10,11	60,08	17,14	12,67	2,56	0,55	0,34
110	10,83	52,89	22,86	13,42	2,44	0,54	0,36
120	11,79	52,77	23,93	11,50	2,66	0,58	0,50
130	10,62	52,60	25,52	11,26	2,78	0,58	0,36
140	8,01	57,24	22,02	12,72	2,41	0,58	0,29
150	8,04	56,67	23,96	11,33	2,31	0,57	0,42
160	7,52	59,42	19,07	13,99	2,31	0,51	0,40
170	12,59	52,32	24,16	10,92	2,47	0,63	0,31
200	19,28	46,93	7,53	26,25	3,08	0,52	0,59
210	11,07	54,63	23,28	11,02	2,57	0,55	0,43
220	10,40	51,03	27,32	11,25	1,78	0,57	0,28
230	15,95	54,32	15,23	14,51	2,68	0,56	0,35
240	11,44	50,33	26,57	11,66	1,93	0,52	0,38
250	9,93	47,79	27,87	14,41	2,11	0,55	0,45
260	11,14	48,99	29,51	10,36	1,97	0,49	0,30
270	12,19	50,17	25,99	11,65	1,58	0,21	0,55
280	11,02	40,37	41,11	7,50	2,07	0,69	0,21
290	13,57	47,00	29,51	9,92	1,81	0,53	0,26
300	20,50	50,43	18,52	10,56	1,97	0,72	0,19
310	17,80	49,05	21,73	11,41	1,78	0,67	0,10
320	21,51	41,41	29,21	7,87	1,49	0,72	0,31
330	34,00	21,03	39,23	5,74	1,97	1,75	0,25
340	33,46	24,90	34,63	7,01	1,90	1,01	0,24
360	36,12	19,18	36,97	7,74	1,82	1,06	0,37
370	35,08	17,99	41,21	5,72	1,86	1,12	0,31

B5: Results of the wet-chemical analysis of samples from sediment core PS69/851-1

Processor *A. Borchers*
Expedition *ANT-XXIII/9*
Core *PS69/851-1*
Date *11.11.2008*
Device *ICP-OES Perkin Elmer Optima 3000 xl*
Remarks *Precision GSD-5 standard: 0.1 - 12.7 %*

Depth	Al_2O_3	Ba	CaO	Fe_2O_3	K_2O	Li	MgO	MnO	Na_2O	P_2O_5	TiO_2
	%	ppm	%	%	%	%	%	%	%	%	%
50 cm	10.34	772.50	1.63	3.11	2.81	< 25	1.00	0.08	2.49	0.11	0.58
80 cm	16.82	560.00	0.85	6.29	3.64	33.00	2.22	0.17	3.12	0.12	0.77
260 cm	16.44	685.00	1.43	6.43	4.28	38.00	2.74	0.06	3.67	0.16	0.85
290 cm	16.72	555.00	0.88	7.08	3.85	31.00	2.48	0.04	3.09	0.13	0.76
360 cm	15.64	660.00	1.08	6.08	3.95	30.00	2.21	0.05	2.99	0.13	0.79
430 cm	12.38	817.50	1.74	5.11	3.10	< 25	1.80	0.06	2.85	0.12	0.69
520 cm	10.58	822.50	4.06	3.52	2.94	< 25	1.11	0.06	2.55	0.12	0.61
550 cm	16.01	665.00	1.31	6.61	3.76	33.00	2.36	0.06	3.07	0.13	0.78
570 cm	8.69	635.00	12.59	2.84	2.44	< 25	0.93	0.05	2.33	0.08	0.51
590 cm	10.30	745.00	10.88	3.93	2.77	< 25	1.39	0.05	2.57	0.10	0.60
620 cm	14.12	670.00	1.16	5.79	3.46	29.50	2.03	0.07	2.77	0.13	0.74
800 cm	9.26	675.00	5.88	2.60	2.53	< 25	0.87	0.05	2.36	0.09	0.53
860 cm	15.92	630.00	1.02	6.29	4.01	30.50	2.17	0.05	2.79	0.13	0.79

	Al	Ba	Ca	Fe	K	Li	Mg	Mn	Na	P	Ti
	%	ppm	%	%	%	ppm	%	%	%	%	%
50 cm	5.48	772.50	1.17	2.17	2.34	< 25	0.61	0.06	1.85	0.05	0.35
80 cm	8.90	560.00	0.61	4.40	3.03	33.00	1.34	0.13	2.32	0.05	0.46
260 cm	8.70	685.00	1.03	4.50	3.55	38.00	1.65	0.05	2.73	0.07	0.51
290 cm	8.85	555.00	0.63	4.95	3.20	31.00	1.50	0.03	2.29	0.06	0.46
360 cm	8.28	660.00	0.78	4.25	3.28	30.00	1.33	0.04	2.22	0.06	0.48
430 cm	6.55	817.50	1.25	3.58	2.58	< 25	1.09	0.05	2.12	0.05	0.42
520 cm	5.60	822.50	2.90	2.46	2.44	< 25	0.67	0.04	1.89	0.05	0.37
550 cm	8.48	665.00	0.94	4.63	3.13	33.00	1.43	0.05	2.28	0.06	0.47
570 cm	4.60	635.00	9.00	1.99	2.03	< 25	0.56	0.04	1.73	0.03	0.31
590 cm	5.45	745.00	7.78	2.75	2.30	< 25	0.84	0.04	1.91	0.04	0.36
620 cm	7.48	670.00	0.83	4.05	2.88	29.50	1.23	0.05	2.05	0.06	0.44
800 cm	4.90	675.00	4.20	1.82	2.10	< 25	0.53	0.04	1.75	0.04	0.32
860 cm	8.43	630.00	0.73	4.40	3.33	30.50	1.31	0.04	2.07	0.06	0.47

B6: Weight percentages of the major grain-size fractions after wet-sieving and Atterberg separation of sediment core PS69/851-1

Depth [cm]	Clay [%]	Silt [%]	Sand [%]	Gravel [%]	Depth [cm]	Clay [%]	Silt [%]	Sand [%]	Gravel [%]
1	5.83	11.83	32.72	6.01	430	10.36	11.82	10.17	2.86
10	7.37	6.73	17.23	6.82	440	12.78	14.01	18.15	8.58
20	6.66	17.04	32.96	1.03	450	11.82	14.56	11.74	1.97
30	5.26	14.55	35.01	0.85	460	9.71	19.82	32.87	1.18
40	5.90	12.05	32.00	0.79	470	3.10	6.85	0.92	5.80
50	4.59	17.84	26.58	2.32	480	11.12	20.35	1.51	23.53
60	13.19	12.40	9.81	0.53	490	7.93	26.50	4.52	13.13
70	16.92	9.63	1.07	4.40	500	16.53	11.30	2.30	0.03
80	19.44	7.29	0.06	0.00	510	20.31	6.65	0.02	0.00
90	19.00	7.18	0.67	0.08	520	7.39	18.27	16.32	0.27
100	18.47	11.64	1.28	0.22	530	7.29	20.45	20.29	0.82
110	16.90	10.17	2.31	0.19	540	19.51	21.82	10.18	2.17
120	11.68	7.44	7.83	0.34	550	17.61	7.87	1.66	0.06
130	22.76	11.56	1.23	0.59	560	8.28	19.30	9.27	1.48
140	20.80	9.49	0.32	0.01	570	6.70	25.38	19.12	0.25
150	21.02	9.98	0.77	0.03	580	8.88	14.76	4.07	0.38
160	19.16	8.21	8.24	1.24	590	11.76	17.71	10.99	0.23
166	2.84	1.53	1.82	0.17	600	11.75	17.82	7.26	0.84
170	22.38	7.16	1.32	0.03	610	13.91	11.07	5.49	0.28
180	23.02	10.56	0.70	0.02	620	19.09	12.65	5.72	0.27
183	18.96	15.33	2.15	1.69	630	24.91	7.75	0.13	0.00
190	20.89	11.16	6.84	0.68	640	15.52	6.83	5.87	0.18
200	17.91	8.67	5.56	0.17	650	17.56	9.59	2.65	3.03
210	27.01	10.70	5.98	0.61	660	19.34	18.24	25.20	0.46
220	15.46	6.05	0.94	0.00	670	21.44	14.13	27.43	1.23
230	20.18	6.69	0.02	0.00	680	14.13	11.85	1.67	0.09
240	17.40	5.78	0.72	0.00	690	15.35	11.39	2.86	0.26
250	21.11	8.15	2.43	0.15	700	15.00	12.76	1.11	0.12
260	24.39	7.00	0.01	0.00	710	26.48	22.04	4.01	0.22
265	19.25	13.46	2.76	0.06	720	26.22	23.65	6.92	0.47
270	21.72	10.10	1.03	0.00	730	25.08	13.31	4.26	0.16
280	14.99	7.54	6.85	0.72	740	23.97	10.13	7.49	0.34
290	20.50	6.31	0.09	0.00	750	26.91	7.39	0.43	0.00
300	21.17	6.95	0.72	0.04	760	24.37	12.95	2.89	0.13
310	26.75	10.16	0.12	0.00	770	25.20	21.65	5.31	0.61
320	23.57	9.03	0.09	0.00	780	22.48	14.12	7.48	6.27
330	19.85	7.06	2.25	0.13	790	19.85	20.57	17.67	0.95
340	24.98	17.93	1.96	0.26	803	11.05	24.10	35.21	54.76
350	5.04	2.49	0.07	0.00	810	27.36	10.61	3.80	0.28
360	19.58	11.03	1.41	0.11	820	26.88	9.49	4.29	0.08
370	23.35	16.97	1.62	0.01	830	28.50	10.91	1.01	1.28
380	19.53	7.27	0.35	0.06	840	23.88	11.21	2.41	0.09
390	24.63	11.54	2.23	1.24	850	24.98	14.92	0.87	0.03
400	21.32	16.85	7.52	0.75	860	22.36	11.39	1.33	0.00
410	16.87	12.85	10.96	1.09	870	17.23	9.33	0.81	2.97
420	11.30	13.48	17.59	17.84					

B7: Clay mineral percentages and non-clay mineral ratios of minerals in the clay fraction (Hb = hornblende, 8.4 Å; KFsp = K-feldspar, 3.24 Å; Plag = plagioclase, 3.19 Å; Qz = quartz, 3.34 Å) and in the bulk sediment (CC = calcite, 3.03 Å) of sediment core PS69/851-1

Depth [cm]	Sm [%]	Ill [%]	Kao [%]	Chl [%]	KFsp/Plag	5/10A	Hb/Qz	CC/Qz bulk
1	4.85	76.05	13.17	5.93	0.50	0.19	0.38	0.01
10	3.40	73.22	16.43	6.95	0.58	0.21	0.29	0.02
20	6.20	71.46	16.71	5.63	0.58	0.22	0.37	0.00
30	7.89	69.96	19.13	3.02	0.61	0.19	0.24	0.00
40	10.34	69.06	17.10	3.49	0.51	0.17	0.43	0.00
50	8.47	75.58	12.55	3.40	0.51	0.22	0.40	0.00
60	15.60	52.91	29.45	2.04	0.73	0.18	0.30	0.00
70	18.07	40.06	39.77	2.10	1.10	0.21	0.30	0.01
80	23.48	36.45	39.21	0.86	1.20	0.21	0.22	0.02
90	22.35	43.99	32.34	1.32	1.21	0.26	0.24	0.02
100	21.28	44.01	33.70	1.01	0.86	0.23	0.28	0.01
110	19.48	40.75	37.99	1.78	0.98	0.26	0.22	0.01
120	17.70	44.64	35.52	2.14	1.02	0.22	0.25	0.00
130	14.57	45.87	36.62	2.94	1.13	0.25	0.34	0.01
140	20.81	42.98	33.15	3.06	0.87	0.28	0.20	0.01
150	26.05	40.88	30.71	2.36	1.19	0.22	0.29	0.01
160	22.44	46.61	27.67	3.28	0.95	0.28	0.24	0.01
170	24.68	45.33	26.85	3.14	1.24	0.23	0.25	0.01
180	18.49	51.77	27.25	2.49	0.85	0.21	0.24	0.02
190	13.91	57.75	24.27	4.07	0.72	0.19	0.33	0.00
200	9.24	58.06	29.38	3.33	0.65	0.28	0.31	0.01
210	4.54	64.62	27.11	3.73	0.67	0.29	0.25	0.01
220	4.46	61.56	29.06	4.92	0.71	0.26	0.27	0.02
230	6.74	63.73	24.51	5.01	0.70	0.27	0.17	0.02
240	2.95	66.15	27.15	3.75	0.56	0.20	0.22	0.02
250	7.22	62.94	25.09	4.74	0.69	0.24	0.33	0.08
260	2.86	63.91	28.06	5.17	0.68	0.22	0.29	0.01
270	21.86	45.51	28.67	3.97	0.77	0.34	0.24	0.01
280	25.89	41.21	28.67	4.23	0.88	0.26	0.19	0.00
290	25.16	41.86	28.49	4.49	1.05	0.28	0.17	0.01
300	23.49	40.50	31.58	4.43	1.16	0.24	0.15	0.01
310	18.07	49.00	26.56	6.38	0.98	0.22	0.16	0.01
320	9.46	50.85	32.66	7.03	1.04	0.32	0.20	0.01
330	18.06	46.03	29.83	6.09	0.42	0.28	0.19	0.01
340	19.51	45.91	28.64	5.95	1.01	0.27	0.16	0.01
350	20.16	43.33	30.87	5.63	0.91	0.28	0.28	0.01
360	18.84	46.93	28.17	6.06	0.92	0.22	0.21	0.01
370	15.80	51.23	26.98	5.98	0.74	0.21	0.14	0.00
380	8.68	48.71	35.32	7.28	0.89	0.31	0.25	0.01
390	15.76	51.77	27.20	5.27	0.79	0.28	0.31	0.01
400	14.54	57.39	23.85	4.22	0.81	0.16	0.37	0.01

Depth [cm]	Sm [%]	Ill [%]	Kao [%]	Chl [%]	KFsp/Plag	5/10A	Hb/Qz	CC/Qz bulk
410	7.91	61.01	25.29	5.79	0.59	0.23	0.34	0.01
420	13.24	60.10	20.47	6.20	0.69	0.33	0.35	0.01
430	18.61	57.78	17.02	6.59	0.58	0.19	0.40	0.01
440	13.71	63.27	17.48	5.54	0.58	0.18	0.49	0.01
450	14.77	59.41	21.22	4.61	0.65	0.23	0.21	0.01
460	15.18	61.21	17.79	5.82	0.66	0.30	0.34	0.00
470	23.85	55.82	14.73	5.60	0.72	0.27	0.38	0.01
480	13.44	60.56	20.97	5.03	0.74	0.20	0.49	0.01
490	19.92	50.27	26.40	3.42	0.99	0.22	0.14	0.02
500	22.10	46.52	27.62	3.76	0.90	0.25	0.27	0.01
510	18.13	49.92	29.04	2.90	0.94	0.26	0.21	0.01
520	12.00	60.35	23.31	4.34	0.64	0.34	0.26	0.08
530	9.42	63.85	21.21	5.52	0.65	0.21	0.31	0.13
540	13.51	55.07	26.25	5.17	0.78	0.22	0.23	0.01
550	13.49	50.61	31.53	4.37	0.83	0.26	0.26	0.03
560	12.52	56.08	26.44	4.96	0.74	0.23	0.22	0.33
570	18.21	56.15	22.91	2.73	0.85	0.23	0.24	0.36
580	15.35	54.06	26.98	3.61	0.81	0.26	0.17	0.41
590	11.60	58.08	27.49	2.83	0.76	0.25	0.19	0.62
600	12.06	63.34	20.02	4.58	1.09	0.17	0.37	0.39
610	9.78	63.52	22.50	4.19	0.69	0.23	0.25	0.03
620	20.21	48.15	28.17	3.47	1.14	0.24	0.32	0.02
630	22.25	34.05	41.59	2.11	1.23	0.33	0.22	0.03
640	20.44	43.64	33.58	2.34	1.10	0.28	0.15	0.02
650	11.82	51.48	32.87	3.83	0.93	0.26	0.18	0.53
660	16.19	55.49	25.13	3.19	0.82	0.18	0.35	0.50
670	12.59	47.36	36.29	3.76	1.01	0.30	0.17	0.01
680	13.94	57.60	24.50	3.96	0.89	0.23	0.26	0.19
690	13.76	56.02	26.35	3.87	0.83	0.17	0.22	0.12
700	10.76	62.16	22.60	4.47	0.84	0.18	0.37	0.18
710	14.57	56.48	24.67	4.27	0.91	0.26	0.24	0.08
720	21.32	46.48	29.39	2.81	1.00	0.22	0.27	0.02
730	16.65	49.01	30.49	3.85	0.90	0.22	0.12	0.01
740	5.91	54.62	34.79	4.68	0.92	0.23	0.19	0.01
750	8.10	50.69	36.42	4.79	0.83	0.37	0.12	0.01
760	27.52	39.24	30.83	2.41	0.90	0.21	0.24	0.03
770	19.94	44.71	30.00	5.35	1.10	0.27	0.14	0.03
780	14.07	56.01	24.72	5.21	0.80	0.16	0.12	0.02
790	12.04	60.76	21.49	5.71	0.74	0.17	0.11	0.14
803	16.67	57.95	22.00	3.37	0.79	0.28	0.09	0.18
810	31.89	30.62	34.68	2.81	1.03	0.26	0.11	0.01
820	25.19	39.25	32.65	2.92	1.25	0.30	0.06	0.01
830	23.19	36.94	35.39	4.48	0.93	0.28	0.07	0.01
840	23.20	37.44	36.03	3.34	0.98	0.25	0.28	0.02
850	20.80	41.76	32.34	5.10	1.07	0.25	0.10	0.01
860	18.88	46.09	29.73	5.31	0.93	0.24	0.26	0.01
870	15.15	52.34	25.72	6.79	0.85	0.24	0.15	0.03

B8: Calcite/ quartz ratio (CC/Qz) of the bulk sediment of sediment core PS69/853-1

Depth [cm]	CC/Qz	Depth [cm]	CC/Qz
1	0.01	440	0.01
10	0.01	450	0.01
20	0.00	460	0.01
30	0.01	470	0.01
40	0.01	480	0.01
50	0.01	490	0.01
60	0.01	500	0.01
70	0.01	510	0.01
80	0.00	640	0.20
90	0.01	650	0.02
100	0.01	660	0.01
110	0.00	670	0.45
120	0.01	680	0.82
130	0.01	690	0.75
140	0.01	700	0.89
150	0.01	710	0.86
160	0.01	720	0.89
170	0.00	730	0.28
180	0.01	740	0.10
190	0.00	750	0.09
200	0.01	760	0.10
210	0.01	770	0.36
220	0.01	780	0.52
230	0.01	790	0.41
240	0.02	800	0.27
250	0.02	810	0.25
260	0.01	820	0.25
270	0.02	830	0.39
280	0.02	840	0.30
290	0.02	850	0.21
300	0.01	860	0.08
310	0.01	870	0.07
320	0.01	880	0.07
330	0.01	890	0.19
340	0.02	900	0.03
350	0.01	910	0.05
360	0.01	920	0.62
370	0.01	930	0.66
380	0.01		
390	0.02		
400	0.02		
410	0.02		
420	0.01		
430	0.01		

B9: Palaeomagnetic properties of sediment core PS69/851-1

Depth [cm]	Incl.	Decl.	ARM 100mT	Depth [cm]	Incl.	Decl.	ARM 100mT
3	-72.3	325	8.37E+01	263	-57.8	106.9	4.81E+00
7	-79.2	183.1	1.88E+02	268	n.d.	n.d.	5.73E+00
12.5	-83.6	256	1.58E+02	273	-83.4	172.1	5.60E+01
17.5	-52	204	1.12E+02	278	-76	203.1	1.07E+02
22.5	n.d.	n.d.	1.22E+02	283	-79.8	153.7	9.59E+01
27.5	-59.6	349.9	8.89E+01	288	-78.3	215	8.18E+01
32.5	-69.4	49.9	6.70E+01	293	-9.7	1.5	6.92E+01
37.5	-60.7	184.3	7.53E+01	298	-76.4	195.2	6.25E+01
42.5	-75	147.3	5.48E+01	303	-71.3	153.8	5.66E+01
48	-80.5	111.6	8.04E+01	308	-67.2	171.2	4.13E+01
52.5	-82.1	102	9.47E+01	313	-66.2	152.7	1.37E+01
58.5	-72.6	274.1	1.21E+02	318	-56.3	171.2	3.54E+01
63	-81.1	216.8	3.51E+02	322	-63.4	185	5.32E+01
68	-81	222.3	3.35E+02	328	-63.6	190.9	9.19E+01
73	-66.4	45.2	9.76E+00	333	-57.2	196.6	2.27E+01
77.5	-86	179.7	5.20E+01	338	-76.3	215.2	6.12E+00
83	-81.8	179	1.41E+02	343	-70.9	181.2	8.97E+01
87	-75.5	186.3	1.48E+02	348	-73.2	189.8	1.18E+02
93	-60.6	179.3	9.92E+00	353	-71.7	184.2	5.85E+01
98	-76.7	315.9	1.52E+01	358	-69.7	210.2	1.14E+02
103	-56.7	116.4	1.93E+01	363	n.d.	n.d.	1.27E+02
108	n.d.	n.d.	3.23E+01	368	n.d.	n.d.	5.63E+01
113	-81.4	240.5	1.22E+02	373	-78.2	198.3	6.99E+01
118	-73.5	224.3	1.67E+02	378	n.d.	n.d.	9.03E+01
123	-87.2	127.4	1.60E+01	383	-73.9	162.2	8.28E+01
128	n.d.	n.d.	4.56E+01	387.5	-86.4	299.4	9.71E+01
133	-82.4	179.3	4.77E+01	393	-57.6	116	2.24E+01
138	-53	113.1	1.92E+01	397.5	-38	162.3	4.04E+01
143	-69.7	44.8	3.11E+01	403	-80.9	272.2	2.11E+01
148	-78.3	146.9	1.31E+02	407.5	-74.7	215.6	3.91E+01
153	-71.8	170.2	1.86E+02	413	n.d.	n.d.	2.23E+01
158	-72.8	231.8	2.22E+02	417.5	-77.8	168	1.91E+01
163	-67.1	213.6	1.31E+02	423	14.1	296.2	1.49E+01
168	-59.5	207.8	1.43E+02	427.5	-65.2	9.7	6.12E+01
173	-43.5	216.5	2.28E+01	433	-12	58.8	2.70E+01
178	-64.1	41.7	6.98E+00	438	-14	65.5	2.93E+01
184.5	n.d.	n.d.	9.65E+00	443	-85.7	267.3	1.12E+02
187.5	n.d.	n.d.	8.98E+00	448	-85.2	85.6	1.56E+02
193	-33.3	134.3	1.07E+02	453	-66.5	172.5	1.58E+02
198	-77.4	197.3	1.79E+02	457	-47.9	180.5	9.77E+01
203	-79.3	134.1	1.25E+02	463	54.7	75.6	7.28E+01
208	-73.6	219.5	3.45E+02	468	n.d.	n.d.	2.30E+01
213	-72.7	212.7	3.38E+02	473	-32.8	354.4	4.58E+01
218	-64.3	229.7	3.47E+02	478	81.4	111	2.20E+02
223	-69.1	213.4	3.56E+02	483	-69.3	278.6	1.96E+02
228	-65.3	182.1	3.60E+02	488	-74.6	14.4	1.38E+02
233	-73.1	185.6	3.84E+02	493	-80.3	295.8	9.77E+01
238	-75.7	206.2	3.98E+02	498	-82.4	199.7	1.55E+02
243	-73.2	208.2	4.14E+02	503	65.3	333.3	1.65E+02
248	-64.4	240.6	3.70E+02	508	-52.3	309.6	1.29E+02
253	-66.8	202.7	3.43E+02	513	-69	280.3	1.86E+02
258	-54.8	236.3	6.90E+01	518	-80.8	218.8	1.52E+02

Depth [cm]	Incl.	Decl.	ARM 100mT	Depth [cm]	Incl.	Decl.	ARM 100mT
523	-78.7	206.3	1.26E+02	703	85.3	79.3	1.22E+02
528	-63.9	261.7	1.28E+02	707.5	79.2	62.2	1.24E+02
533	n.d.	n.d.	1.06E+02	713	86.5	84.7	2.34E+02
538	-6.1	3.6	1.06E+02	718	71.3	35.8	2.04E+02
543	76.5	125.2	2.60E+02	723	42.5	329.9	2.00E+02
548	-82.4	90.3	1.45E+02	728	74.3	179.3	1.72E+02
553	47.8	167.3	9.60E+01	733	48.9	22.6	2.99E+02
558	18.8	93.8	1.26E+02	738	72.4	108.5	3.65E+02
563	58.4	82.1	1.08E+02	743	61.3	349.7	3.32E+02
568	n.d.	n.d.	9.74E+01	748	81.9	168.8	4.62E+02
573	19.2	92.4	1.10E+02	753	83.6	62.1	9.40E+01
577.5	76.6	75.8	2.04E+02	757.5	34.9	252.2	1.07E+01
583	62.8	71.4	1.98E+02	763	71.3	165.9	1.34E+02
587.5	60.5	69.3	2.22E+02	767.5	n.d.	n.d.	8.49E+00
593	60.1	64.8	2.01E+02	773	22.3	147.7	3.52E+00
597.5	61.8	85.3	1.54E+02	777	n.d.	n.d.	2.47E+00
603	76	84.9	1.35E+02	783	47.8	22.6	3.29E+00
607	73.6	79.1	2.28E+02	788	60.8	120.7	3.92E+00
613	69.5	234.2	2.16E+02	792	33.8	320.1	3.07E+00
617.5	67.7	300.2	1.30E+02	796.5	39.9	284.8	5.59E+00
623	68.7	123.5	1.57E+02	800.5	-17.7	96.7	8.65E+00
626.5	83.7	133	1.28E+02	806.5	65.4	45.5	1.61E+02
632.5	80	133.6	2.05E+02	812	76.1	230.7	1.38E+02
637	78.3	139.5	2.39E+02	816.5	71.2	222.7	1.38E+02
642	76.7	145.5	1.67E+02	822	78.1	218.2	1.55E+02
646.5	59.8	82.2	1.37E+02	827.5	n.d.	n.d.	1.54E+02
653	78.9	63.4	2.12E+02	832.5	74.2	188.2	1.62E+02
657	71.4	88	1.72E+02	837.5	68.6	183	1.65E+02
663	78.5	105.6	1.76E+02	842.5	88.5	54	1.62E+02
666.5	67.4	99.6	2.26E+02	847.5	64.5	199.4	1.54E+02
672	78.7	60	2.29E+02	852.5	62.7	185.7	1.46E+02
677.5	79.7	63.9	2.53E+02	857	78.4	169.7	1.37E+02
683	78.7	212.4	2.28E+02	862.5	87.8	101.4	1.36E+02
688	85.3	52.2	2.71E+02	867	84.5	89.2	1.20E+02
693	78	136.5	1.47E+02	871.5	61.2	183.3	4.52E+00
698	80.1	116	1.21E+02				

B10: Palaeomagnetic properties of sediment core PS69/853-1

Sample	Incl.	Decl.	ARM 100mT	Sample	Incl.	Decl.	ARM 100mT
4	-71,2	311,4	1,85E+02	258	-76,2	92,6	8,08E+00
8	-77,7	320,9	1,63E+02	263	-29,7	4,2	1,02E+01
14	-77,7	356,1	2,10E+02	269	-54,6	40,2	7,58E+00
18	-79,6	26,8	2,28E+02	274	-72,3	94,4	8,69E+00
24	-74,9	335,6	1,85E+02	278	-72,1	32	5,53E+00
28	-66,8	307,4	1,81E+02	283	-82	267,3	6,46E+00
33	-73,7	309,7	4,96E+01	288	-72,1	145,4	5,24E+00
38	-62,3	308,2	1,40E+02	293	-70,7	332,7	6,56E+00
43,5	-78,2	12,3	1,62E+02	298	-83,3	78,7	2,82E+01
48	-86,4	347,1	1,72E+02	303	-78,3	78,5	4,84E+01
53	-80,5	5,8	1,76E+02	308	-75,7	45,6	3,33E+01
58	-82,1	34,9	1,78E+02	312,5	-78,5	61,5	9,21E+01
63	-82,1	49,9	3,56E+02	318	-80,8	80,4	3,41E+02
68	-81,4	6,1	1,94E+02	322,5	-80,5	28,5	3,22E+02
72,5	-77,3	32,7	1,51E+02	326	-68,4	327,8	3,15E+02
78	-77,8	356,6	1,61E+02	332	-78,4	17,9	2,78E+02
83	-77	29,1	1,89E+02	337	-75,9	6	2,61E+02
86,5	-87,2	87,6	1,91E+02	342	-79,6	9,8	2,28E+02
92	-74,7	87,7	9,83E+01	347	-78,3	31	3,96E+02
98	-83,1	7,6	1,26E+02	352	-76,7	14,1	3,00E+02
103	-84	326,7	1,46E+02	357	-76,1	17,4	3,42E+02
106,5	-83,7	350	8,61E+01	362	-73,6	26,6	4,01E+02
113,5	-80,7	41,8	2,17E+02	367	-70,3	36,3	3,66E+02
117,5	-79,2	42,6	2,37E+02	372	-81,8	37,3	3,02E+02
123	-78	42,2	2,17E+02	377	-69,5	355,4	1,04E+02
127,5	-84,5	42,1	2,18E+02	383	n.d.	n.d.	3,06E+00
132,5	-85,5	348,2	1,91E+02	387	-32,8	131,7	4,94E+00
138	-78,2	297,9	1,68E+02	392	-77,4	60	2,60E+01
143	n.d.	n.d.	5,63E+00	397	-80,6	43,1	1,29E+02
147	-72,9	93,8	2,66E+01	402	-75	27	1,18E+02
153	-77,4	92,1	3,33E+00	407	-78,5	62	8,74E+00
157	-77,9	56	1,73E+00	412	-66,3	15,5	1,28E+01
163	-66,7	6,6	3,73E+00	417	-76,8	70,9	1,38E+01
168	-79,4	350,4	8,64E+01	422	-76,7	82,7	1,49E+01
173	n.d.	n.d.	9,51E+00	427	-81,1	131,7	1,96E+01
178	-78,5	109,1	1,02E+01	432	-83,2	91	2,06E+01
183	-55,5	34,6	2,33E+01	437	-84,2	41,8	2,07E+01
188	n.d.	n.d.	4,09E+01	442	-73,1	102,6	2,72E+01
193	-76,2	70,7	5,01E+01	447	-67	55,1	1,12E+01
198	-88,1	45,2	1,45E+01	452	-87	87,8	1,88E+01
203	-71,2	202	4,45E+00	457	-63,1	217,6	1,07E+01
208	-73,7	27,4	3,56E+00	462	n.d.	n.d.	1,46E+01
213	-80,9	38	6,81E+00	467	-79,7	82,8	2,13E+01
217	n.d.	n.d.	1,11E+01	472	-76,6	100,8	3,94E+01
223	-81,3	96,9	8,26E+00	477	-74	67	2,29E+01
228	n.d.	n.d.	7,16E+00	482	-75,7	52,2	2,70E+01
233	n.d.	n.d.	1,03E+01	487	-78	74,6	3,62E+01
238	-84,8	146,5	5,02E+00	492	-38,1	46,6	1,77E+01
243	-79,8	67,2	8,56E+00	497	-64,5	97,5	1,28E+01
248	-84,9	119,2	8,11E+00	502	-79,6	252	1,65E+01
253	-84,2	145,7	8,10E+00	507	-80,4	64	7,52E+01

Sample	Incl.	Decl.	ARM 100mT	Sample	Incl.	Decl.	ARM 100mT
512	-83,3	323,8	4,29E+01	727	69,1	342	2,09E+02
517	-78,1	113,1	8,30E+01	732	77,8	290,4	1,90E+02
522	-72,9	82,5	6,81E+01	737	76,9	293,5	1,56E+02
527	-76,2	126,5	7,91E+01	742	75	333	2,01E+02
532	-78,5	88,5	1,98E+01	747	77	341,1	1,31E+02
537	-79,5	0,3	4,51E+01	752	52,6	305	1,59E+02
542	-72,4	52	1,37E+01	757	74,9	326,3	2,24E+02
547	-55,7	125,5	8,17E+00	762	82,4	312,2	2,33E+02
552	-76,3	88,3	4,82E+01	767	61,3	294,7	1,86E+02
557	-53	64,5	1,23E+01	772	73,3	349,9	2,32E+02
562	57	51,3	2,03E+02	777	70,1	335,5	2,13E+02
567	45,4	351,9	2,53E+02	782	63,3	340,4	2,35E+02
572	-78,2	15,4	2,29E+02	787	76,6	357,4	2,13E+02
577	77,5	82,8	1,64E+02	792	82	1,3	2,04E+02
582	69,5	129	1,35E+02	797	77,6	346,1	2,38E+02
587	-8,4	84,1	1,27E+01	802	78,2	327,9	3,02E+02
592	67,7	30,2	1,63E+02	807	62	328,7	2,87E+02
597	78,6	284,4	2,28E+02	812	73,6	349,6	2,79E+02
602	72,3	296,4	1,74E+02	817	62,6	90,2	2,85E+02
607	-71,1	53,7	1,81E+02	822	74,9	325,2	2,11E+02
612	n.d.	n.d.	1,58E+02	827	76,2	330,3	2,56E+02
617	-84,3	8,6	2,11E+02	832	81,6	283,3	2,81E+02
622	-56,6	67,3	1,70E+02	837	78,1	316	2,40E+02
627	-65,5	83,6	1,49E+02	842	61,9	283,8	2,52E+02
632	-82,2	213,6	2,17E+02	847	67,2	326,7	2,41E+02
637	-84,1	131,3	1,83E+02	852	72,6	298,7	2,64E+02
642	-76,1	92,8	1,69E+02	857	69,7	326,2	2,17E+02
647	-20,3	73,2	2,96E+02	862	59,7	300,9	3,12E+02
652	20,9	341,3	2,40E+02	867	76,9	329	3,44E+02
657	72,6	324,8	1,86E+02	872	73,7	18,2	3,69E+02
662	73,6	345,4	2,48E+02	877	51,6	0,9	3,06E+02
667	76,9	274,9	2,31E+02	882	79,7	41,1	6,74E+01
672	82,8	317,5	2,40E+02	887	71,9	328,1	1,36E+02
677	76,6	321	1,88E+02	892	72,6	298,5	2,22E+02
682	84	287,4	1,96E+02	897	74,4	299,1	2,51E+02
687	78,1	273,1	1,60E+02	902	76	317,1	3,07E+02
692	78,6	267,1	1,40E+02	907	84,3	308,1	3,70E+02
697	70,3	293,7	2,30E+02	912	81,8	251,1	4,30E+02
702	74,3	0,4	2,28E+02	917	87,7	79,6	2,50E+02
707	57,5	299,4	2,16E+02	922	81,8	294,4	2,16E+02
712	58,2	356,6	1,82E+02	927	66,3	224,4	2,23E+02
717	83,1	57,9	2,13E+02	932	63,9	272,9	1,75E+02
722	80,2	267,5	1,59E+02	937	76,8	263,7	1,18E+02